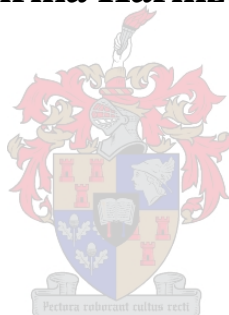


# **Study of nanofibrous membranes for application in postharvest technology**

**By**

**Elrika Harmzen**



*Thesis presented in partial fulfillment of the requirements for the degree of Master of Science (Polymer Science)*

**Supervisors:** Prof Bert Klumperman

**Co-supervisor:** Dr Lizl Cronje

University of Stellenbosch  
Department of Chemistry and Polymer Science

April 2014

## DECLARATION

By submitting this thesis electronically, I declare the entirety of the work contained therein is my own, original work, that I am the owner of the copyright thereof (unless to the extent explicitly otherwise stated) and that I have not previously in its entirety or in part submitted it for obtaining any qualification.

Elrika Harmzen

December 2013

## ABSTRACT

Grapes are lost annually due to spoilage by *Botrytis cinerea*. *Botrytis cinerea* is currently controlled using fungicides and SO<sub>2</sub> fumigation in storage rooms but with limited success.

Although these techniques have been used for decades they have been associated with numerous of disadvantages. Fungicides are restricted from being used during storage due to legislation and toxicity of the fungicides present on the surface of the berries. SO<sub>2</sub> fumigation does not kill the dormant infections present inside the grape tissue and if the SO<sub>2</sub> concentration is too high the berries are damaged.

During this study two different polymer nanofibrous platforms was synthesized in an attempt to prevent the rotting effect of *B. cinerea*.

The first polymer was modified to yield a polymer with a positively charged quaternized nitrogen moiety, which was subsequently reacted with sodium metabisulfite through an ion exchange process. The modified polymer was electrospun into nanofibrous mats for the benefit of the nanofibers' high available surface area. A further functionalization was done to increase the quantity of sodium metabisulfite on the surface of the polymer nanofibers. Sodium metabisulfite salt released SO<sub>2</sub> gas upon reaction with water vapour present in the atmosphere which resulted in the inhibition of conidial germination of *B. cinerea*.

The second polymer was synthesized and then electrospun into polymer nanofibrous mats followed by chemical modification of the electrospun polymer nanofibers. This post-electrospun modification resulted in the covalent attachment of a fungicide-derivative to the surface of the polymer nanofibers. The fungicide-derivative showed excellent inhibition of *B. cinerea* mycelium growth.

Anti-fungal studies were conducted using the two modified polymer nanofibrous mats against *B. cinerea* to evaluate these nanofibrous surfaces as *B. cinerea* inhibiting membranes. Results indicated that *B. cinerea* conidial germination and mycelium growth were successfully inhibited.

## OPSOMMING

Druive bederf jaarliks weens die verrottende effek van die fungi *Botrytis cinerea*. *Botrytis cinerea* word tans beheer deur gebruik te maak van swamdoders en swaweldioksied ( $\text{SO}_2$ ) besproeiings in stoorkamers, maar met beperkte sukses.

Alhoewel hierdie tegnieke al vir dekades in gebruik is, word dit geassosieer met verskeie probleme. Die gebruik van swamdoders word in stoorkamers verbied, weens die moontlike skadelike inname daarvan deur die mens aangesien die swamdoders op die druive se oppervlakte teenwoordig is.  $\text{SO}_2$ -gasbesproeiings maak nie dormante infeksies binne-in die druive self dood nie en indien  $\text{SO}_2$ -konsentrasies te hoog is kan dit die druive beskadig.

Tydens hierdie studie is twee verskillende polimeer-nanoveselplatforms gesintetiseer met die doel om die verrottende effek van *B. cinerea* te voorkom.

Die eerste polimeer is aangepas met 'n primêre amienverbinding met die doel dat dit deur 'n opvolgende modifikasie reaksie verander om sodoende 'n polimeer met 'n kwaternêre ammoniumgroep te verkry. Die doel van die kwaternêre eienskap is dat ioniese uitruiling plaasvind tussen die anioon van die polimeer en die natruimmetabisulfiet-anioon van die sout. Die voorbereide kopolimeer is geëlektrospon in nanoveselmatte deur middel van die enkelnaald-en-enkelbal-elektrospon tegniek om SMI-qC<sub>12</sub> nanovesels te lewer wat gefunksionaliseer is. Die nanoveselmatte is na die elektrosponproses verder aangepas om die hoeveelheid natruimmetabisulfiet op die oppervlak van die nanovesels te verhoog.

Die natruimmetabisulfiet stel  $\text{SO}_2$ -gas vry sodra dit in aanraking kom met waterdamp in die lug wat 'n beperkende effek op spoorontkieming van *B. cinerea* tot gevolg het.

Die tweede polimeer is voor en na die elektrosponproses gefunksionaliseer met gesintetiseerde organiese verbindings (swamdoder). Die aanpassing van die polimeer met die organiese verbindings het plaasgevind op 'n kovalente wyse om te verhoed dat die organiese verbinding vrygelaat word tydens gebruik. Die organiese verbindings het effektiewe beperking van miselium-groei getoon.

Anti-swamstudies is uitgevoer tussen die twee gefunksionaliseerde polimeer platforms en *B. cinerea* om die oppervlaktes van die gefunksionaliseerde polimeer/nanovesels te evalueer as *B. cinerea* beperkende platforms. Resultate het aangetoon dat spoorontkieming en miselium groei van *B. cinerea* suksesvol beperk is.

## TABLE OF CONTENTS

DECLARATION .....	iii
ABSTRACT .....	iv
OPSOMMING .....	v
TABLE OF CONTENTS .....	vii
List of Tables .....	xvii
List of Figures .....	xviii
List of Equations .....	xxiii
List of symbols .....	xxiv
List of acronyms.....	xxv
CHAPTER I: INTRODUCTION AND OBJECTIVES .....	1
1.1 Introduction .....	1
1.2 Objectives .....	3
1.3 Layout of thesis .....	5
1.4 References.....	7
CHAPTER II: HISTORICAL AND THEORETICAL BACKGROUND .....	9
2.1 Introduction .....	9
2.2 Microorganisms responsible for food spoilage.....	10
2.2.1 Introduction to microorganisms.....	10
2.2.2 Microorganisms responsible for spoilage.....	11
2.2.2.1 Bacteria .....	12
a) Gram-positive bacteria .....	13
b) Gram-negative bacteria .....	13
2.2.2.2 Fungi .....	13
2.3 Mechanisms of spoilage.....	15
2.4 Spoilage of fruit and vegetables .....	18
2.4.1 Introduction to spoilage of fruit and vegetables.....	18
2.4.2 Factors and processing operations that affect quality of minimally fresh processed plant foods .....	19
2.5 Grape spoilage.....	20

2.5.1 Introduction to grape spoilage.....	20
2.5.2 Microorganisms responsible for spoilage of grapes .....	20
2.5.2.1 <i>Penicillium</i> .....	21
2.5.2.2 <i>Pseudomonas</i> .....	21
2.5.2.3 <i>Botrytis cinerea</i> .....	22
2.6 Prevention and control measures of microorganisms in postharvest foods.....	23
2.6.1 Introduction to preventions and control measures.....	23
2.6.2 Emerging technologies for maintaining quality of minimally fresh processed fruit and vegetables.....	25
2.6.2.1 Liquid-phase chemicals .....	25
a) Hydrogen peroxide .....	25
b) Electrolyzed water (EOW) .....	26
c) Organic acids .....	26
d) Dipping solutions.....	27
2.6.2.2 Gas-phase chemicals .....	27
a) Ozone .....	27
b) Ethylene (C <sub>2</sub> H <sub>4</sub> ).....	27
c) Biocontrol .....	28
2.7 Prevention and control measures of microorganisms in grapes.....	28
2.7.1 Introduction to preventions and control measures.....	28
2.7.2 Emerging technologies for maintaining quality of grapes .....	29
2.7.2.1 Liquid-phase chemicals .....	30
a) Ethanol.....	30
b) Naturally occurring oils .....	30
c) Fungicides.....	31
2.7.2.2 Gas-phase chemicals .....	31
a) Ozone .....	31
b) Ethylene (C <sub>2</sub> H <sub>4</sub> ).....	32
2.7.2.3 Biocontrol .....	32
2.7.2.4 Equilibrium modified atmosphere (EMA) packaging.....	33
2.7.2.5 Modified atmosphere packaging (MAP) .....	33
2.8 SO <sub>2</sub> generating sheets .....	35
2.9 Organic compounds .....	38
2.9.1 Introduction to fungicides .....	38



2.9.2 Mepanipyrim ( <i>N</i> -(4-methyl-6-prop-1-ynylpyrimidin-2-yl) aniline) .....	40
2.10 Polymers .....	41
2.11 Electrospinning .....	42
2.11.1 Single needle electrospinning process .....	44
2.11.2 Ball electrospinning process .....	46
2.11.3 Electrospinning process parameters .....	50
2.11.4 Electrospinning process parameters affecting fiber diameter .....	51
2.11.4.1 Viscosity .....	52
2.11.4.2 Electric Field .....	53
2.11.4.3 Surface tension of the solution .....	54
2.11.4.4 Electrical conductivity .....	54
2.11.4.5 Distance between needle tip/ball and target .....	54
2.11.4.6 Flow rate of polymer solution .....	55
2.12 Conclusion .....	55
2.13 References.....	57

CHAPTER III: SYNTHESIS AND CHARACTERIZATION OF FUNCTIONALIZED POLYMER NANOFIBERS THROUGH THE INCORPORATION OF SODIUM METABISULFITE AS COUNTERION.....64

3.1 Introduction .....	64
3.2 Synthesis of SMA polymer .....	66
3.3 Synthesis of SMI polymer and functionalized SMI-qC <sub>12</sub> polymer .....	66
3.3.1 Synthesis of SMI polymer .....	66
3.3.2 Synthesis of SMI-qC <sub>12</sub> polymer .....	68
3.4 Electrospinning of the modified polymer .....	69
3.4.1 Introduction to single needle electrospinning .....	69
3.4.2 Introduction to single ball electrospinning .....	70
3.4.3 Electrospinning of neat polymer, and polymer and salt .....	71
3.4.4 Modification of polymer nanofibers after electrospinning.....	72
3.5 SO <sub>2</sub> detection test .....	73
3.6 Characterization of SMA and the modified SMI polymers.....	75
3.6.1 Characterization of SMA.....	75
3.6.1.1 <sup>1</sup> H-NMR .....	75
3.6.1.2 <sup>13</sup> C-NMR.....	77

3.6.2 Characterization of SMI .....	78
3.6.2.1 <sup>1</sup> H-NMR .....	78
3.6.2.2 <sup>13</sup> C-NMR .....	80
3.6.3 Characterization of SMI-qC <sub>12</sub> .....	81
3.6.3.1 <sup>1</sup> H-NMR .....	81
3.6.3.2 <sup>13</sup> C-NMR .....	83
3.6.4 Characterization of polymers using ATR-FTIR spectroscopy .....	84
3.6.5 SEM analysis: Characterization of single needle and single ball electrospun SMI-qC <sub>12</sub> polymer nanofibers .....	87
3.6.6 SEM analysis: Characterization of single needle and single ball electrospun SMI-qC <sub>12</sub> and added salt polymer nanofibers .....	88
3.6.7 SEM analysis: Crosslinked single ball electrospun SMI-qC <sub>12</sub> and salt polymer nanofibers .....	89
3.6.8 SEM analysis: Characterization of single ball electrospun SMI-qC <sub>12</sub> polymer nanofibers submerged in saturated salt solution .....	90
3.7 SO <sub>2</sub> test results .....	91
3.8 Conclusion .....	92
3.9 Experimental .....	93
3.9.1 Chemicals .....	93
3.9.2 Characterization techniques .....	94
3.9.2.1 Scanning Electron Microscopy (SEM) .....	94
3.9.2.2 Attenuated total reflectance Fourier transform infrared (ATR-FTIR) spectroscopy .....	94
3.9.2.3 Size exclusion chromatography (SEC) .....	94
3.9.2.4 Nuclear magnetic resonance spectroscopy (NMR) .....	95
3.9.3 Synthesis of styrene- <i>alt</i> -maleic anhydride copolymer (SMA) .....	95
3.9.4 Synthesis of styrene-[ <i>N</i> -3-( <i>N</i> ', <i>N</i> '-dimethylamino) propyl maleimide] copolymer (SMI) .....	97
3.9.5 Synthesis of styrene-[ <i>N</i> -3-( <i>N</i> '-dodecyl- <i>N</i> ', <i>N</i> '-dimethylammonium) propyl maleimide] copolymer (SMI-qC <sub>12</sub> ) .....	98
3.9.6 Single needle electrospinning of styrene-[ <i>N</i> -3-( <i>N</i> '-dodecyl- <i>N</i> ', <i>N</i> '-dimethylammonium) propyl maleimide] copolymer (SMI-qC <sub>12</sub> ) .....	99
3.9.7 Single ball electrospinning of styrene-[ <i>N</i> -3-( <i>N</i> '-dodecyl- <i>N</i> ', <i>N</i> '-dimethylammonium) propyl maleimide] copolymer (SMI-qC <sub>12</sub> ) .....	100
3.9.8 Single needle electrospinning of styrene-[ <i>N</i> -3-( <i>N</i> '-dodecyl- <i>N</i> ', <i>N</i> '-dimethylammonium) propyl maleimide] copolymer (SMI-qC <sub>12</sub> ) and sodium metabisulfite .....	100

3.9.9 Single ball electrospinning of styrene-[ <i>N</i> -3-( <i>N</i> '-dodecyl- <i>N</i> ', <i>N</i> '-dimethylammonium) propyl maleimide] copolymer (SMI-qC <sub>12</sub> ) and sodium metabisulfite.....	101
3.9.10 Modification after electrospinning.....	101
3.9.11 SO <sub>2</sub> detection test.....	101
3.10 References.....	102

## CHAPTER IV: SYNTHESIS AND CHARACTERIZATION OF ANTI-FUNGAL POLYMER NANOFIBERS AGAINST *Botrytis cinerea*..... 105

4.1 Introduction .....	105
4.2 Synthesis of fungicide-derivatives .....	107
4.2.1 Synthesis of <i>S</i> -methylisothiourea (1) using thiourea and methyl iodide.....	109
4.2.2 Synthesis of 4-hydroxy-6-methyl-2-(methylthio)-pyrimidine (2) using <i>S</i> -methylisothiourea and ethyl acetoacetate.....	109
4.2.3 Synthesis of 4--6-methyl-2-(methylthio)-pyrimidine (3) using 4-hydroxy-6-methyl-2-(methylthio)-pyrimidine and phosphorous oxychloride .....	109
4.2.4 Synthesis of 4-iodo-6-methyl-2-(methylthio)-pyrimidine (4) using 4-chloro-6-methyl-2-(methylthio)-pyrimidine and hydroiodic acid.....	110
4.2.5 Palladium cross-coupling reaction yielding 4-methyl-2-(methylthio)-6-((trimethylsilyl) ethynyl) pyrimidine (5) .....	110
4.2.6 Synthesis of 4-methyl-2-(methylsulfonyl)-6-((trimethylsilyl) ethynyl) pyrimidine (6) via an oxidation reaction of 4-methyl-2-(methylthio)-6-((trimethylsilyl) ethynyl) pyrimidine....	110
4.2.7 Synthesis of <i>N</i> -(4-methyl-6-((trimethylsilyl) ethynyl) pyrimidin-2-yl)- <i>N</i> -phenylformamide (7) via the addition of formanilide to 4-methyl-2-(methylsulfonyl)-6-((trimethylsilyl) ethynyl) pyrimidine .....	111
4.2.8 TBAF-mediated desilylation of <i>N</i> -(4-methyl-6-((trimethylsilyl) ethynyl) pyrimidin-2-yl)- <i>N</i> -phenylformamide to obtain <i>N</i> -(4-ethynyl-6-methylpyrimidin-2-yl)- <i>N</i> -phenylformamide .....	111
4.2.9 Synthesis of 4-ethynyl-6-methyl- <i>N</i> -phenylpyrimidin-2-amine (8) via an oxidation reaction of <i>N</i> -(4-methyl-6-((trimethylsilyl) ethynyl) pyrimidin-2-yl)- <i>N</i> -phenylformamide .....	111
4.3 Synthesis of polymers .....	112
4.3.1 Synthesis of poly(4-vinylbenzyl chloride- <i>alt</i> -maleic anhydride) copolymer (P(S <sub>Cl</sub> - <i>alt</i> -MANh)) .....	112

4.3.2	Synthesis of functionalized poly(4-vinylbenzyl azide- <i>alt</i> -maleic anhydride) copolymer (P(S <sub>N</sub> - <i>alt</i> -MANh))	112
4.3.3	Synthesis of functionalized polymer by immobilizing <i>N</i> -(4-ethynyl-6-methylpyrimidin-2-yl)- <i>N</i> -phenylformamide on to P(S <sub>N</sub> - <i>alt</i> -MANh) copolymer yielding anilinopyrimidine <sub>7</sub> -derivative copolymer (P(S <sub>AP7</sub> - <i>alt</i> -MANh))	113
4.4	Electrospinning of polymers	115
4.4.1	Electrospinning of poly(4-vinylbenzyl chloride- <i>alt</i> -maleic anhydride) copolymer (P(S <sub>Cl</sub> - <i>alt</i> -MANh))	115
4.4.2	Electrospinning of functionalized poly(4-vinylbenzyl azide- <i>alt</i> -maleic anhydride) copolymer (P(S <sub>N</sub> - <i>alt</i> -MANh))	116
4.4.3	Post-electrospinning modification of P(S <sub>Cl</sub> - <i>alt</i> -MANh) polymer nanofibers to yield P(S <sub>N</sub> - <i>alt</i> -MANh) polymer nanofibers	116
4.4.4	Post-electrospinning functionalization of P(S <sub>N</sub> - <i>alt</i> -MANh) polymer nanofibers by immobilizing <i>N</i> -(4-ethynyl-6-methylpyrimidin-2-yl)- <i>N</i> -phenylformamide onto polymer nanofibers yielding anilinopyrimidine <sub>7</sub> -derivative polymer (P(S <sub>AP7</sub> - <i>alt</i> -MANh))	117
4.5	Characterization of synthesized compounds and polymers	117
4.5.1	Characterization of <i>S</i> -methylisothiourea	118
4.5.1.1	<sup>1</sup> H-NMR	118
4.5.1.2	<sup>13</sup> C-NMR	119
4.5.2	Characterization of 4-hydroxy-6-methyl-2-(methylthio)-pyrimidine	120
4.5.2.1	<sup>1</sup> H-NMR	120
4.5.2.2	<sup>13</sup> C-NMR	121
4.5.3	Characterization of 4-chloro-6-methyl-2-(methylthio)-pyrimidine	123
4.5.3.1	<sup>1</sup> H-NMR	123
4.5.3.2	<sup>13</sup> C-NMR	124
4.5.4	Characterization of 4-iodo-6-methyl-2-(methylthio)-pyrimidine	125
4.5.4.1	<sup>1</sup> H-NMR	125
4.5.4.2	<sup>13</sup> C-NMR	126
4.5.5	Characterization of 4-methyl-2-(methylthio)-6-((trimethylsilyl) ethynyl) pyrimidine	127
4.5.5.1	<sup>1</sup> H-NMR	127
4.5.5.2	<sup>13</sup> C-NMR	128
4.5.6	Characterization of 4-methyl-2-(methylsulfonyl)-6-((trimethylsilyl) ethynyl) pyrimidine	130
4.5.6.1	<sup>1</sup> H-NMR	130
4.5.6.2	<sup>13</sup> C-NMR	131

4.5.7	Characterization of <i>N</i> -(4-methyl-6-((trimethylsilyl) ethynyl) pyrimidin-2-yl)- <i>N</i> -phenylformamide.....	133
4.5.7.1	<sup>1</sup> H-NMR.....	133
4.5.7.2	<sup>13</sup> C-NMR.....	134
4.5.8	Characterization of <i>N</i> -(4-ethynyl-6-methylpyrimidin-2-yl)- <i>N</i> -phenylformamide.....	136
4.5.8.1	<sup>1</sup> H-NMR.....	136
4.5.8.2	<sup>13</sup> C-NMR.....	137
4.5.9	Characterization of 4-ethynyl-6-methyl- <i>N</i> -phenylpyrimidin-2-amine .....	139
4.5.9.1	<sup>1</sup> H-NMR.....	139
4.5.9.2	<sup>13</sup> C-NMR.....	140
4.5.10	Characterization of poly(4-vinylbenzyl chloride- <i>alt</i> -maleic anhydride) copolymer (P(S <sub>Cl</sub> - <i>alt</i> -MAh)) .....	142
4.5.10.1	<sup>1</sup> H-NMR.....	142
4.5.10.2	<sup>13</sup> C-NMR.....	143
4.5.11	Characterization of poly(4-vinylbenzyl azide- <i>alt</i> -maleic anhydride) copolymer (P(S <sub>Cl</sub> - <i>alt</i> -MAh)) .....	144
4.5.11.1	<sup>1</sup> H-NMR.....	144
4.5.11.2	<sup>13</sup> C-NMR.....	145
4.5.12	Characterization of functionalized anilinopyrimidine <sub>7</sub> -derivative copolymer (P(S <sub>AP7</sub> - <i>alt</i> -MAh)). .....	147
4.5.12.1	<sup>1</sup> H-NMR.....	147
4.5.13	Characterization of P(S <sub>Cl</sub> - <i>alt</i> -MAh), P(S <sub>Cl</sub> - <i>alt</i> -MAh) and P(S <sub>AP7</sub> - <i>alt</i> -MAh) copolymers using ATR-FTIR spectroscopy.....	148
4.5.14	SEM analysis: Characterization of single needle- and single ball electrospun P(S <sub>Cl</sub> - <i>alt</i> -MAh) polymer nanofibers .....	150
4.5.15	SEM analysis: Characterization of single needle- and single ball electrospun P(S <sub>N</sub> - <i>alt</i> -MAh) polymer nanofibers .....	151
4.5.16	SEM and ATR-FTIR analysis: Characterization of post-electrospinning modified P(S <sub>N</sub> - <i>alt</i> -MAh) polymer nanofibers.....	152
4.5.17	SEM and ATR-FTIR analysis: Characterization of post-electrospinning functionalized anilinopyrimidine <sub>7</sub> -derivative polymer nanofibers (P(S <sub>AP7</sub> - <i>alt</i> -MAh)) .....	154
4.6	Conclusion .....	156
4.7	Experimental.....	156
4.7.1	Chemicals.....	156

4.7.2 Characterization techniques .....	157
4.7.2.1 Nuclear magnetic resonance spectroscopy (NMR) .....	157
4.7.2.2 Attenuated total reflectance Fourier transform infrared (ATR-FTIR) spectroscopy .....	157
4.7.2.3 Scanning electron microscopy (SEM) .....	158
4.7.2.4 Size exclusion chromatography (SEC) .....	158
4.7.3 Synthesis of <i>S</i> -methylisothiourea using thiourea and methyl iodide .....	159
4.7.4 Synthesis of 4-hydroxy-6-methyl-2-(methylthio)-pyrimidine from <i>S</i> -methylisothiourea and ethyl acetoacetate .....	159
4.7.5 Synthesis of 4-chloro-6-methyl-2-(methylthio)-pyrimidine from 4-hydroxy-6-methyl-2-(methylthio)-pyrimidine and phosphorous oxychloride .....	160
4.7.6 Synthesis of 4-iodo-6-methyl-2-(methylthio)-pyrimidine from 4-chloro-6-methyl-2-(methylthio)-pyrimidine and hydroiodic acid.....	160
4.7.7 Palladium cross-coupling reaction yielding 4-methyl-2-(methylthio)-6-((trimethylsilyl) ethynyl) pyrimidine .....	161
4.7.8 Synthesis of 4-methyl-2-(methylsulfonyl)-6-((trimethylsilyl) ethynyl) pyrimidine via an oxidation reaction of 4-methyl-2-(methylthio)-6-((trimethylsilyl) ethynyl) pyrimidine....	162
4.7.9 Synthesis of <i>N</i> -(4-methyl-6-((trimethylsilyl) ethynyl) pyrimidin-2-yl)- <i>N</i> -phenylformamide via the addition of formanilide to 4-methyl-2-(methylsulfonyl)-6-((trimethylsilyl) ethynyl) pyrimidine.....	162
4.7.10 TBAF-mediated desilylation of <i>N</i> -(4-methyl-6-((trimethylsilyl) ethynyl) pyrimidin-2-yl)- <i>N</i> -phenylformamide to yield <i>N</i> -(4-ethynyl-6-methylpyrimidin-2-yl)- <i>N</i> -phenylformamide .....	163
4.7.10 Synthesis of 4-ethynyl-6-methyl- <i>N</i> -phenylpyrimidin-2-amine via an oxidation reaction of <i>N</i> -(4-methyl-6-((trimethylsilyl) ethynyl) pyrimidin-2-yl)- <i>N</i> -phenylformamide .....	164
4.7.11 Synthesis of poly(4-vinylbenzyl chloride- <i>alt</i> -maleic anhydride) copolymer (P(S <sub>Cl</sub> - <i>alt</i> -MANh)) .....	165
4.7.12 Synthesis of functionalized poly(4-vinylbenzyl azide- <i>alt</i> -maleic anhydride) (P(S <sub>N</sub> - <i>alt</i> -MANh)) copolymer .....	166
4.7.13 Synthesis of functionalized polymer by immobilizing <i>N</i> -(4-ethynyl-6-methylpyrimidin-2-yl)- <i>N</i> -phenylformamide on to P(S <sub>N</sub> - <i>alt</i> -MANh)) copolymer yielding anilinopyrimidine-7-derivative copolymer (P(S <sub>AP7</sub> - <i>alt</i> -MANh)).....	166
4.7.14 Single needle electrospinning of poly(4-vinylbenzyl chloride- <i>alt</i> -maleic anhydride) copolymer (P(S <sub>Cl</sub> - <i>alt</i> -MANh)).....	167

4.7.15 Single ball electrospinning of poly(4-vinyl benzyl chloride- <i>alt</i> -maleic anhydride) copolymer (P(S <sub>Cl</sub> - <i>alt</i> -MANh)).....	167
4.7.16 Single needle- and single ball electrospinning of poly(4-vinyl benzyl azide- <i>alt</i> -maleic anhydride) copolymer (P(S <sub>N</sub> - <i>alt</i> -MANh)).....	168
4.7.17 Post-electrospinning modification of P(S <sub>Cl</sub> - <i>alt</i> -MANh) polymer nanofibers to yield P(S <sub>N</sub> - <i>alt</i> -MANh) polymer nanofibers.....	168
4.7.18 Post-electrospinning functionalization of P(S <sub>N</sub> - <i>alt</i> -MANh) polymer nanofibers by immobilizing <i>N</i> -(4-ethynyl-6-methylpyrimidin-2-yl)- <i>N</i> -phenylformamide onto polymer nanofibers yielding anilinopyrimidine <sub>7</sub> -derivative polymer nanofibers (P(S <sub>AP7</sub> - <i>alt</i> -MANh)) .....	169
4.8 References.....	170

## CHAPTER V: ANTI-FUNGAL STUDIES BETWEEN FUNCTIONALIZED POLYMERS AND

<i>Botrytis cinerea</i> .....	172
5.1 Introduction .....	172
5.2 Materials and methods .....	173
5.2.1 <i>B. cinerea</i> isolates and preparation.....	173
5.2.2 Functionalized polymer preparation .....	173
5.2.2.1 Functionalized SMI-qC <sub>12</sub> nanofibrous mats with incorporated sodium metabisulfite salt .....	173
5.2.2.2 Fungicide-derivatives.....	173
5.2.3 Media preparation.....	174
5.2.4 Conidial and mycelium sensitivity assay .....	174
5.2.4.1 Conidial germination sensitivity using SMI-qC <sub>12</sub> nanofibrous mats with incorporated sodium metabisulfite salt .....	174
5.2.4.2 Mycelium sensitivity assay to fungicide-derivatives.....	175
5.3 Results.....	176
5.3.1 Conidial sensitivity assay regarding functionalized SMI-qC <sub>12</sub> polymer nanofibers .....	176
5.3.2 Mycelium sensitivity assay regarding the synthesized fungicide-derivatives .....	177
5.3.3 Inhibition assay of mycelium growth using functionalized anilinopyrimidine <sub>7</sub> -derivative copolymer (P(S <sub>AP7</sub> - <i>alt</i> -MANh)) against <i>B. cinerea</i> .....	177
5.4 Discussion and conclusion .....	178
5.4.1 Discussion on conidial sensitivity assay regarding functionalized SMI-qC <sub>12</sub> polymer nanofibers .....	178

5.4.2 Discussion on mycelium sensitivity assay regarding the synthesized fungicide-derivatives .....	178
5.4.3 Conclusion.....	179
5.5 References.....	180
CHAPTER VI: CONCLUSIONS AND RECOMMENDATIONS FOR FUTURE RESEARCH ....	182
6.1 Conclusions .....	182
6.1.1 Functionalization of polymers .....	182
6.1.1.1 Functionalization of SMI-qC <sub>12</sub> polymer nanofibers with incorporated sodium metabisulfite .....	182
6.1.1.2 Synthesis of functionalized polymer through immobilization of anilinopyrimidine-derivatives onto poly(4-vinylbenzyl azide- <i>alt</i> -maleic anhydride) copolymer yielding anilinopyrimidine-derivative polymers .....	183
6.1.2 Anti-fungal studies .....	184
6.2 Recommendations for future research .....	184
ACKNOWLEDGMENTS.....	186



## List of Tables

Table	Page
<i>Table 3.1 The solvents that were selected for dissolving the active salt and electrospinning both the salt and SMI-qC<sub>12</sub> polymer .....</i>	69
<i>Table 3.2 Electrospinning results regarding the single needle and single ball electrospinning of the neat polymer and the polymer with the incorporated sodium metabisulfite .....</i>	72
<i>Table 3.3 SO<sub>2</sub> release data regarding SMI-qC<sub>12</sub> fibers with incorporated sodium metabisulfite..</i>	91
<i>Table 5.1 The percentage of conidium inhibition of two different isolates of B. cinerea using sodium metabisulfite. In each experiment 30 spores were evaluated for germination.....</i>	176
<i>Table 5.2 The Percentage inhibition of mycelium growth is expressed as a function of concentration against the two B. cinerea isolates.....</i>	177

## List of Figures

Figure	Page
<i>Figure 2.1 Data indicating the quantity of food eaten compared to the quantity of food lost for different food types.<sup>18</sup></i>	9
<i>Figure 2.2 Illustration of B. cinerea grape bunch rot (A) and P. expansum fruit rot (B).</i>	15
<i>Figure 2.3 Illustration of grape bunches with bruising, cracks and punctures.</i>	17
<i>Figure 2.4 Histogram representing the increase in the number of scientific articles published in the electrospinning field over the last decade.<sup>75</sup></i>	43
<i>Figure 2.5 Different fields and potential applications of polymer nanofibers in the industry.<sup>69</sup></i>	44
<i>Figure 2.6 Illustration of the spinning tip, the polymer droplet, the Taylor cone region and the bending instability region.<sup>82</sup></i>	45
<i>Figure 2.7 The multiple ball electrospinning setup is illustrated. Multiple balls are used to create electrospun nanofibers. In a solution container (2) multiple loose balls (1) are rotated. The polymer solution (3) within the container is able to be electrospun. An electric field is created between the balls (1) and a collector (5) by means of a high voltage power supply (4). A contact plate (6) supports the balls while the trough is moved by one of a few different methods, including by means of pistons (7). The motion can be controlled by using an automatic valve assembly (8). When sufficient electrical charge is applied to the balls, electrospinning jets (9) eject from the surface of the balls and are deposited on the collector as nanofibers.<sup>87</sup></i>	47
<i>Figure 2.8 A) Representation of an electric wave running over the surface of the ball, dashed-red wave at lower frequency and solid-blue wave at a higher frequency.<sup>133</sup> B) A schematic illustration of the different amount of jets which are able of being ejected from the surface of the glass ball. In the figure B): (i) fewer amounts of peaks due to a lower frequency (red wave) and (ii) more wavelengths due to a higher frequency wave (blue wave) therefore more peaks and more jets are able to eject from the surface of the glass ball.</i>	49
<i>Figure 3.1 Conventional radical copolymerization of SMA and the repeat unit of SMA.</i>	66
<i>Figure 3.2 Schematic illustration of the modification of SMA via nucleophilic addition of a primary N-alkylamine to the reactive maleic anhydride group of SMA.</i>	67
<i>Figure 3.3 The schematic illustration of the SMA modification reaction to yield the relevant SMI precursor and the quaternization step via the SMI precursor to yield SMI-qC<sub>12</sub>.</i>	68

<i>Figure 3.4 The lab scale ball electrospinning setup used in this study. The setup consists of 1) the glass ball within the solution holder, 2) the aluminum covered collector collecting the nanofiber, 3) the rotation drum that is covered with aluminum foil, 4) the motor that rotates the glass ball, 5) the positive electrode coupled to the solution via the solution holder and 6) the negative electrode coupled to the collector. ....</i>	70
<i>Figure 3.5 A schematic illustration of the ions present to interchange during the ion exchange between the bromide and the sodium metabisulfite ions. ....</i>	73
<i>Figure 3.6 The experimental setup for the SO<sub>2</sub> detection test. ....</i>	74
<i>Figure 3.7 <sup>1</sup>H-NMR spectrum of SMA and the assignment of the relevant peaks. ....</i>	75
<i>Figure 3.8 <sup>13</sup>C-NMR spectrum of SMA and the assignment of the relevant peaks. ....</i>	77
<i>Figure 3.9 <sup>1</sup>H-NMR spectrum of styrene-[N-3-(N',N'-dimethylamino) propyl maleimide] copolymer (SMI).....</i>	78
<i>Figure 3.10 <sup>13</sup>C-NMR spectrum of styrene-[N-3-(N',N'-dimethylamino) propyl maleimide] copolymer (SMI).....</i>	80
<i>Figure 3.11 <sup>1</sup>H-NMR spectrum of styrene-[N-3-(N'-dodecyl-N',N'-dimethylammonium) propyl maleimide] copolymer (SMI-qC<sub>12</sub>). ....</i>	81
<i>Figure 3.12 <sup>13</sup>C-NMR spectrum of styrene-[N-3-(N'-dodecyl-N',N'-dimethylammonium) propyl maleimide] copolymer (SMI-qC<sub>12</sub>). ....</i>	83
<i>Figure 3.13 ATR-FTIR spectra of (a) SMA (top), (b) SMI (middle), (c) SMI-qC<sub>12</sub> (bottom). ....</i>	84
<i>Figure 3.14 SEM images of SMI-qC<sub>12</sub> polymer nanofibers using single needle and single ball electrospinning. Image A was obtained using the single needle electrospinning process: Polymer concentration 20 wt. %; applied voltage 20 kV, ambient humidity &lt;50%, temperature 24 °C, 10 cm spinning distance and a flow rate of 0.07 mL.min<sup>-1</sup>. Image B was obtained using the single ball electrospinning process: Polymer concentration 25 wt. %, applied voltage 50 kV, 10 cm spinning distance and an ambient humidity &lt;50%. ....</i>	87
<i>Figure 3.15 SEM images of SMI-qC<sub>12</sub> polymer and salt nanofibers formed using single needle and single ball electrospinning. Image A was obtained using the single needle electrospinning process: Polymer concentration, 20 wt. %; salt, 0.6 wt. %, applied voltage 20 kV, temperature 24 °C, 10 cm spinning distance, ambient humidity &lt;50% and a flow rate of 0.07 mL.min<sup>-1</sup>. Image B was obtained using the single ball electrospinning process: Polymer concentration, 25 wt. %; salt, 0.6 wt. %, applied voltage 50 kV, 10 cm spinning distance and an ambient humidity &lt;50%. ....</i>	88
<i>Figure 3.16 SEM images of SMI-qC<sub>12</sub> and add salt polymer nanofibers cross-linked under vacuum at 130 °C for 24 hours.....</i>	89

Figure 3.17 SEM images of the submerged SMI-qC <sub>12</sub> nanofibers containing sodium metabisulfite salt on the surface of the nanofibers. Images A - C were obtained after submerging the fibers for 20 minutes. Images D - F were obtained after submerging the fibers for 40 minutes. The images differ only in the magnification at which the images were taken.....	90
Figure 3.18 Graph illustrating the incremental quantity of SO <sub>2</sub> gas that is released in the first 96 hours if moisture is present in the system. ....	92
Figure 3.19 Synthesis of styrene-[N-3-(N',N'-dimethylamino) propyl maleimide] copolymer. ....	97
Figure 3.20 Synthesis of styrene-[N-3-(N'-dodecyl-N',N'-dimethylammonium)propyl maleimide] copolymer (SMI-qC <sub>12</sub> ). ....	98
Figure 4.1 Mepanipyrim compound with the chemical name 3-methyl-N-phenyl-5-(prop-1-yn-1-yl) aniline.....	107
Figure 4.2 Synthesis route for the synthesis of the anilinopyrimidine compounds. Precursors include : (1) S-methylisothiourea, (2) 4-Hydroxy-6-methyl-2-(methylthio)-pyrimidine, (3) 4-Chloro-6-methyl-2-(methylthio)-pyrimidine, (4) 4-Iodo-6-methyl-2-(methylthio)-pyrimidine, (5) Palladium cross-coupling reaction yielding 4-methyl-2-(methylthio)-6-((trimethylsilyl) ethynyl) pyrimidine, (6) 4-methyl-2-(methylsulfonyl)-6-((trimethylsilyl) ethynyl) pyrimidine, (7) N-(4-methyl-6-((trimethylsilyl) ethynyl) pyrimidin-2-yl)-N-phenylformamide, and (8) 4-methyl-N-phenyl-6-((trimethylsilyl) ethynyl) pyrimidin-2-amine. ....	108
Figure 4.3 Poly(4-vinylbenzyl chloride-alt-maleic anhydride) copolymer (P(S <sub>Cl</sub> -alt-MANh) monomer units. ....	112
Figure 4.4 The functionalized poly(4-vinylbenzyl azide-alt-maleic anhydride) copolymer monomer units.....	113
Figure 4.5 The schematic illustration of the anilinopyrimidine <sub>7</sub> -derivative polymer (P(S <sub>APT</sub> -alt-MANh).....	114
Figure 4.6 <sup>1</sup> H-NMR spectrum of S-methylisothiourea and the assigned peaks.....	118
Figure 4.7 <sup>13</sup> C-NMR spectrum of S-methylisothiourea and the assigned peaks .....	119
Figure 4.8 <sup>1</sup> H-NMR spectrum of 4-hydroxy-6-methyl-2-(methylthio)-pyrimidine and the assignment of the peaks. ....	120
Figure 4.9 <sup>13</sup> C-NMR spectrum of 4-hydroxy-6-methyl-2-(methylthio)-pyrimidine and the assignment of the relevant peaks.....	121
Figure 4.10 <sup>1</sup> H-NMR spectrum of 4-chloro-6-methyl-2-(methylthio)-pyrimidine and the assignment of the peaks. ....	123

Figure 4.11 <sup>13</sup> C-NMR spectrum of 4-chloro-6-methyl-2-(methylthio)-pyrimidine and the assignment of the peaks. ....	124
Figure 4.12 <sup>1</sup> H-NMR spectrum of 4-iodo-6-methyl-2-(methylthio)-pyrimidine and the assignment of the relative peaks. ....	125
Figure 4.13 <sup>13</sup> C-NMR spectrum of 4-iodo-6-methyl-2-(methylthio)-pyrimidine and the assignment of the peaks. ....	126
Figure 4.14 <sup>1</sup> H-NMR spectrum of 4-methyl-2-(methylthio)-6-((trimethylsilyl) ethynyl) pyrimidine and the assignment of the peaks. ....	127
Figure 4.15 <sup>13</sup> C-NMR spectrum of 4-methyl-2-(methylthio)-6-((trimethylsilyl) ethynyl) pyrimidine and the assignment of the peaks. ....	128
Figure 4.16 <sup>1</sup> H-NMR spectrum of 4-methyl-2-(methylsulfonyl)-6-((trimethylsilyl) ethynyl) pyrimidine and the assignment of the peaks. ....	130
Figure 4.17 <sup>13</sup> C-NMR spectrum of 4-methyl-2-(methylsulfonyl)-6-((trimethylsilyl) ethynyl) pyrimidine and the assignment of the peaks. ....	131
Figure 4.18 <sup>1</sup> H-NMR spectrum of N-(4-methyl-6-((trimethylsilyl) ethynyl) pyrimidin-2-yl)-N-phenylformamide and the assignment of the peaks. ....	133
Figure 4.19 <sup>13</sup> C-NMR spectrum of N-(4-methyl-6-((trimethylsilyl) ethynyl) pyrimidin-2-yl)-N-phenylformamide and the assignment of the peaks. ....	134
Figure 4.20 <sup>1</sup> H-NMR spectrum of N-(4-ethynyl-6-methylpyrimidin-2-yl)-N-phenylformamide and the assignment of the peaks. ....	136
Figure 4.21 <sup>13</sup> C-NMR spectrum of N-(4-ethynyl-6-methylpyrimidin-2-yl)-N-phenylformamide and the assignment of the peaks. ....	137
Figure 4.22 <sup>1</sup> H-NMR spectrum of 4-ethynyl-6-methyl-N-phenylpyrimidin-2-amine and the assignment of the peaks. ....	139
Figure 4.23 <sup>13</sup> C-NMR spectrum of 4-ethynyl-6-methyl-N-phenylpyrimidin-2-amine and the assignment of the peaks. ....	140
Figure 4.24 <sup>1</sup> H-NMR spectrum of poly(4-vinylbenzyl chloride-alt-maleic anhydride) copolymer and the assignment of the peaks. ....	142
Figure 4.25 <sup>13</sup> C-NMR spectrum of poly(4-vinylbenzyl chloride-alt-maleic anhydride) copolymer and the assignment of the peaks. ....	143
Figure 4.26 <sup>1</sup> H-NMR spectrum of poly(4-vinylbenzyl azide-alt-maleic anhydride) copolymer and the assignment of the peaks. ....	144
Figure 4.27 <sup>13</sup> C-NMR spectrum of poly(4-vinylbenzyl azide-alt-maleic anhydride) copolymer and the assignment of the peaks. ....	145

Figure 4.28  $^{13}\text{C}$ -NMR spectra of functionalized anilinopyrimidine<sub>7</sub>-derivative copolymer ( $P(\text{S}_{\text{AP}7}\text{-alt-MAh})$ ) and the assignment of the peaks.....147

Figure 4.29 ATR-FTIR spectra of (a)  $P(\text{S}_{\text{Cl}}\text{-alt-MAh})$  (top), (b)  $P(\text{S}_{\text{N}}\text{-alt-MAh})$  (middle) and .149

Figure 4.30 SEM images of  $P(\text{S}_{\text{Cl}}\text{-alt-MAh})$  polymer nanofibers using single needle and single ball electrospinning. Image A was obtained using the single needle electrospinning process: Polymer concentration 25 wt. %; applied voltage 16 kV, , ambient humidity <50%, temperature 20 °C, 15 cm spinning distance and a flow rate of 0.2 mL.min<sup>-1</sup>. Images B and C were obtained using the single ball electrospinning process: Polymer concentration 25 wt. %, applied voltage 55 kV, 10 cm spinning distance and an ambient humidity <50%. ....151

Figure 4.31 SEM images of post-electrospinning  $P(\text{S}_{\text{Cl}}\text{-alt-MAh})$  nanofibers to obtain azide functionalized  $P(\text{S}_{\text{N}}\text{-alt-MAh})$  nanofibers. Images A and B are functionalized nanofibers without washing (crystal present on surface of nanofibers). Images C and D are functionalized nanofibers that were thoroughly washed.....152

Figure 4.32 ATR-FTIR spectra of (a)  $P(\text{S}_{\text{Cl}}\text{-alt-MAh})$  polymer nanofibers modified for 2 hours (top), (b)  $P(\text{S}_{\text{Cl}}\text{-alt-MAh})$  polymer nanofibers modified for 5 hours (middle), (c)  $P(\text{S}_{\text{Cl}}\text{-alt-MAh})$  polymer nanofibers modified for 16 hours (bottom). ....153

Figure 4.33 SEM images of functionalized anilinopyrimidine<sub>7</sub>-derivative polymer ( $P(\text{S}_{\text{AP}7}\text{-alt-MAh})$ ).....154

Figure 4.34 ATR-FTIR spectra of post-electrospinning modification to yield functionalization anilinopyrimidine<sub>7</sub>-derivative polymer nanofibers ( $P(\text{S}_{\text{AP}7}\text{-alt-MAh})$ ).....155

## List of Equations

Equation	Page
Equation 2.1 Electric field strength equation. Units being measured in are: <sup>a</sup> = kV/cm, <sup>b</sup> = kV and <sup>c</sup> = cm.....	53

## **List of symbols**

%	Percentage
°C	Degree Celsius
d	Distance the polymer jet needs to travel
$\mathcal{D}$	Dispersity
E	Electric field strength
g	gram
kg	Kilogram
kPa	Kilopascal
kV	Kilovolts
M	Molar concentration
mg	Milligram
mL	Milliliter
mmol	Millimole
$M_n$	Number average molecular weight
mV	Millivolts
$M_w$	Weight average molecular weight
nm	Nanometer
V	Voltage difference between electrodes
wt. %	Weight-weight percentage



**List of acronyms**

$^{13}\text{C}$ -NMR	Carbon nuclear magnetic resonance spectroscopy
$^1\text{H}$ -NMR	Proton nuclear magnetic resonance spectroscopy
1-MCP	1-Methylcyclopropene
Acetone- $\text{d}_6$	Deuterated acetone
AIBN	2, 2' Azobis (isobutyronitrile)
Ar	Argon
ATR-FTIR	Attenuated reflectance Fourier transform infrared spectroscopy
Br- $\text{C}_{12}$	Bromododecane
$\text{C}_2\text{H}_4$	Ethylene
CA	Controlled atmosphere
$\text{CDCl}_3$	Deuterated chloroform
Cl	Chloride
$\text{Cl}_2$	Chlorine
$\text{CO}_2$	Carbon dioxide
$\text{Cu(I)Br}$	Copper(I) bromide
CuAAC	Copper (I)-catalyzed Azide-Alkyne Cyclo-addition
$\bar{D}$	Dispersity or Degree of polymerization
DCM	Dichloromethane
DMAPA	3-( <i>N, N</i> -dimethylamino)-1-propylamine
DMF	<i>N, N</i> -Dimethylformamide
DMSO	Dimethyl sulfoxide
$\text{DMSO-}\text{d}_6$	Deuterated dimethyl sulfoxide
DNA	Deoxyribonucleic acid
DRI	Differential refractive index
EA	Ethyl acetate

EMA	Equilibrium modified atmosphere
EOW	Electrolyzed water
GMP	Good manufacturing practices
GRAS	Generally recognized as safe
H <sub>2</sub> O <sub>2</sub>	hydrogen peroxide
H <sub>2</sub> SO <sub>3</sub>	Sulfurous acid
IPE	Isopropyl ether
IR	Infrared
KMnO <sub>4</sub>	Potassium permanganate
LAB	Lactic acid bacteria
MAnh	Maleic anhydride
MAP	Modified atmosphere packaging
Mel	Methyl iodide
MEK	Methyl ethyl ketone
MeOH	Methanol
MgSO <sub>4</sub>	Magnesium sulphate
min	Minutes
NaCl	Sodium chloride
NaN <sub>3</sub>	Sodium azide
NaOH	Sodium hydrogen
NH <sub>4</sub> Cl	Ammonium chloride
O <sub>2</sub>	Oxygen
OH	Hydroxide ion or group
PCN	Penicillin
Pd (PPh <sub>3</sub> ) <sub>2</sub> Cl <sub>2</sub>	Bis (triphenylphosphine) palladium (II) dichloride
PMDETA	<i>N,N,N',N'',N'''</i> -Pentamethyldiethylenetriamine
POCl <sub>3</sub>	Phosphorous oxychloride
ppm	Parts per million

PPO	Polyphenol oxidase
rH	Relative humidity
ROS	Reactive oxygen species
S <sub>Cl</sub>	4-Vinylbenzyl chloride
SEC	Size exclusion chromatography
SEM	Scanning electron microscope
SMA	Styrene- <i>alt</i> -maleic anhydride copolymer
SMI	Styrene-[ <i>N</i> -3-( <i>N</i> , <i>N</i> -dimethylamino) propyl maleimide)] copolymer
SMI-qC <sub>12</sub>	Styrene-[( <i>N</i> -dodecyl)- <i>N</i> ' , <i>N</i> ' -dimethyl)-3-propyl maleimide] copolymer
SO <sub>2</sub>	Sulphur dioxide
SSO	Specific spoiling organism
St	Styrene
TBAF	Tetra- <i>N</i> -butyl ammonium fluoride
TEA	Triethylamine
THF	Tetrahydrofuran
TLC	Thin layer chromatography
TMS	Trimethylsilane
USDA	United States Department of Agriculture
UV-C	Ultraviolet-C
P(S <sub>Cl</sub> - <i>alt</i> -MAh)	Poly(4-vinylbenzyl chloride- <i>alt</i> -maleic anhydride)
P(S <sub>N</sub> - <i>alt</i> -MAh)	Poly(4-vinylbenzyl azide- <i>alt</i> -maleic anhydride)
P(S <sub>AP7</sub> - <i>alt</i> -MAh)	poly({4-vinylbenzyl-N-[4-methyl-6-(1H-1,2,3-triazol-4-yl)pyrimidin-2-yl]-N-phenylformamide}- <i>alt</i> -maleic anhydride) copolymer also anilinopyrimidine <sub>7</sub> -derivative copolymer
Zn/Se	Zinc selenide

## CHAPTER I: INTRODUCTION AND OBJECTIVES

### 1.1 Introduction

The worldwide grape production per year has increased in the last ten years to an estimate of 69 million tons/year.<sup>1,2</sup> South Africa is the 9<sup>th</sup> largest grape producing country in the world and the 3<sup>rd</sup> largest leading exporting company of table grapes in the world.<sup>2,3</sup> It is estimated that for 2013 between 53.8 and 55.1 million cartons of grapes (~ 4.5 kg per carton) will be harvested.<sup>2,4</sup> Before consumption, the fruit is exposed to widely different conditions during either storage or shipping, which may lead to the spoilage of the fruit due to the presence of microorganisms such as fungi.<sup>5</sup> Such microorganisms can be found on a large number of economically important agricultural and horticultural crops, including grapes, which can cause serious fruit damage and hence a massive economic loss.

Among other fungi, *Botrytis cinerea* Pers.: Fr. is well known for its activity on grape tissue during storage. *Botrytis cinerea* is a ubiquitous and sophisticated fungal pathogen causing a disease known by the common name “grey mould” in over 200 plant species in the temperate zone worldwide.<sup>6,7</sup> The fungus is destructive, neurotropic and a high risk to farmers and consumers.<sup>8,9</sup> All plant organs, including the flowers, leaves, shoots, rachin and soil storage organs are susceptible to grey mould attacks.<sup>10</sup> However, the most important damage to plant fruits is caused either by pre- and/or post-harvest decay.<sup>10</sup>

On the grapes surface during storage are sclerotia (a compact mass of hardened fungal mycelium containing food reserves) from overwintering. The sclerotia can produce abundant conidia, which can infect susceptible tissue. The infected tissue develops into latent infections due to the inoculum present on the surface of the berries. In addition, the fruits peel/surface can be damaged creating wounds in the form of punctures or bruises during harvest or postharvest handling. These wounds are the major avenues for infections by microorganisms (fungi). The study focuses on the spoilage fungi *B. cinerea*.

Postharvest *B. cinerea* bunch rot can largely be ascribed to infection during storage. Currently, grey mould on table grapes is primarily controlled in the field, by pre-harvest fungicide applications (chemical fungicides sprayed onto grapes in a spray program).<sup>7</sup> However, during fruit storage (post-harvest), growth is restricted by the use of sulphur dioxide (SO<sub>2</sub>), which can be applied via either weekly fumigations or via the use of an SO<sub>2</sub>-precursor i.e. sodium metabisulfite.<sup>5,11,12</sup> In the second control technique, the SO<sub>2</sub>-precursor is imbedded in sheets, called SO<sub>2</sub> generating sheets, placed on top of the grape package, which upon contact with atmospheric moisture release SO<sub>2</sub> gas.<sup>8,11,13-16</sup>

Although fumigation is the most commonly used post-harvest method, this method is associated with a number of disadvantages. For example, it can cause bleaching injuries of the berries surface, browning of the rachins and the residues can be health risk to human. In addition, the use of SO<sub>2</sub> is restricted only in fighting *B. cinerea* in the storage rooms, as well as its restriction in organically certified farms. Furthermore, SO<sub>2</sub> is only active against growing species and does not affect the dormant infections present inside the berry tissue, which can cause the fruit spoilage at a later stage during storage.<sup>7,8</sup> To overcome this limitation, a preprogrammed SO<sub>2</sub> fumigation is required in order to prevent any *B. cinerea* development.

Besides the use of SO<sub>2</sub> in fighting *B. cinerea*, other types of fungicides are also commonly used via means of spraying programs pre-harvest in the field. The fungicides are effective and can kill dormant infections present inside the berry tissue, but many key fungicides have been withdrawn because of concerns over the safety of food supply and environment. However, the use of such fungicides is generally also restricted by disease resistance, legislations and consumer-demand for lower residues in the fruit.<sup>17</sup> The fungicides are also restricted from being used in post-harvest periods due to “free” fungicides that are present on the grape berry surface. Such limitations increase the demand for new health-friendly fungicides that can be used against a wide spectrum of fungi as well as for more effective and practical methods to apply these fungicides.<sup>16,18</sup>

Some new fungicides, focused on the inhibition of *B. cinerea*, with different modes of action by which the fungicides inhibit the growth or developments of *B. cinerea* have recently been registered. These new fungicides include phenylpyrrole derivatives, hydroxyanilide derivatives and anilinopyrimidine derivatives.<sup>17,19</sup> The anilinopyrimidine group, especially the mepanipyrim

fungicide, have a broad-spectrum activity against several plant pathogens, including a potent fungicidal activity against *B. cinerea*.<sup>16,20</sup>

However, due to practice and health limitations associated with the above-mentioned methods, this study focuses on developing new effective methods against *B. cinerea*. In this study, two approaches were conducted; the first approach is based on the SO<sub>2</sub> fumigation, while the second approach focuses on the use of immobilized fungicides.

In the first approach, the SO<sub>2</sub>-precursor is incorporated in polymeric nanofibrous mats that can be used to outline the package, which insures a better fumigation of the fruit.

The second approach of the study is to investigate an alternative method to limit *B. cinerea* growth by using a fungicide that is covalently attached to a polymer system, and hence no “free” fungicides is present on the surface of the berries. Literature shows mepanipyrim is effective in inhibiting *B. cinerea*.<sup>18</sup> In order to attach mepanipyrim to polymer chains with functional groups, it is necessary to modify the mepanipyrim and introduce active sites that selectively react with functional groups on the polymer.

These two approaches and newly proposed methods to control *B. cinerea* in a more effective manner are used for *in vitro* sensitivity assays between 1) the fibers containing the SO<sub>2</sub>-precursor *i.e.* active sodium metabisulfite and 2) the immobilized organic compounds on a polymer against *B. cinerea*. The sensitivity assays were done to evaluate and compare conidial and mycelium growth inhibition of *B. cinerea* using the proposed techniques (using sodium metabisulfite fibers and compound amended fibers have).

## **1.2 Objectives**

The basic motivation for this work was to synthesize an inhibition platform against *Botrytis cinerea* in packaging systems during storage. The study was taken in two approaches.

The objectives of the study can therefore be summarized as follows:

1. To synthesize a high molar mass alternating poly(styrene-*alt*-maleic anhydride) (SMA) and poly(4-vinylbenzyl chloride-*alt*-maleic anhydride) (P(S<sub>Cl</sub>-*alt*-MANh)) copolymer using conventional radical copolymerization
2. To synthesize poly(styrene-*alt*-maleimide) copolymer (SMI) and quaternized poly(styrene-*alt*-[(*N*-dodecyl)-*N,N*-dimethyl]-3-propyl maleimide] copolymer (SMI-qC<sub>12</sub>) that can be electrospun into polymer nanofibers.
3. To incorporate sodium metabisulfite salt within the functionalized polymer nanofibers via an ion exchange transfer reaction.
4. To synthesize poly(4-vinylbenzyl azide-*alt*-maleic anhydride) copolymer P(S<sub>N</sub>-*alt*-MANh) through pre- and post-electrospinning modification by first electrospinning the pristine P(S<sub>Cl</sub>-*alt*-MANh) polymer into polymer nanofibers and thereafter surface functionalization with NaN<sub>3</sub> to yield P(S<sub>N</sub>-*alt*-MANh) polymer nanofibers and secondly, modifying the pristine P(S<sub>Cl</sub>-*alt*-MANh) polymer before electrospinning to yield P(S<sub>N</sub>-*alt*-MANh) polymer.
5. To successfully synthesize *N*-(4-ethynyl-6-methylpyrimidin-2-yl)-*N*-phenylformamide (anilinopyrimidine<sub>7</sub>-derivative) and 4-ethynyl-6-methyl-*N*-phenylpyrimidin-2-amine (anilinopyrimidine<sub>8</sub>-derivative).
6. To functionalize P(S<sub>N</sub>-*alt*-MANh) copolymer before electrospinning, as well as surface-functionalizing the P(S<sub>N</sub>-*alt*-MANh) polymer nanofibers post-electrospinning with *N*-(4-ethynyl-6-methylpyrimidin-2-yl)-*N*-phenylformamide (anilinopyrimidine<sub>7</sub>-derivative) and 4-ethynyl-6-methyl-*N*-phenylpyrimidin-2-amine (anilinopyrimidine<sub>8</sub>-derivative) to yield functionalized polymers with immobilized anilinopyrimidine-derivatives (anilinopyrimidine-derivatives polymer (P(S<sub>AP</sub>-*alt*-MANh)).
7. To evaluate the inhibition effect of the SMI-qC<sub>12</sub> polymer nanofibers with the incorporated salt on *B. cinerea*. Germination inhibition is done to determine the percentage inhibition in the presence of sodium metabisulfite on the surface of the nanofibers.
8. To evaluate the inhibition effect of the synthesized anilinopyrimidine<sub>7</sub>-derivative and anilinopyrimidine<sub>8</sub>-derivative against *B. cinerea*. In this case, the inhibition of mycelium growth is determined to evaluate the effect of the fungicide.

9. To evaluate the inhibition effect of the immobilized anilinopyrimidine-derivative polymer on *B. cinerea* mycelium growth.

### 1.3 Layout of thesis

This thesis consists of six chapters. A short description of each chapter follows:

**Chapter 1:** A brief introduction describes the scope of this study, it also give the objectives of this study.

**Chapter 2:** In this chapter, a literature survey on the relevant studies on deterioration of fruit and vegetables including grapes is given here. It describes the limitation and the problems associated with these preservation techniques specifically those used in preventing *B. cinerea* growth. It highlights the important factors, which have to be taken into consideration in developing new polymer platforms for the control of *B. cinerea*.

**Chapter 3:** This chapter describes the methods used to synthesize and characterize functionalized polymer nanofibers and the incorporation of sodium metabisulfite salt. It also gives a brief description on the electrospinning procedure of this functionalized polymer.

**Chapter 4:** This chapter describes the synthesis and characterization of *N*-(4-ethynyl-6-methylpyrimidin-2-yl)-*N*-phenylformamide (anilinopyrimidine<sub>7</sub>-derivative) and 4-ethynyl-6-methyl-*N*-phenylpyrimidin-2-amine (anilinopyrimidine<sub>8</sub>-derivative) and the covalent attachment onto poly(4-vinylbenzyl azide-*alt*-maleic anhydride) copolymer (P(S<sub>N</sub>-*alt*-MANh)) before electrospinning.

This chapter also describes the electrospinning of poly(4-vinylbenzyl chloride-*alt*-maleic anhydride) copolymer (P(S<sub>Cl</sub>-*alt*-MANh)) and surface modifying the polymer nanofibers post-electrospinning to yield poly(4-vinylbenzyl azide-*alt*-maleic anhydride) (P(S<sub>N</sub>-*alt*-MANh)) polymer nanofibers and further functionalizing the P(S<sub>N</sub>-*alt*-MANh) polymer nanofibers via immobilization the anilinopyrimidine<sub>7</sub>-derivative and anilinopyrimidine<sub>8</sub>-derivative on the surface of the polymer nanofibers.



**Chapter 5:** This chapter shows the anti-fungal studies of the two approaches mentioned above.

**Chapter 6:** Conclusions and recommendations for future research are discussed in this chapter.

## 1.4 References

1. Mogala, M. Department: Agricultural, Forestry and Fisheries. [www.webapps.daff.gov.za/mis](http://www.webapps.daff.gov.za/mis).
2. Ntombela, S.; Moobi, M. *South African fruit trade flow*. **2013**, 8, 1-11.
3. Tonietto, J.; Carbonneau, A. *Agric. For. Meteorol.* **2004**, 1, 81-97.
4. Geier, B. *The World of Organic Agriculture*. **2006**, 9, 62-65.
5. Mustonen, H.M. *Aust. J. Exp. Agr.* **1992**, 32 (3), 389-393.
6. Zhu, P.; Xu, L.; Zhang, C.; Toyoda, H.; Gan, S. *Postharvest Biol. Technol.* **2012**, 69, 23-29.
7. Qin, G.; Zong, Y.; Chen, Q.; Hua, D.; Tian, S. *Int. J. Food Microbiol.* **2010**, 1, 145-150.
8. de Kock, P.J; Holtz, S. *Afr. J. Enol. Vitic.* **1994**, 23, 33-40.
9. Vermeulen, T.; Schoonbeek, H.; De Waard, M. A. *Pest Manag. Sci.* **2001**, 5, 393-402.
10. Veloukas, T.; Karaoglanidis, G. S. *Pest Manag. Sci.* **2012**, 6, 858-864.
11. Zutahy, Y.; Lichter, A.; Kaplunov, T.; Lurie, S. *Postharvest Biol. Technol.* **2008**, 50, 12-17.
- 12.. Nelson, K. E; Gentry, J. P. *J. Enol. Vitic.* **1964** , 4, 290-301.
13. Palou, L.; Crisosto, C. H.; Garner, D.; Basinal, L. M.; Smilanick, J. L.; Zoffoli, J. P. *Am. J. Enol. Vitic.* **2002**, 2, 110-115.
14. Gabler, F. M.; Mercier, J.; Jiménez, J. I.; Smilanick, J. L. *Postharvest Biol. Technol.* **2010**, 2, 78-84.

15. Del Nobile, M.A.; Sinigaglia, M.; Conte, A.; Speranza, B.; Scrocco, C.; Brescia, I.; Bevilacqua, A.; Laverse, J.; La Notte, E.; Antonacci, D. *Postharvest Biol. Technol.* **2008**, *47*, 389–396.
16. Serey, R. A.; Torres, R.; Latorre, B. A. *Ciencia e investigación agraria.* **2007**, *3*, 215-224.
17. Couderchet, M. *Vitis.* **2003**, *4*, 165-171.
18. Nagata, T.; Masuda, K.; Maeno, S.; Miura, I. *Pest Manag. Sci.* **2004**, *4*, 399-407.
19. Myresiotis, C.K.; Karaoglanidis, G.S; Tzavella-Klonari, K. *Plant Dis.* **2007**, *94*, 407- 413.
20. Yourman, L.; Jeffers, S. *Plant Dis.* **1999**, *6*, 569-575.

## CHAPTER II: HISTORICAL AND THEORETICAL BACKGROUND

### 2.1 Introduction

Fruit and vegetables are lost annually due to microorganisms causing spoilage. The spoilage of fruit and vegetables to the extent that it is not edible are estimated to be as high as 40% of all fresh produce produced for human consumption. This large amount of fruit and vegetables lost annually has an enormous economic impact.<sup>16,17</sup> According to a study done by the United States Department of Agriculture (USDA) - Economic Research Service in 2010, nearly 9 billion kilograms of fresh vegetables and fruits are lost per annum due to spoilage, increasing each year. The graph in Figure 2.1 illustrate the quantity of fruit and vegetables lost annually.<sup>18</sup>

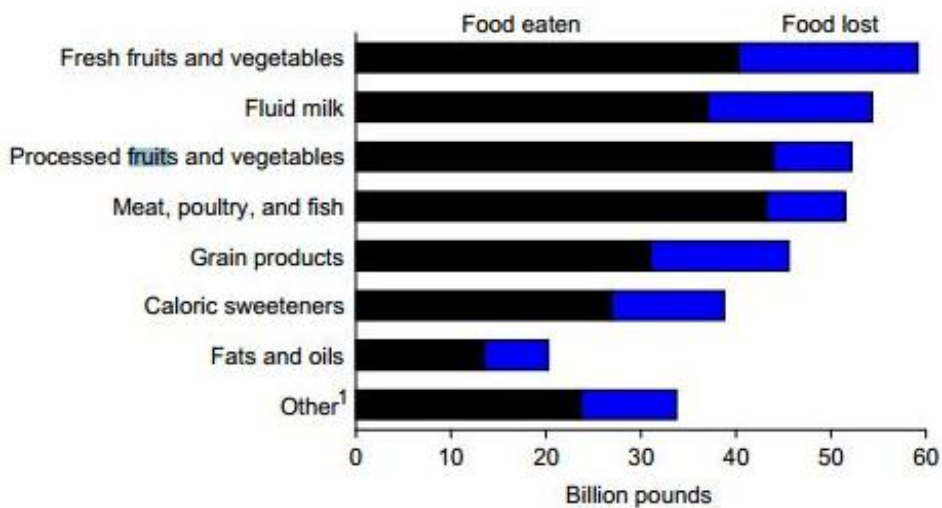


Figure 2.1 Data indicating the quantity of food eaten compared to the quantity of food lost for different food types.<sup>18</sup>

Increasing the shelf life of fresh produce is therefore of great significance as the annual consumption of fresh fruit and vegetables increases rapidly around the world. The disadvantage of increasing the shelf life of any produce is that outbreaks of foodborne illnesses increases as the demand for fresh produce increases. These outbreaks vary in size affecting only one person to thousands of people. Organisms involved in the deterioration of fruit and vegetables include bacteria, viruses and parasites.

The deterioration of fruit and vegetables can occur at any time along the food chain and is therefore dependent on the proceeding time from harvest to consumption. During this time period the fruit and vegetables are subjected to physiological ageing, biochemical changes and microbial spoilage.<sup>19</sup>

Agricultural, operational and preparation procedures are responsible for most of the contamination of produce. Spoilage occurs mainly due to the use of unsafe water for rinsing and sprinkling to keep produce fresh, and due to ice, soil, birds and insects, as well as handling of the product and physical damage (bruising, freezing, packaging, etc.), inborn enzyme activity in the plant tissue from within the cells, chemical changes (involving oxygen), harvesting, processing equipment and during transportation. During harvesting and processing of the fruit and vegetables damage to the surface can be obtained causing changes in the rate of respiration of the cells, the quantity of ethylene given off, water movement through the produce and enzymatic activity in living tissues. These changes have an effect on the texture (the loss of crispness or juiciness), colour (discolouration), flavour (off-flavours) and nutritional values (loss of water and minerals) of the produce.

## ***2.2 Microorganisms responsible for food spoilage***

### **2.2.1 Introduction to microorganisms**

At any given time from harvest to consumption, all food products contain possible specific and characteristic micro-flora. A variety of microorganisms and microbial activity are the cause of food spoilage. At the point of spoilage, the microbial flora consists of microorganisms that colonize and dominate a product. The spoilage activity of an organism is the organism's ability to produce spoilage metabolites. The higher the spoilage activity of microorganisms, the more metabolites will be produced. Understanding how major preservation parameters affect microbial growth, a prediction can be made regarding the microorganisms responsible for dominating and deteriorating that produce. Understanding the microbial ecology, the raw material and processing techniques, patterns appear in which microorganisms are connected to

the food they spoil as a function of the temperature, the origin of the product, the base of the substrate, pH, water activity and atmosphere.

Collaborative behaviour between different microorganisms determines the selection and/or the metabolism of the microorganisms and as a result spoilage follows. This collaborative interaction of microorganisms is important in microbial food spoilage and includes microbes that suppress any activity of plant pathogens and microbes that are dependent on the plant.

Most microorganisms found on the surface of whole fruit and vegetables are soil populations. Soil populations make up a diverse and wide community of microbes that are mutually accountable for maintaining a dynamic ecological balance within most agricultural systems. These microbes are transferred through the air via spores, soil particles and irrigation water. Fruit and vegetables that are in the developing stages can be infected by bacteria and fungi. These microorganisms can be completely nonthreatening to the produce's health or, in many cases, provide a natural biological barrier towards microorganisms causing crop damage. Other ways by which microorganisms can be introduced to fruit and vegetables are through the seed itself, harvesting of the produce, during postharvest handling, or during storage and transportation.

In most cases not only one microorganism can be held responsible for the spoilage of a certain product. Due to the possibility of having multiple microorganisms able to spoil one commodity of produce, it is very difficult to make a distinction between the microbial composition and the presence of microbial metabolites as both play a role in microbial spoilage. Metabolites are formed during biochemical spoilage. The quantity of metabolites formed is generally very low and difficult to detect, having an effect on the understanding of the biochemical process taking place during spoilage. The biochemical processes are poorly understood and little is known about the interaction of microbial and chemical spoilage of fruit and vegetables.

### 2.2.2 Microorganisms responsible for spoilage

A wide variety of microorganisms can be found on fruit and vegetables, namely Gram-negative bacteria, Gram-positive bacteria and fungi, including yeast and moulds. Although uncommon, some viruses have also been identified as plant pathogens. Parasites can also be a concern

regarding food borne illness but do not spoil or affect the sensory qualities of fruit and vegetables.

### 2.2.2.1 Bacteria

When food is contaminated by bacteria, the bacteria enter the lag phase. In the lag phase the growth rate is slow. After the lag phase, the log phase is entered, which means that growth is initiated, the bacteria adjust to the surroundings, and the bacteria population grows in a logarithmic fashion. As the bacteria feed on nutrients, a stationary phase is entered. In this phase the growth rate is equal to the rate of death, and the viable number of bacteria cells remains the same. After a time period, the nutrients will be depleted and the bacteria's rate of death will exceed the rate of growth as no nutrition is available to support the metabolism. This phase is called the decline phase. If the homeostasis of microorganisms (the internal equilibrium) is disturbed, they won't be able to multiply (they will remain in the lag-phase after which death will follow). Different species will react differently to certain conditions. Even in specific species, the strains can act differently under the same conditions. When conditions for cell growth are unfavourable, the bacteria produces cells called endospores. These endospores are metabolically inactive and are formed in a process called sporulation. Endospores are called such because the spore forms within the cell. Endospores become dormant, can outlast unfavourable conditions for long periods and are resistant to harsh environments. If the conditions should change to more favourable conditions, stimuli will activate the endospores to germinate. Germination is the irreversible conversion of endospores to metabolically active cells. Rapid and complete germination only occur after activation and is triggered by specific germination-inducing agents. These viable cells can initiate exponential growth, in which the number of cells doubles each time in a fixed period of time.

Bacteria can be divided into Gram-positive and Gram-negative bacteria. A method was formulated by Hans Christian Gram to be able to distinguish between these two different types of bacteria based on the structural differences in the cell walls. The test uses crystal violet dye to differentiate between two types of bacteria. Bacteria that retain the dye do so because of the thick layer of peptidoglycan and are referred to as Gram-positive bacteria. Gram-negative bacteria will stain red/pink because the bacteria's cell wall can't retain the crystal violet dye due to their thin peptidoglycan layer.

#### a) Gram-positive bacteria

The internal structure of Gram-positive and Gram-negative bacteria is similar, but they have very different external structures. For the purpose of this study, details of the cell wall structure will not be discussed. The most abundant Gram-positive bacteria are unicellular bacteria which have very simple internal structures compared to eukaryotic cells. Gram-positive bacteria have rigid cell walls because they are protected by a thick peptidoglycan layer. Many Gram-positive bacteria have one or even more plasmids with antibiotic resistance genes on them. If a Gram-positive microbial transformation takes place it results in deterioration of the food and food poisoning can occur.

#### b) Gram-negative bacteria

Gram-negative bacteria require a rigid cell wall to support and protect them because these bacteria only have thin peptidoglycan layers. Gram-negative bacteria have thinner peptidoglycan layers, but consist of a more complex and relatively impermeable cell wall. If a Gram-negative microbial transformation takes place it results in deterioration of the food and food poisoning can occur. Some of the pathogens include *Bacillus*, *Staphylococcus* and *Clostridium*.

The most common Gram-negative bacteria (*Bacillus*) are rod-shaped bacteria which are responsible for the spoilage of fresh, chilled produce under refrigerated and modified atmosphere packaging (MAP) conditions. Although minimal growth is observed at temperatures of 0 - 3 °C, they grow rapidly at temperatures above 5 - 10 °C.

#### 2.2.2.2 Fungi

Fungi are single-celled or multicellular organisms. Yeasts are single-celled fungi that reproduce primarily asexually and undergo anaerobic fermentation. Moulds reproduce both sexually and asexually (with hyphae, branched filaments) and are mostly aerobic respirators. Moulds are multicellular fungi that reproduce by the formation of spores. Spores are formed in large numbers and are easily dispersed through the air. If these spores land on a substrate they will grow and reproduce, if conditions are favourable.



Yeast species of the genera *Saccharomyces*, *Candida*, *Torulopsis*, and *Hansenula* have been associated with the fermentation of fruit. In addition to those responsible for fermentation, yeast is responsible for quality loss and includes *Rhodotorula mucilaginosa*, *Rhodotorula glutinis*, *Zygosaccharomyces bailii*, *Zygosaccharomyces bisporus*, and *Zygosaccharomyces rouxii*. Although these species have been isolated from fresh fruit and vegetables individually, the specific species that are responsible for the spoilage are rarely identified. Yeasts are commonly known for the off-flavours and off-odours they create and have a slightly higher growth rate than moulds. Moulds are commonly present in postharvest diseases regarding fruit and vegetables. Spoilage of fresh produce due to moulds, especially fresh fruit, is mostly caused by the genera: *Penicillium*, *Phytophthora*, *Alternaria*, *Botrytis*, *Fusarium*, *Cladosporium*, *Phoma*, *Trichoderma*, *Aspergillus*, *Alternaria*, *Rhizopus*, *Aureobasidium*, and *Colletotrichum*. Similar to yeast, mould populations have been reported in a wide variety of fresh-cut fruit and vegetables. Moulds are mostly observed as visible spoilage and the deterioration due to moulds result in inedible fresh-cut fruits. Moulds not only produce observable spoilage, but can spoil food through the formation of mycotoxins. Mycotoxins are secondary metabolites that are toxic and are produced by fungi to initiate the pathogenic process.

In general, the changes due to spoilage from these microorganisms are of a sensory nature, including visible growth, rots and discolorations (blue mould rot, grey mould rot, botrytis rot and brown rot) or pigmented growth on the surface, production of slime, fermentation of sugars to produce acids, gas or alcohols or the development of off-odours and off-flavours.

*Penicillium expansum* and *Botrytis cinerea* are two wound pathogens, and if they are not thoroughly cleaned from the surface or if the produce that is infected has not been removed from the bunch, they can cause significant crop loss (Refer to Figure 2.2 for an illustration of the spoilage). At the wounds where the spoilage is initiated, the cells will be degraded causing lesions and the pathogens will cross-contaminate the adjacent fruit and vegetables.

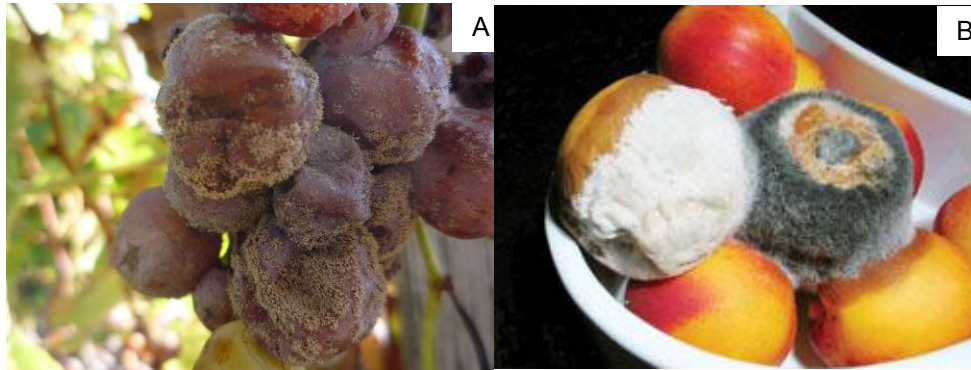


Figure 2.2 Illustration of *B. cinerea* grape bunch rot (A) and *P. expansum* fruit rot (B).

The factors affecting the growth of fungi are similar to those affecting bacteria. The optimum pH for the growth of most microorganisms is near neutrality (pH 7.0), but fungi (yeast and moulds) are mostly acid tolerant and are therefore associated with the spoilage of more acidic foods.<sup>20</sup> Moulds can grow in a wide pH range of 2 - 11, but favours more acidic regions and yeast grows in a pH range of 3 - 10.<sup>21</sup> In terms of water requirements for growth, yeast is intermediate between bacteria and moulds. Yeast and moulds are also relatively tolerant to low water activity, low temperature and the presence of preservatives. In previous research, it was explained that yeast and moulds can use a large variety of substrates to survive (as food) and are therefore found in a wide variety of environments.<sup>21,22</sup>

### **2.3 Mechanisms of spoilage**

It is necessary to understand the mechanisms of food spoilage to be able to minimize food spoilage and predict the quality of the produce. Different food commodities house different specific spoiling organisms (SSOs). One needs to identify and control the growth of these SSOs. Not many SSOs have been identified, thus making the prediction of the quality of the food product difficult and dependable on the quantification of the total number of microorganisms. Not only does one need to identify the SSOs, but one also has to understand the complexity of the interaction between these SSOs and any other microorganisms or their metabolites (synergism/antagonism). Although it is difficult to differentiate between microbial and biochemical spoilage, the interaction between the two mechanisms needs to be clarified.

Microorganisms possess a series of survival mechanisms as they can adapt rapidly to environmental change, colonize and grow on a wide variety of substrates. Microorganisms can also outlive stressed environments. If the optimum temperature, pH and water activity is unavailable they will adapt to survive. Microorganisms have an adaptive response to any osmotic stress. The external stimuli stimulate cell processes to be able to adapt to unfavorable conditions. These mechanisms have to be understood before controlling and predicting the growth of spoilage microorganisms are attempted. The reaction of microorganisms to external stresses also needs to be understood, in order to find ways that will enable interference with these diverse mechanisms through which microbes develop resistance against physical and chemical treatments.

One of the most important characteristics of fresh fruit and vegetable products are that their metabolic processes continue although they have been harvested. The metabolic process keeps the respiration activities going and supplies the plant cells with sufficient energy to stay alive and continue with the physiological and biochemical processes. The maturity stage and type of produce and also the storage conditions after harvesting affects the respiration rate of the produce. Wounding of a commodity promotes the release of ethylene that initiates enzyme-catalyzed processes in the cells, and this converts substrates into more complex products. This process is called biosynthesis, and stimulates respiration, which results in an increase in the respiration rate.

Spoilage microorganisms enter plant tissues during fruit development, either through the calyx (flower end) or along the stem, or through various specialized water and gas exchange structures of leafy matter. To be successfully established the microbes need to overcome multiple natural protective barriers, as fruit and vegetables possess an epidermis and epiphytic microorganisms on the outermost surface, which form a further barrier to these spoiling organisms. How the microorganisms overcome these barriers is complicated and won't be discussed for the purpose of this study. Spoilage microorganisms exploit the host, growing and releasing extracellular lytic enzymes into the surrounding liquid of the host. These enzymes can degrade any polymers within the host and will release water and the host's other intracellular liquids and nutrients for the growth of the microorganisms itself. Fungi in particular produce an excess of extracellular hemi-cellulases and pectinases, which are enzymes that hydrolyze polysaccharides. These enzymes are of utmost importance for fungal spoilage to occur.

External damage, e.g. bruising, cracks and punctures, are possible sites for the colonization and outgrowth of spoilage microbes. Two wound pathogens that occur frequently are *P. expansum* and *B. cinerea*. These microorganisms are able to reproduce rapidly within the open wound only days after the damage occurred. If the wound is infected and not carefully cleaned before storage or the infected fruit is not taken out of the lot, significant crop loss can be seen as the pathogens eventually degrade the wound site, creating lesion and cross-contaminate adjacent fruit.



Figure 2.3 Illustration of grape bunches with bruising, cracks and punctures.

Veld and co-workers have stated in a study in 1996 that SSOs are initially present in low quantities and natural micro-flora is a negligible part of these SSOs.<sup>21</sup> In storage, the SSOs generally reproduce faster than the natural micro-flora present and produce metabolites responsible for off-odours/flavours and slime, finally causing sensory spoilage. Changing the extrinsic conditions, for instance the storage temperature, is a method to delay spoilage. Storage at acceptable low temperatures will delay spoilage as the bacteria will still be able to grow, but the deterioration will be limited mostly to psychotropic microorganisms (some yeast and mould). Although yeasts and moulds cannot outlive bacteria at low temperatures, bacteria grow under certain conditions such as acid foods (low pH), foods with high sugar or salt concentrations, where the yeasts and moulds become dominant.

## **2.4 Spoilage of fruit and vegetables**

### 2.4.1 Introduction to spoilage of fruit and vegetables

Food spoilage is a very complex process and is caused by a wide range of reactions, which are mainly physical or chemical in nature, including the actions of enzymes or microorganisms. Although the raw materials and process conditions are heterogenic, the micro-flora that spoils food can be predicted by investigating the source of the produce, the base substrate and basic preservation parameters including storage and transport temperature, atmospheric volume around the produce, pH and the water activity. The microorganisms responsible for the spoilage of fruit are mainly yeast and moulds as the pH of fruit is too low to support bacterial growth. Detailed analysis including microbiological, chemical and sensory analysis can be done on individual products to determine the specific spoilage organisms responsible for the spoilage. Bacteria and yeast spoilage are less visible than the microbial spoilage due to moulds. Moulds manifest themselves as visible growth in the form of large pigmented colonies.

The microorganisms produce gas that results in a decrease in pH and the formation of slime becomes visible. Enzymes diffuse through the cells causing softening and rotting. Off-odours and –flavours are the end result.

The quality loss of the fresh produce is generally defined by an irreversible, permanent loss of quality, as these kinds of products will never be able to increase in quality during storage. However, the quality can be retained or the deterioration can be delayed. Quality changes are classified in two different categories. One category includes off-odours, toxic by-products, pH-changes within the produce and gas-and slime-formation. The other category is the oxidation of phospholipids and pigments in fat-containing foods resulting in off-odours, compounds with adverse biological effects or discolouration. Little is known how these two categories interact with each other under different packaging and storage conditions.

## 2.4.2 Factors and processing operations that affect quality of minimally fresh processed plant foods

There are many factors affecting the shelf-life and microbial quality of fresh fruit and vegetables. The initial microbial flora on the commodities plays an important role in the spoilage. Intrinsic food properties, including endogenous enzymes, the substrate, sensitivity towards light and oxygen, pH of the cell's liquids, the water activity, nutritional contents of the produce, antimicrobial constituents, and the oxidation-reduction potential and biological structures are primary factors influencing spoilage. Other factors include agricultural techniques, hygiene during harvesting, handling and processing (heating and acidification), the water quality, packaging systems, storage conditions and distribution.

Of all the agricultural techniques, storage conditions and temperature are the most important environmental factors that influence the deterioration rate of harvested produce. During storage, microorganisms can infest, multiply and initiate deterioration. It is therefore crucial that the temperature needs to be carefully controlled. To determine the influence of the cold chain on the products, the time-temperature conditions need to be known. During storage and processing the products are also subjected to mechanical damage including washing, peeling, cutting, disinfection and dewatering.

These damages cause wounds on the surface of the fruit and vegetables. The wound's ethylene ( $C_2H_4$ ) production will increase due to the mechanical damage that initiates enzyme-catalyzed processes in the cells that stimulates respiration, resulting in an increase in the respiration rate. This leads to various biochemical deterioration processes such as browning, an increase in moisture content and cell leakage including loss of nutrients, which can be the substrate for microbial growth.<sup>17,23,24</sup>

## **2.5 Grape spoilage**

### **2.5.1 Introduction to grape spoilage**

Table grapes are a member of the genus *Vitis* and the family *Vinifera*. Grapes are a non-climactic fruit and consist of a berry, which is more or less spherical with pulp and seeds inside. Various quantities of minerals (calcium and phosphorous) and sugars (glucose and fructose) are in grapes. In many countries grapes are a big component in the fruit diet and they are consumed raw with minimal washing. Grapes in the vineyard already stand a chance to become infected from the inoculum present in the field, which can develop into latent infections. These infections have the possibility to develop into visible spoilage at a later stage during storage or transport.<sup>25</sup>

The quality-loss characteristics of grapes that affect the shelf-life are physiological disorders including weight loss (berry and stem), stem (rachis) dehydration and browning, sulphur dioxide (SO<sub>2</sub>) injury, decay and lack of berry firmness.<sup>26</sup> Although grapes are a non-climactic fruit, firmness weakens and softening occurs as well as colour change accelerates during postharvest storage and contributes to quality loss and a reduction of the shelf-life.<sup>27</sup> Texture and colour are important parameters to consumers that need to be intact.

### **2.5.2 Microorganisms responsible for spoilage of grapes**

The spoilage of grapes is defined by the weight loss of berries, colour change, softening that occurs, browning of the rachis and high incident berry deterioration. All these properties lead to an overall loss of quality and high occurrence of decay is observed when storage is prolonged.<sup>27</sup> Microorganisms found on grapes are very diverse. They can be divided into 3 groups: 1) Species without fermentation ability, 2) species with some fermentation ability and 3) species that are the main fermentation agents.

During the ripening stages of grapes, the ratios in which these groups are present differ. Group 1 is dominant during the onset of ripening whereas at harvesting the species of group 2 are dominant.<sup>28</sup> During storage, rapid quality loss occurs and the fruit are susceptible to fungal colonization and decay, especially *B. cinerea*.<sup>1</sup> In addition to *B. cinerea* being the most destructive fungus, other filamentous fungi that are commonly present in vineyards include Spp. *Pseudomonas*, *Aspergillus niger*, *Cladosporium herbarum*, *Penicillium expansum*, and *Rhizopus stolonifer*.<sup>25</sup> Species that contribute to the annual spoilage of grapes will be discussed in the subsequent sub-sections.

#### 2.5.2.1 *Penicillium*

Penicillin (PCN) refers to a group of  $\beta$ -lactam antibiotics obtained from fungi of the genus *Penicillium*. *Penicillium* can be used to treat bacterial infection (Gram-positive organisms) but can also spoil food. Storage decay in table grapes is caused by the plant pathogen *Penicillium expansum*. *Penicillium* species are filamentous fungi that are widely distributed in nature.<sup>29</sup> This fungus has been frequently isolated from healthy clusters of grapes and some strains of *Penicillium* produce patulin. Patulin is a thermal-resistant, mutagenic, immunologic, and neurotoxic mycotoxin known to contaminate grapes.<sup>30</sup>

#### 2.5.2.2 *Pseudomonas*

*Pseudomonas* spp. (e.g. *Pseudomonas marginalis*) is the most commonly found and important spoilage microorganism of food containing high water levels, pH of 7 and that are stored aerobically.<sup>17,21</sup> *Pseudomonas* spp. is a Gram-negative rod-shaped and severe aerobic organism.<sup>17</sup> These species are widely dispersed in the environment and are found on animals and plants. They can contaminate from many sources but often proliferate on inadequately cleaned surfaces and grow from a wide variety of substrates. *Pseudomonas* are heat sensitive although found in heat-processed food and are not very sensitive to drying or gamma radiation.<sup>17</sup> They are however still able to multiply rapidly at low temperatures and dominate the micro-flora of foods stored at low temperature.<sup>31</sup> They grow mostly aerobically, but can grow anaerobically in nitrate-containing substrates. The colonies are usually yellow-green but have been reported to appear blue or orange, depending on the environment and the specific species playing a role.<sup>17</sup>



### 2.5.2.3 *Botrytis cinerea*

*Botrytis cinerea* is an unselective and sophisticated plant pathogen that is able to degrade plants rich in pectin and is the focus of this study. *Botrytis cinerea* is seen as a massive economy-influencing plant pathogen that is destructive, neurotropic and a high risk to farmers and consumers. It causes grey mould in over 200 horticultural crops such as grapes, asparagus, bean, beet, carrot, celery, chicory, crucifers, cucurbits, eggplant, endive, lettuce, onion, pepper, potato, raspberry, rhubarb, rutabaga, shallot, strawberry, tomato, turnip, and many others.<sup>7</sup> Grey mould is caused in both pre- and postharvest periods.<sup>32</sup> *Botrytis cinerea* is such a destructive fungus because of its ubiquitous occurrence, broad host spectrum and genetic heterogeneity that makes it possible to have wide natural variability and readily develop resistance to fungicides.<sup>33</sup> *Botrytis cinerea* is considered the most destroying disease of the grape commodity and uncontrolled infections can lead to airborne mycelium spreading rapidly to adjacent berries with severe economic repercussions.<sup>27,34</sup>

Spreading of *B. cinerea* during storage mostly originates from the flower part that was initially infected during flowering. The pathogen enters the plant and persevere unnoticed as an endophyte (without causing any apparent disease) and emerges later to cause postharvest grey mould.<sup>35</sup> The infected fruit can be packed and stored with the hidden contamination of the pathogen on the fruit.<sup>7</sup> The contamination can lead to an outbreak of grey mould or bunch rot when the grapes are in storage and conditions become favourable.<sup>7</sup> It is not known what initiates the latent infections to become viable and cause the berries to rot. The berries that are infected and old flower parts are the biggest source that causes the other berries in the bunch to rot. The presence of resistant strains of *B. cinerea* complicates the efficacy to try and delay the spoilage.<sup>36</sup>

For the purpose of the study we are focused on the most destructive fungi spoiling grapes named *B. cinerea*.

## ***2.6 Prevention and control measures of microorganisms in postharvest foods***

### **2.6.1 Introduction to preventions and control measures**

Two critical factors contributing to the shelf-life and deterioration of fruit and vegetables are the products' integrity at the time of harvest and postharvest storage temperature management from harvest to consumption.<sup>17,27</sup> Directly after harvesting, the most important step is sanitizing and/or washing of the produce. Chemicals used for the prevention and control of spoilage can be divided into gas-phase methods and liquid-phase methods. The most widely used chemical treatment is the use of chlorinated water.

Effective sanitizing agents remove excess soil and microorganisms from the surface of the produce. Some other sanitizing agents include sodium hypochlorite, calcium hypochlorite or an antimicrobial solution.<sup>37,38</sup> Alternatively to the liquid-phase chemicals used are the gas-phase sanitation methods. Allende and co-workers have discussed the use of chlorine ( $\text{Cl}_2$ ) and ozone.<sup>24</sup> The use of gas-phase methods have the drawback that a special in-line closed system is needed for the treatment and can also be harmful for the applicator (human).<sup>17,39</sup>

The products are subsequently cooled to slow down the metabolism and growth of spoilage microbes.<sup>17</sup> If the metabolism of microorganisms is reduced, the respiration rate decreases and in turn decreases the rate of deterioration.<sup>17</sup> Although washing and sanitizing is very important, some pathogens have been reported to survive and manifest itself on the produce.<sup>16</sup>

To prevent microorganisms from becoming resistant towards these active washing methods, other methods and factors play a role in the prevention of microbial spoilage.<sup>17</sup> These methods include the quality of the raw product, packaging and temperature management, the processing techniques and manufacturing practices. When using a clean, high-quality raw material it can reduce the possibility for surface contamination and maximize the plant's self-defense system.<sup>17</sup>

Climactic fruits have shown to increase their respiration prior to ripening. The increase in respiration rate leads to a reduction of the fruits' resistance to pathogens. Processing and procedures like washing, peeling, cutting and dewatering increase the produce's susceptibility to

microbial spoilage. If the fruit is damaged during these procedures the inner cells are exposed to microbial attack and if the outer cells of the fruit are damaged the natural epidermal barriers are removed. The removal of the external barriers results in a buildup of surface moisture, decrease of moisture content in the tissue, and cell leakage occurs that will support microbial growth.<sup>17</sup> A wounded or damaged surface possesses an increased rate of respiration, leading to cellular ageing or cell death and shows an increase in fungal colonization and browning.<sup>17</sup>

Browning can occur due to enzymatic or non-enzymatic reactions. Artes and co-workers has shown in studies conducted that enzymatic/oxidative browning consists of different components.<sup>39,40</sup> The components mainly consist of enzymes such as polyphenol oxidase (PPO) and peroxidase (POD), a substrate and co-substrates such as oxygen (O<sub>2</sub>) and hydrogen peroxide (H<sub>2</sub>O<sub>2</sub>).<sup>38</sup> The initiation of browning starts at the damaged surface area of the produce due to compartmentalization that occurs when cells are broken, where enzymes and substrates are delocalized that leads to various biochemical deterioration allowing substrates and oxidizers to come into contact.<sup>17, 23</sup> The development of a brown colour is related primarily to the oxidation of phenolic compounds including monophenols, triphenols, o- and p-diphenols and o-quinones.<sup>38,41</sup> Enzymatic browning and shrinking, being the most limiting sensory disorder of fresh-cut produce, can be retarded through low temperature storage techniques.<sup>42</sup>

Many of the conventional preservation techniques cannot be used on minimally processed fruit and vegetables. Only a few traditional techniques such as optimization of the processing techniques, the use of an optimal chilling chain, packaging conditions, application of enzymatic inhibitors, and the use of chemical and mild heat treatments (40 - 50 °C) can be used.<sup>38</sup> Microorganisms have the ability to change and adapt to outlive conventional food preservation techniques, therefore new techniques need to be developed for inhibiting microbial growth. As a result thereof, many non-conventional methods, such as fungicides, ozone, ultraviolet-C (UV-C), high-intensity pulsed light, pulsed electric fields, light magnetic fields, high hydrostatic pressure, new edible coatings and the use of safe antimicrobials are now being investigated.

## 2.6.2 Emerging technologies for maintaining quality of minimally fresh processed fruit and vegetables

Barth studied thermal and non-thermal technologies that have been developed to control microorganisms on fresh-cut produce.<sup>17</sup> The raw material quality, the processing technologies, good manufacturing practices (GMP) and storage temperature management play an intricate role in fungal control. The use of agro-chemicals for the protection of minimally fresh processed fruit and vegetables against quality losses, diseases, physiological disorders and insects, has shifted to the use of alternative techniques that are safer for humans.<sup>17,38</sup> These alternative techniques include biological control, cultural adaptations and physical methods such as irradiation, controlled atmosphere (CA) and modified atmosphere packaging (MAP), with MAP being one of the most important extrinsic factors that can prevent microbial spoilage of fruit and vegetable.<sup>17,38</sup> Following are some of the techniques with a short description of each:

### 2.6.2.1 Liquid-phase chemicals

#### a) Hydrogen peroxide

For centuries, hydrogen peroxide ( $H_2O_2$ ) has been known for its germicidal properties.  $H_2O_2$  is listed to be generally recognized as safe (GRAS) in FDA regulations (21 CFR 184.1366) when used as a bleaching agent in food and in cotton fabrics for dry food packaging.<sup>43,44</sup>  $H_2O_2$  has not yet been approved as an antimicrobial wash but is used to disinfect surfaces.<sup>38</sup> In addition to certain bactericidal effects observed in biological systems and virucidal properties,  $H_2O_2$  can be a spore killing chemical if the concentration used is high enough.<sup>45</sup> Some instances have been reported where cells protect themselves against  $H_2O_2$  toxicity either through catalases or by repairing the damage, in the case of deoxyribonucleic acid (DNA) damage, after it has taken place.<sup>46</sup>

$H_2O_2$  does not leave residues since it is rapidly decomposed to water and oxygen by enzymatic catalysis.<sup>43</sup> Various antimicrobial methods for the preservation of foods using  $H_2O_2$  have been investigated and have shown to reduce microbial populations by extending the shelf-life without causing a loss of any quality.<sup>38</sup> Artes has reported that the bactericidal effects observed in biological systems due to  $H_2O_2$  usage is due to the growth inhibition of one bacterial species by

another and killing of invading microorganisms by activated phagocytic cells.<sup>38</sup> H<sub>2</sub>O<sub>2</sub> has demonstrated to be somewhat harmful to some commodities due to bleaching of the fruit or vegetables. The cytotoxicity of H<sub>2</sub>O<sub>2</sub> is due to its oxidizing capacity, facilitated by transition metal ions, generating more reactive and cytotoxic oxygen species.<sup>38</sup>

#### b) Electrolyzed water (EOW)

Electrolyzed water is also known as electro-activated water, electrolyzed oxidizing water or electro-chemically activated water. Electrolyzed water can be obtained through the electrolysis of ordinary tap water that contains dissolved sodium chloride.<sup>47</sup> Tap water typically contains sufficient quantities of salt so that when electrolysis occurs a solution of sodium hypochlorite is obtained. The resulting solution is known as a sanitizer and has been shown to kill spores, some viruses and bacteria. The effectiveness of EOW increases as the pH decreases causing acidic electrolysed water. Acidic electrolysed water is preferred for sanitation purposes. Due to the antimicrobial and antiviral activities of acidic electrolysed water having a pH of 2.6 and an oxidation reduction potential of 1140 mV it is efficient in prolonging fruit and vegetables' shelf-life. The use of this sanitation method alone to delay spoilage is limited to some products only and mild heat treatment is needed to enhance this bactericidal effect.<sup>43,48</sup>

#### c) Organic acids

An organic acid is an organic compound with some acidic properties. Organic acids may retard and/or prevent the growth of some microorganisms. Seymour reported in 1999 that the antimicrobial activity of organic acids is due to the interference with the cells' ability to sustain a natural homeostasis (pH), disruption of the substrates transport and inhibiting metabolic pathways and not due to killing of the cells.<sup>49</sup>

The mode of action of organic acids regarding bacteria includes non-dissociated organic acids that easily penetrate the bacterial cell wall and disrupt the normal physiology of the bacteria and thus the bacteria's buffer system, and can therefore not maintain a constant pH inside of the cells. Although this technique has been used for centuries, there is a need to improve the continued effectiveness and sustainability of using only organic acids. Another drawback of using organic acids is that they are only applicable to bacteria.<sup>49</sup>

#### d) Dipping solutions

Dipping solutions contain compounds such as sulphites and ascorbic acid, which act as PPO inhibitors and antimicrobial agents that prevent browning by reducing quinones back to their parent o-diphenols. Some antioxidants,  $\text{Cl}_2$ , antimicrobial solutions and acidulate can be used for washing to avoid browning.<sup>38</sup>

#### 2.6.2.2 Gas-phase chemicals

##### a) Ozone

Ozone is a natural substance in the atmosphere.<sup>50</sup> Ozone is applied as a sanitizer and is seen as one of the more effective sanitizers against a wide spectrum of microorganisms. It is generally recognized as safe for food contact applications as no residues are left on commodities due to ozone degrading.

The mode of action of ozone involves the progressive oxidation of vital cellular components. The cell surface is the main target of ozonation that leads to the death of the microorganisms.<sup>27,38</sup> To enhance the antimicrobial efficiency of ozone, this technique is used in combination with other chemical (hydrogen peroxide) or physical (UV-C radiation) treatments for prolonged decay control.<sup>4,51</sup>

##### b) Ethylene ( $\text{C}_2\text{H}_4$ )

The production of ethylene is induced by any stresses on the produce such as chilling or wounding through damaging of the produce during harvesting or processing.<sup>17</sup> The metabolism of fruit and vegetables stored at optimum storage temperatures and  $\text{O}_2$  concentrations are reduced and the emission of  $\text{C}_2\text{H}_4$  lowered. In addition to this conventional method to reduce the emission of  $\text{C}_2\text{H}_4$ , numerous chemicals are available as  $\text{C}_2\text{H}_4$  absorbent materials to remove  $\text{C}_2\text{H}_4$  from the packaging atmosphere around the produce. Formulations of potassium permanganate ( $\text{KMnO}_4$ ) and ozone are efficient oxidizers of  $\text{C}_2\text{H}_4$ . In addition to using chemicals to remove  $\text{C}_2\text{H}_4$ , compounds can also be used to prevent the formation of  $\text{C}_2\text{H}_4$ . Carbon dioxide ( $\text{CO}_2$ ) and a number of unsaturated cyclic olefins, such as 1-methylcyclopropene (1-MCP) have been shown by Abeles and co-workers to have inhibitory effects on the production of ethylene.<sup>17</sup>

However, it was reported that 1-MCP treatment is not as effective for leafy tissues as for floral organs.

### c) Biocontrol

Controlling postharvest diseases primarily depends on the use of synthetic fungicides.<sup>5</sup> Restrictions of chemicals used in plant foods exist due to the ecological problems they can cause and because they are potentially harmful to humans.<sup>38</sup> Microbial agents have been developed to control postharvest decay, instead of using toxic chemicals. One example of a biocontrol agent is the use of the lactic acid bacteria (LAB) for the fermentative preservation of food.<sup>17</sup> LAB's mode of action is that this bacterium is able to produce a wide range of inhibitory metabolites. These metabolites include organic acids, hydrogen peroxide, low-molecular-weight metabolites and bacteriocins.<sup>52</sup> The production of metabolites acts as inhibitor of pathogenic growth. The production of these metabolites increases as the conditions become more favourable for bacterial growth. To control spoilage due to bacteria in fresh fruit and vegetables, an antimicrobial agent that produces these metabolites, combined with optimum storage temperature and good handling techniques, are needed.<sup>17</sup>

## ***2.7 Prevention and control measures of microorganisms in grapes***

### 2.7.1 Introduction to preventions and control measures

The same prevention and control used for general fruit and vegetables can be used for grapes. Microorganisms causing spoilage of grapes have an enormous influence on the quality of the grapes. They do not necessarily result in severe diseases before harvest in the field but cause a considerable loss of product during the storage and marketing stages. Therefore, this study focusses on the packaging of grapes to reduce or prevent spoilage due to microorganisms.

Table grapes are stored at 0 °C but are subjected to large quantities of water loss and decay during postharvest storage. Grey mould caused by *B. cinerea* is the main spoilage fungus that cause decay during postharvest storage. Prevention of decay during postharvest storage is

through the presence of SO<sub>2</sub> fumigation, either through weekly fumigations of the storage room, or the use of generating sheets containing sodium metabisulfite. Worldwide, these SO<sub>2</sub> generating sheets are used to fumigate table grapes for the control of grey mould caused by *B. cinerea*.

Fungicides are restricted due to the registration restrictions, maximum tolerance of the fungicides that can be used and less effective due to the development of resistant strains towards the fungicides.<sup>12</sup> Fungicides are the most commonly known method to reduce or inhibit the growth of *B. cinerea* in the field. *Botrytis cinerea* populations have shown resistance towards these fungicides and because of the resistance compromises the efficiency of the fungicides. Resistance to these well-established fungicides complicates the management of diseases caused by *B. cinerea* and can lead to serious economic losses.<sup>15</sup> It is thus of importance to establish effective treatments or control method with low toxic risk.

These methods, SO<sub>2</sub> fumigation and the use of fungicides, have limited success and to date, no literature showed the successful inhibition of *B. cinerea* during storage.<sup>1</sup>

Although SO<sub>2</sub> fumigation and the use of fungicides are the most widely used techniques, some other conventional methods are used as well. These methods include lowering the temperature during storage and the removal of water from the surface of the produce and the storage container. The industry as a whole, and specifically the grape industry, is looking for techniques to achieve and maintain fresh-like quality for longer shelf-life times and products that are safe for human consumption with a high nutritional value.<sup>17</sup>

### 2.7.2 Emerging technologies for maintaining quality of grapes

The same technologies that are used and explained in Section 2.6 are used in the grape industry but some of the new technologies in the grape industry are discussed in the following sub-sections.



### 2.7.2.1 Liquid-phase chemicals

#### a) Ethanol

Ethanol is the most commonly used microbiological and medical disinfectant. Ethanol has the potential to eliminate dangerous food-borne pathogens, and kill microorganisms responsible for spoilage of grapes.<sup>6</sup> Pinto and co-workers reported that ethanol dipping effectively kills spores of *Botrytis*, *Rhizopus stolonifer* and *Aspergillus niger*, the major postharvest pathogens of grapes.<sup>6</sup> The removal of spoilage microorganisms from grapes using ethanol is influenced by the specific species involved, as anatomical variations have been observed among different species that have an effect on the quantity of contact between the attached microorganisms and the ethanol.<sup>6</sup> Ethanol dipping results in effective inhibition of cell germination compared to SO<sub>2</sub> treatment but only for short storage times.

The advantage of using ethanol treatment is that no opposing effects have yet been observed on the appearance or the taste of grapes. If the humidity during storage is high enough, ethanol treatment does not prevent the rachis turning brown but keeps the stem green, unlike SO<sub>2</sub> that bleaches the rachis. A very low residue has been found to build up during the treatment of ethanol in the fruit and is comparable to the natural levels found in other fruit. Different cultivars of grapes, the physiological conditions of the grapes and the storage conditions will influence the quantity of residues retained.<sup>6</sup> The drawback of using ethanol is that a solution is needed, the berries need to be dipped and extra equipment is needed for the dipping process. The fruit also needs to be dried and repacked after the dipping process.

#### b) Naturally occurring oils

Naturally occurring plant oils have been documented for centuries to act as antimicrobial agents. Some natural oils include eugenol, thymol or menthol, with eugenol being the most effective of the three. These oils have shown to reduce microbial populations and are more effective against yeast and moulds than mesophilic aerobic bacteria that grow only at moderate temperatures. Modified atmosphere packaging can be combined with these natural oils to maintain table grape quality parameters and to reduce microbial spoilage.<sup>27</sup>

The drawback is that in harvested fruit and vegetables there is little evidence of the use of these compounds during postharvest storage to prevent fruit spoilage.

### c) Fungicides

Fungicides are used in the field in spray programs to protect the grapes against *B. cinerea*.<sup>1</sup> Dipping and spraying of the grapes are not possible during postharvest periods or in the store rooms due to machinery needed for the application and are thus not accepted commercially. The infield spraying of grape bunches to reduce infection has been successful, but using the fungicide during postharvest periods is not possible due to the possibility that the fungicide stays on the surface of the berries and can be indigested by humans or animals.

The industry is seeking control methods that give good control against *B. cinerea* (being the most destructive fungus in the grape industry) but that are safe for human consumption.

#### 2.7.2.2 Gas-phase chemicals

##### a) Ozone

Ozone was described under Section 2.6.2.2. Ozone is a biocide and the biocidal activity is related to ozone's high oxidation potential, reacting with organic material up to 3000 times faster than chlorine.<sup>38</sup>

Ozone fumigation can be combined with biocontrol methods through the continuous in-package fumigation using *Muscodor albus*. Ozone is a fast and effective method for initial sanitation which reduces the viable inoculum on grapes, while *M. albus* can suppress the grey mould that can develop in the plant tissue due to the infections that occurred earlier which ozone could not kill.<sup>4</sup>

A single fumigation with concentrated ozone during storage is able to reduce grey mould decay in grapes. In a study done by Palou, it was observed that the continuous fumigation of stored grapes with a low dose of ozone (0.1 - 0.3 L.L<sup>-1</sup>) for 7 weeks at 5 °C, prevented aerial mycelia growth (nesting) from *B. cinerea*.<sup>3</sup> However the number of grey mould infections observed did not decrease, even if ozone was used in combination with modified atmosphere packaging.<sup>4</sup>

One drawback of using ozone is that machinery is needed to ensure that all the microorganisms on the surface of the fruit are exposed to ozone and then removed. Kim and co-workers and Norton and co-workers have respectively reported after independent studies that ozone could

have harmful effects, especially in the case of grapes having very thin skin, which ozone can easily penetrate and leave the fruit to be oxidized.<sup>4,53</sup>

#### b) Ethylene (C<sub>2</sub>H<sub>4</sub>)

Refer to Section 2.6.2.2 for the detailed discussion of C<sub>2</sub>H<sub>4</sub> to prevent and/or delay the spoilage of fruit.

#### 2.7.2.3 Biocontrol

Biocontrol is discussed under Section 2.6.2.2 as well. This section of biocontrol as a method to control postharvest diseases is focused on grapes. Biocontrol employs naturally occurring microorganisms to help control postharvest pathogens and to increase the product quality. Microorganisms, including bacteria and filamentous fungi, have shown to protect fruit against postharvest pathogens.<sup>54</sup> Biocontrol agents must be specifically chosen for the environment in which they will be used. Due to a large number of effective biocontrol agents that have different ecological functions and different modes of action, it is possible to use two or more microorganisms in combination with each other.

Epiphytic and endophytic microorganisms' mode of action is to compete for space in the host and nutrients, introducing resistance in the host tissue and producing hydrolytic enzymes.<sup>55</sup> Epiphyte refers to a microorganism growing upon or attached to a living plant and endophytic microorganisms associate more closely within the host. These are abundant in most plant species and result in a more persistent and stronger protection.<sup>56</sup> These fungi can live in the host without causing any indications of infection and produce compounds that have antibacterial and antifungal activity thereby inducing microbial-mediated resistance.<sup>55</sup>

Biocontrol agents can be applied pre-harvest with the same equipment used for conventional chemical application. The use of biocontrol agents during postharvest storage can also reduce the use of water-based treatments that can have an influence on the appearance of fruit such as strawberries and table grapes.<sup>55</sup>

Bio-fumigators are included in biocontrol techniques. Volatile-producing fungus *M. albus* can act as a bio-fumigator. *Muscodor albus* also have a continuous long-term release of activated volatiles that is able to protect grapes during storage and transport.<sup>4</sup> The volatiles produced by *M. albus* are fungicidal to most postharvest pathogens and can control decay taking place during

storage in a number of commodities (grapes included). A developed bio-fumigation formulation containing *M. albus* consists of dried rye grain, which is populated by the fungus that needs to be activated for postharvest usage through rehydration.<sup>4</sup> The fumigation formulation is applied in a passive form into a pad/sachet system, whereby upon hydration, the *M. albus* is activated and the boxes containing fruit are fumigated.<sup>4</sup> *Muscodor albus* produces a “musky” odour that declines rapidly within the packages after the sachets have been hydrated.

The storage temperature plays an important role in the level of bio-fumigation activity. The disadvantage of using *M. albus* is that the fungus is alive and keeps producing life dependent nutrients. The efficacy of this method is dependent on the substrate (the rye grain) on which it grows. *Muscodor albus* needs to be rehydrated, after which it requires at least two hours at ambient temperatures to reactivate for the use at cold temperatures.<sup>4</sup> Another disadvantage of *M. albus* is that it doesn't provide fast postharvest fumigation, in contrast to sulphur dioxide and ozone which are much more efficient in a shorter time period.<sup>4</sup>

#### 2.7.2.4 Equilibrium modified atmosphere (EMA) packaging

This is a mild preservation technique that uses oxygen (O<sub>2</sub>) at 1 - 5 kPa in combination with CO<sub>2</sub> at 3 - 10 kPa and entails that the products' respiration rates are lowered which reduces the overall metabolic process. This results in better preservation of the physiological state of the commodities and subsequently inhibits the growth of spoilage microorganisms.<sup>42</sup> Reducing the storage temperature decrease the growth rate of mesophilic micro-flora significantly and favours psychotropic microorganisms.<sup>39</sup> The storage temperature is thus an important factor because insufficient CO<sub>2</sub> is available in the storage room to alone slow down or stop the microbial activity. The storage temperature determines the microorganisms' metabolisms, subsequently influencing the respiration rates of the produce. Due to the packaging film being permeable for O<sub>2</sub>, CO<sub>2</sub> and water vapour and the change in respiration changes occurs within the atmospheres of the EMA-packages.<sup>42</sup> New developments within the packaging systems include the use of micro-perforated films and interline packaging.<sup>17</sup>

#### 2.7.2.5 Modified atmosphere packaging (MAP)

In the last decade, a number of new MAP systems have been developed, which are aimed at preventing microbial growth through the active introduction of antimicrobial agents in the

packaging. Polymer-based materials which are selectively permeable to gases such as CO<sub>2</sub>, O<sub>2</sub>, as well as UV and moisture, led to the development of MAP. Packaging systems with MAP technology are able to generate an atmosphere around the produce that enables the shelf-life to be extended, uphold sensory qualities of the fresh processed fruit and vegetables and improve the safety of the produce to users.<sup>17</sup>

MAP is an effective method to retard the softening process in grapes. Storage under modified atmosphere packaging (high CO<sub>2</sub> atmosphere) was able to maintain berry quality and reduce the decay, although some injuries (rachis browning and off-flavours) occurred. Packages need to be stored at 1 °C.<sup>27</sup> Conventional MAP has moderate-to-low O<sub>2</sub> and high CO<sub>2</sub> levels. MAP is focused on creating an atmosphere around the produce that will decrease the rate of respiration and therefore the rate of deterioration in such a way that the minimal O<sub>2</sub> or maximum CO<sub>2</sub> concentrations tolerated by the fruit are not exceeded.<sup>17</sup> By not exceeding these concentrations, the shift towards fermentation or other metabolic and/or biochemical disorders is avoided.<sup>39,42</sup> If the metabolic processes and ethylene biosynthesis are not inhibited, weight loss, softening, chilling injuries and deterioration will be observed.<sup>17</sup>

All living organisms need a minimum amount of oxygen. If the O<sub>2</sub> concentrations in the MAP packaging are too low and insufficient, it will lead to anaerobic conditions. Anaerobic conditions will lead not only to the production of mal-odorous compounds but also to the growth of anaerobic pathogens.<sup>34</sup>

Passive MAP consists of a carefully selected film with sufficient gas permeability to obtain the optimal O<sub>2</sub> and CO<sub>2</sub> atmosphere within the packaging.<sup>34</sup> Passive modified atmosphere packaging has the restriction that the appropriate films needed are not able to provide gas fluxes, be selective, and be temperature compensating to function effectively.<sup>34</sup> Passive MAP has the limitation that the system needs to regulate atmospheres that were passively established, therefore active modified atmosphere packaging is preferred. Active MAP consists essentially of flushing a gas such as O<sub>2</sub>, CO<sub>2</sub> and ethylene into the packaging to establish equilibrium conditions within the packaging system more quickly.

A modification of conventional MAP is the super atmospheric O<sub>2</sub> conditions within the packaging (higher than 70 kPa). Super atmospheric O<sub>2</sub> levels affect the metabolism, respiration rate, colour and texture of the produce as well as reduce the microbial growth and decay.<sup>39</sup> Using high oxygen concentrations overcome the conventional anaerobic atmosphere packaging system.

High oxygen concentrations have shown to be effective in reducing microbial growth, prevent anaerobic fermentation, and also inhibit discolouration due to enzymatic activity.<sup>17</sup>

Oxygen itself has a low reactivity. Reactive O<sub>2</sub> is formed from an excited state (singlet O<sub>2</sub>) or a semi-reduced radical. During a microorganisms' aerobic cellular metabolism, reactive oxygen species (ROS) are formed and these include O<sub>2</sub>, hydroxyl radicals, hydrogen peroxide and a singlet O<sub>2</sub>. These reactive species induce DNA and nucleoprotein damage as well as lipid and protein damage in microorganisms.

Combining super atmospheric oxygen with increasing CO<sub>2</sub> concentration inhibits enzymatic discolorations and retards microbial growth in fresh-cut fruit and vegetables and prevents anaerobic fermentation reactions to occur.<sup>38</sup> CO<sub>2</sub> has antimicrobial activity as it increases the lag phase duration and the relative size of the intervals of offspring production of the microorganisms and it forms carbonic acid (possibly lowering the pH of the food to bacteriostatic levels).<sup>38</sup> Packaging systems having high CO<sub>2</sub> and O<sub>2</sub> levels can control microbial growth, but stand an increased chance of the commodities inside the packaging recontaminating.

Modified packaging can be combined with eugenol, thymol, menthol, acetic acid, Cl<sub>2</sub> gas, ozone, SO<sub>2</sub> and antimicrobials, which leads to an additional delay in both berry and firmness losses. The next two sections are the techniques taken further in the study.

## **2.8 SO<sub>2</sub> generating sheets**

Extending the shelf-life of products increases the time the pathogens have to multiply and become more developed microorganisms, increasing the possibility of spoilage.<sup>6</sup> Since the 1920s, the grey mould caused by *B. cinerea*, is controlled by fumigations of SO<sub>2</sub>.<sup>3</sup> SO<sub>2</sub> gas is the most common synthetic fungicide used to kill both spores and mycelia during storage.

The grape industry uses boxes lined with a polyethylene film/liner. Each liner-type has different numbers and sizes of perforations and is characterized by these properties. The number and size of perforations influence the atmospheric conditions in the packaging around the produce.<sup>26</sup> Liners consisting of no perforations maintain an almost 100% relative humidity (rH) during cold storage and a shelf period of 7 days.<sup>26</sup> High humidity results in delayed stem loss quality and, in the presence of SO<sub>2</sub>, significantly increases the injury due to SO<sub>2</sub> incidence of the berries during storage. Table grapes can be stored for months at 0 °C and high humidity.

Perforated liners on the other hand improve the cooling rate of the fruit and reduce the relative humidity inside the container. Liners having too many perforations maintain too low humidity and result in stems being dehydrated and browning increases when compared to non-perforated liners.<sup>26</sup> A large difference in berry firmness is observed between the two types of liners. The highest decay of grapes occurs in liners with fewer perforations. The perforation area of the liner needs to be adjusted after taking the release rate of the SO<sub>2</sub> sheet into consideration.

An SO<sub>2</sub> generating sheet is placed on top of the fruit. The generating pad consists of pockets containing sodium metabisulfite salt. In the presence of water vapour in the atmosphere, the salt will react with the water vapour and emit SO<sub>2</sub> at low concentrations within the packaging. SO<sub>2</sub> gas is also applied in vapour form at field temperature, during pre-cooling or frequent fumigations in storage rooms (- 0.5 °C). Fumigation should take place for 2 - 6 hours weekly or by packaging the grapes in a box containing a polyethylene liner with an SO<sub>2</sub> generator sheet on top of the fruit.<sup>4,6</sup>

SO<sub>2</sub> fumigation has shown to be more effective than fumigation with ozone or *M. albus*.<sup>4,57</sup> Through an ionization–entrapment mechanism, sulphur dioxide in solution can diffuse through membranes and thus accumulate in microorganisms. Grapes consist of an epicuticular wax that makes grapes more tolerant toward sulphur dioxide, minimizing SO<sub>2</sub> penetration into the berries thus reducing berry injury. The quantity of SO<sub>2</sub> in injured berries, pedicels, and the rachis, can accumulate and cause bleaching of the fruit.

During storage of grapes, the spreading of *B. cinerea* primarily originates from the flower axil that was infected during flowering and where the pathogen survived unnoticed as an endophyte, and develop later to cause postharvest grey mould.<sup>50</sup> An increase in SO<sub>2</sub> concentration in the pedicels plays an important role due to *B. cinerea* infecting berries in the pedicel-berry attachment zone.

The first limitation of using SO<sub>2</sub> gas as fumigation agent is that it exhibit anti-fungal activity against *B. cinerea*, but does not kill dormant infections present inside the berry tissue during storage that are able to develop into grey mould at a later stage when favourable conditions occur.<sup>1</sup> SO<sub>2</sub> fumigations only eradicate spores on the surface of the berries.<sup>1</sup>

For this reason, fumigations are needed to prevent grey mould nesting, causing mycelia spreading from infected berries to adjacent healthy berries.<sup>3</sup> A high SO<sub>2</sub> concentration is needed

to kill the inoculum present on the berries surface, but if the concentration is too high, damage to the berries occurs. The second drawback of using SO<sub>2</sub> generating sheets are that the sheets are only placed on top of the box. If SO<sub>2</sub> is released, the release point of SO<sub>2</sub> gas is only from one part of the packaging system. The berries close to the generating sheet might experience higher SO<sub>2</sub> concentrations than the fruit at the bottom. Another disadvantage of using SO<sub>2</sub> sheets or fumigation for the prevention and/or delay of *B. cinerea* spreading in the packaged grapes is that the concentration of SO<sub>2</sub> required for effectiveness may injure both the rachis and berry, may result in the bleaching of the berry colour, browning of the stem and rachis and occurrence of water loss.<sup>27,58</sup> In addition, sulphite residue is a problem. In the industry, the tolerance of SO<sub>2</sub> residue is rarely exceeded, but berries that get wounded or detached can easily accumulate excessive residues.<sup>50</sup>

Although SO<sub>2</sub> has some disadvantages, it is one of the most well-known and used control methods against *B. cinerea*. The first approach of the study is to incorporate the sodium metabisulfite salt within polymer nanofiber mats to have a higher surface area that is able to emit SO<sub>2</sub> gas increasing the efficiency of the SO<sub>2</sub> generating sheet. The nanofibrous material can be placed around the fruit having more surface area exposed to the fruit. The reason this is advantageous is that there is not only one point of release of SO<sub>2</sub>. Section 2.10 that will follow shortly will discuss the polymers that have been chosen for the individual approaches of the study.



## 2.9 Organic compounds

### 2.9.1 Introduction to fungicides

Controlling postharvest diseases primarily depends on the use of synthetic fungicides.<sup>5</sup> The use of fungicides was briefly discussed in Section 2.7.2.1. A technique is needed that will kill the initial fungi present on the surface of the produce. Fungicides that are sprayed onto bunches in the field are able to kill *B. cinerea* deteriorating the grapes at a later stadium. Thus using a fungicide on the surface of the packaging can have the advantage over SO<sub>2</sub> fumigation to kill or prevent the initial *B. cinerea* present on the surface of the berries from growing.

*Botrytis cinerea* can be controlled through the methods stated above, but in many crops, cultural practices cannot provide sufficient disease control and chemical control is therefore of utmost importance.<sup>2</sup> Microorganisms have the ability to change and adapt in order to outlive conventional food preservation techniques, therefore new techniques need to be developed for the inhibition of microbial growth. These non-conventional techniques including ultraviolet treatment (UV-C), the application of shorts bursts of electricity using a high voltage supply, ozone treatment, application of magnetic fields, high-intensity pulsed light, high hydrostatic pressure, new edible coatings and the use of safe antimicrobials are now being investigated.<sup>38</sup>

The protection of fruit in the postharvest storage duration against physiological disorders, quality characteristics losses and microorganisms and insects have shifted from using environmental unfriendly chemicals to various alternative techniques that are safer for the human. These alternative techniques include biological control and physical methods such as irradiation, controlled atmosphere- (CA), modified atmosphere packaging (MAP) and safe fungicides for the control of spreading fungi.<sup>38</sup>

Chemicals used in packaging may react with food constituents, especially Cl<sub>2</sub>-containing fungicides or preservation methods including chlorine, thereby reducing microbiological efficiency coupled with sensorial changes and the formation of potential carcinogenic or mutagenic products. Regarding the dangers these chemicals have for the users and applicators,

questions are being raised. In the near future, regulatory restrictions may require the development of alternative decontamination methodologies.<sup>16,43</sup>

Chemicals being used for protection during postharvest are becoming increasingly restricted as the effects can include human health and environmental concerns.<sup>55</sup> The development of new fungicides can also be costly, but up to now the primary approach for controlling postharvest diseases is the use of synthetic fungicides.<sup>5</sup>

During the last decade modern fungicides with diverse modes of action have been developed for the protection of produce against plant pathogens that cause resistance and huge economic losses. Fungicides can be applied for disease control through pre- and post-infection activity, but a specific fungicide's mode of action and whether the fungicide's activity focusses on pre- or post-infection must be well known to increase the efficiency of the fungicide. If that is known the application timing can be optimized based on the host-pathogen interaction in table grapes.<sup>12</sup>

Some of the older and well-known fungicides include the dicarboximide fungicide family (iprodione, procymidone and vinclozolin) and substances mostly derived from the benzimidazole fungicide family (diethofencarb, phenylcarbamate and carbendazim), the dichlorofluanid, folpet and captan fungicides. These fungicides have been used mainly for the control of grey mould that is responsible for a great loss of fruit and vegetables annually.<sup>14</sup> In earlier years chemical control was primarily accomplished by means of site-specific fungicides belonging to the dicarboximides and benzimidazoles families while multi-specific inhibitors such as phenylpyrrole and captan are only used in mixtures or in rotation with site-specific inhibitors since their efficacy is relatively low if used by itself.<sup>14</sup> Intensive usage of these fungicides led to the rapid development of resistant strains towards the fungicides. Therefore some of the fungicides are not used more than once a year due to resistant strains formed against the fungicides. The development of resistant strains toward these compounds limits the usage of these fungicides.<sup>12,13</sup>

New and more effective fungicide treatments with the lowest possible toxicity and risk for human health are required. Some new botryticides, focused on the inhibition of *B. cinerea*, with different modes of action have recently been registered for the control of grey mould. These new fungicides include the phenylpyrrole fungicide (fludioxonil), the hydroxyanilide derivative (fenhexamid), and the anilinopyrimidine derivatives (pyrimethanil, cyprodinil and mepanipyrim).<sup>11,14</sup> Although the modern fungicides<sup>11</sup> are most probable to lead to the

development of resistant strains, the fungicides are not comparable to the older fungicides that are mostly derived from dicarboximides.

The anilinopyrimidines have a broad-spectrum activity against several important plant pathogens, including a potent fungicidal activity against *B. cinerea*.

Even though chemicals are used in the vineyard for the control of *B. cinerea*, storage decay by *B. cinerea* still occur and needs to be addressed. A possible method could be the development of a polymer system amended with a fungicide which could be attached to the lining of boxes during packaging, therefore reducing the possible development of grey mould decay. Through attaching the fungicide covalently to a polymer system no “free” fungicides will be present on the surface of the berries during storage, reducing decay as well as satisfying consumer demand for fewer residues on the fruit.

### 2.9.2 Mepanipyrim (*N*-(4-methyl-6-prop-1-ynylpyrimidin-2-yl) aniline)

A synthetic fungicide group, namely anilinopyrimidine, was found to be highly effective against *B. cinerea*, although some strains of *B. cinerea* have shown some resistance against certain anilinopyrimidines. Mepanipyrim was the first of the anilinopyrimidine group to be declared a fungicide and is used worldwide for crop protection.<sup>13</sup> The mode of action of anilinopyrimidines consists of the microorganisms’ methionine and amino acids biosynthesis’ being inhibited, as well as the secretion of hydrolytic enzymes being inhibited.<sup>14</sup>

All new fungicides face the possibility of resistance development against them. Although some resistance has been detected against anilinopyrimidines from *B. cinerea*, it is rarely reported and only in low resistance levels. Mepanipyrim have shown excellent activity against *B. cinerea* and will be the fungicide used in the study.<sup>59</sup>

Although most of the fungicides are applied during bunch development in the field it is active against *B. cinerea*, it can be viable to apply these fungicides in the packaging to prevent *B. cinerea* spreading to healthier grape bunches. Instead of using the fungicide in spray form and the sodium metabisulfite that releases SO<sub>2</sub> gas in the generating sheet it can be incorporated into the packaging system itself. This can be achieved through the polymer system chosen for the packaging. A wide variety of polymers is known that is used for packaging. In order to attach mepanipyrim to polymer chains with functional groups, it is necessary to modify

the mepanipyrin and introduce active sites that selectively react with, those function groups on the polymer.

The section that follows will discuss the polymers that were chosen for the individual approaches of the study.

## **2.10 Polymers**

In both approaches of the study, maleic anhydride (an electron-poor monomer) is copolymerized with styrene or a derivative thereof (an electron-rich monomer), which leads to the formation of alternating copolymers.<sup>60</sup>

In the first section of the project, an alternating styrene-maleic anhydride (poly(styrene-*alt*-maleic anhydride)) copolymer is used (SMA). SMA is a cheap, easy to modify and very versatile polymer.<sup>61</sup> SMA is easily synthesized through conventional radical copolymerization in an alternating distribution of the two monomer units. SMA is soluble in a wide variety of solvents due to the polar nature of the maleic anhydride residues and the nonpolar styrene residues in combination.<sup>62</sup> SMA can be used as polymer blend compatibilizers and adhesion promoter.<sup>63</sup> The maleic anhydride group is easy to modify and is reactive towards amidation, esterification and hydrolysis.<sup>64,65</sup> Any chemical group that has a suitable reactive group can thus be covalently attached to the highly maleic anhydride group of SMA via a nucleophilic ring-opening reaction of the 5-membered anhydride group, making it easy to modify and functionalize, with ring-closure occurring upon application of heat.<sup>66</sup> The SMA modification agent had a primary amine moiety that is electron rich with the other end of the modification agent having a tertiary amine tail. The primary amine group was available for the nucleophilic attack on the maleic anhydride unit after which the ring-closure reaction followed. The tertiary amine on the other side of the modification agent side can be reacted further via a quaternization reaction to obtain an alkyl chain with the nitrogen moiety being quaternized giving the polymer a cationic nature.

Other advantages of using SMA is that it has been electrospun, is easy to electrospin and optimization of the electrospinning process has been done. Modification of the polymer can be done before or after electrospinning. Modifying a polymer before the electrospinning procedure can influence the electrospinnability of the polymer, because a new polymer is formed that may require different spinning parameters compared to the neat SMA polymer. If this potential

problem is observed, the SMA polymer can be electrospun and then surface-functionalized after the electrospinning process. One advantage of using this option is that only the surface of the electrospun fibers are modified and less compound is used, compared to the bulk of the polymer being modified and then only electrospun.

In the second approach of this study, a polymer similar to SMA was used, but the modification of the polymer occurred on the styrene residue instead of the maleic anhydride residue. The reason for this is that an azide moiety was needed for the covalent attachment via click chemistry of an organic compound onto the polymer. If the maleic anhydride group is left unmodified, functionalization of the maleic anhydride group can be done at a later stage if additional functionalization is needed. 4-Vinylbenzyl chloride was therefore used instead of styrene, leaving a chloride functionality that can be substituted with an azide functional group. 4-Vinylbenzyl chloride ( $S_{Cl}$ ) and maleic anhydride (MANh) were polymerized in the second approach of the study to yield poly(4-vinylbenzyl chloride-*alt*-maleic anhydride) copolymer ( $P(S_{Cl}$ -*alt*-MANh)).

Polymers are used in a variety of applications, but in the last decade, a vast amount of attention was paid to the electrospinning of polymers. The advantages of using electrospinning to produce polymer nanofibers are the extremely high surface-to-volume ratio, porous architecture, flexibility regarding size and shape of the nanofibers, ability to control the compositions of the fibers, possibility of incorporating compounds within polymer systems and a 3-D environment for anti-fungal activity.<sup>67-69</sup> Due to fibers with higher surface-to-volume ratios and the ability of incorporating compounds within the electrospun polymer nanofibers a possible increased anti-fungal activity can be achieved.

## **2.11 Electrospinning**

The term electrospinning is derived from electrostatic spinning.<sup>69</sup> Electrospinning is a very old, but every day improved technique that was first patented by J.F Cooley in 1900. The first patent for the fabrication of textile yarns was described in 1934 by Anton Formhals.<sup>70</sup> Electrospinning has been known for more than a century. The last couple of years it became an interesting topic and research area due to the surging interest in nanotechnology, as ultrafine, nanofibers can be easily fabricated with this process.<sup>69,71-74</sup>

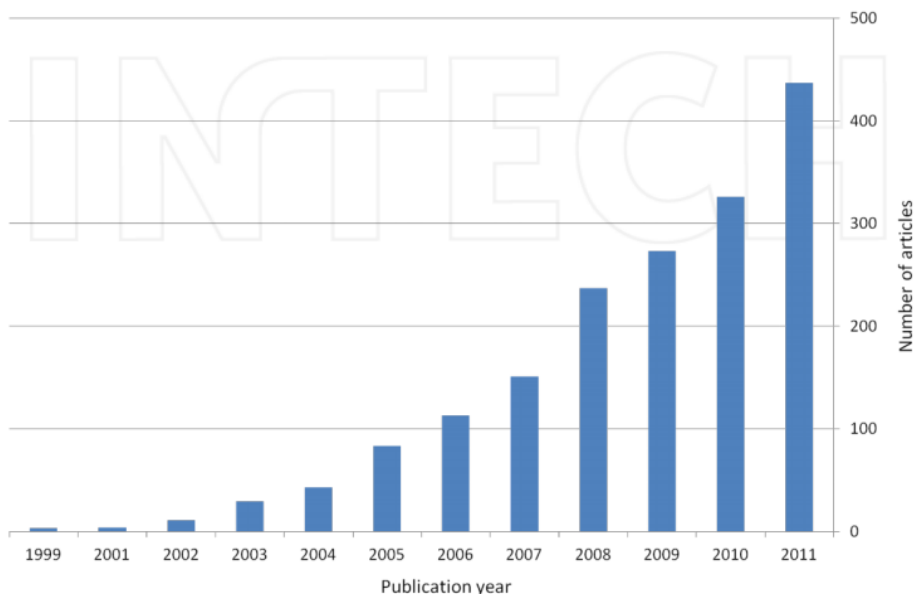


Figure 2.4 Histogram representing the increase in the number of scientific articles published in the electrospinning field over the last decade.<sup>75</sup>

Electrospinning still continues to evolve rapidly as the usefulness of nanofibers is still growing.<sup>74</sup> The data in Figure 2.2 clearly demonstrate that electrospinning has attracted an increasing amount of research in the past decade.<sup>69</sup> Electrospinning can produce continuous polymer nanofibers ranging from several micrometers to just a few nanometers (between 50 - 500 nm in diameter).<sup>76</sup>

The technique is very simple, cost effective and promising since it facilitates the production of multi-functional nanofibers from a wide variety of polymers, polymer blends and polymer composites and ceramics.<sup>76</sup> The modification of polymer nanofibers has generated much interest due to the versatility of the process and the unique properties that are obtained through the process when the fiber diameter is decreased from micrometers to nanometers.<sup>69</sup> These properties include flexibility in surface functionalities, very high specific surface area to volume ratio, and uniformity along the fibers, porosity, high mechanical strength and high aspect ratios.<sup>69,77,78</sup> These outstanding properties make the polymer nanofibers outstanding candidates for a variety of applications.<sup>69</sup> Refer to Figure 2.3 for a range of applications of polymer nanofibers. These applications include, but the applications are not restricted to, food packaging, filtration media, reinforcements of nano-composites, biomedical fields such as drug

delivery, medical applications such as sensors and tissue engineering scaffolds, to name but a few.<sup>74,76</sup>

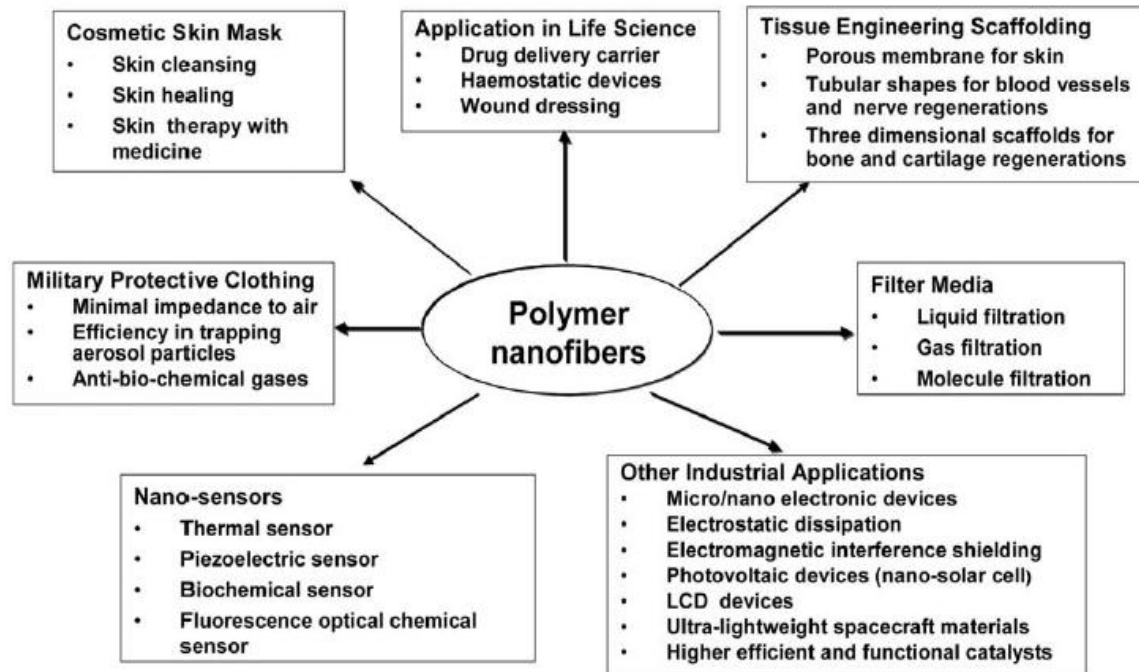


Figure 2.5 Different fields and potential applications of polymer nanofibers in the industry.<sup>69</sup>

### 2.11.1 Single needle electrospinning process

The process of electrospinning entails the following: A blunted needle is attached to a syringe, filled with the desired polymer solution. A high voltage power supply is attached to the needle tip. The needle tip acts as a positive electrode by attaching the positive end of the high voltage power supply to it, a distance away, an aluminum-covered collector is placed that acts as the negative electrode through attaching the negative electrode of the same high voltage power supply. A droplet of polymer solution is pushed through the needle tip using a syringe pump that regulates the flow rate of the polymer solution. The droplet is subjected to the two opposing forces, one being the polymer solution's contractive surface tension and secondly the electrostatic repulsive force caused by the same charge as introduced by the high voltage power supply.<sup>79</sup> The applied voltage induces charge via the electrode within the polymer solution. These similar charges flow through the solution and accumulate on the surface of the

polymer solution droplet at the tip of the needle, thereby increasing the charge density at the surface. The charges repel each other and the electrostatic repulsive force will aim to expand the surface area of the droplet whereas the contractive nature of the surface tension force will aim to reduce the surface area of the droplet.

As the electrostatic force increase the hemispherical surface of the droplet deforms and it elongates to form a conical shape known as the Taylor cone.<sup>69,80,81</sup> Refer to Figure 2.4 for the illustration of the Taylor cone region.

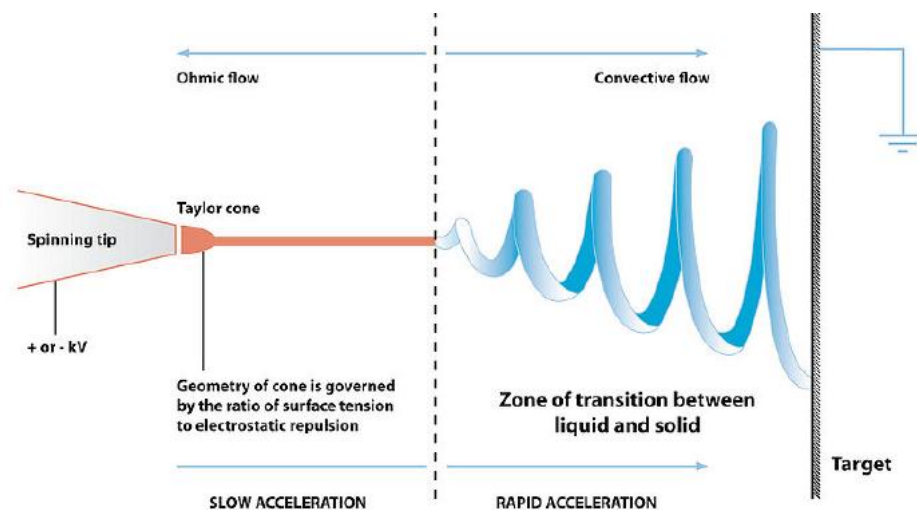


Figure 2.6 Illustration of the spinning tip, the polymer droplet, the Taylor cone region and the bending instability region.<sup>82</sup>

Rayleigh studied the theoretical stability of an isolated charged liquid that becomes unstable and fission at the tip of the deformed droplet becomes visible. Zeleny adapted this theory to the case of an electric field being applied and the droplet losing its stability when jetting begins at its vertex and Taylor corrected his theoretical results.<sup>80</sup>

A critical value is reached if the electric field is further increased. At this value, the electrostatic repulsive force overcomes the surface tension of the polymer solution. The result thereof is a charged polymer jet that is ejected from the tip of the Taylor cone.<sup>69</sup> Straight after the jet is ejected, the jet is stable and straight, where the growing perturbations are still very small. When the jet passes the steady-state segment, it starts what is referred to as a region of instability or bending instability.<sup>80,83</sup> In this region the charged jet is repelled from itself due to the similarly charged ions within the electrospinning jet and undergoes whipping. During the primary



instability region the charged jet deviates from travelling straight towards the collector and coils onto itself repeatedly, each coil having turns of increasing radius.<sup>80,84,85</sup> Refer to Figure 2.4 for an illustration of the bending instability region.

As the charge repulsions along the fiber increase, secondary bending instabilities are observed. The whipping action stretches and elongates the charged jet, therefore decreasing the fiber diameter from micrometers to nanometers. Simultaneously the solvent evaporates and fibers solidify, resulting in dry fibers accumulating on the collector.

A major drawback of the single needle electrospinning process is that very few fibers are produced, varying from 0.1 to 1 g.h<sup>-1</sup>.<sup>86</sup> The use of these nanofibers for the appropriate applications, as mentioned previously, is not economically sustainable or industrially feasible due to the extremely slow production rate. To overcome these problems of slow production rates, research has been done to upscale the production process of single needle electrospinning. Ball electrospinning is one of the techniques that were developed to increase the production rate.

### 2.11.2 Ball electrospinning process

Ball electrospinning is a relatively new high throughput technique for the production of nanofibers. This process is designed to increase the fiber production capacity of the conventional electrospinning process. The process of ball electrospinning was developed at the University of Stellenbosch.<sup>87</sup>

The concept of ball electrospinning is the same as single needle electrospinning. The same parameters play an intricate role in the process, although more parameters play a role and the process does not entail a sharp edge but a free-surface. Refer to Figure 2.5 for the schematic illustration of the basic ball electrospinning setup.

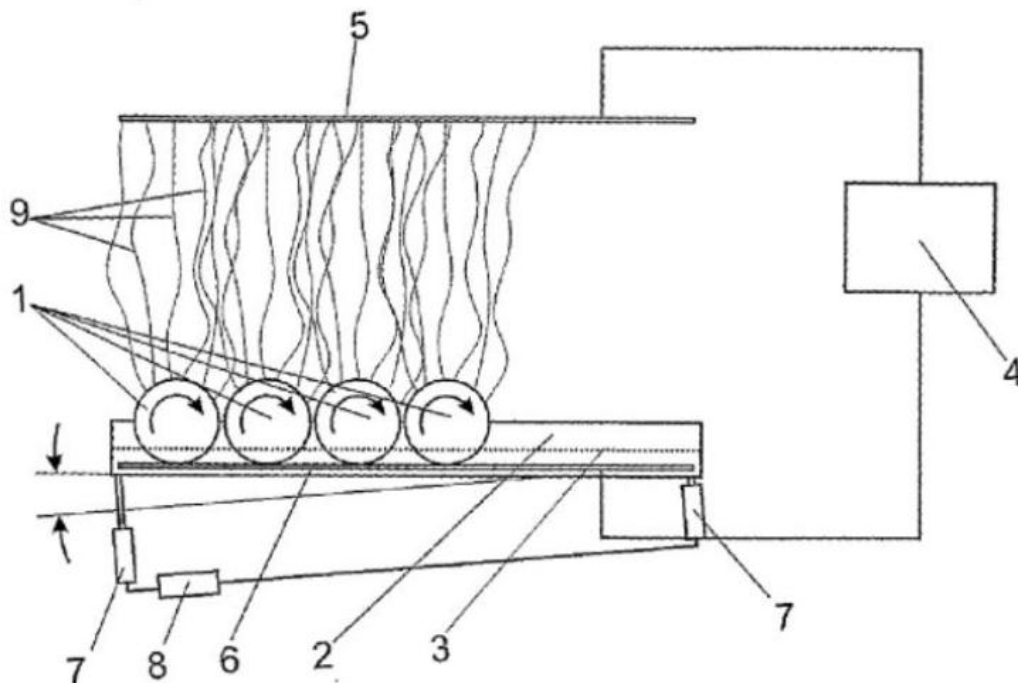


Figure 2.7 The multiple ball electrospinning setup is illustrated. Multiple balls are used to create electrospun nanofibers. In a solution container (2) multiple loose balls (1) are rotated. The polymer solution (3) within the container is able to be electrospun. An electric field is created between the balls (1) and a collector (5) by means of a high voltage power supply (4). A contact plate (6) supports the balls while the trough is moved by one of a few different methods, including by means of pistons (7). The motion can be controlled by using an automatic valve assembly (8). When sufficient electrical charge is applied to the balls, electrospinning jets (9) eject from the surface of the balls and are deposited on the collector as nanofibers.<sup>87</sup>

Ball electrospinning is an upward direction needleless process that produces multiple nanofibers from multiple polymer jets formed simultaneously from the surface of a polymer coated ball. The lab-scale setup used in this study (Refer to Figure 3.4 in Chapter 3) differ from the multiple ball setup (Refer to Figure 2.5) in that only one glass ball is used. The setup consists of a solution holder that is cylindrical and a rotating glass ball that fits in the holder. The glass ball is connected via a glass rod to an electrical device that induces rotation. The rotation speed can be adjusted and is therefore a parameter that can be changed. A rotating drum collector is used and is placed a certain distance away from the rotating ball.

The formed polymer nanofibers accumulate on the rotating drum collector. The speed at which the drum collector rotates can be adjusted and is therefore another parameter that can be

changed. When the speed of the drum collector matches the speed of the dried jets that deposit on the collector, the fibers are tightly collected in a circumferential manner, resulting in fair alignment of the fibers. When the collector speed is slower than the alignment of the fibers, randomly deposited fibers are observed. On the other hand, if the collector speed is more than the maximum speed at which fibers can be aligned, fibers will break.<sup>69</sup>

The solution holder of the ball electrospinning setup is filled with polymer solution. The glass ball is placed inside the holder and as the ball rotates, the ball is submerged and coated with an even layer of polymer solution on the outside of the glass ball.

The solution in the holder is charged via the positive electrode of the high voltage power supply. The negative electrode of the same high voltage power supply is connected to the collector, which is a rotating drum covered with aluminum foil. In the single needle setup, the electric field that is applied deforms the droplet and when the contractive surface tension is overcome by the electrostatic repulsive forces, a charged jet is ejected from the needle tip. The needle tip thus acts as a sharp edge. The same principle applies with ball electrospinning, except that the glass ball doesn't have any sharp edges. Although a sharp edge is absent in ball electrospinning electrical wavelengths moving over the surface of the polymer coated glass ball is present. Refer to Figure 2.6 on the next page for the schematic illustration of a basic electric wave, including a wave peak (tip) and wave trough (bottom) and the quantity of jets that can form.

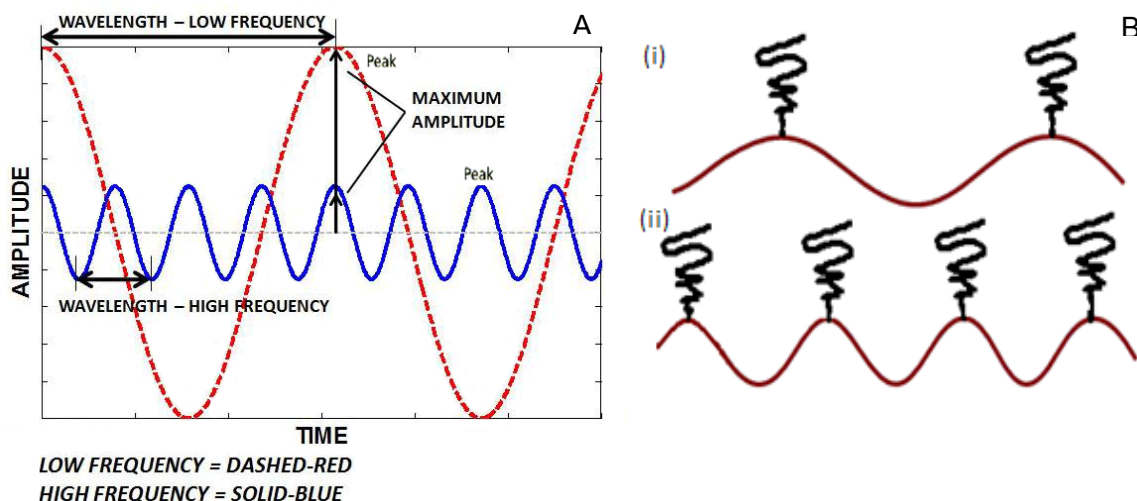


Figure 2.8 A) Representation of an electric wave running over the surface of the ball, dashed-red wave at lower frequency and solid-blue wave at a higher frequency.<sup>133</sup> B) A schematic illustration of the different amount of jets which are able of being ejected from the surface of the glass ball. In the figure B): (i) fewer amounts of peaks due to a lower frequency (red wave) and (ii) more wavelengths due to a higher frequency wave (blue wave) therefore more peaks and more jets are able to eject from the surface of the glass ball.

In ball electrospinning more than one condition or parameter plays a role in the successful production of nanofibers. The first condition is that the jets need to be mechanically strong enough to support the Taylor cones. The second condition is that a continuous polymer solution needs to be fed to the jets on the spinning surface. Therefore, a sufficient viscosity is needed but not too high for the solution must flow freely and feed the jet with fresh polymer solution. The continuous feeding of polymer solution to the jets is supported by the rotating ball that rotates through the polymer solution, to cover the surface of the ball with polymer solution. When the contractive surface tension is overcome by the electrostatic repulsive force a charged jet is ejected from the tip of each wave. The more peaks/tips there are, the more jets can be ejected.

Multiple jets are formed simultaneously from the surface of the rotating ball. The speed at which the ball rotates has an effect on the number of jets formed. If the rotation speed is too low, the multiple jets that form won't be able to "run" over the surface of the ball and the solution on the surface of the ball will get depleted. If the ball rotates too quickly, the fibers will not have sufficient time to undergo solvent evaporation and wet fibers will land on the collector. As more jets are formed, a higher voltage is needed to supply sufficient charge to all the ejecting jets to

stretch and whip as the individual polymer jets travel to the counter electrode. In the stretching and whipping stage, the polymer jets are repelled from themselves and undergo elongation and solvent evaporation.

As in single needle electrospinning the solvent parameters are of utmost importance. The conductivity, viscosity, surface tension and vapour pressure should all be in balance to produce dry, uniform polymer nanofibers on the collector. This technique can produce nanofibrous membranes consisting of millions of nanofibers in shorter times than the conventional single needle electrospinning process.

### 2.11.3 Electrospinning process parameters

The electrospinning process is complex and is influenced by a variety of parameters and processing variables. These parameters interact differently and simultaneously to create polymer jet(s).<sup>80</sup> These parameters are:

- a) The system/operational parameters describing the electrospinning conditions,
- b) The solution parameters such as the spin solutions' physiochemical properties, and
- c) External parameters such as the ambient conditions surrounding the electrospinning setup.

The system parameters include electric field strength, solution feed rate and the effective distance between the capillary and the target. The main solution parameters are the shear and elongational viscosity, conductivity and surface tension.<sup>80,88</sup> Other solution parameters include the dielectric constant of the solution, the molar mass and molar mass distribution of the polymer and the polymer architecture (e.g. linear or branched). The external factors that affect the electrospinning process are the ambient temperature, the relative humidity and the temperature of the solutions.<sup>69,80,88</sup>

Changing one parameter will affect another parameter or more than one.<sup>79</sup> An example of parameters having an effect on each other is the chain entanglements needed for electrospinning. Proper and acceptable number of polymer chain entanglements is needed for fibers to be able to form using the electrospinning process. Polymer chain entanglements are dependent on the molar mass of the polymer and/or the concentration of the polymer solution. Both are parameters that have an effect on the electrospinning process. The molar mass and

concentration of the polymer need to be sufficient for fiber formation, but not so high that the resultant viscosity prevents the polymer jet to be induced by the electric field. In addition, the surface tension of the polymer solution must be low enough and the electric field that supply the charges high enough for a polymer jet to be ejected. The viscosity of the polymer solution must also be sufficient to prevent the jet from collapsing into droplets due to incomplete solvent evaporation resulting in beads-on-a-string forming.<sup>69,81</sup> By changing the electrospinning process parameters and solution parameters, as mentioned in b) and c) above, almost any polymer solutions can be electrospun.<sup>89</sup>

For the purpose of this study, nanofibers had to be spun with high surface area to unit mass ratio for optimum availability of the antifungal compound and release of SO<sub>2</sub>. Although numerous research papers have been published regarding the influence of the various parameters on the electrospinning process, only those parameters affecting fiber diameter will be discussed further.<sup>79</sup>

#### 2.11.4 Electrospinning process parameters affecting fiber diameter

Formation of nanofibers on the collector is the result of solvent evaporation and solidification of the polymer jets and the diameter of the fibers primarily depend on the size of the jets and the polymer solution.<sup>69</sup> Viscosity, applied electric field strength (applied voltage), solution conductivity, distance between capillary and target and polymer solution flow rate are the electrospinning parameters that have the biggest influence on the diameter of the fibers.<sup>80, 90</sup> The applied voltage and the distance between the needle tip and the collector determine the strength of the electric field felt by the polymer jet. These parameters influence the extent of whipping and elongation the polymer jet undergoes, and therefore they have a direct influence on the fiber diameter.

#### 2.11.4.1 Viscosity

The viscosity of a solution is the resistance of a solution to flow. The viscosity of a polymer solution is determined by the concentration and the molar mass of the polymer. Viscosity is a key parameter affecting the electrospun fiber diameter.<sup>91</sup> For instance, if the concentration of the polymer solution increases, more polymer chain entanglements are found to happen and the resistance to flow increases. An increase in solution concentration and molar mass increases the viscosity.

If the viscosity is too low, there are not sufficient polymer chain entanglements to stabilize the formed jet and electrospinning is observed. The phenomenon occurs due to the jet that breaks up into droplets due to the Rayleigh instability and spray towards the collector.<sup>91</sup> Polymer concentration also affects the formation of beads or beads-on-a-string.<sup>69</sup> As the concentration increases, the observed beading will get less until smooth, bead-free fibers are produced.<sup>92,93</sup> Beaded fibers are also a consequence of high surface tension. Surface tension aims to reduce the surface area per unit and if the electric field does not overcome the surface tension, the jet will break up and form beads-on-a-string. If a higher viscosity solution is used, the solution will be able to stretch more without breaking up and beading will be reduced.<sup>92</sup>

If the viscosity is too high, a jet will not be easily induced. Even if the electric field strength is increased further, due to polymer chain entanglements that inhibit the solution from flowing and deforming fast enough to form the Taylor cone region.<sup>69,90,94,95</sup> Demir and co-workers reported that the fiber diameter is proportional to the cube of the polymer concentration.<sup>69</sup> At higher viscosities, the path that the jet travels is reduced since the bending instability becomes smaller and the jet undergoes less whipping and stretching. As the viscosity of the polymer solution increases, so does the fiber diameter of the electrospun fiber. More polymer chain entanglements result in greater resistance of the solution to stretching and elongation.<sup>96-98</sup>

A minimum and maximum viscosity is observed for different solutions and polymer systems. Changing the viscosity within these electrospinnable ranges affects the fiber diameters. An increase in viscosity increases the fiber diameters obtained through the electrospinning process.<sup>99,100</sup> This observation can possibly be explained due to two effects. Firstly, at higher viscosities a lower portion of the jet consists of solvent and less solvent thus needs to evaporate during the whipping and elongation period. Secondly, as the viscosity increases the number of

chain entanglements increases, resulting in less solution flowing during the whipping and elongation process, producing thicker fibers.

#### 2.11.4.2 Electric Field

Electric field is another parameter that affects the fiber diameter to a significant extent. For electrospinning to take place, an electric field is needed between the needle tip, filled with a polymer solution, and the collector. The observed electric field is a function of the applied voltage and the distance between the needle tip and the collector as defined by the following equation:

$$E = V/d$$

---

Where E = Electric field strength <sup>a</sup>

V = Voltage difference between electrodes <sup>b</sup>

d = Distance between electrodes <sup>c</sup>

*Equation 2.1 Electric field strength equation. Units being measured in are: <sup>a</sup> = kV/cm, <sup>b</sup> = kV and <sup>c</sup> = cm*

Only when the electrostatic forces overcome the solutions' surface tension does a jet eject from the droplet.<sup>101</sup> A charged polymer jet undergoes whipping and elongation in the bending instability region due to the electrostatic repulsive charges within the jet. During the whipping and elongation the fiber decreases in diameter continuously until all solvent has evaporated and land as dry fibers on the collector.<sup>96</sup>

The higher the applied electric field, the more charges accumulate at the polymer droplet surface. The more charges on the surface of the newly ejected polymer jet the more whipping and stretching the jet undergoes and thus finer fibers are collected on the collector.<sup>72,91,93,95</sup> The higher the charge density carried by the polymer jet surface, the fewer beads are formed.<sup>90</sup> Bead formation is also greatly influenced by the applied electric field. As the concentration of the polymer solution increases, the applied electric field also need to increase to induce a polymer jet, indicating that a higher electric force is needed to form a jet.<sup>81</sup>



#### 2.11.4.3 Surface tension of the solution

Prior to Taylor cone formation, during the jet initiation period and during bending instability does the surface tension parameter play an enormous role. The electric field charge therefore needs to be high enough to overcome the surface tension of the polymer solution in order for Taylor cone formation and subsequent jetting to occur. If the electric field strength is not high enough, the surface tension of the polymer solution will be the dominant force.<sup>72,102</sup>

#### 2.11.4.4 Electrical conductivity

Electrical conductivity of a solution refers to its ability to transfer charges via the polymer molecules, solvent molecules, additives or impurities in the solution. The mutual charges that repel each other in the polymer solution when the jet is ejected cause the jet to be whipped and stretched. These charges need to be carried and therefore solution conductivity is a key parameter in the electrospinning process. The higher the solution conductivity, the more charges can be carried, resulting in more whipping and stretching taking place, producing finer diameter fibers.<sup>91</sup> A solution with zero conductivity cannot be electrospun due to the absence of charge transfer. As the solution conductivity increases, lower electrical forces are required to overcome the solutions' surface tension to eject a polymer jet. Adding a salt to the polymer solution, increasing the temperature or using different solvents can increase the electrical conductivity of a solution. If the solvent allows dissociation of the salt, the dissociated salt has the advantage of positive and negative ions being present. These individual ions move independently of each other, each able to carry part of the charge. The charge carrying capacity increases and thus an increase in the electrical conductivity is observed.<sup>69</sup>

#### 2.11.4.5 Distance between needle tip/ball and target

As seen above in Section 2.11.4.2, refer Equation 2.1, the field strength is directly influenced by the distance between the needle tip and the collector. Increasing the distance results in a decrease in the fiber diameter due to the travelling time of the jet increasing, giving the polymer jet more time to whip and stretch.<sup>72,81,94</sup> If the electric field is high but the distance is small, thicker fibers may form on the collector due to more fluid ejected in a jet and the travelling time decreasing, thus the polymer jet does not whip and stretch sufficiently.<sup>69</sup> Wet fibers or a film

may form on the collector due to the solvent not having sufficient time to evaporate before reaching the collector. An effective spinning distance will ensure complete drying of the fibers as well as enough time for the fibers to stretch and elongate to form thinner fibers.

#### 2.11.4.6 Flow rate of polymer solution

A syringe pump is used to control the flow rate of the polymer solution through the needle. A variation in fiber diameter can be seen with a variation in the flow rate.<sup>92</sup> Increasing the flow rate of the polymer solution increase the fiber diameter, due to more polymer solution that is able to be drawn from the tip of the capillary.<sup>72,92</sup> If the flow rate is too high, the polymer solution will start dripping from the needle tip as the excess solution cannot be carried away fast enough by the available charge.<sup>95,103</sup> If the flow rate is too low, the Taylor cone will disappear due to the absence of solution available to deform, resulting in a discontinuous jet. If the flow rate is optimal, a stable Taylor cone can be observed for the same size capillary.<sup>80</sup> The optimal flow rate is observed if the rate of polymer solution being pumped to the needle tip is the same as the quantity of polymer solution being carried away by the jet.

## 2.12 Conclusion

To conclude this chapter, spoilage in general has been discussed, as well as the spoilage of fruit and vegetable and in particular the spoilage of grapes. Details about the specific microorganisms and fungi responsible for the spoilage of grapes have been described. The dangers regarding the techniques used up to now to delay or retard spoilage of fresh fruit and vegetable have been highlighted with the background on why. Emerging technologies addressing the dangers and efficiency of the technologies have been considered, one being an improved SO<sub>2</sub> generating pad/nanofiber mat concept and secondly the use of a fungicide on the surface of the film in the inside of the boxes. Although the fungicides are used in the field, the mode of action can be carried over to the film, having the same mode of action when the fungi come in contact with the fungicide-modified film.

Since the 1920s, the grey mould that is caused by *Botrytis cinerea*, is controlled through fumigations with SO<sub>2</sub> gas and fungicides that is sprayed onto the fruit in the vineyard.<sup>3</sup> SO<sub>2</sub> gas is the most commonly known synthetic fungicide used to inhibit both spores and mycelium of *B. cinerea*. Initial SO<sub>2</sub> treatment kills fungal inoculum present on the fruit surface but not the

microorganisms within the berry tissue. For that reason, fumigations are needed to prevent grey mould nesting, causing mycelia spread from infected berries to adjacent healthy berries.<sup>3</sup> On the other side, the synthetic fungicide group, namely anilinopyrimidine, was found to be highly effective against *B. cinerea*, although some strains have shown some resistance against certain anilinopyrimidines. Mepanipyrim was the first of the anilinopyrimidine group to be declared as a fungicide and is used worldwide for crop protection in the field.<sup>13</sup>

The aim of the study is to incorporate SO<sub>2</sub> fumigation and the use of organic compounds as fungicides into different polymer systems. Electrospinning such a polymer system has various advantages. The electrospinning technique produces polymer nanofibers that have larger surface to volume ratio that have the advantage over a pad or film, more surface area is able to be modified or functionalized.

In the first part of the study, modification of a polymer to be able to have specific ionic interactions between the polymer and the salt can improve the release of SO<sub>2</sub> due to the production of nanofibers which have higher surface to volume ratio, more surface to interact with salt. The salt that is used is the same as in the generating sheets, i.e. sodium metabisulfite, which react to atmospheric moisture present in the packaging, releasing SO<sub>2</sub> gas needed for control of decay. A polymer, poly(styrene-*alt*-maleic anhydride) copolymer (SMA), has been identified that is easily reacted and modified with suitable chemical moieties to be able to have ionic interactions with the salt used.

The SO<sub>2</sub> generating sheets are used during packaging and contain sodium metabisulfite salt

In the second part of the study no SO<sub>2</sub> was used, as SO<sub>2</sub> can cause both berry and rachis injury, and may manifest as berry colour being bleached, browning of the stem and rachis and water loss occurring.<sup>27,58</sup> Anilinopyrimidine-derivatives are synthesized, which can be covalently attached to a polymer. Poly(4-vinylbenzyl chloride-*alt*-maleic anhydride) copolymer (P(S<sub>Cl</sub>-*alt*-MANh)) has been identified as the polymer to be used. The polymer can easily be modified, via a substitution reaction to contain a functional moiety available for the covalent attachment of the organic compound. Electrospinning the functionalized polymer will also have the advantage of a high surface area of the electrospun material is able to be functionalized.

In summary, in both approaches of the study, through electrospinning each of the task-specific modified polymers into polymer nanofibers, membranes aimed to improve the control *B. cinerea* deterioration can be developed.

## 2.13 References

1. Rahman, S.; Jin, Y.; Oh, D. *Food Microbiol.* **2011**, 3, 484-491.
2. Barth, M. ;Hankinson, T.R.; Zhuang, H.; Breidt, F. *Food Microbiol.* **2010**, 27, 135-183.
3. Nellemann, C. *The Environmental Food Crisis: The Environment's Role in Averting Future Food Crises: a UNEP Rapid Response Assessment*; UNEP/Earthprint. **2009**.
4. Gram, L.; Ravn, L.; Rasch, M.; Bruhn, J. B.; Christensen, A. B.; Givskov, M. *Int. J. Food Microbiol.* **2002**, 2, 79-97.
5. Madigan, M. T.; Martinko, J. M.; Parker, J.; Brock, T. D. *Biology of microorganisms.* **1997**, 985, 1-17.
6. Huis in't Veld, Jos. *Int. J. Food Microbiol.* **1996**, 1, 1-18.
7. Mossel, D.; Vega, C. L.; PUT, H. *J. Appl. Microbiol.* **1975**, 1, 15-22.
8. Varoquaux, P.; Wiley, R. C. *Minimally processed refrigerated fruits & vegetables*, Springer: **1994**, 226-268.
9. Ahvenainen, R.; Hurme, E. *Food Addit. Contam.* **1997**, 7, 753-763.
10. Serey, R.A.; Torres, R., Latorre, B. A *Cien. Inv. Agr.* **2007**, 3, 215-224.
11. Ngcobo, M. E. K.; Opara, U. L.; Thiart, G. D. *Packag. Technol. Sci.* **2012**, 25, 73-84.
12. Valverde, J.M.; Guillean, F.;Martinez-Romero, D.; Castillo, S.; Serrano, M.; Valero, D. *J. Agric. Food Chem.* **2005**, 53, 7458-7464.
13. Renouf, V.; Strehaiano, P.; Lonvaud-Funel, A. *J Int Sci Vigne et du Vin.* **2007**, 1, 51.
14. de Kock, P.J.; Holtz,G.S. *Arf. J. Enol. Vitic.* **1994**, 23, 33-40.
15. Irkin, R.; Korukluoglu, M. *J. Med. Food.* **2009**, 1, 193-197.

16. Díaz, G. A.; Yañez, L.; Latorre, B. A. *Am. J. Enol. Vitic.* **2011**, 4, 542-546.
17. Dr P Voysey, Campden & Chorleywood Microbial food spoilage. [www.biotopics.co.uk/pot/foodsp.html](http://www.biotopics.co.uk/pot/foodsp.html).
18. Zhu, P.; Xu, L.; Zhang, C.; Toyoda, H.; Gan, S. *Postharvest Biol. Technol.* **2012**, 66, 23-29.
19. Choquer, M.; Fournier, E.; Kunz, C.; Levis, C.; Pradier, J.; Simon, A.; Viaud, M. *FEMS Microbiol. Lett.* **2007**, 1, 1-10.
20. Suty, A.; Pontzen, R.; Stenzel, K. In Bayer-English Edition, Ed. **1999**, 52, 145-157.
21. Charles, F.; S.; Charles, F.; Sanchez, J.; Gontard, N. *J. Food Sci.* **2006**, 5, 1736-1742.
22. Elmer, P.; Hoyte, S.; Vanneste, J.; Reglinski, T.; Wood, P.; Parry, F. *N.Z J Plant Prot.* **2005**, 58, 47-54.
23. Wicks, T.; Hall, B. *D:\web stuff\grape\botrytis\Botrytis Fungicides.doc.* **2005**.
24. Allende, A.; Luo, Y.; McEvoy, J.L.; Artés, F.; Wang, C.Y. *Postharvest Biol Tec.* **2004**, 1, 51-59.
25. Artés, F.; Allende, A. *Food Sci Technol Int.* **2009**, 10, 3076-3105.
26. Allende, A.; Padilla, E.; F. Artés *Acta Hort.* **2003**, 91, 753-760.
27. Piližota, V.; Šubarić, D. *Food Technol Biotech.* **1998**, 3, 1-8.
28. Mayer, A. M.; Harel, E. *Phytochemistry.* **1979**, 2, 193-215.
29. Jacxsens, L.; Devlieghere, F.; Debevere, J. *Postharvest Biol. Technol.* **2002**, 1, 59-73.
30. Sapers, G.; Miller, R.; Pilizota, V.; Mattrazzo, A. *J. Food Sci.* **2001**, 2, 345-349.
31. Senti, F. R. *Ind Eng Chem Res.* **1981**, 2, 237-246.
32. Klapes, N. A.; Vesley, D. *Appl. Environ. Microbiol.* **1990**, 2, 503-506.

33. Juven, B. J.; Pierson, M. D. *J. Food Prot.* **1996**, 11, 1233-1241.
34. Huang, Y.; Hung, Y.; Hsu, S.; Huang, Y.; Hwang, D. *Food Control.* **2008**, 4, 329-345.
35. Koseki, S.; Yoshida, K.; Kamitani, Y.; Isobe, S.; Itoh, K. *Food Microbiol.* **2004**, 5, 559-566.
36. Ricke, S. *Poult. Sci.* **2003**, 4, 632-639.
37. Gabler, F. M.; Mercier, J.; Jimenez, J.; Smilanick, J. *Postharvest Biol. Technol.* **2010**, 2, 78-84.
38. Allende, A.; Aguayo, E.; Artés, F. *Int J Food Microbiol.* **2004**, 2, 109–117.
39. Gabler, F. M.; Mercier, J.; Jiménez, J. I.; Smilanick, J. L. *Postharvest Biol Technol.* **2010**, 2, 78-84.
40. Del Nobile, M.A.; Sinigaglia, M.; Conte, A.; Speranza, B.; Scrocco, C.; Brescia, I.; Bevilacqua, A.; Laverse, J.; La Notte, E.; Antonacci, D. *Postharvest Biol. Technol.* **2009**, 51, 21-26.
41. Breidt, F.; Fleming, H. P. *Food Technol.* **1997**, 9, 44-51.
42. Serey, R. A.; Torres, R.; Latorre, B. A. *Ciencia e investigación agraria.* **2007**, 3, 215-224.
43. Yourman, L.; Jeffers, S. *Plant Dis.* **1999**, 6, 569-575.
44. Pinto, R.; Lichter, A.; Danshin, A.; Sela, S. *Postharvest Biol. Technol.* **2006**, 39, 308-313.
45. Palou, L.; Crisosto, C. H.; Garner, D.; Basinal, L. M.; Smilanick, J. L.; Zoffoli, J. P. *Am. J. Enol. Vitic.* **2002**, 2, 110-115.
46. Kim, J.; Yousef, A. E.; Dave, S. *J. Food Prot.* **1999**, 9, 1071-1087.
47. Long, C.; Wu, Z.; Deng, B. *Eur. Food Res. Technol.* **2005**, 2, 197-201.
48. Schena, L.; Nigro, F.; Pentimone, I.; Ligorio, A.; Ippolito, A. *Postharvest Biol. Technol.* **2003**, 30, 209-220.

49. Krechel, A.; Faupel, A.; Hallmann, J.; Ulrich, A.; Berg, G. *Can. J. Microbiol.* **2002**, 9, 772-786.
50. Cantín, C.; Palou, M.; Bremer, L.; Michailides, V.; Crisosto, T. J. *Postharvest Biol. Technol.* **2011**, 2, 150-158.
51. Valero, D.; Valverde, J.M.; Mart´inez-Romero, D.; Guill´en, F.; Castillo, S.; Serrano, M. *Postharvest Biol Technol.* **2006**, 41, 317-327.
52. Vermeulen, T.; Schoonbeek, H.; De Waard, M. A. *Pest Manag. Sci.* **2001**, 5, 393-402.
53. Myresiotis, C.K.; Karaoglanidis, G.S.; Tzavella-Klonari, K. *Plant Dis.* **2007**, 91, 407-413.
54. Nagata, T.; Masuda, K.; Maeno, S.; Miura, I. *Pest Manag. Sci.* **2004**, 4, 399-407.
55. Couderchet, M. *Vitis* **2003**, 4, 165-171.
56. Forster, B.; Staub, T. *Crop Prot.* **1996**, 6, 529-537.
57. Klumperman, B. *J. Polym. Chem.* **2010**, 5, 558-562.
58. Lai, X.; Sun, C.; Tian, H.; Zhao, W.; Gao, L. *Int. J. Pharm.* **2008**, 1, 66-73.
59. Shulkin, A.; Stöver, H. D. *J. Membr. Sci.* **2002**, 2, 421-432.
60. Lessard, B.; Marić, M. *Macromolecules.* **2009**, 2, 879-885.
61. Stoilova, O.; Ignatova, M.; Manolova, N.; Godjevargova, T.; Mita, D.; Rashkov, I. *Eur Polym J.* **2010**, 10, 1966-1974.
62. Vermeesch, I.; Groeninckx, G.; Coleman, M. *Macromolecules.* **1993**, 24, 6643-6649.
63. Pompe, T.; Zschoche, S.; Herold, N.; Salchert, K.; Gouzy, M.; Sperling, C.; Werner, C. *Biomacromolecules.* **2003**, 4, 1072-1079.
64. Chew, S.; Wen, Y.; Dzenis, Y.; Leong, K. *Curr. Pharm. Des.* **2006**, 36, 4751.

65. Willemse, A. C. *Electrospinning bicomponent nanofibres for platinum ion extraction from acidic solutions*, MSc Thesis, University of Stellenbosch, South Africa. **2013**.
66. Huang, Z.; Zhang, Y.; Kotaki, M.; Ramakrishna, S. *Composites Sci. Technol.* **2003**, 15, 2223-2253.
67. Formhals, A. *Process and apparatus for preparing artificial threads: US, 1975504*. **1934**.
68. Chakrapani, V. Y.; Gnanamani, A.; Giridev, V.; Madhusoothanan, M.; Sekaran, G. *J. Appl Polym Sci.* **2012**, 4, 3221-3227.
69. Subbiah, T.; Bhat, G.; Tock, R.; Parameswaran, S.; Ramkumar, S. *J. Appl Polym Sci.* **2005**, 2, 557-569.
70. Ojha, S. S.; Afshari, M.; Kotek, R.; Gorga, R. E. *J. Appl Polym Sci.* **2008**, 1, 308-319.
71. Reneker, D. H.; Yarin, A. L. *Polymer.* **2008**, 10, 2387-2425.
72. Salles, V.; Seveyrat, L.; Fiorido, T.; Hu, L.; Galineau, J.; Eid, C.; Guiffard, B.; Brioude, A.; Guyomar, D. *In Tech Open.* **2012**.
73. Uyar, T.; Besenbacher, F. *Polymer.* **2008**, 24, 5336-5343.
74. Lee, S. J.; Tatavarty, R.; Gu, M. B. *Biosens. Bioelectron.* **2012**, 1, 302-307.
75. Cui, W.; Li, X.; Zhou, S.; Weng, J. *Polym. Degrad. Stab.* **2008**, 3, 731-738.
76. Cronje, L. *Surface modification of styrene maleic anhydride nanofibers for efficient capture of Mycobacterium tuberculosis*, PhD Thesis, University of Stellenbosch, South Africa. **2012**.
77. Yarin, A.; Koombhongse, S.; Reneker, D. *J. Appl. Phys.* **2001**, 9, 4836-4846.
78. Doshi, J.; Reneker, D. H. *J. Electrostatics* **1995**, 2, 151-160.
79. Schenke-Layland Lab. <http://www.schenke-layland-lab.com/>. **2010**.
80. Willemse, A. C. *Electrospinning bicomponent nanofibres for platinum ion extraction from acidic solutions*, MSc Thesis, University of Stellenbosch, South Africa. **2013**.



81. Theron, S.; Yarin, A.; Zussman, E.; Kroll, E. *Polymer*. **2005**, 9, 2889-2899.
82. Mitchell, S.; Sanders, J. *J Biomed Mater Res A*. **2006**, 1, 110-120.
83. Alamein, M. A.; Liu, Q.; Stephens, S.; Skabo, S.; Warnke, F.; Bourke, R.; Heiner, P.; Warnke, P. H. *Adv. Healthcare Mater*. **2012**.
84. Smit, A. E.; Sanderson, R. D. *Method and apparatus for the production of fine fibres*. **2009**.
85. Chronakis, I. S.; Milosevic, B.; Frenot, A.; Ye, L. *Macromolecules*. **2006**, 1, 357-361.
86. Agarwal, S.; Wendorff, J. H.; Greiner, A. *Polymer*. **2008**, 26, 5603-5621.
87. Frenot, A.; Chronakis, I. S. *Curr. Opin. Colloid Interface Sci*. **2003**, 1, 64-75.
88. Kilic, A.; Oruc, F.; Demir, A. *Text. Res. J*. **2008**, 6, 532-539.
89. Teo, W.; Ramakrishna, S. *Composites Sci. Technol*. **2009**, 11, 1804-1817.
90. Macossay, J.; Marruffo, A.; Rincon, R.; Eubanks, T.; Kuang, A. *Polym. Adv. Technol*. **2007**, 3, 180-183.
91. Thompson, C.; Chase, G.; Yarin, A.; Reneker, D. *Polymer*. **2007**, 23, 6913-6922.
92. Beachley, V.; Katsanevakis, E.; Zhang, N.; Wen, X. *Biomedical Applications of Polymeric Nanofibers*; Springer. **2012**, 171-212.
93. McKee, M. G.; Wilkes, G. L.; Colby, R. H.; Long, T. E. *Macromolecules*. **2004**, 5, 1760-1767.
94. Dersch, R.; Steinhart, M.; Boudriot, U.; Greiner, A.; Wendorff, J. *Polym. Adv. Technol*. **2005**, 2-3, 276-282.
95. Huang, C.; Chen, S.; Lai, C.; Reneker, D. H.; Qiu, H.; Ye, Y.; Hou, H. *Nanotechnology*. **2006**, 6, 1558.
96. Ryu, Y. J.; Kim, H. Y.; Lee, K. H.; Park, H. C.; Lee, D. R. *Eur Polym J*. **2003**, 9, 1883-1889.

97. Koombhongse, S.; Liu, W.; Reneker, D. H. *J Polym Sci Part B: Polym Phys.* **2001**, 21, 2598-2606.
98. Taylor, G. *Proc. R. Soc. Lon. A. Math. Phys Sci.* **1969**, 1515, 453-475.
99. Ding, W.; Wei, S.; Zhu, J.; Chen, X.; Rutman, D.; Guo, Z. *Macromol Mater Eng.* **2010**, 10, 958-965.
100. Rutledge, G. C.; Li, Y.; Fridrikh, S.; Warner, S.; Kalayci, V.; Patra, P. *Annual Report (M98-D01).* **2001**, 1-10.
101. Sohraby, K.; Minoli, D.; Znati, T. *WSN: technology, protocols, and applications*; John Wiley & Sons. **2007**.

## **CHAPTER III: SYNTHESIS AND CHARACTERIZATION OF FUNCTIONALIZED POLYMER NANOFIBERS THROUGH THE INCORPORATION OF SODIUM METABISULFITE AS COUNTERION**

### ***3.1 Introduction***

In recent years post-polymerization modification of polymers has been done to produce polymers with specific properties toward the application it is intended for. Considerable attention has also been paid to electrospinning in the last decade as a versatile processing method to produce polymer nanofibers.<sup>1</sup>

This chapter describes the preparation of functionalized polymer nanofibers that have been modified before or after electrospinning. The modification of polymer nanofibers has generated much interest due to the versatility of the process and the unique properties that are obtained through the process.<sup>2</sup> These properties can be used in applications for food packaging, biomedical devices, electronics, catalysis, sensor devices, bio-mimicking, post-surgical anti-adhesion barriers, drug delivery, bone grafting, tissue engineering scaffolds and advanced biological and therapeutic applications.<sup>3</sup>

Modification of a polymer before electrospinning can change the polymer properties considerably thus affecting the electrospinnability of that polymer. When the polymer properties change, the electrospinning parameters might be different compared to the parent polymer.<sup>4</sup> Through adjustment of these electrospinning parameters, such as flow rate, spinning distance, voltage, and humidity as well as polymer solution properties, such as concentration (viscosity), surface tension and solution conductivity, most polymers should be electrospinnable.

Electrospinning is a highly versatile technique to produce polymer nanofibers with properties such as very large surface-to-volume ratio, small pore sizes of the electrospun membrane, decreased structural defects and superior mechanical characteristics.<sup>4,5</sup> Although the technique is simple it is a rather intricate process that depends on the polymer's molecular properties, solvent properties and technical parameters.<sup>4</sup>

One of the main characteristics of poly(styrene-*alt*-maleic anhydride) (SMA), the polymer selected for this study, is that it is relatively easy to modify due to the reactivity of the maleic anhydride moiety. SMA is an inexpensive, biocompatible and thermoplastic polymer with high heat resistance and high dimensional stability.<sup>3,5-8</sup> When the polymer is modified before electrospinning, covalent bond formation is preferred between the parent polymer and the modification agent as covalent bonding prevents a loss of durability of the modified polymer's properties. Any suitable modification agent should have a reactive group that can be covalently attached to SMA through a ring-opening reaction of the maleic anhydride unit.<sup>4,9,10</sup> Polymer nanofibers with new functionalities can thus be synthesized through selecting chemical compounds with primary amines or alcohol moieties to functionalize SMA. For ring-opening to occur on the anhydride group strong nucleophilic anhydride reactive coupling agents are needed. Amines have a greater nucleophilic character compared to alcohols, and are therefore the coupling agent of choice.<sup>4-8</sup>

The modification agents used for the functionalization of SMA were selected based on possible interaction of the modified polymer with sodium metabisulfite, which releases SO<sub>2</sub> gas if environmental moisture is present. The modification agents have a primary amine functional group available for nucleophilic attack on the reactive maleic anhydride moiety of SMA, resulting in a ring-opening reaction that takes place within the 5-membered ring, yielding an amide. Further stabilization occurs when the amide undergoes heat treatment to yield a stable 5-membered cyclic imide.<sup>4,10-12</sup> A further substitution reaction was done where the cyclic imide reacted with an alkyl halide to yield a modified SMI polymer (SMI-qC<sub>12</sub>) with a positively charged aliphatic quaternized ammonium moiety. The negatively charged sodium metabisulfite can interact as counter ion with the quaternized ammonium group.

In this chapter we report the synthesis, characterization and electrospinning of poly(styrene-*alt*-maleic anhydride) (SMA), functionalized styrene-[*N*-3-(*N,N'*-dimethylamino) propyl maleimide] copolymer (SMI) and quaternized styrene-[(*N*-dodecyl)-*N,N*-dimethyl]-3-propyl maleimide] copolymer (SMI-qC<sub>12</sub>).<sup>9</sup> The general procedure entailed that SMA was first modified with an *N*-alkyl amine to obtain a polymer having a tertiary amine moiety after which a quaternization reaction followed. SMI-qC<sub>12</sub> polymer was subsequently dissolved with sodium metabisulfite in a suitable solvent system to be electrospun into functionalized polymer nanofibers functionalized with sodium metabisulfite. The various modified polymers were characterized using <sup>1</sup>H-NMR and <sup>13</sup>C-NMR spectroscopy and attenuated reflectance Fourier transform infrared spectroscopy

(ATR-FTIR). The functionalized electrospun polymer nanofibers were characterized using scanning electron microscopy (SEM).

### 3.2 Synthesis of SMA polymer

The synthesis started with the alternating copolymerization of maleic anhydride (MAh) with styrene (St) using conventional radical copolymerization to yield SMA polymer.<sup>9</sup> Refer to Figure 3.1 for the schematic illustration of the monomer units that were used for the conventional radical copolymerization of SMA ( $M_w = 198049$  g/mol,  $\bar{D} = 4.09$ , MAh content: 50%).

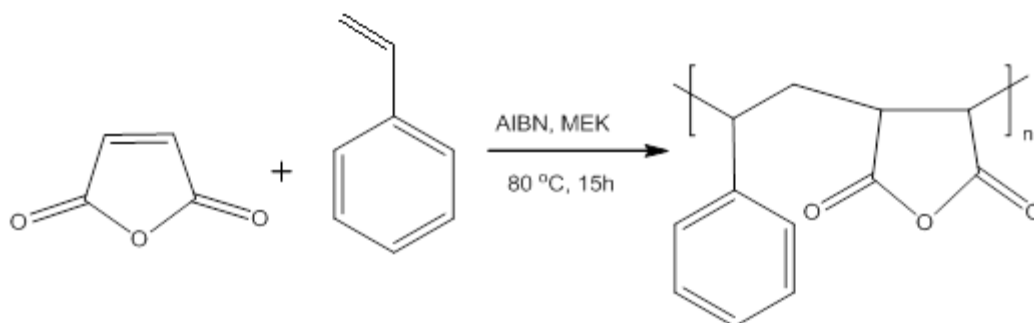


Figure 3.1 Conventional radical copolymerization of SMA and the repeat unit of SMA.

### 3.3 Synthesis of SMI polymer and functionalized SMI- $qC_{12}$ polymer

#### 3.3.1 Synthesis of SMI polymer

After its synthesis, SMA was modified at the cyclic maleic anhydride moiety via a nucleophilic addition reaction of a primary *N*-alkylamine resulting in a ring-opening reaction of the 5-membered ring to form a secondary amide and a carboxylic acid group, also known as maleamic acid.<sup>10</sup> Further stabilization occurred when the amide generated upon reaction of the primary amine with the maleic anhydride group underwent heat treatment and water loss to yield a stable 5-membered cyclic maleimide. The ring-closed maleimide is far more stable than the ring-opened compound and is less susceptible to hydrolysis.<sup>11-13</sup> The schematic illustration of the modification reaction of SMA is shown in Figure 3.2.

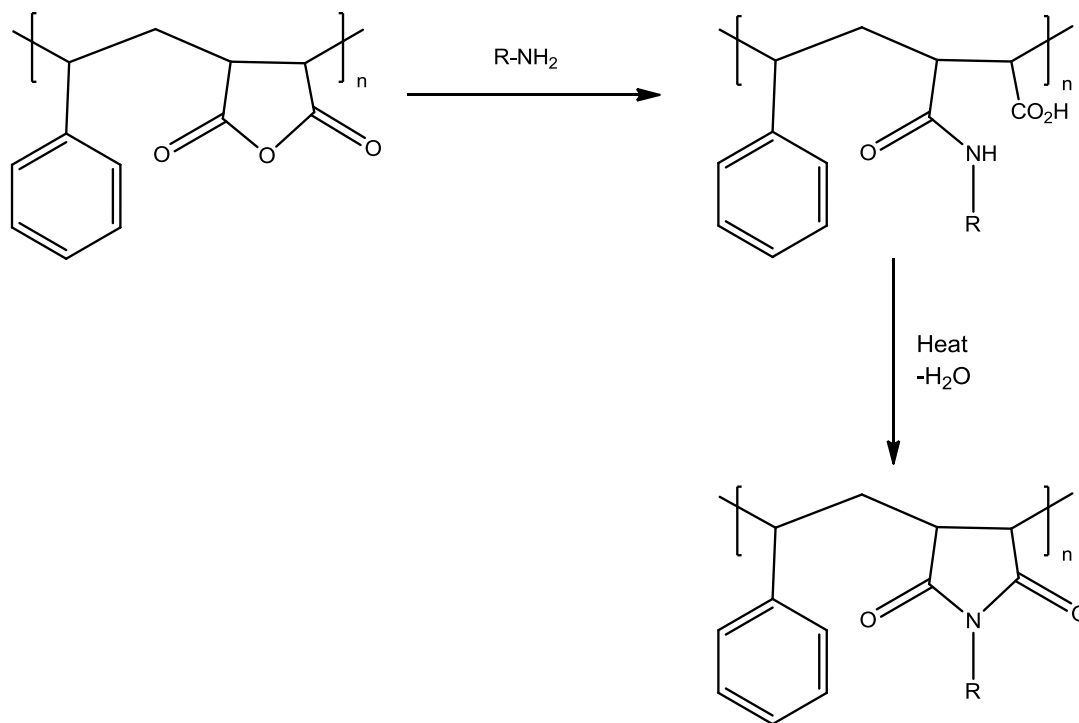


Figure 3.2 Schematic illustration of the modification of SMA via nucleophilic addition of a primary N-alkylamine to the reactive maleic anhydride group of SMA.

SMA was dissolved in dimethylformamide (DMF) and reacted with 3-(*N,N*-dimethylamino)-1-propylamine (DMAPA).<sup>10,11</sup> The ring-opening amidation reaction took place at room temperature and without a catalyst. The ring-opened SMA polymer modified with an N-alkyl compound synthesized in this study was insoluble in DMF and precipitated as a white polymer upon addition of the N-alkylamine to a solution of SMA in DMF. With an increase in temperature to 125 °C, the white precipitate started to dissolve and became a yellow solution. The reaction mixture was refluxed at 170 °C for 6 hours to achieve ring closure to form the cyclic maleimide.<sup>11,14</sup> After precipitation of the modified SMI polymer in diethyl ether to remove any unreacted monomer, the polymer was filtered and dried under vacuum at 40 °C for 24 hours to remove any residual solvent and yield styrene-[*N*-3-(*N,N*'-dimethylamino) propyl maleimide] copolymer (SMI).

### 3.3.2 Synthesis of SMI-qC<sub>12</sub> polymer

SMI-qC<sub>12</sub> was prepared via the SMI precursor using an addition-substitution reaction with a suitable bromoalkane, namely bromododecane (Br-C<sub>12</sub>). The schematic illustration of the SMA modification reaction and quaternization of the SMI precursor is shown in Figure 3.3.

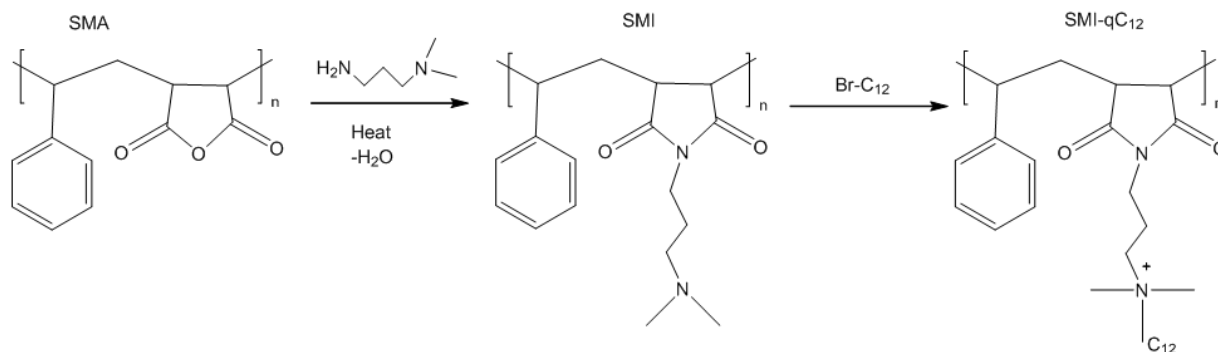


Figure 3.3 The schematic illustration of the SMA modification reaction to yield the relevant SMI precursor and the quaternization step via the SMI precursor to yield SMI-qC<sub>12</sub>.

In previous work done in 2008 by Bshena and co-workers, bromobutane, bromooctane and bromododecane alkyl halides were used as quaternization agents.<sup>15</sup> Murata and co-workers investigated the effect of charge density on the polymer chain and chain length of polymeric quaternized brushes and found the surface charge density to be a critical element in designing a surface for maximum killing efficiency.<sup>16</sup> It was also shown through the work of Bshena that longer aliphatic chains showed more promising results toward antimicrobial efficiency. Br-C<sub>12</sub> was therefore selected as the alkyl halide of choice. The addition reaction resulted in the quaternization of the tertiary amine functional group on the maleimide moiety of SMI to yield the relevant quaternized styrene-[(N-dodecyl)-N,N-dimethyl]-3-propyl maleimide] copolymer (SMI-qC<sub>12</sub>). The quaternized polymer was subsequently dissolved in a suitable solvent system and electrospun to yield functionalized polymer nanofibers.

### 3.4 Electrospinning of the modified polymer

#### 3.4.1 Introduction to single needle electrospinning

For the basic illustration setup and discussion of single needle electrospinning refer to Chapter 2, Section 2.11.1. As discussed previously, a variety of parameters play an intricate role in the electrospinning process. The parameters do not act or influence the electrospinning process individually but there is interplay between them.<sup>4</sup> Some of these parameters include flow rate of the polymer solution, electrical field applied and properties of the solvent that should possess a specific balance between the solution conductivity, viscosity, surface tension and vapour pressure.<sup>5</sup>

The quaternized SMI-qC<sub>12</sub> was dissolved in a DMF/THF mixture with a 1:1 ratio. Solvents had to be used that dissolved the polymer as well as the salt. Table 3.1 shows the solvent systems that were investigated.

*Table 3.1 The solvents that were selected for dissolving the active salt and electrospinning both the salt and SMI-qC<sub>12</sub> polymer*

Solvent/Mixture	Solubility of salt	Solubility of Polymer
Methanol	No	No
Ethanol	Yes	No
DMF	Partially	Yes
THF	Partially	Yes
Acetonitrile	No	No
Chloroform	No	Yes
Acetone	No	Yes
Isopropanol	No	No
DMSO	Yes	Partially
Ethylene glycol	Yes	No
DMF/THF	Yes	Yes



The polymer nanofibers were crosslinked using a heat treatment under vacuum according to a poorly understood in-house developed protocol. After heat treatment, the fibers became insoluble in water and organic solvents including THF/DMF. This is essential since the fibers will be exposed to high humidity environments within packaging and need to maintain their nanofibrous structure.<sup>4</sup> The mechanism by which the fibers undergo crosslinking has not been established to this date.

### 3.4.2 Introduction to single ball electrospinning

Ball electrospinning, known as free surface needleless electrospinning, is a relatively new high throughput technique for the production of nanofibers. The concept of ball electrospinning is the same as single needle electrospinning and has been discussed in detail in Chapter 2, Section 2.11.2. Refer to Figure 3.4 for the lab scale single ball electrospinning setup used in this study.

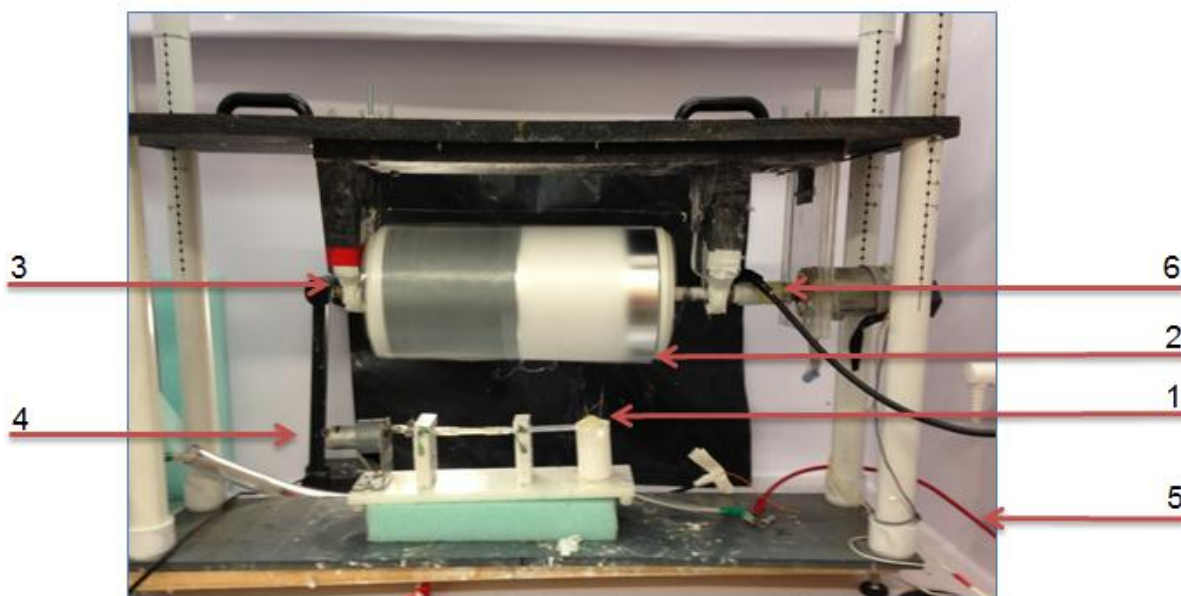


*Figure 3.4 The lab scale ball electrospinning setup used in this study. The setup consists of 1) the glass ball within the solution holder, 2) the aluminum covered collector collecting the nanofiber, 3) the rotation drum that is covered with aluminum foil, 4) the motor that rotates the glass ball, 5) the positive electrode coupled to the solution via the solution holder and 6) the negative electrode coupled to the collector.*

The glass ball (1) is connected via a glass rod to an electrical device (4) that induces rotation of the glass ball within the solution holder filled with polymer solution, resulting in a constant layer of polymer solution being formed on the surface of the glass ball. The rotation speed can be adjusted and therefore become a variable parameter. A positive electrode from a high voltage power supply is connected to the solution holder (5) and the negative electrode of the same high voltage power supply (6) is connected to the collector (3). The rotating drum is covered with aluminum foil (2). In the single needle electrospinning setup the applied electric field deforms the droplet at the tip of the needle into a cone-like shape. This phenomenon is only possible when the surface tension, which is contracting in nature, is overcome by the repulsive electrostatic force applied via the high voltage power supply. Only then is Taylor cone formation observed and a charged jet is ejected from the deformed polymer droplet at the needle tip. Although ball electrospinning does not entail any sharp edges the same phenomenon of charged polymer jets ejected from a deformed polymer surface is observed due to electrical waves moving over the surface of the polymer solution-coated glass ball as explained in Section 2.11.2 of Chapter 2. The ball electrospinning process affords hassle-free simultaneous jets operating under self-regulated and self-assembled cone-jet conditions.

### 3.4.3 Electrospinning of neat polymer, and polymer and salt

The neat SMI-qC<sub>12</sub> polymer synthesized in Section 3.3 was single needle and single ball electrospun after which a suitable solvent system was chosen for the electrospinning of the polymer (SMI-qC<sub>12</sub>) and sodium metabisulfite combination. The optimum solvent was found to be a 1:1 mixture of DMF/THF for the neat polymer and the polymer-and-salt combination. With this solvent system a higher concentration of salt could be dissolved within the polymer solution.

Table 3.2 Electrospinning results regarding the single needle and single ball electrospinning of the neat polymer and the functionalized polymer with the sodium metabisulfite

Electrospinning (E/s) results			
	E/s process	Concentration (wt. %)	Fiber diameter (nm)
Neat polymer	Single needle	20	238 ± 47
	Single ball	25	373 ± 76
Polymer and salt	Single needle	20	410 ± 98
	Single ball	25	465 ± 175

From the table above the electrospinning results can be seen (refer Table 3.2). A concentration of 20 wt. % was found to be sufficient for an acceptable number of polymer chain entanglements for the single needle electrospinning process.<sup>21</sup> A concentration of 25 wt. % was found to be sufficient for an acceptable number of polymer chain entanglements for the single ball electrospinning process.<sup>21</sup> The fiber diameter increased slightly from single needle electrospinning to ball electrospinning. This observation can possibly be explained due to multiple jets initiating from the surface of the polymer-coated glass ball in single ball electrospinning (refer Section 2.11.2 in Chapter 2). To obtain the same fiber diameters in single ball electrospinning a high voltage is needed for the multiple jets to whip and elongate sufficiently. If a lower voltage is used an increase in fiber diameter is observed. The nanofibers were dried under vacuum to remove any residual solvents.

#### 3.4.4 Modification of polymer nanofibers after electrospinning

The polymer nanofibers obtained in Section 3.4.3 were further functionalized to increase the amount of salt incorporated on the polymer nanofibers' surface. To be able to incorporate the active salt with the polymer nanofibers it is necessary that the nanofibrous structure of the polymer nanofibers is preserved throughout the reaction. The polymer nanofibers were found to be soluble. The solvent/water soluble electrospun SMI-qC<sub>12</sub> polymer nanofibers were crosslinked using an additional heat treatment at 130 °C under vacuum for 24 hours to achieve

crosslinking of the polymer. After heat treatment, the fibers became insoluble in water and organic solvent including THF/DMF.

An ion exchange reaction occur between the counter bromide anion from the SMI-qC<sub>12</sub> polymer and the anionic sodium metabisulfite salt (Refer to Figure 3.5). Subsequently the insoluble polymer nanofibers were submerged in a saturated solution of sodium metabisulfite in DMF/THF for set periods of time. These fibers were finally washed with clean DMF/THF solvent and dried.

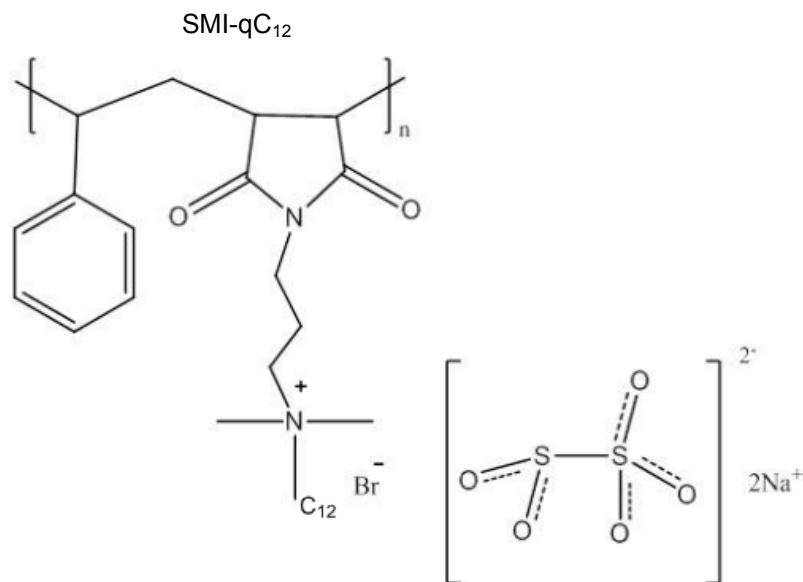


Figure 3.5 A schematic illustration of the ions present to interchange during the ion exchange between the bromide and the sodium metabisulfite ions.

### 3.5 SO<sub>2</sub> detection test

For the polymers nanofibers to function as antifungal platforms they must be able to release SO<sub>2</sub> gas. The detection of SO<sub>2</sub> is based on a method that was published in accordance with Article 15 (2) of The Commission Regulations (EC) No 606/2009 on 10 July 2009.<sup>2</sup> The wine industry uses this method to detect the free amount of SO<sub>2</sub> and total amount of SO<sub>2</sub> present in wine samples although the total amount might not be released into the atmosphere as a volatile gas. Refer to Figure 3.6 for a picture of the setup used for the detection of SO<sub>2</sub>. The same method was used for the detection of SO<sub>2</sub> that are given off by the nanofibers functionalized with the sodium metabisulfite salt.

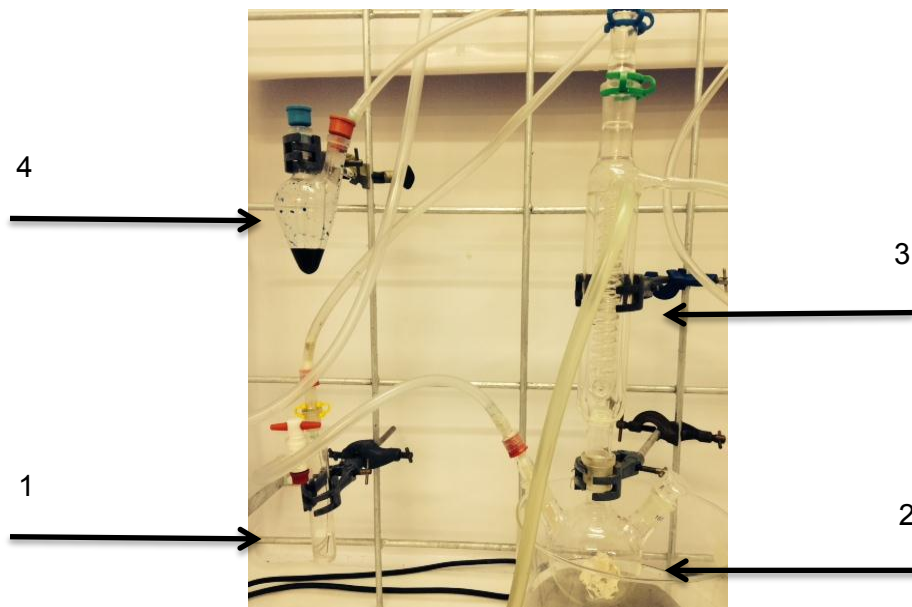


Figure 3.6 The experimental setup for the  $\text{SO}_2$  detection test.

Argon is bubbled through water into the system (1) and is thus water saturated before entering the system. This establishes a water saturated atmosphere within the round bottom containing the nanofibers. The nanofibers are placed inside the closed system (2). The sodium metabisulfite will release  $\text{SO}_2$  if in contact with water vapour. The Ar is used to carry any free  $\text{SO}_2$  that is released from the fibers through a condenser (3) into a solution of hydrogen peroxide, indicator and sodium hydroxide (NaOH) (4). The NaOH is used to neutralize the hydrogen peroxide solution to pH 7. This is done to ensure any colour change occurring to be due to the  $\text{SO}_2$  reacting with the hydrogen peroxide, oxidizing the  $\text{SO}_2$  into sulfurous acid ( $\text{H}_2\text{SO}_3$ ) thus changing the indicator. If NaOH is not used the flask containing the hydrogen peroxide will start in acid conditions. After set times, the indicator solution will be back titrated to neutral using NaOH. The volume NaOH used to neutralize the sulfurous acid that formed are back calculated using this back titration method to calculate the amount of  $\text{SO}_2$  that was given off by the fibers.

### 3.6 Characterization of SMA and the modified SMI polymers

SMA, SMI and SMI-qC<sub>12</sub> were characterized using <sup>13</sup>C and <sup>1</sup>H nuclear magnetic resonance spectroscopy (NMR) and attenuated total reflectance Fourier transform infrared (ATR-FTIR). The electrospun mats were characterized using scanning electron microscopy (SEM).

#### 3.6.1 Characterization of SMA

SMA was synthesized using conventional radical copolymerization.<sup>9</sup>

##### 3.6.1.1 <sup>1</sup>H-NMR

Refer to Figure 3.7 for the <sup>1</sup>H-NMR spectrum of SMA and the assignments of the relevant peaks.

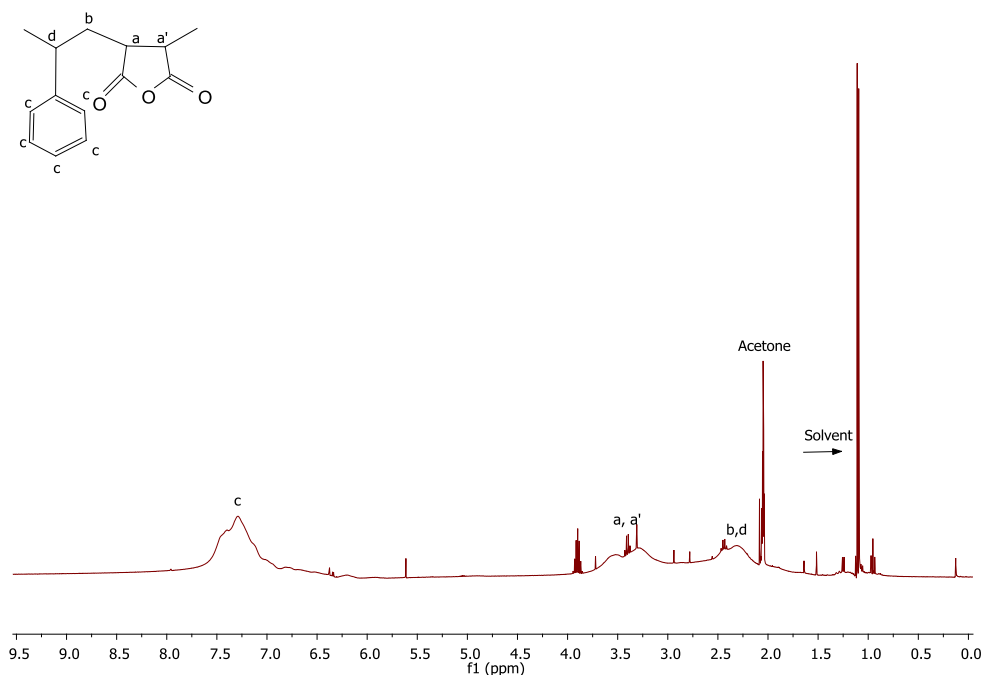


Figure 3.7 <sup>1</sup>H-NMR spectrum of SMA and the assignment of the relevant peaks.

SMA is characterized by a broad peak at a chemical shift of 6.8 - 7.3 ppm that relates to the aromatic ring protons of the styrene unit (c). The methine and methylene protons originate from

the maleic anhydride and styrene monomers forming the backbone of the polymer respectively (a, a', b, d).<sup>5</sup> It is observed as two broad peaks at 3.0 - 3.5 ppm and 1.9 - 2.2 ppm that are poorly resolved due to peak overlapping. The maleic anhydride's methine hydrogens are deshielded by the anisotropy of the adjacent carbonyl moiety, whereas the methine hydrogen of the styrene unit is deshielded by the anisotropic field of the aromatic ring, but the shift is smaller, due to one proton that gets removed by one of the carbons from the aromatic ring, reducing the deshielding effect. The methine and methylene protons of the styrene unit are observed as one broad peak due to the deshielding effect of the aromatic ring. The results are in good agreement with literature.<sup>9</sup>

The <sup>1</sup>H-NMR spectrum (Refer to Figure 3.7) was used to calculate the respective maleic anhydride contents by integrating the ratio of the aromatic protons of the styrene moiety to the methine protons of the maleic anhydride unit. It was found that an alternating SMA copolymer with a 1:1 ratio of maleic anhydride to styrene (50%) was synthesized in this study.

### 3.6.1.2 $^{13}\text{C}$ -NMR

The results obtained from the  $^1\text{H}$ -NMR spectrum were confirmed by interpreting the  $^{13}\text{C}$ -NMR spectrum. The  $^{13}\text{C}$ -NMR spectrum of SMA and the assignment of the relevant peaks are shown in Figure 3.8.

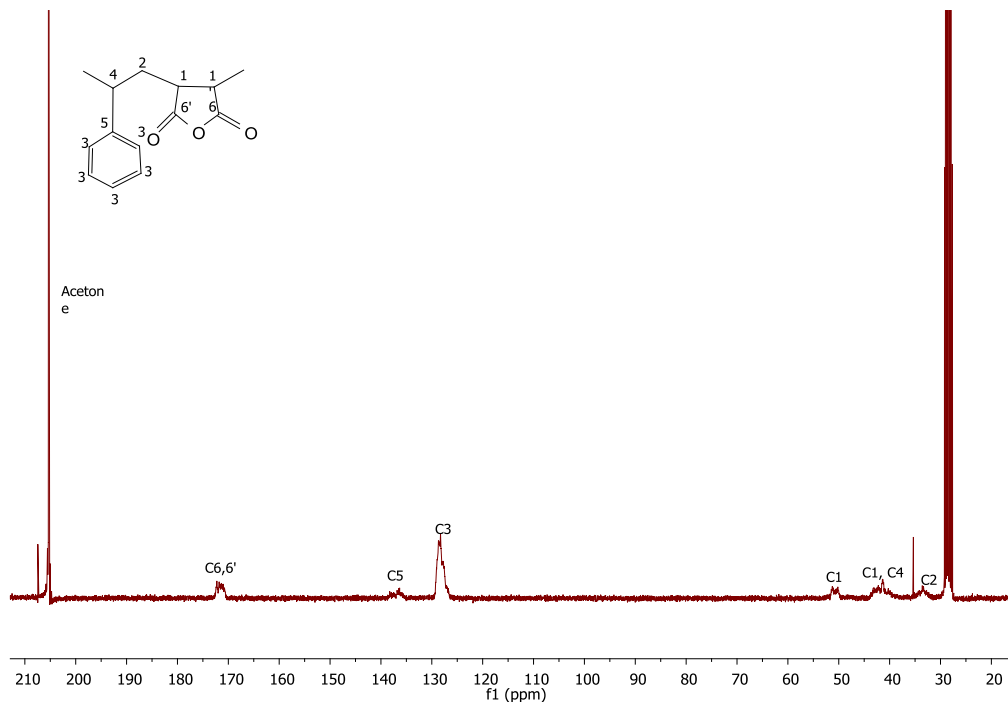


Figure 3.8  $^{13}\text{C}$ -NMR spectrum of SMA and the assignment of the relevant peaks.

A peak is observed at 172.2 ppm and is designated to the carbonyl carbons of the maleic anhydride unit (C6). Peaks observed at 137.4 ppm and 128.4 ppm correspond to the aromatic carbons of the styrene unit (C5, C3) and peaks at 50.8 ppm, 39.4 - 43.1 ppm and 33.4 ppm are designated to the methylene and methine carbons of the SMA copolymer backbone (C1, C4, C2). These peaks are in good correspondence with literature.<sup>17</sup>



### 3.6.2 Characterization of SMI

The presence of amines, ammonium moieties and the imide nitrogens make the interpretation of the NMR spectra a bit challenging in the relevant styrene-maleic anhydride copolymers. Peak overlapping also made quantitative analysis difficult.

Amine compounds have two distinctive types of hydrogen atoms, namely those that are attached to the nitrogen itself and then those attached to the carbons adjacent to the nitrogens, called the alpha ( $\alpha$ ) carbon. The chemical shifts of the N-H are usually very variable and can appear over a wide chemical shift, mostly 0.5 - 4.0 ppm. Solvents used, temperature, acidity and the extent of hydrogen bonding taking place influences the position of these NH peaks. NH peaks are usually broad and weak. The protons on the  $\alpha$ -carbon are slightly more deshielded than the rest of the carbons due to the electronegativity of the nitrogen atom resulting in a downfield appearance of the peak.<sup>12,18</sup>

#### 3.6.2.1 $^1\text{H-NMR}$

Figure 3.9 shows the  $^1\text{H-NMR}$  spectrum of styrene-[*N*-3-(*N,N'*-dimethyl amino) propyl maleimide] copolymer (SMI) and the assignments of the relevant peaks.

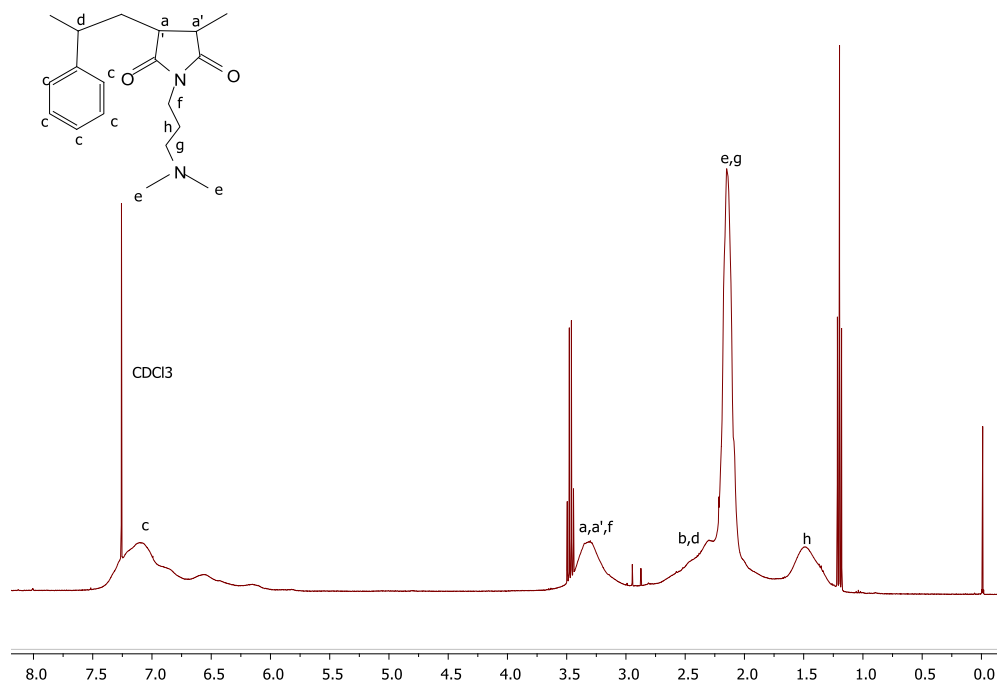


Figure 3.9  $^1\text{H-NMR}$  spectrum of styrene-[*N*-3-(*N,N'*-dimethylamino) propyl maleimide] copolymer (SMI).

The  $^1\text{H-NMR}$  spectrum of SMI is characterized by three relatively broad peaks at 6.6 - 7.4 ppm, 3.01 - 3.5 ppm and 2.19 - 2.7 ppm, respectively, due to the aromatic protons on the styrene unit (c), the methine protons of the maleimide unit (a, a' and f) and the methylene protons from the styrene (b, d), in the polymer backbone. The broad peak at 1.5 ppm is characteristic of the methylene protons (h) of the propyl chain, whereas the peak at 2.03 - 2.19 ppm corresponds to the methyl protons (e) and the methylene protons (g) adjacent to the tertiary amine.<sup>19,20</sup> The electronegativity of the nitrogen deshields the proton on the adjacent carbon ( $\alpha$ -carbon), resulting in the methylene proton (g) overlapping with the methyl protons. The methylene protons (f) adjacent to the imide nitrogen are influenced by the electron rich nitrogen, having an effect on the chemical shift of the methylene protons, due to deshielding and resulting in peak shifting more downfield. The methine protons of the maleic unit (a, a') and the methylene protons (f) therefore overlap at 3.01 - 3.5 ppm.

3.6.2.2  $^{13}\text{C}$ -NMR

The results of the  $^1\text{H}$ -NMR spectrum were confirmed by interpretation of the  $^{13}\text{C}$ -NMR spectrum of SMI. Refer to Figure 3.10 for the  $^{13}\text{C}$ -NMR spectrum of SMI and the assignment of the relevant peaks.

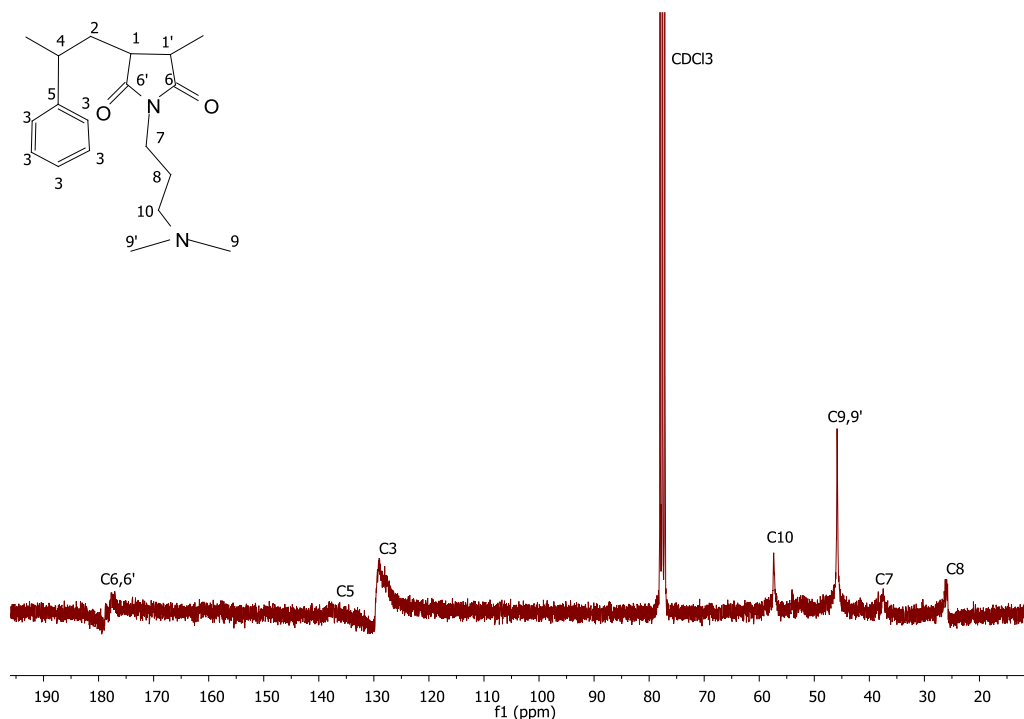


Figure 3.10  $^{13}\text{C}$ -NMR spectrum of styrene-[*N*-3-(*N*',*N*'-dimethylamino) propyl maleimide] copolymer (SMI).

A peak at 177.3 ppm is indicative of the imide carbons (C6) and the peaks at 136 ppm and 129 ppm are indicative of the aromatic ring carbons from the styrene unit (C5 and C3). Imidization that took place is confirmed by the peaks at 57.3 ppm and 45.8 ppm, which are characteristic of the *N*-alkyl amine's methyl carbons (C10) and methylene carbons (C9) that are present, that was not present in SMA. A peak at 37.5 ppm and 26 ppm corresponds to the methylene carbon adjacent to the imide nitrogen (C7) and the methylene carbon (C8) of the aliphatic chain, respectively.<sup>20-22</sup>

The  $^1\text{H}$ -NMR and  $^{13}\text{C}$ -NMR spectra of the SMI copolymer confirmed the successful modification of SMA with 3-(*N,N*-dimethylamino)-1-propylamine to yield styrene-[*N*-3-(*N*',*N*'-dimethylaminopropyl) maleimide] copolymer (SMI).

### 3.6.3 Characterization of SMI-qC<sub>12</sub>

SMI was subsequently reacted with a suitable bromoalkane, which resulted in the quaternization of the tertiary amine moiety of SMI to yield the relevant modified styrene-maleimide copolymer. In this study *N*-bromododecane was used for quaternization to obtain styrene-[*N*-3-(*N'*-dodecyl-*N',N'*-dimethylammonium) propyl maleimide] copolymer (SMI-qC<sub>12</sub>).<sup>18</sup>

#### 3.6.3.1 <sup>1</sup>H-NMR

Refer to Figure 3.11 for the <sup>1</sup>H-NMR spectrum of styrene-[*N*-3-(*N'*-dodecyl-*N',N'*-dimethylammonium) propyl maleimide] copolymer (SMI-qC<sub>12</sub>) and the assignments of the relevant peaks.

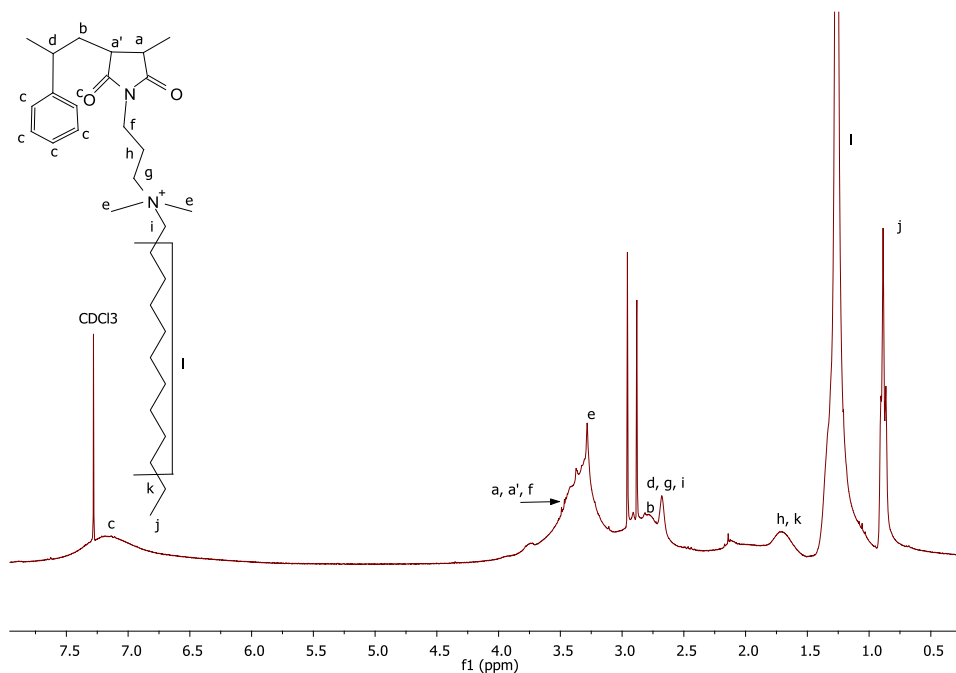


Figure 3.11 <sup>1</sup>H-NMR spectrum of styrene-[*N*-3-(*N'*-dodecyl-*N',N'*-dimethylammonium) propyl maleimide] copolymer (SMI-qC<sub>12</sub>).

The <sup>1</sup>H-NMR spectrum of SMI-qC<sub>12</sub> is characterized by four peaks at 6.9 - 7.4 ppm, 3.35 - 3.50 ppm, 2.85 ppm and 2.6 ppm, respectively, and corresponds to the aromatic protons on the styrene unit (c), the methine and methylene protons of the maleimide unit (a, a' and f), the methylene protons in the polymer backbone (b) and the methine protons from the styrene unit and the methylene protons from the alkyl chain (d, g, i).

The broad peak at 1.65 ppm is characteristic of the methylene protons (h, k) of the propyl chain and dodecyl chain, whereas the peak at 3.35 ppm corresponds to the methyl protons (e) that are adjacent to the quaternary ammonium moiety.<sup>20,23</sup> A peak at 0.83 ppm is attributed to the methyl protons (j) at the end of the aliphatic chain and the strong intensity of the peak at 1.23 ppm corresponds to the methylene protons (l) of the aliphatic chain. The presence of these three peaks confirms the successful quaternization of SMI to yield SMI-qC<sub>12</sub>.

The electronegativity of the nitrogen in the aliphatic chain deshielded the proton on the adjacent carbon ( $\alpha$ -carbon), resulting in the methylene proton from the styrene unit (d) overlapping with the methylene protons (g, i). The methylene protons (f) adjacent to the imide nitrogen are influenced by the electron rich nitrogen, having an effect on the chemical shift of the methylene protons, due to deshielding and resulting in the peak shifting more downfield. The methine protons of the maleimide unit (a, a') and the methylene protons (f) therefore overlap at 3.35 - 3.50 ppm.

After quaternization of the tertiary amine moiety of SMI with *N*-bromododecane, the peak at 2.03 - 2.19 ppm that corresponds to the methyl protons (e) and the methylene protons (g) adjacent to the tertiary amine shifted downfield to 3.35 ppm (Refer to Figure 3.9 and Figure 3.11).<sup>20,23</sup> This chemical shift position is characteristic of methyl and methylene protons attached to an ammonium moiety.<sup>20,23</sup> Confirmation of the quaternization reaction that took place is the presence of the methyl protons (j) at 0.83 ppm.

3.6.3.2  $^{13}\text{C}$ -NMR

The  $^{13}\text{C}$ -NMR spectrum confirmed the results obtained from the  $^1\text{H}$ -NMR spectrum. Figure 3.12 represents the  $^{13}\text{C}$ -NMR spectrum of styrene-[*N*-3-(*N'*-dodecyl-*N',N'*-dimethyl ammonium) propyl maleimide] copolymer (SMI-qC<sub>12</sub>) and shows the assignment of the relevant peaks.

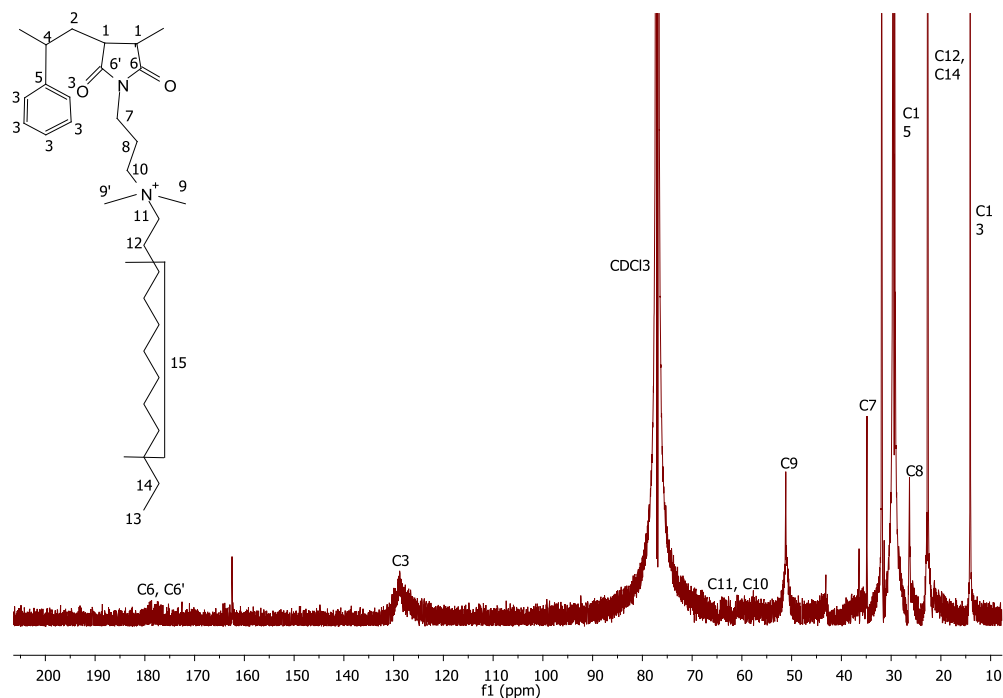


Figure 3.12  $^{13}\text{C}$ -NMR spectrum of styrene-[*N*-3-(*N'*-dodecyl-*N',N'*-dimethylammonium) propyl maleimide] copolymer (SMI-qC<sub>12</sub>).

The *N*-alkyl amine's methyl carbons' (C9) and methylene carbons' (C10) at 45.8 ppm and 57.3 ppm (Refer to Figure 3.11), shifted downfield to 51.2 ppm (C9) and 58.6 ppm (C10) (when quaternization took place). These peak shifts serve as confirmation that the quaternization reaction occurred.<sup>23,24</sup> The presence of two new peaks at 63.3 ppm and 14.1 ppm is due to the methylene carbon (C11) of the aliphatic chain attached to the ammonium nitrogen and the methyl carbon (C13) of the same chain.<sup>18</sup> Other prominent peaks are the peaks at 22.7 ppm and 29.6 ppm due to the methylene carbons of the aliphatic chain (C12, C14) and the methylene carbons of the rest of the chain (C15). These peaks also serve as confirmation that quaternization took place to yield SMI-qC<sub>12</sub> copolymer.

### 3.6.4 Characterization of polymers using ATR-FTIR spectroscopy

SMA, SMI and SMI-qC<sub>12</sub> were dried at 60 °C under vacuum to remove any residual solvent and characterized using ATR-FTIR. Refer to Figure 3.13 for the representative ATR-FTIR spectra of

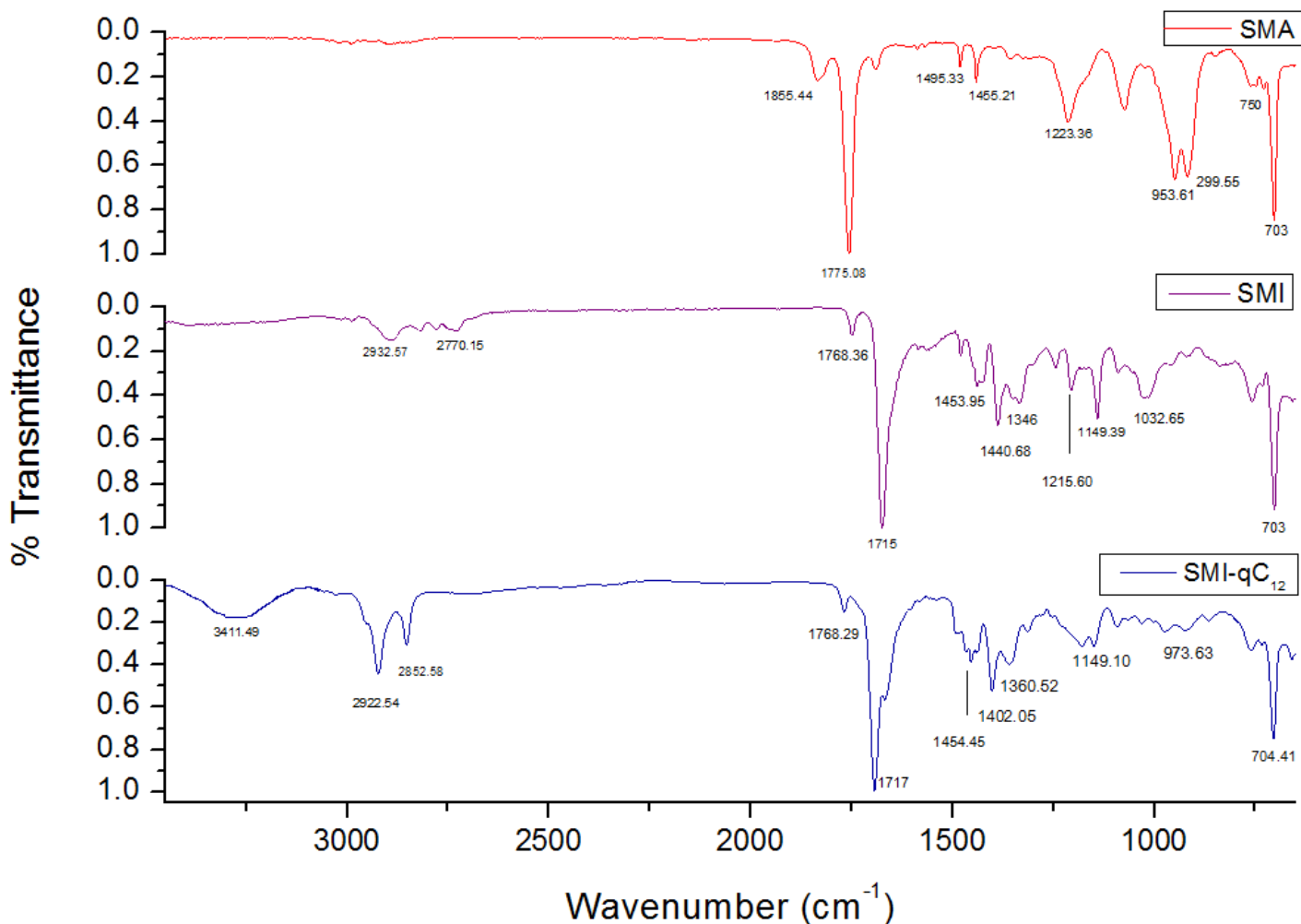


Figure 3.13 ATR-FTIR spectra of (a) SMA (top), (b) SMI (middle), (c) SMI-qC<sub>12</sub> (bottom).

(a) SMA, (b) SMI and (c) SMI-qC<sub>12</sub>.

SMA is characterized by a pair of bands of the carbonyls absorbing at 1775.08 cm<sup>-1</sup> and 1855.44 cm<sup>-1</sup> and can be seen in Figure 3.13 (a). This is due to the symmetrical and asymmetrical carbonyl stretch vibrations of the anhydride moiety. A characteristic band appears at 1223.36 cm<sup>-1</sup> corresponding to the C-O stretch vibrations of the cyclic five-membered anhydride. The small peak at 3061 cm<sup>-1</sup> is due to sp<sup>2</sup> aromatic C-H bend vibrations of the

styrene unit and the bands at  $2929.31\text{ cm}^{-1}$  is due to the  $\text{sp}^3$  aliphatic C-H bending vibrations of the polymer chain. The peaks at  $1455.21\text{ cm}^{-1}$  and  $1495.33\text{ cm}^{-1}$  correspond to the C=C stretching vibrations of the styrene aromatic ring and the C-H stretching vibrations of the polymer chain. The peaks at  $703\text{ cm}^{-1}$  and  $750\text{ cm}^{-1}$  are characteristic of the C-H out-of-plane stretching vibrations of a mono substituted aromatic ring of the styrene group. These results are in good agreement with literature.<sup>5,7,9,25</sup>

After imidization of SMA with 3-(*N,N*-dimethylamino)-1-propylamine, followed by a heat-induced ring closure, the C-O peak at  $1775.08\text{ cm}^{-1}$  disappeared. A new strong band at  $1715\text{ cm}^{-1}$  appeared that is characteristic of a cyclic imide bond (Refer to Figure 3.13 (b)). The cyclic imide formed due to an amidation reaction of a primary amine, 3-(*N,N*-dimethylamino)-1-propylamine, and the maleic anhydride unit of SMA after heat-induced ring closure of the maleamic acid that formed. Further confirmation of the ring closure that occurred is the absence of an N-H bending absorption of a secondary amine at  $\sim 1550\text{ cm}^{-1}$ .<sup>17,26,27</sup> The peak at  $1223.36\text{ cm}^{-1}$  is characteristic of the C-O stretch vibration for SMA due to the cyclic anhydride disappearing when the anhydride moiety was modified via the addition of the primary amine. A new peak at  $1346\text{ cm}^{-1}$  is evident of the bending absorption of methyl groups, due to the presence of the carbon chains.<sup>22,25,28</sup> A peak indicative of a tertiary amine vibrating band appeared at  $1149.39\text{ cm}^{-1}$ . The peaks at  $2932.57\text{ cm}^{-1}$  and  $2770.15\text{ cm}^{-1}$  are indicative of the  $\text{sp}^3$  aliphatic C-H bending vibrations of the added propyl hydrocarbon chain. These peaks are not as evident in the spectrum because the attached propyl chain only has three addition methylene groups, which would not increase the intensity of the peaks at  $2902.57\text{ cm}^{-1}$  and  $2770.15\text{ cm}^{-1}$ .

After quaternization of the tertiary amine in SMI, a new peak appeared at  $3411.19\text{ cm}^{-1}$  that is indicative of a quaternized ammonium nitrogen (Refer to Figure 3.13 (c)).<sup>28</sup> This peak confirms the successful quaternization of the SMI precursor. Further confirmation of the quaternization reaction that took place is the disappearance of the tertiary amine vibrating band at  $1149.39\text{ cm}^{-1}$ . The peak at  $1360\text{ cm}^{-1}$  is characteristic of the bending absorption of methyl groups, due to the presence of the carbon chains.<sup>22,25,28</sup> The peaks at  $2922.54\text{ cm}^{-1}$  and  $2852.58\text{ cm}^{-1}$  are indicative to the  $\text{sp}^3$  aliphatic C-H bending vibrations of the  $\text{C}_{12}$  hydrocarbon chain. These peaks are more prominent in the spectrum because the attached hydrocarbon chain increased in chain length.

When comparing these three spectra, a shift in the carbonyl absorption band can be seen, namely a peak disappearing at  $1775.08\text{ cm}^{-1}$  and appearing at  $1715\text{ cm}^{-1}$  that is characteristic of a cyclic imide bond. Peaks designated to  $\text{sp}^3$  aliphatic C-H bending vibrations appeared and the higher intensity of the  $\text{sp}^3$  aliphatic C-H bending vibrations in SMI-q $\text{C}_{12}$  are most probably due to



length of the aliphatic C<sub>12</sub> - chain. A peak indicative of a tertiary amine vibrating band appeared at 1149.39 cm<sup>-1</sup> in the SMI spectrum and disappeared in the SMI-qC<sub>12</sub> spectrum. In the SMI-qC<sub>12</sub> spectrum a peak appeared at 3111.19 cm<sup>-1</sup> that is indicative of quaternized ammonium nitrogens.

### 3.6.5 SEM analysis: Characterization of single needle and single ball electrospun SMI-qC<sub>12</sub> polymer nanofibers

SMI-qC<sub>12</sub> was dissolved in a suitable solvent system (1:1 DMF: THF solution) at a concentration adequate for polymer chain entanglements and single needle electrospun and single ball electrospun. Conditions at which single needle electrospinning was done varied in electric field strength and spinning distance. SEM images with regard to fiber diameter morphology indicated that the optimum electrospinning concentration was 20 wt. % for SMI-qC<sub>12</sub> (Refer to Figure 3.14). The conditions at which the single ball electrospinning process was conducted varied in electric field strength, spinning distance, humidity and rotating speed of the glass ball. SEM images with regard to fiber diameter and fiber morphology indicated that the optimum spinning distance was 10 cm and an electrospinning polymer concentration of 25 wt. %. SEM images indicated that the average fiber diameter of the single needle electrospun SMI-qC<sub>12</sub> polymer nanofibers was  $238 \pm 47$  nm and for the single ball electrospun SMI-qC<sub>12</sub> polymer nanofibers was  $373 \pm 76$  nm.

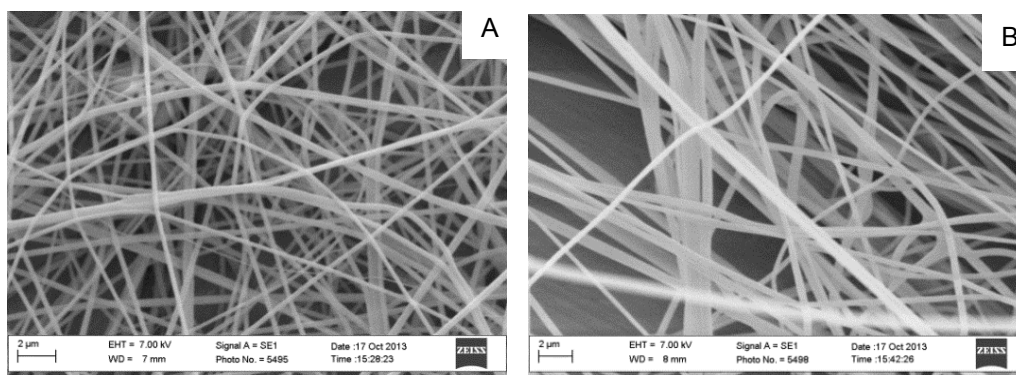


*Figure 3.14 SEM images of SMI-qC<sub>12</sub> polymer nanofibers using single needle and single ball electrospinning. Image A was obtained using the single needle electrospinning process: Polymer concentration 20 wt. %; applied voltage 20 kV, ambient humidity <50%, temperature 24 °C, 10 cm spinning distance and a flow rate of 0.07 mL.min<sup>-1</sup>. Image B was obtained using the single ball electrospinning process: Polymer concentration 25 wt. %, applied voltage 50 kV, 10 cm spinning distance and an ambient humidity <50%.*

### 3.6.6 SEM analysis: Characterization of single needle and single ball electrospun SMI-qC<sub>12</sub> and added salt polymer nanofibers

Different concentrations of SMI-qC<sub>12</sub> polymer and sodium metabisulfite in a 1:1 DMF/THF solvent solution were prepared and single needle and single ball electrospun. Conditions at which the single needle electrospinning process was done varied in electric field strength and spinning distance. SEM images with regard to fiber diameter and fiber morphology indicated that the optimum electrospinning concentration of the polymer was 20 wt. % and 0.6 wt. % for the salt (Refer to Figure 3.15). The conditions at which the single ball electrospinning process was conducted varied in electric field strength, spinning distance, humidity and rotating speed of the glass ball. SEM images with regard to fiber diameter and fiber morphology indicated that the optimum electrospinning concentration was 25 wt. % for SMI-qC<sub>12</sub> and 0.6 wt. % for the salt. SEM images indicated that the average fiber diameter of the single needle electrospun SMI-qC<sub>12</sub> polymer and salt nanofibers was  $410 \pm 98$  nm and for the single ball electrospun SMI-qC<sub>12</sub> polymer and salt nanofibers was  $465 \pm 175$  nm

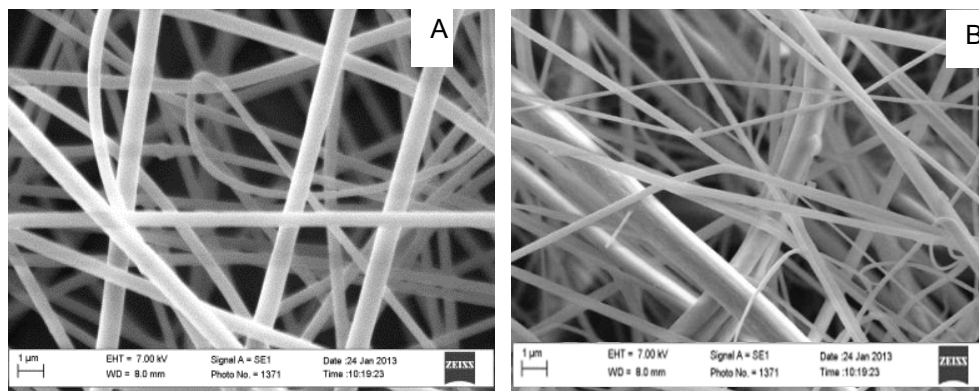


*Figure 3.15 SEM images of SMI-qC<sub>12</sub> polymer and salt nanofibers formed using single needle and single ball electrospinning. Image A was obtained using the single needle electrospinning process: Polymer concentration, 20 wt. %; salt, 0.6 wt. %, applied voltage 20 kV, temperature 24 °C, 10 cm spinning distance, ambient humidity <50% and a flow rate of 0.07 mL.min<sup>-1</sup>. Image B was obtained using the single ball electrospinning process: Polymer concentration, 25 wt. %; salt, 0.6 wt. %, applied voltage 50 kV, 10 cm spinning distance and an ambient humidity <50%.*

### 3.6.7 SEM analysis: Crosslinked single ball electrospun SMI-qC<sub>12</sub> and salt polymer nanofibers

The process of single ball electrospinning has been designed to increase the fiber production capacity of the conventional electrospinning process. The single ball electrospinning experiments resulted in smooth fibers without any beads. With the advantage that the single ball electrospinning process has over the conventional single needle electrospinning, the ball electrospinning setup was used for the production of fibers for further experiments. The SMI-qC<sub>12</sub> ball electrospun nanofibers were dried under vacuum at 130 °C for 24 hours to render water and solvent insoluble polymer nanofibers. The mechanism through which the crosslinking occurs cannot be explained, but was observed in two other studies in the research group.<sup>15,29</sup> Refer to Figure 3.16 for the SEM image of the cross-linked fibrous mats.

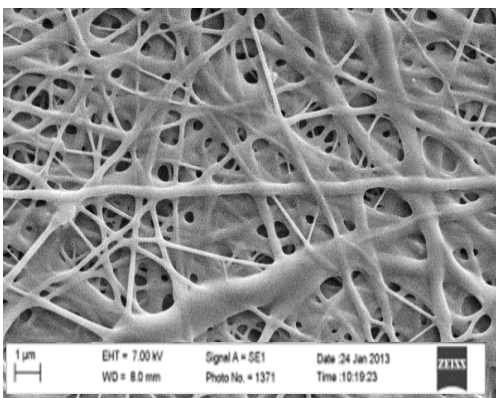


*Figure 3.16 SEM images of SMI-qC<sub>12</sub> and add salt polymer nanofibers cross-linked under vacuum at 130 °C for 24 hours.*

### 3.6.8 SEM analysis: Characterization of single ball electrospun SMI-qC<sub>12</sub> polymer nanofibers submerged in saturated salt solution

Fibers that were crosslinked as detailed in Section 3.4.4 (Refer to Figure 3.16 in Section 3.6.7) were submerged in a saturated sodium metabisulfite solution for different periods of time. The SEM images (Refer to Figure 3.17) indicated the presence of sodium metabisulfite crystals on the surface of the fibers. These salt crystals were not present in earlier SEM images. It can be seen from the images that increasing the time from 20 to 40 minutes increased the amount of salt crystals formed on the surface of the nanofibers.

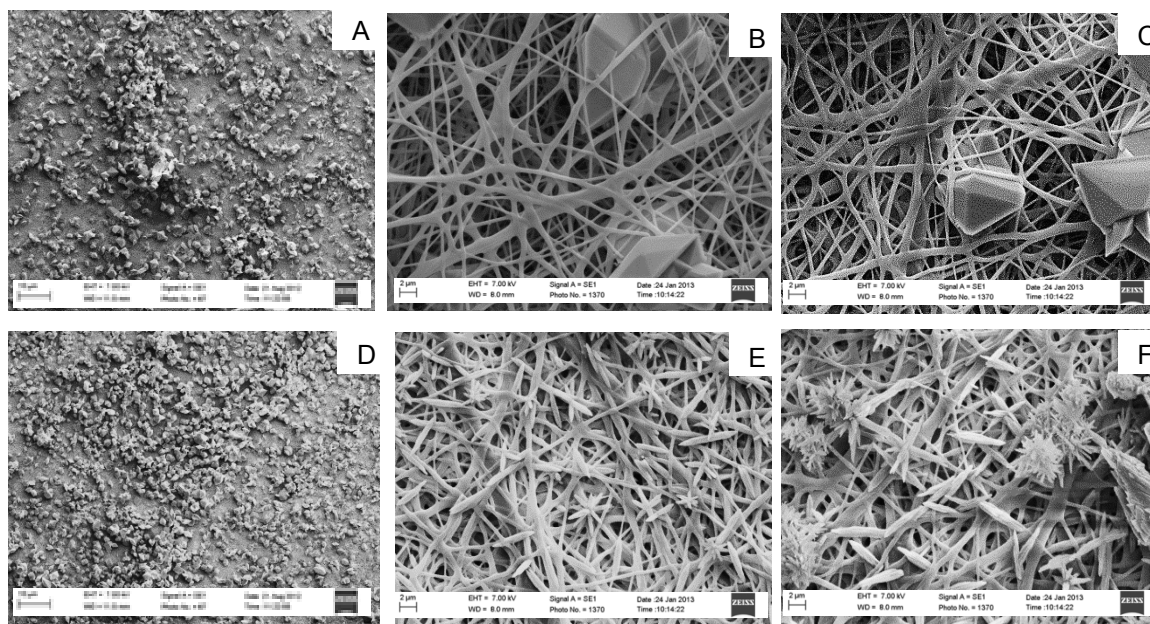


Figure 3.17 SEM images of the submerged SMI-qC<sub>12</sub> nanofibers containing sodium metabisulfite salt on the surface of the nanofibers. Images A - C were obtained after submerging the fibers for 20 minutes. Images D - F were obtained after submerging the fibers for 40 minutes. The images differ only in the magnification at which the images were taken.

### 3.7 SO<sub>2</sub> test results

Different variations of SO<sub>2</sub> generating pads exist but all SO<sub>2</sub> generating sheets entails sulfite (sodium metabisulfite) and in the presence of moisture SO<sub>2</sub> gas is released. The SO<sub>2</sub> release data were obtained using the SO<sub>2</sub> detection method described in Section 3.5. Refer Table 3.3 for the data on the SO<sub>2</sub> release and Figure 3.18 for the representation of the SO<sub>2</sub> release data in a graph.

*Table 3.3 SO<sub>2</sub> release data regarding functionalized SMI-qC<sub>12</sub> fibers with incorporated sodium metabisulfite*

Time (hours)	Incremental quantity of SO <sub>2</sub> released (mg)	Cumulative amount of SO <sub>2</sub> released (mg)
0	0	0.00
1	0.64	0.64
2	4.64	5.28
5	2.56	7.87
7	2.56	10.40
9	1.6	12.00
11	0.64	12.64
12	5.76	18.40
24	4.8	23.20
48	0.64	23.84
72	0.65	24.49
96	0.64	25.13

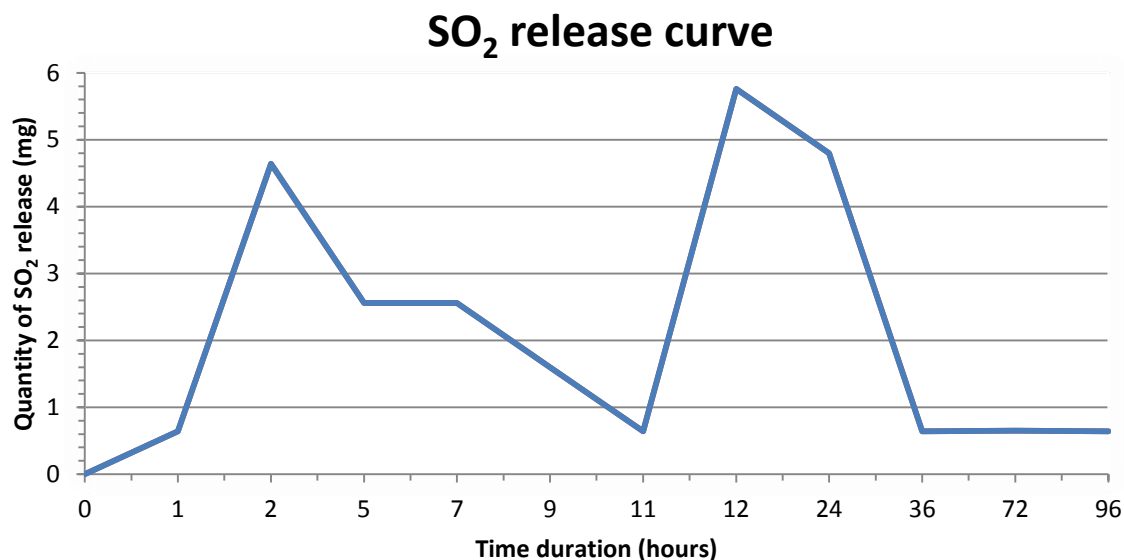


Figure 3.18 Graph illustrating the incremental quantity of SO<sub>2</sub> gas that is released in the first 96 hours if moisture is present in the system.

Back titration using NaOH to calculate the quantity of SO<sub>2</sub> that is released indicated that over 72 hours 25.13 mg of SO<sub>2</sub> was released. An initial quick release of SO<sub>2</sub> gas was observed (Refer to Figure 3.18) after which the quantity of SO<sub>2</sub> gas released decrease every two hours up to 11 hours. After 12 hours the quantity of SO<sub>2</sub> gas released increased quickly and then decreased again up to 96 hours. The initial functionalized polymer nanofibers had 215 mg of sodium metabisulfite incorporated. In 96 hours 11.7% of the total sodium metabisulfite was released as SO<sub>2</sub> gas when in contact with atmospheric moisture. Having 11.7% of the total SO<sub>2</sub> released in 4 days and only releasing low concentrations of SO<sub>2</sub> after 36 hours it is expected to have slow SO<sub>2</sub> release for up to weeks (8 - 10).<sup>30</sup>

The advantage of the polymers nanofibers compared to the SO<sub>2</sub> generating sheets is the small amount of fibers needed to incorporate sodium metabisulfite.

### 3.8 Conclusion

SMA was successfully synthesized using conventional radical copolymerization and modified to yield SMI-qC<sub>12</sub> via an SMI intermediate. This modification entailed a nucleophilic addition reaction of an *N*-alkyl amine agent to the reactive maleic anhydride moiety of the SMA. The functionalized SMI polymer was heat treated to achieve ring closure of the maleamic acid that

formed to yield a stable cyclic imide. SMI was further modified via an addition-substitution reaction with a suitable alkyl halide to yield SMI-qC<sub>12</sub> with an aliphatic quaternary ammonium moiety.

The SMI-qC<sub>12</sub> polymer and salt were simultaneously dissolved and electrospun into a nanofibrous mat with an average fiber diameter of ~ 465 nm. Using SEM for analysis it was seen that smooth, bead-free fibers were obtained. These polymer nanofibers were subsequently crosslinked in an additional heat treatment step at 130 °C under vacuum. The crosslinked fiber mats were submerged in a saturated sodium metabisulfite solution to increase the amount of salt present on the surface of the nanofibers.

The successful synthesis and modification of SMA was confirmed with <sup>1</sup>H-NMR and <sup>13</sup>C-NMR spectroscopy and ATR-FTIR. Electrospun nanofibrous mats were characterized using SEM. The nanofibrous structure of the fibers before and after crosslinking and the preservation of the nanofibrous structure after the polymer nanofibers were submerged in the saturated salt solution were confirmed using SEM.

The work discussed in this chapter thus confirms the successful synthesis and modification of the SMA, SMI and SMI-qC<sub>12</sub>. It is confirmed that a polymer with a reactive site can be modified using a modification agent with a suitable reactive group and that these modified polymers can be successfully electrospun into functionalized nanofibers that can be further modified after the electrospinning process. Nanofibers could therefore be modified post-electrospinning to incorporate salt for possible SO<sub>2</sub> gas release.

## **3.9 Experimental**

### **3.9.1 Chemicals**

Potassium hydroxide pellets >85% (Merck Chemicals), sodium hydroxide pellets >85% (Merck Chemicals), styrene monomer 99.5% (Fluka chemika), maleic anhydride 99% (Sigma-Aldrich), 3-(*N,N*-dimethylamino)-1-propylamine 99% (Sigma-Aldrich), methyl ethyl ketone ≥99.7% (Sigma-Aldrich), isopropanol (Kimix), sodium metabisulfite >99% (Sigma-Aldrich), 1-bromododecane 98% (Sigma-Aldrich), hydrogen peroxide 30% (Merck Chemicals) and diethyl ether (Kimix) were used without purification. 2, 2'-Azo-bis (isobutyronitrile) (AIBN) (Riedel de



Haen) was recrystallized twice using methanol and dried under vacuum before use. Tetrahydrofuran (Kimix), *N,N*-dimethylformamide (Kimix) and methanol (Kimix) were distilled and kept on 4 Å molecular sieves.

## 3.9.2 Characterization techniques

### 3.9.2.1 Scanning Electron Microscopy (SEM)

Images of neat SMI-qC<sub>12</sub> and SMI-qC<sub>12</sub> with sodium metabisulfite that was electrospun were obtained using a Leo® 1430VP Scanning Electron Microscope (SEM). For each fiber mat that was analysed, small squares, approximately 0.5 cm x 0.5 cm, were cut out and attached to a SEM stub using carbon double sided tape. The carbon tape is used to ensure that good conductivity between the SEM stub and the sample is established. Prior to imaging the SEM stubs with samples were sputter-coated with gold under vacuum for 3 minutes. After imaging, the images were analysed using an image analysis program, SEM Image Studio, to obtain data regarding fiber diameter. An average of 100 fiber diameters was measured per sample and the average fiber diameter and the standard deviation were calculated using Microsoft Excel 2010.

### 3.9.2.2 Attenuated total reflectance Fourier transform infrared (ATR-FTIR) spectroscopy

Infrared spectra were recorded using a Nicolet FTIR spectrometer (model Nexus) from Thermo-Fischer equipped with a Smart Golden Gate ATR accessory with a diamond/ZnSe internal reflection crystal. The spectra were recorded from 3750 cm<sup>-1</sup> to 700 cm<sup>-1</sup> with a spectral resolution of 8 cm<sup>-1</sup> and a sum of 64 individual scans.

Samples were run in solid state and no sample preparation was necessary. Omnic software was used for data acquisition and Origin software was used for processing the data.

### 3.9.2.3 Size exclusion chromatography (SEC)

Molar mass and dispersity ( $\mathcal{D}$ ) were obtained using size exclusion chromatography (SEC). SEC analysis was carried out on a THF solvent system. The SEC instrument consists of a Waters

1515 isocratic HPLC pump, a Waters 717 plus auto-sampler, Waters 600E system controller (run by Breeze Version 3.30 SPA) and a Waters in-line Degasser AF. A Waters 2414 differential refractometer was used at 30 °C in series with a Waters 2487 dual wavelength absorbance UV/Vis detector operating at variable wavelengths. Tetrahydrofuran (THF, HPLC grade, stabilized with 0.125% BHT) was used as eluent at flow rates of 1 ml min<sup>-1</sup>. The column oven was kept at 30 °C and the injection volume was 100  $\mu$ l. Two PLgel (Polymer Laboratories) 5  $\mu$ m Mixed-C (300 x 7.5 mm) columns and a pre-column (PLgel 5  $\mu$ m Guard, 50 x 7.5 mm) were used. Calibration was done using narrow polystyrene standards ranging from 580 to 2x10<sup>6</sup> g.mol<sup>-1</sup>. All molecular weights were reported as polystyrene equivalents. Data acquisition was done using Millennium software, version 4.

Samples were prepared dissolving samples in BHT stabilized THF (2mg/ml). Sample solutions were filtered via syringe through 0.45  $\mu$ m nylon filters before subjected to analysis.

#### 3.9.2.4 Nuclear magnetic resonance spectroscopy (NMR)

A Varian Inova 300 MHz and 400 MHz NMR spectrometer and Varian Inova 600 MHz NMR spectrometer were used for the NMR analysis. After the samples were run Mestrenova computer software (Version 6.0.2-5475) was used from interpretation of the spectra obtained. Characterization and integration was done using Mestrenova.

Deuterated dimethyl sulfoxide (Sigma-Aldrich®, 99.9 atom % DMSO-d<sub>6</sub>), deuterated acetone (Sigma-Aldrich®, 99.9 atom % Acetone-d<sub>6</sub>) and deuterated chloroform (Sigma-Aldrich®, 99.9 atom % CDCl<sub>3</sub>) were used for NMR sample preparations.

#### 3.9.3 Synthesis of styrene-*alt*-maleic anhydride copolymer (SMA)

Conventional radical copolymerization was used to synthesize an alternating copolymer of styrene and maleic anhydride monomers in a 1:1 molar ratio styrene: maleic anhydride.<sup>9</sup>

Maleic anhydride (MAh) (18.8 g, 192 mmol), styrene monomer (20 g, 192 mmol) and 2, 2' azobis (isobutyronitrile) (AIBN, 0.65 g, 3.96 mmol) were dissolved in 250 mL methyl ethyl ketone (MEK). The reaction mixture was purged with Argon (Ar) for 45 min at room temperature and emerged into a 60 °C preheated oil bath. The Ar needle was taken out of the solution, but

kept in the round bottom flask for another 50 min. After 50 min the Ar needle was removed and the reaction mixture was stirred overnight for 15 hours. The reaction mixture was allowed to cool down to room temperature after which the polymer was precipitated in diethyl ether. The polymer was dried under vacuum at 80 °C for 1.5 hours and left under vacuum for 16 hours to remove any unreacted monomer and residual solvent. Analyses were done using SEC.  $M_w = 198049$  g/mol,  $\bar{D} = 4.09$ , MAnh content: 50%.

Major IR absorptions: 2929.31, 1855.44, 1768.39, 1708.10, 1495.33, 1455.21, 1223.36, 1080.94, 953.61, 922.28, 749.55, 703.59  $\text{cm}^{-1}$ .

$^1\text{H-NMR}$  ( $\text{CDCl}_3$ ):  $\delta$  (ppm) = 6.8 - 7.3 (s broad, 5H aromatic), 3.0-3.5 (s broad, 2H, -**CH-CH**-), 1.9 - 2.2 (s broad, 3H, -**CH<sub>2</sub>-CH**-).

$^{13}\text{C-NMR}$  ( $\text{CDCl}_3$ ):  $\delta$  (ppm) = 172.2 (-**O-C=O**), 137.4 (aromatic -**C**-), 128.4 (aromatic -**C=**), 50.8 (-**CH-CH**-), 39.4 - 43.1 (-**CH**-), 33.4 (-**CH<sub>2</sub>**).

### 3.9.4 Synthesis of styrene-[*N*-3-(*N*',*N*'-dimethylamino) propyl maleimide] copolymer (SMI)

The synthetic work of Vermeesch and Evenson was used as basis for this procedure.<sup>10, 11</sup> Refer to Figure 3.19 for the schematic illustration of the synthetic route taken to yield SMI.

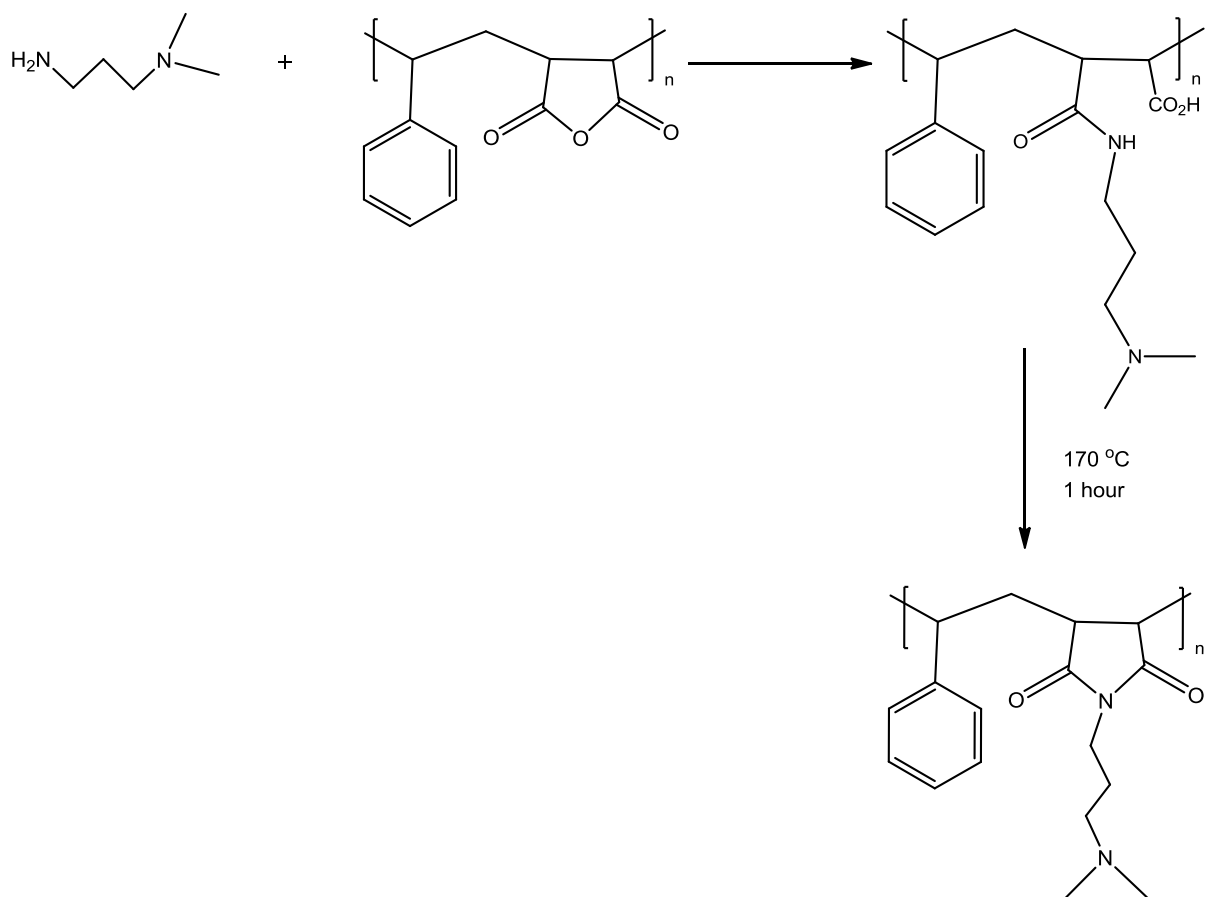


Figure 3.19 Synthesis of styrene-[*N*-3-(*N*',*N*'-dimethylamino) propyl maleimide] copolymer.

SMI was prepared by treating SMA with 3-dimethylaminopropylamine (DMAPA) as follows: SMA (7.189 g, 35.5 mmol) was dissolved in 100 mL DMF and an excess amount of 3-(*N*,*N*-dimethylamino)-1-propylamine (13 mL, 0.103 mmol) in 50 mL DMF was added dropwise to the solution over a period of 30 minutes.<sup>15</sup> Precipitation of the polymer out of solution was observed. The polymer suspension was heated gradually to bring the solution temperature to reflux for 6 hours. The suspension gradually became clear and turned a light yellow. The solution was allowed to cool down to room temperature after which precipitation in diethyl ether followed. The

polymer was filtered and re-dissolved in methanol and precipitated in diethyl ether to remove any unreacted monomer. The polymer was filtered and dried under vacuum at 40 °C for 24 hours to remove any residual solvent.

Major IR absorptions: 3444.66, 2932.57, 2770.15, 1768.36, 1708.10, 1494.38, 1453.95, 1400.68, 1346.00, 1254.85, 1215.50, 1149.39, 1032.76, 759.42, 704.41  $\text{cm}^{-1}$ .

$^1\text{H-NMR}$  ( $\text{CDCl}_3$ ):  $\delta$  (ppm) 6.6 - 7.4 (s broad, 5H, aromatic), 3.01 - 3.5 (s broad, 4H), 2.19 - 2.7 (s broad, 3H), 2.03 - 2.19 (s broad, 8H), 1.5 (s, 2H).

$^{13}\text{C-NMR}$  ( $\text{CDCl}_3$ ):  $\delta$  (ppm) = 177.3 (-N-C=O), 136 (aromatic -C-), 129 (aromatic -C=), 57.3 (-CH<sub>2</sub>-CH<sub>2</sub>-N-), 45.8 (-N-CH<sub>3</sub>), 37.5 (-N-CH<sub>2</sub>-CH<sub>2</sub>-), 26 (CH<sub>2</sub>-CH<sub>2</sub>-CH<sub>2</sub>).

### 3.9.5 Synthesis of styrene-[*N*-3-(*N'*-dodecyl-*N',N'*-dimethylammonium) propyl maleimide] copolymer (SMI-qC<sub>12</sub>)

Refer to Figure 3.20 for the schematic illustration of the synthetic route taken to yield SMI-qC<sub>12</sub>.

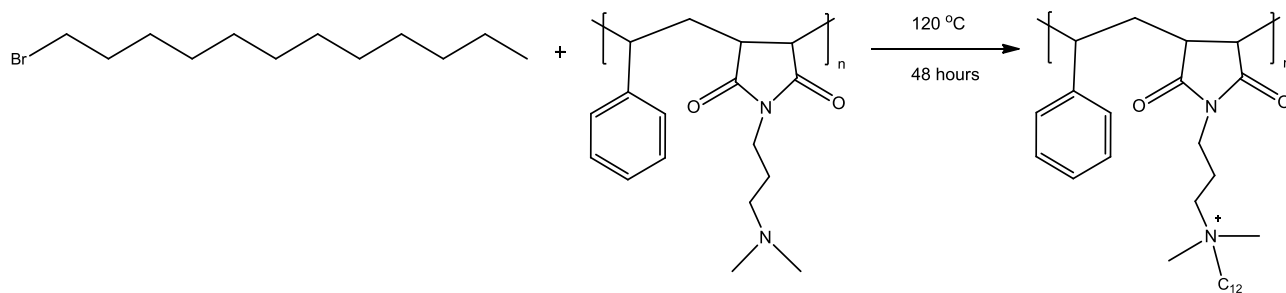


Figure 3.20 Synthesis of styrene-[*N*-3-(*N'*-dodecyl-*N',N'*-dimethylammonium)propyl maleimide] copolymer (SMI-qC<sub>12</sub>).

SMI-qC<sub>12</sub> was prepared by treating SMI with a 12-carbon alkyl bromide as follows:

1-Bromododecane (3.24 g, 13 mmol) in 5 mL DMF was added dropwise to a solution of styrene-[*N*-3-(*N',N'*-dimethylamino) propyl maleimide] copolymer (3 g, 10.4 mmol) in 50 mL DMF at room temperature. The polymer solution was heated gradually till 100 °C. The solution was

stirred overnight for 24h. The resulting light brown solution was allowed to cool down to room temperature and the quaternized polymer was precipitated in diethyl ether and dried under vacuum at 50 °C for 24h.

Major IR absorptions: 3411.19, 2922.54, 2852.58, 1767.29, 1708.10, 1454.45, 1402.05, 1360.52, 1179.65, 1149.18, 1091.43, 973.64, 759.84, 704.41  $\text{cm}^{-1}$ .

$^1\text{H-NMR}$  ( $\text{CDCl}_3$ ):  $\delta$  (ppm) 6.9-7.4 (s broad, 5H, aromatic), 3.35 - 3.50 (s, 4H), 3.35 (s, 6H), 2.85 (s broad, 2H), 2.6(s, 5H), 1.65 (s broad, 4H), 1.23 (s, 18H), 0.83 (s, 3H).

$^{13}\text{C-NMR}$  ( $\text{CDCl}_3$ ):  $\delta$  (ppm)= 178.09 (-N-C=O), 138.98 (aromatic -C-), 129.10 (aromatic -C-), 64.39 (-N-CH<sub>2</sub>-), 62.26 (-N-CH<sub>2</sub>-), 51.28 (-N-CH<sub>3</sub>), 45.99 (-CH-), 35.00 ((CO)<sub>2</sub>N-CH<sub>2</sub>-), 32.05 (-CH<sub>2</sub>-), 29.77 (-CH<sub>2</sub>-), 26.59 (-CH<sub>2</sub>-), 22.99 (-CH<sub>2</sub>-), 22.80 (-CH<sub>2</sub>-), 14.20 (-CH<sub>3</sub>).

### 3.9.6 Single needle electrospinning of styrene-[*N*-3-(*N'*-dodecyl-*N',N'*-dimethylammonium) propyl maleimide] copolymer (SMI-qC<sub>12</sub>)

SMI-qC<sub>12</sub> was dissolved in a 1:1 THF/DMF solution to a concentration of 20 wt. %. Electrospinning took place in a top to bottom direction. The prepared solution was placed in a single needle electrospinning setup prepared beforehand, refer to Section 2.11.1 in Chapter 2. The setup involved a 1 mL plastic syringe with a 21 Gauge blunted needle. The syringe is placed upside down and connected to a syringe pump (Harvard, Model 33 Twin Syringe Pump). The high voltage supply is capable of generating positive DC voltages from 0 to 25 kV, the positive electrode of the high voltage supply was connected to the blunt needle and the negative electrode of the same high voltage power supply was connected to an aluminum covered collector. The positive charge was set at 10 kV and the negative at 10 kV. The flow rate was set to 0.07 mL.min<sup>-1</sup>. The stationary aluminum covered collector was placed at a distance of 8 cm and 10 cm away from the needle tip. Environmental conditions while electrospinning were ambient humidity <50% and temperature 24 °C. The collected electrospun nanofibers were placed under vacuum at 40 °C to remove any residual solvent.

### 3.9.7 Single ball electrospinning of styrene-[*N*-3-(*N*'-dodecyl-*N*',*N*'-dimethylammonium) propyl maleimide] copolymer (SMI-qC<sub>12</sub>)

SMI-qC<sub>12</sub> was dissolved in 1:1 DMF/THF solution. The concentration of the polymer was 25 wt. %. The prepared solution was placed in the solution holder, refer to Section 2.11.2 in Chapter 2 for the detailed description of the setup and Figure 3.4 for the schematic illustration of the setup. The rotating drum collector was placed at a distance of 8 cm and 10 cm from the rotating glass ball. The positive electrode of the high voltage power supply was attached to the cup holder and the negative electrode of the same high voltage power supply was attached to the rotating drum collector. The high voltage power supply is capable of generating positive DC voltages from 0 to 25 kV and was set at maximum for the experiments. The rotating ball was attached to an electrical device to automatically turn the glass ball through the solution. The device was set at 7.5 kV and the drum collector device at 12 kV. Environmental conditions while electrospinning were ambient humidity <50% and temperature 24 °C. The nanofibers collected were placed under vacuum at 40 °C to remove any residual solvent that might be present.

The nanofibrous mats were placed under vacuum at 130 °C for 24 hours. After the procedure the nanofibrous mats became insoluble in water and organic solvents.

### 3.9.8 Single needle electrospinning of styrene-[*N*-3-(*N*'-dodecyl-*N*',*N*'-dimethylammonium) propyl maleimide] copolymer (SMI-qC<sub>12</sub>) and sodium metabisulfite

The same procedure was followed as in Section 3.9.6 with the same conditions. A concentration of 20 wt. % polymer was used. Sodium metabisulfite was dissolved with the polymer solution making a 0.6 wt. % concentration.

### 3.9.9 Single ball electrospinning of styrene-[*N*-3-(*N'*-dodecyl-*N',N'*-dimethylammonium) propyl maleimide] copolymer (SMI-qC<sub>12</sub>) and sodium metabisulfite

The same procedure was followed as in section 3.9.7 with the same conditions. A concentration of 25 wt. % polymer was used. Sodium metabisulfite was dissolved with the polymer solution to make a 0.6 wt. % concentration of salt within the polymer solution.

### 3.9.10 Modification after electrospinning

The crosslinked fibers were submerged in a saturate sodium metabisulfite solution in 1:1 THF/DMF for 20 - 40 min. The salt interacted with the fibers via an ionic exchange process and through increasing the submerging time an increase in the amount of salt crystals was observed.

### 3.9.11 SO<sub>2</sub> detection test

660 mg nanofibers containing sodium metabisulfite salt (445 mg polymer nanofibers functionalized with 215 mg salt) were placed in a closed round bottom. Argon was bubbled through water and was thus water saturated before entering the system. The sodium metabisulfite releases SO<sub>2</sub> gas upon reaction with the water vapour present in the system. The Ar is used to carry any SO<sub>2</sub> that is released through the condenser into the hydrogen peroxide solution. The hydrogen peroxide solution is diluted and neutralized using NaOH (5 mL H<sub>2</sub>O<sub>2</sub>, neutralized with NaOH). 4 Drops of indicator reagent (in 50 mL methanol, 24.9 mg Methylene Blue and 53.0 mg Methyl Red) is added to the H<sub>2</sub>O<sub>2</sub> solution. The SO<sub>2</sub> is oxidized by the hydrogen peroxide. The sulfuric acid formed is determined by titrating with a standard solution of sodium hydroxide (0.1 M). 445 mg polymer nanofibers were submerged for 30 minutes after which 215 mg sodium metabisulfite was incorporated.



### 3.10 References

1. Subbiah, T.; Bhat, G.; Tock, R.; Parameswaran, S.; Ramkumar, S. *J. Appl. Polym. Sci.* **2005**, *2*, 557-569.
2. Yao, C.; Li, X.; Neoh, K.; Shi, Z.; Kang, E. *J. Membr. Sci.* **2008**, *1*, 259-267.
3. Yoo, H. S.; Kim, T. G.; Park, T. G. *Adv. Drug Deliv. Rev.* **2009**, *12*, 1033-1042.
4. Cronje, L. *Surface modification of styrene maleic anhydride nanofibers for efficient capture of Mycobacterium tuberculosis*, PhD Thesis, University of Stellenbosch, South Africa. **2012**.
5. Tang, C.; Ye, S.; Liu, H. *Polymer.* **2007**, *15*, 4482-4491.
6. Donati, I.; Gamini, A.; Vetere, A.; Campa, C.; Paoletti, S. *Biomacromolecules.* **2002**, *4*, 805-812.
7. Stoilova, O.; Ignatova, M.; Manolova, N.; Godjevargova, T.; Mita, D.; Rashkov, I. *Eur. Polym. J.* **2010**, *10*, 1966-1974.
8. Lai, X.; Sun, C.; Tian, H.; Zhao, W.; Gao, L. *Int. J. Pharm.* **2008**, *1*, 66-73.
9. Jeong, J.; Byoun, Y.; Ko, S.; Lee, Y. *J. Ind. Een. Chem.* **2001**, *5*, 310-315.
10. Evenson, S.; Badyal, J. *J. Phys. Chem. B.* **1998**, *28*, 5500-5502.
11. Vermeesch, I.; Groeninckx, G. *J. Appl. Polym. Sci.* **1994**, *10*, 1365-1373.

12. Soer, W. J.; Ming, W.; Klumperman, B.; Koning, C.; van Benthem, R. *Polymer*. **2006**, *22*, 7621-7627.
13. Henry, S. M.; El-Sayed, M. E.; Pirie, C. M.; Hoffman, A. S.; Stayton, P. S. *Biomacromolecules*. **2006**, *8*, 2407-2414.
14. Pompe, T.; Zschoche, S.; Herold, N.; Salchert, K.; Gouzy, M.; Sperling, C.; Werner, C. *Biomacromolecules*. **2003**, *4*, 1072-1079.
15. Bshena, O. E. S. *Synthesis of Permanent Non-Leaching Antimicrobial Polymer Nanofibers*, PhD Thesis, University of Stellenbosch, Stellenbosch. **2012**.
16. Murata, H.; Koepsel, R. R.; Matyjaszewski, K.; Russell, A. J. *Biomaterials*. **2007**, *32*, 4870-4879.
17. Vermeesch, I.; Groeninckx, G.; Coleman, M. *Macromolecules*. **1993**, *24*, 6643-6649.
18. Pavia, D. L. *Introduction to spectroscopy*. Brooks/Cole Pub Co; **2009**.
19. Shenoy, S. L.; Bates, W. D.; Frisch, H. L.; Wnek, G. E. *Polymer*. **2005**, *10*, 3372-3384.
20. Huang, F.; Wu, H.; Wang, D.; Yang, W.; Cao, Y. *J. Mater. Chem*. **2004**, *4*, 708-716.
21. Qin, C.; Xiao, Q.; Li, H.; Fang, M.; Liu, Y.; Chen, X.; Li, Q. *Int. J. Biol. Macromol*. **2004**, *1*, 121-126.
22. Kim, C. H.; Choi, J. W.; Chun, H. J.; Choi, K. S. *Poly. Bull*. **1997**, *4*, 387-393.
23. Roy, S.; Dasgupta, A.; Das, P. K. *Langmuir*. **2006**, *10*, 4567-4573.

24. Huang, Z.; Zhang, Y.; Kotaki, M.; Ramakrishna, S. *Composites Sci. Technol.* **2003**, 15, 2223-2253.
25. Chen, G.; Zhang, Y.; Zhou, X.; Xu, J. *J. Appl. Surf. Sci.* **2006**, 3, 1107-1110.
26. Wang, K.; Huang, W.; Xia, P.; Gao, C.; Yan, D. *React. Funct. Polym.* **2002**, 3, 143-148.
27. Lee, S.; Ahn, T. O. *J. Appl. Polym. Sci.* **1999**, 7, 1187-1196.
28. Kim, T. G.; Park, T. G. *Biotechnol. Prog.* **2006**, 4, 1108-1113.
29. Cronje, L.; Klumperman, B. *Eur. Polym. J.* **2013**, 49, 3814-3824.
30. Mustonen, H.M. *Aust J. Exp. Agr.* **1992**, 32, 389-393.

## CHAPTER IV: SYNTHESIS AND CHARACTERIZATION OF ANTI-FUNGAL POLYMER NANOFIBERS AGAINST *Botrytis cinerea*

### 4.1 Introduction

Grape berries become infected primarily during harvest, packaging and storage periods, it is thus important to find a method that will be able to reduce *Botrytis cinerea* spreading on harvested grapes. Spoilage due to *B. cinerea* during storage and transportation starts from the inoculum present on the berries that came from the vineyard. The inoculum on the berries surface is present as a dormant infection with the possibility of later forming grey mould in packaged grapes.<sup>1</sup>

In the previous chapter, the release of sulphur dioxide (SO<sub>2</sub>) gas was discussed using the industrially known and used sodium metabisulfite salt that was incorporated with electrospun polymer nanofibers. The limitation of using SO<sub>2</sub> gas is that it exhibits anti-fungal activity against *B. cinerea*, but does not kill dormant infections present inside the berry tissue during storage that are able to develop into grey mould at a later stage when favourable conditions occur.<sup>2</sup> Due to the disadvantages of using SO<sub>2</sub>, a more effective method is needed.

In literature there is no method yet discussed to completely remove the inoculum present on the berries surface that is completely safe for consumption. The approach discussed in this chapter aims to synthesize a fungicidal compound that can be attached to a polymer system to keep the inoculum from spreading to adjacent healthy grape bunches.

Fungicides have been known and used for decades. One of the newer fungicides, an anilinopyrimidine specifically the mepanipyrim fungicide, have a broad-spectrum activity against several important plant pathogens specifically including a potent fungicidal activity against *B. cinerea*.<sup>3,4</sup>

In this study compounds will be synthesized that are similar to mepanipyrim (fungicide-derivative) but with modifications that allow the covalent attachment to a polymer system. The defining mechanistic feature of the aforementioned method is that it is not based on the gradual release of a volatile gas (SO<sub>2</sub>). Some non-leaching antibacterial materials have been developed by other investigators, but literature could not be found that discuss a fungicide to be attached to a surface to act against *B. cinerea*.

The covalent attachment of such a compound is seen as overall modifying a parent polymer. As described in the previous chapter the final step entails electrospun polymer nanofibers having advantages such as higher surface-to-volume ratios. The modification of a polymer system consists of immobilizing a modification agent physically or chemically onto a polymer. Chemical immobilization of modification agents onto a polymer is favoured above physical immobilization due to the covalent bond that is formed through the reactive groups that react with each other. Another advantage of chemically modifying a polymer is if an active compound against specific microorganisms is used for the modification the covalent bond between the polymer and the modification agent prevents the leaching out of the active compound during use. A requirement needed when a polymer's surface is modified using chemical modification agent is that a covalent bond needs to be able to form between the fibers and the modification agent due to the presence of a reactive site on the polymer and a suitable reactive group on the modification agent. Through immobilizing the fungicide-derivative onto the polymer system, the disadvantage of having a "free" fungicide on the berry surface is ruled out and the fungicide can't leach out of the system due to the covalent attachment of the fungicide-derivative to the polymer.

In the previous chapter, the polymer that was used was an alternating SMA copolymer. To be able to attach the desired fungicide-derivative onto the polymer system, the polymer itself had to be modified to be able to attach the compound covalently to the polymer system. Thus in the present chapter, the polymer of choice is poly(4-vinylbenzyl chloride-*alt*-maleic anhydride) copolymer (P(S<sub>Cl</sub>-*alt*-MANh)).

In this chapter, we report the synthesis and characterization of the fungicide-derivatives and the synthesis, characterization and electrospinning of poly(4-vinylbenzyl chloride-*alt*-maleic anhydride) copolymer (P(S<sub>Cl</sub>-*alt*-MANh)) and the pre- and post-electrospinning modification of the pristine polymer to functionalized poly(4-vinylbenzyl azide-*alt*-maleic anhydride) copolymer (P(S<sub>N</sub>-*alt*-MANh)). The last procedure is to attach the synthesized fungicide-derivatives onto the P(S<sub>N</sub>-*alt*-MANh) polymer and polymer nanofibers.

The general procedure entailed that P(S<sub>Cl</sub>-*alt*-MANh) copolymer was modified pre- and post-electrospinning with sodium azide to obtain P(S<sub>N</sub>-*alt*-MANh) polymer and polymer nanofibers. Further functionalization occurred through the immobilization of the newly synthesized fungicide-derivatives onto the P(S<sub>N</sub>-*alt*-MANh) polymer. The synthesized fungicide-derivatives were characterized using <sup>1</sup>H-NMR and <sup>13</sup>C-NMR spectroscopy and mass spectroscopy. The pristine polymer P(S<sub>Cl</sub>-*alt*-MANh), P(S<sub>N</sub>-*alt*-MANh) polymer and functionalized anilinoimidopyrimidine-

derivative copolymer (P(S<sub>AP7</sub>-*alt*-MA<sub>nh</sub>)) were characterized using <sup>1</sup>H-NMR and <sup>13</sup>C-NMR spectroscopy and attenuated reflectance Fourier transform infrared spectroscopy (ATR-FTIR). The functionalized electrospun polymer nanofibers were characterized using scanning electron microscopy (SEM) and ATR-FTIR.

The new approach, if successful, will have a direct-in-contact fungicidal action and not a volatile action as with SO<sub>2</sub> gas against *B. cinerea*. Although fungicide-derivatives are synthesized, it needs to be covalently attached to a polymer system, which overall needs to have an anti-fungal activity, but prevent the leakage or indigestion of free compounds.

## 4.2 Synthesis of fungicide-derivatives

Although a relatively large number of new fungicides are available, the anilinopyrimidine group has shown the largest efficacy against *B. cinerea* as well as a broad spectrum against other fungi.<sup>5</sup> The fungicide-derivatives that were synthesized are based on the commercially available mepanipyrim compound used in the field to act against *B. cinerea*. Refer to Figure 4.1 for the schematic illustration of the original mepanipyrim compound.

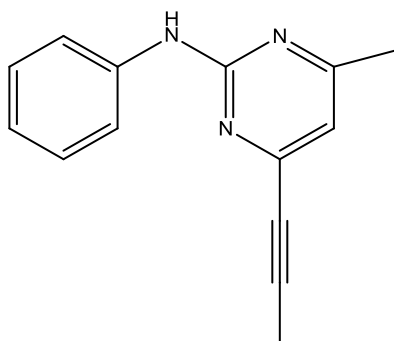


Figure 4.1 Mepanipyrim compound with the chemical name 3-methyl-N-phenyl-5-(prop-1-yn-1-yl) aniline.

The final fungicide-derivatives that is synthesized had to be modified from the original mepanipyrim compound to be able to have a reactive moiety to attach covalently onto a polymer system. In previous work done by Nagata and co-workers, a series of 2-anilinopyrimidines were examined for fungicidal activity against *B. cinerea*. It was observed that the activity fell sharply with any substitution on the anilinobenzene ring.<sup>5</sup> For this reason the compound synthesized in this study was modified at the alkyl chain end to attach to the polymer through the alkyne

functionality. The synthesis of the fungicide-derivatives consisted of various steps and the synthesis was based on previous work done by T Nagata and co-workers, D Davey and co-workers, and Rowley and co-workers.<sup>5-7</sup> The synthesis route of the final compounds, *N*-(4-ethynyl-6-methylpyrimidin-2-yl)-*N*-phenylformamid (anilinopyrimidine<sub>7</sub>-derivative) and 4-ethynyl-6-methyl-*N*-phenylpyrimidin-2-amine (anilinopyrimidine<sub>8</sub>-derivative), is shown in Figure 4.2. The compounds without the trimethylsilane (TMS) protecting groups will be tested for fungicidal activity against *B. cinerea*.

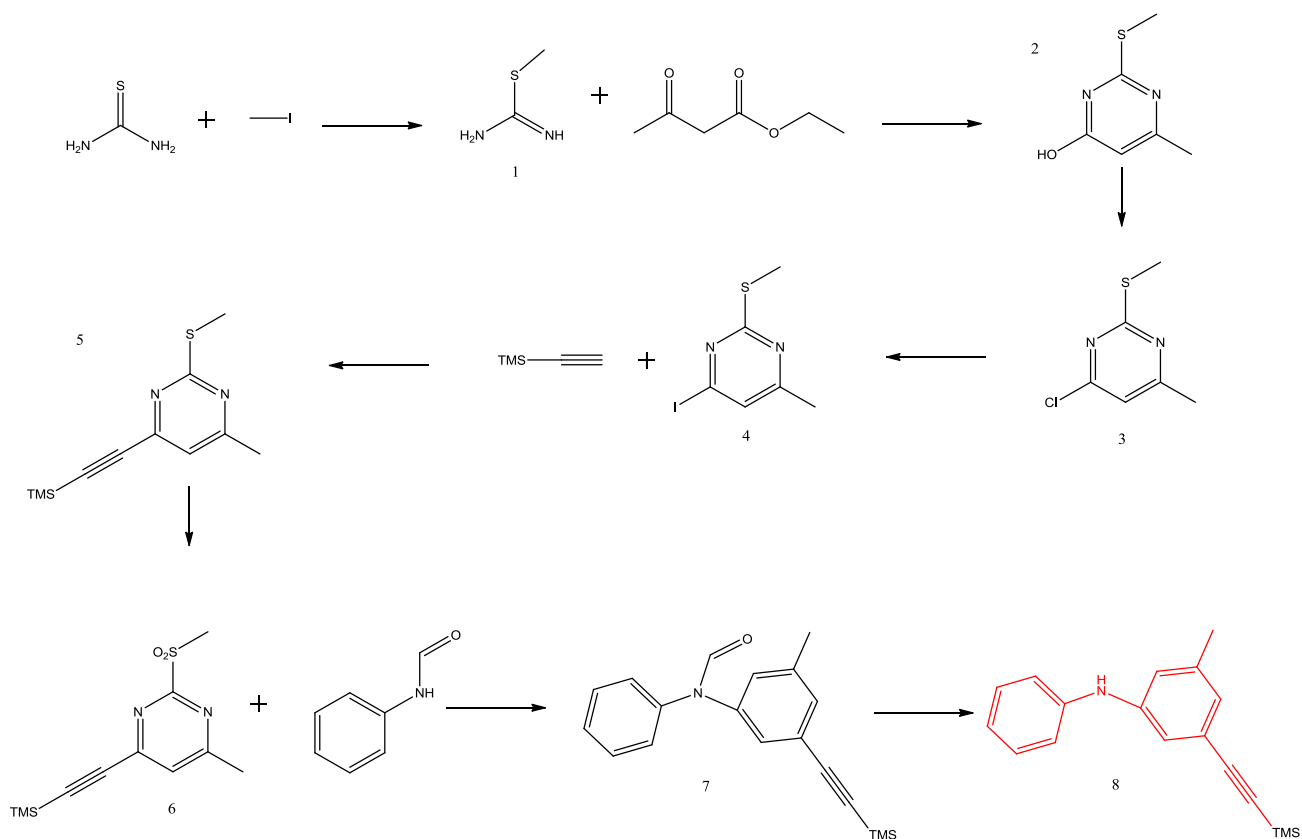


Figure 4.2 Synthesis route for the synthesis of the anilinopyrimidine compounds. Precursors include : (1) *S*-methylisothiourea, (2) 4-Hydroxy-6-methyl-2-(methylthio)-pyrimidine, (3) 4-Chloro-6-methyl-2-(methylthio)-pyrimidine, (4) 4-Iodo-6-methyl-2-(methylthio)-pyrimidine, (5) Palladium cross-coupling reaction yielding 4-methyl-2-(methylthio)-6-((trimethylsilyl) ethynyl) pyrimidine, (6) 4-methyl-2-(methylsulfonyl)-6-((trimethylsilyl) ethynyl) pyrimidine, (7) *N*-(4-methyl-6-((trimethylsilyl) ethynyl) pyrimidin-2-yl)-*N*-phenylformamide, and (8) 4-methyl-*N*-phenyl-6-((trimethylsilyl) ethynyl) pyrimidin-2-amine.

#### 4.2.1 Synthesis of *S*-methylisothiurea (1) using thiourea and methyl iodide

Thiourea being a thio-ether can be readily alkylated to give *S*-methylisothiurea. Methyl iodide is used as methylation reagent and alkylation occurs upon heating.

#### 4.2.2 Synthesis of 4-hydroxy-6-methyl-2-(methylthio)-pyrimidine (2) using *S*-methylisothiurea and ethyl acetoacetate

Pyrimidines are easily synthesized through a condensation reaction of  $\beta$ -ketoesters (dicarbonyl derivatives) and unsubstituted amidine compounds (having an N-C-N functionality) in the presence of sodium carbonate. The N-C-N moiety is most frequently an amidine, a guanidine, urea or thiourea. The synthesis of the pyrimidine is achieved through the condensation reaction of *S*-methylisothiurea with ethyl acetoacetate in an alkaline solution to yield 4-hydroxy-6-methyl-2-phenyl-pyrimidine.<sup>8,9</sup>

#### 4.2.3 Synthesis of 4--6-methyl-2-(methylthio)-pyrimidine (3) using 4-hydroxy-6-methyl-2-(methylthio)-pyrimidine and phosphorous oxychloride

The reaction of hydroxypyrimidines with phosphorous oxychloride ( $\text{POCl}_3$ ) is a complicated substitution reaction to prepare chlorinated pyrimidine compounds or intermediates for further reactions.<sup>10</sup> The procedure generally involves heating a hydroxyl-containing compound in excess  $\text{POCl}_3$  ( $\text{POCl}_3$  activating the OH group) to reflux in the presence of an organic base. Large scale reactions using excess amounts of  $\text{POCl}_3$  need careful attention. Attention need to be paid when quenching excess  $\text{POCl}_3$  due to the potential of latent exothermic events.



#### 4.2.4 Synthesis of 4-iodo-6-methyl-2-(methylthio)-pyrimidine (4) using 4-chloro-6-methyl-2-(methylthio)-pyrimidine and hydroiodic acid

The chloropyrimidine compound followed an iodination step using hydroiodic acid to substitute the chloride with iodide to obtain the corresponding 4-iodo-6-methyl-2-(methylthio)-pyrimidine.<sup>10</sup>

#### 4.2.5 Palladium cross-coupling reaction yielding 4-methyl-2-(methylthio)-6-((trimethylsilyl) ethynyl) pyrimidine (5)

Palladium cross-coupling reactions also known as Sonogashira couplings have great flexibility and value of adding new acetylenic moieties to compounds. Copper and palladium contribute to the reaction as the catalyst.

Aryl iodides are the most frequently used intermediate and the reactions are done at elevated temperatures. Corresponding bromides and chlorides are less prone to participate due to more vigorous conditions that are required to activate the halide. Aryl compounds having terminal iodide functionalities construct aromatic acetylenes through acetylene cross-coupling, forming carbon-carbon alkyne bonds.

#### 4.2.6 Synthesis of 4-methyl-2-(methylsulfonyl)-6-((trimethylsilyl) ethynyl) pyrimidine (6) via an oxidation reaction of 4-methyl-2-(methylthio)-6-((trimethylsilyl) ethynyl) pyrimidine

Thio-ethers are easily oxidized to sulfoxides, which themselves can be further oxidized to sulfones. Thiopyrimidines are oxidized using an oxidizing agent to obtain sulfonylpyrimidines. Sulfones are not stable and should be used soon after synthesis or need to be stored under anhydrous conditions. Isolation of the sulfone compound is unnecessary as the follow up step will not react unless the compound has the sulfone functionality.

#### 4.2.7 Synthesis of *N*-(4-methyl-6-((trimethylsilyl) ethynyl) pyrimidin-2-yl)-*N*-phenylformamide (7) via the addition of formanilide to 4-methyl-2-(methylsulfonyl)-6-((trimethylsilyl) ethynyl) pyrimidine

Sulfonylpyrimidines can be reacted with benzyl formaldehyde in the presence of a base to yield *N*-formylanilinopyrimidines. Large quantities of side reactions occurred. Starting material and unwanted side reaction compounds had to be removed before continuing. Column chromatography was necessary to obtain the desired compound.

#### 4.2.8 TBAF-mediated desilylation of *N*-(4-methyl-6-((trimethylsilyl) ethynyl) pyrimidin-2-yl)-*N*-phenylformamide to obtain *N*-(4-ethynyl-6-methylpyrimidin-2-yl)-*N*-phenylformamide

The protecting TMS moiety on the compound needs to be removed to have an alkyne moiety available for click chemistry. TBAF is an organic-soluble fluoride ion that removes trimethylsilyl protecting groups. De-protection of the trimethylsilyl moiety on the compound synthesized in section 4.2.7 is done using tetra-*N*-butyl ammonium fluoride (TBAF).

#### 4.2.9 Synthesis of 4-ethynyl-6-methyl-*N*-phenylpyrimidin-2-amine (8) via an oxidation reaction of *N*-(4-methyl-6-((trimethylsilyl) ethynyl) pyrimidin-2-yl)-*N*-phenylformamide

Hydrolysis of *N*-formylanilinopyrimidines yields the desired anilinopyrimidine. Column chromatography is necessary to obtain the desired 4-ethynyl-6-methyl-*N*-phenylpyrimidin-2-amine compound. Side reactions occurred and undesired compounds had to be removed to obtain pure 4-ethynyl-6-methyl-*N*-phenylpyrimidin-2-amine compound. TBAF desilylation is unnecessary due to the removal of the TMS moiety under the reaction conditions of this step.

### 4.3 Synthesis of polymers

#### 4.3.1 Synthesis of poly(4-vinylbenzyl chloride-*alt*-maleic anhydride) copolymer (P(S<sub>Cl</sub>-*alt*-MAh))

The polymer of choice is poly(4-vinylbenzyl chloride-*alt*-maleic anhydride) copolymer (P(S<sub>Cl</sub>-*alt*-MAh). Conventional radical copolymerization of styrene and maleic anhydride monomers results in the formation of a close to 1:1 alternation of the monomer units, refer Section 3.2 in Chapter 3, for the illustration of the copolymerization reaction.<sup>11</sup> A similar trend is expected for the current maleic anhydride and 4-vinylbenzyl chloride copolymerization.<sup>11,12</sup>

The synthesis started with the alternating copolymerization of maleic anhydride (MAh) with 4-vinylbenzyl chloride (S<sub>Cl</sub>) to obtain poly(4-vinylbenzyl chloride-*alt*-maleic anhydride) copolymer (P(S<sub>Cl</sub>-*alt*-MAh). The functionalization of the polymer occurs at the chloride moiety. Refer to Figure 4.3 for the schematic illustration of the polymer monomer units. ( $M_n = 101662$  g/mol,  $\bar{D} = 1.904$ , MAh content: 45 - 50%)

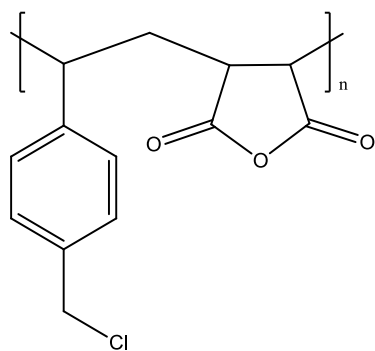


Figure 4.3 Poly(4-vinylbenzyl chloride-*alt*-maleic anhydride) copolymer (P(S<sub>Cl</sub>-*alt*-MAh)) monomer units.

#### 4.3.2 Synthesis of functionalized poly(4-vinylbenzyl azide-*alt*-maleic anhydride) copolymer (P(S<sub>N</sub>-*alt*-MAh))

The benzyl chloride group in the P(S<sub>Cl</sub>-*alt*-MAh) polymer is a very reactive group and can easily be converted to various functional moieties. P(S<sub>Cl</sub>-*alt*-MAh) polymer was modified at the

chloride moiety using sodium azide ( $\text{NaN}_3$ ) via a nucleophilic substitution reaction. The chloride moiety is easily substituted to an azide moiety. Sodium azide was suspended in a suitable solvent and the  $\text{P}(\text{S}_{\text{Cl}}\text{-}alt\text{-MAh})$  copolymer was simultaneously dissolved and added drop wise. The modification reaction was performed at room temperature overnight to obtain the functionalized poly(4-vinylbenzyl azide-*alt*-maleic anhydride) copolymer ( $\text{P}(\text{S}_{\text{N}}\text{-}alt\text{-MAh})$ ). Refer to Figure 4.4 for the schematic illustration of the modified  $\text{P}(\text{S}_{\text{N}}\text{-}alt\text{-MAh})$  copolymer.

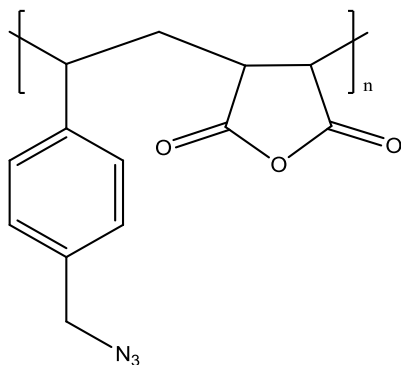


Figure 4.4 The functionalized poly(4-vinylbenzyl azide-*alt*-maleic anhydride) copolymer monomer units.

#### 4.3.3 Synthesis of functionalized polymer by immobilizing *N*-(4-ethynyl-6-methylpyrimidin-2-yl)-*N*-phenylformamide on to $\text{P}(\text{S}_{\text{N}}\text{-}alt\text{-MAh})$ copolymer yielding anilinopyrimidine<sub>7</sub>-derivative copolymer ( $\text{P}(\text{S}_{\text{AP7}}\text{-}alt\text{-MAh})$ )

Before attachment of the fungicide-derivatives onto the synthesized polymer, the fungicide-derivatives were tested for fungicidal activity. Due to the alterations on the synthesized fungicide-derivatives when compared to mepanipyrim, it was necessary to determine if the alteration had any effect on the fungicidal activity. Both *N*-(4-ethynyl-6-methylpyrimidin-2-yl)-*N*-phenylformamide (anilinopyrimidine<sub>7</sub>-derivative) and 4-ethynyl-6-methyl-*N*-phenylpyrimidin-2-amine (anilinopyrimidine<sub>8</sub>-derivative) were tested *in vitro* in sensitivity assays against *B. cinerea* to evaluate and compare mycelium growth determining the inhibition of *B. cinerea* growth. From the pilot study the results indicated that anilinopyrimidine<sub>7</sub>-derivative had an overall higher activity compared to anilinopyrimidine<sub>8</sub>-derivative towards the inhibition of *B. cinerea* (as described in Chapter 5). From the sensitivity results it was found applicable to functionalize  $\text{P}(\text{S}_{\text{N}}\text{-}alt\text{-MAh})$  copolymer with anilinopyrimidine<sub>7</sub>-derivative covalently to obtain poly({4-vinylbenzyl-*N*-[4-methyl-6-(1H-1,2,3-triazol-4-yl)pyrimidin-2-yl]-*N*-phenylformamide}-*alt*-maleic

anhydride) copolymer that will be abbreviated as follows: anilinopyrimidine<sub>7</sub>-derivative copolymer (P(S<sub>AP7</sub>-*alt*-MANh)) for the rest of the thesis.

Anilinopyrimidine<sub>7</sub>-derivative, without the TMS protecting group had a terminal alkyne available and the polymer contained the available azide moiety. Copper (I)-catalyzed Azide-Alkyne Cycloaddition (CuAAC) is used to yield anilinopyrimidine<sub>7</sub>-derivatives polymer (P(S<sub>AP7</sub>-*alt*-MANh)). Refer to Figure 4.5 for the schematic illustration of the functionalized polymer having the new triazole and fungicide-derivative attached to the polymer backbone (P(S<sub>AP7</sub>-*alt*-MANh)). CuAAC is preferred over the uncatalyzed cycloaddition as elevated temperatures are needed for the 1, 3 - dipolar-cycloaddition for an azide-alkyne Huisgen cycloaddition to form a 1, 2, 3-triazole without any catalyst.<sup>12-15</sup> The CuAAC reaction is faster than the uncatalyzed 1, 3-dipolar cycloaddition reaction and succeeds over a broader temperature range, the reaction is insensitive to aqueous conditions and pH between 4 - 12 can be used. The CuAAC reactions also tolerate a broader range of functional groups.

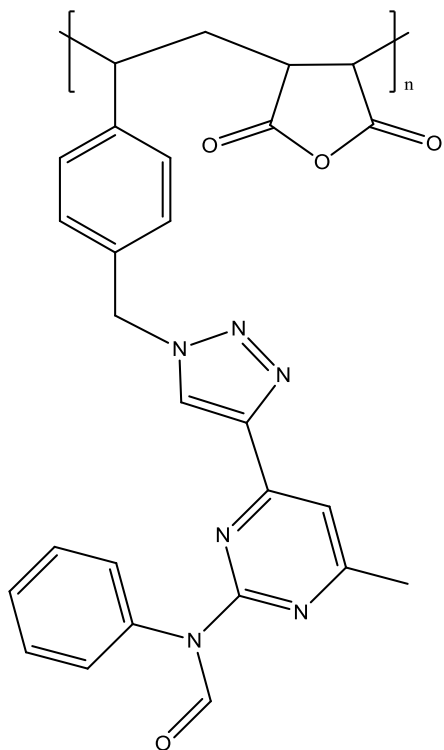


Figure 4.5 The schematic illustration of the anilinopyrimidine<sub>7</sub>-derivative polymer (P(S<sub>AP7</sub>-*alt*-MANh)).

## 4.4 Electrospinning of polymers

Single needle electrospinning and single ball electrospinning were done to produce polymer nanofibers. Refer Section 3.4 in Chapter 3, for an introduction to both these electrospinning processes.

### 4.4.1 Electrospinning of poly(4-vinylbenzyl chloride-*alt*-maleic anhydride) copolymer (P(S<sub>Cl</sub>-*alt*-MAh))

It is the first time that the electrospinning process was used to produce P(S<sub>Cl</sub>-*alt*-MAh) polymer nanofibers. The P(S<sub>Cl</sub>-*alt*-MAh) neat polymer that was synthesized in Section 4.3.1 was single needle and single ball electrospun. Before electrospinning could be done a suitable solvent system had to be chosen for the electrospinning of the polymer. The solvent system has a big influence on the electrospinning process. The optimal solvent system should have a proper balance between a variety of parameters, such as surface tension, vapour pressure and solvent conductivity. The optimum solvent was found to be a 1:1 mixture of DMF/THF to obtain polymer nanofibers within the nano-scale region.

Single needle electrospinning was done at various concentrations. A concentration of 25 wt. % was found to be sufficient for an acceptable number of polymer chain entanglements to yield smooth, bead-free fibers. An average fiber diameter of  $515 \pm 83$  nm was observed.<sup>16</sup> The nanofibers were dried under vacuum to remove any residual solvents.

Single ball electrospinning was done with the same polymer. In single ball electrospinning the same polymer concentration of 25 wt. % was found to be sufficient for an acceptable number of polymer chain entanglements to obtain smooth, bead-free polymer nanofibers. An average fiber diameter of  $585 \pm 113$  nm was observed. The diameter increased slightly between single needle electrospinning and ball electrospinning. This observation can possibly be explained due to multiple jets being initiated from the surface of the glass ball in single ball electrospinning compared to single needle electrospinning. These multiple jets need more charge to whip and elongate sufficiently for collection of dry fibers on the collector. The nanofibers were dried under vacuum to remove any residual solvents.

#### 4.4.2 Electrospinning of functionalized poly(4-vinylbenzyl azide-*alt*-maleic anhydride) copolymer (P(S<sub>N</sub>-*alt*-MAh))

The synthesized polymer was isolated and dried in vacuum. After isolation of the polymer the polymer was not able to dissolve in a suitable solvent in a high enough concentration for an acceptable number of chain entanglements. The polymer was found to rather make a “gel” than an electrospinnable solution. Dimethyl sulfoxide (DMSO) was found to dissolve the polymer the best, in the highest concentration, but due to the rather high melting point of DMSO the polymer solution froze in the syringe and needle when electrospinning was attempted. Electrospinning was unsuccessful attempting to electrospin P(S<sub>N</sub>-*alt*-MAh).

Post-electrospinning modification of P(S<sub>Cl</sub>-*alt*-MAh) electrospun polymer nanofibers will be done to surface-functionalize the polymer nanofibers through substituting the chloride moiety with an azide moiety.

#### 4.4.3 Post-electrospinning modification of P(S<sub>Cl</sub>-*alt*-MAh) polymer nanofibers to yield P(S<sub>N</sub>-*alt*-MAh) polymer nanofibers

The chloride moieties on the surface of the nanofibers will undergo a nucleophilic substitution reaction to form azide moieties on the surface of the polymer nanofibers. Prepared electrospun P(S<sub>Cl</sub>-*alt*-MAh) nanofibrous mats, obtained in Section 4.4.1, are functionalized with a surface-functionalization agent (NaN<sub>3</sub>) under room temperature conditions and without a catalyst. The post-electrospun functionalized P(S<sub>N</sub>-*alt*-MAh) fibers are thoroughly washed with a solvent to remove any unreacted surface-functionalization agent. To preserve the nanofibrous structure during the functionalization procedure, a non-solvent for the fibers had to be chosen being a solvent for the NaN<sub>3</sub> and the side product sodium chloride (NaCl) and a non-solvent for the functionalized fibers.

Functionalized P(S<sub>N</sub>-*alt*-MAh) mats were characterized using ATR-FTIR spectroscopy and SEM analysis was done to confirm the preservation of the nanofibrous structure and integrity after the functionalization reaction.

#### 4.4.4 Post-electrospinning functionalization of P(S<sub>N</sub>-*alt*-MANh) polymer nanofibers by immobilizing *N*-(4-ethynyl-6-methylpyrimidin-2-yl)-*N*-phenylformamide onto polymer nanofibers yielding anilinopyrimidine<sub>7</sub>-derivative polymer) (P(S<sub>AP7</sub>-*alt*-MANh))

Post-electrospinning modified P(S<sub>N</sub>-*alt*-MANh) nanofibrous mats obtained in Section 4.4.3 were functionalized and reacted with *N*-(4-ethynyl-6-methylpyrimidin-2-yl)-*N*-phenylformamide (anilinopyrimidine<sub>7</sub>-derivative) (synthesized in Section 4.2) via a click reaction (CuAAC). To preserve the nanofibrous structure during the functionalization procedure, a solvent system had to be chosen that is a non-solvent for the fibers but a solvent for the organic compound and a non-solvent for the functionalized fibers.

The anilinopyrimidine<sub>7</sub>-derivative polymer nanofibers (P(S<sub>AP7</sub>-*alt*-MANh)) were thoroughly washed with solvent to remove any unreacted compound. The functionalized P(S<sub>AP7</sub>-*alt*-MANh) polymer nanofibers were characterized using ATR-FTIR spectroscopy and SEM analysis was done to confirm the preservation of the nanofibrous structure and integrity after the functionalization reaction.

### **4.5 Characterization of synthesized compounds and polymers**

Synthesized compounds and polymers were characterized using <sup>13</sup>C and <sup>1</sup>H nuclear magnetic resonance spectroscopy (NMR), mass spectroscopy and attenuated total reflectance Fourier transform infrared (ATR-FTIR).



## 4.5.1 Characterization of S-methylisothiurea

### 4.5.1.1 $^1\text{H-NMR}$

The  $^1\text{H-NMR}$  spectrum of S-methylisothiurea and the assignments of the relevant peaks are shown in Figure 4.6.

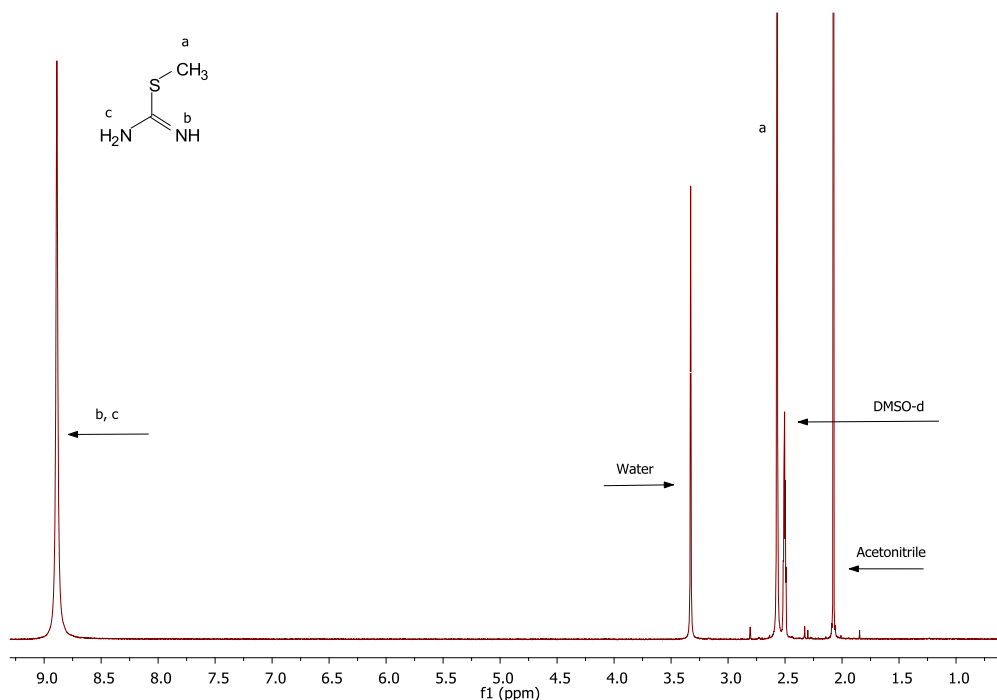


Figure 4.6  $^1\text{H-NMR}$  spectrum of S-methylisothiurea and the assigned peaks.

S-methylisothiurea is characterized by a peak at a chemical shift of 8.7 - 9.05 ppm that relates to the NH and  $\text{NH}_2$  protons (b, c). The chemical shift observed can possibly be explained by the electronegativity of the nitrogen. The more electronegative the element the hydrogens are attached to, the greater the chemical shift. Electronegative elements have an electron-withdrawing effect, reducing the valence electron density around the protons. These electrons shield the proton from the applied magnetic field. Substituents that have this type of effect are said to deshield the protons. The greater the electronegativity of the substituent, the more it deshields the protons and hence the greater the chemical shift of those protons.<sup>17</sup> Hydrogen bonding also has an influence on the absorption position. The more hydrogen bonding, the

more deshielded a proton becomes and the greater the chemical shift. Two different peaks for the two nitrogen hydrogens are expected, but due to fast occurring resonance interaction and the rate of the NMR transition being slower than the different resonance structures being formed thus only one peak is observed.<sup>17</sup>

The methyl protons (a) are observed as a singlet at 3.56 ppm, correlating with known literature.<sup>17</sup> The integration of the methyl protons are 3:3 in relation to the overlapping NH and NH<sub>2</sub> hydrogen atoms.

#### 4.5.1.2 <sup>13</sup>C-NMR

The results obtained from the <sup>1</sup>H-NMR spectrum were confirmed by <sup>13</sup>C-NMR spectroscopy. Figure 4.7 shows the <sup>13</sup>C-NMR spectrum of S-methylisothiourea and the assignment of the relevant peaks.

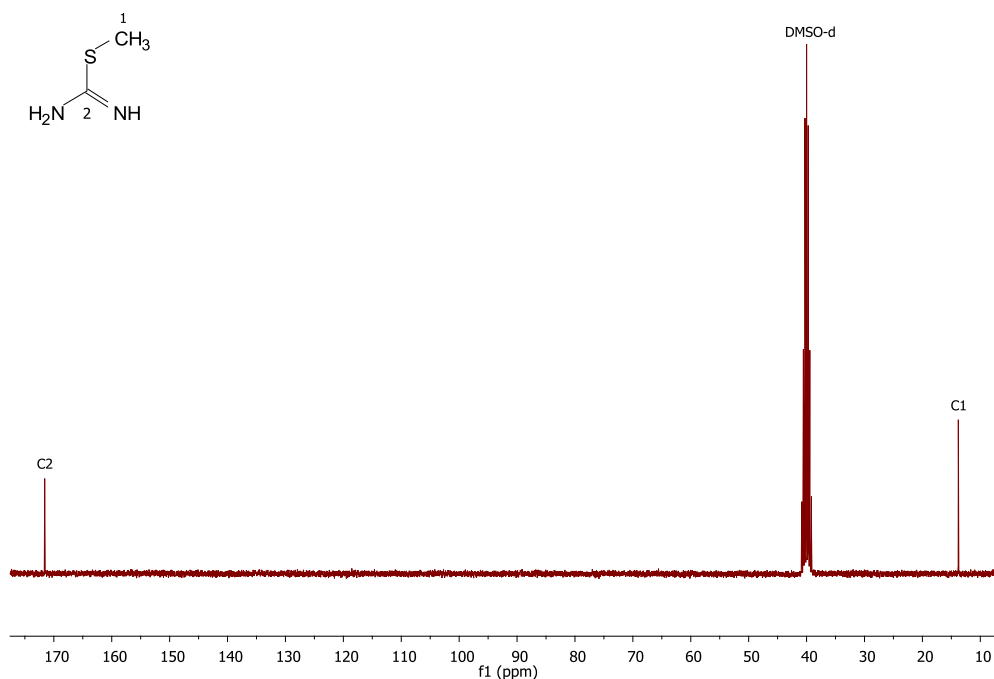


Figure 4.7 <sup>13</sup>C-NMR spectrum of S-methylisothiourea and the assigned peaks.

A peak is observed at 171 ppm, designated to the methine carbon (C2) adjacent to the sulphur and two nitrogen atoms. Electronegativity, hybridization and anisotropy all affect <sup>13</sup>C chemical shifts in nearly the same fashion as they affect <sup>1</sup>H chemical shifts, although <sup>13</sup>C chemical shifts are almost 20 times larger.<sup>17</sup> The methine carbon is surrounded with electronegative atoms causing deshielding to occur that produce a large downfield shift. A peak corresponding to the

methyl carbon (C1) is observed at 13.9 ppm, which is in agreement with the proposed structure and literature.<sup>17</sup>

## 4.5.2 Characterization of 4-hydroxy-6-methyl-2-(methylthio)-pyrimidine

### 4.5.2.1 <sup>1</sup>H-NMR

Figure 4.8 shows the <sup>1</sup>H-NMR spectrum of 4-Hydroxy-6-methyl-2-(methylthio)-pyrimidine and the assignments of the relevant peaks.

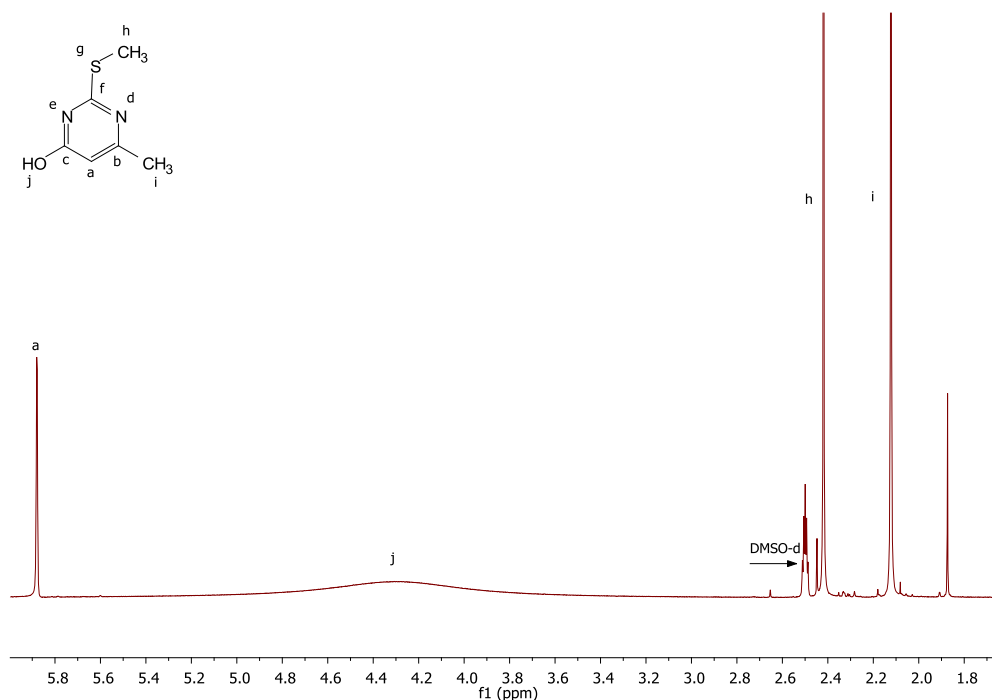


Figure 4.8 <sup>1</sup>H-NMR spectrum of 4-hydroxy-6-methyl-2-(methylthio)-pyrimidine and the assignment of the peaks.

4-Hydroxy-6-methyl-2-(methylthio)-pyrimidine is characterized by a peak at a chemical shift of 5.88 ppm that relates to the aromatic proton (a). Aromatic ring protons of a benzenoid system appear around 7 ppm, but due to the lone pair interactions on the O atom in the *anti*-position to the C-H bond, shifts the proton more upfield.<sup>18</sup>

Two peaks with an integration of 3 are observed at 2.4 and 2.1 ppm correlating to the two methyl proton moieties (h, i). The electronegativity of the sulphur atom deshields the methyl

hydrogens (h) causing a more down field chemical shift in comparison of the methyl hydrogens (i) attached to the aromatic ring.

OH hydrogens exhibit hydrogen bonding that can have extremely variable absorption positions over a wide range. The position of the peak depends on the concentration, solvent and the temperature.<sup>17</sup> The more hydrogen bonding that occurs, the more deshielded a proton become, appearing more downfield. A broad peak at 3.65 - 4.8 ppm correlates to the OH group of the compound (j).

#### 4.5.2.2 <sup>13</sup>C-NMR

The results obtained from the <sup>1</sup>H-NMR spectrum were confirmed by <sup>13</sup>C-NMR spectroscopy. Figure 4.9 shows the <sup>13</sup>C-NMR spectrum of 4-hydroxy-6-methyl-2-(methylthio)-pyrimidine and the assignment of the relevant peaks.

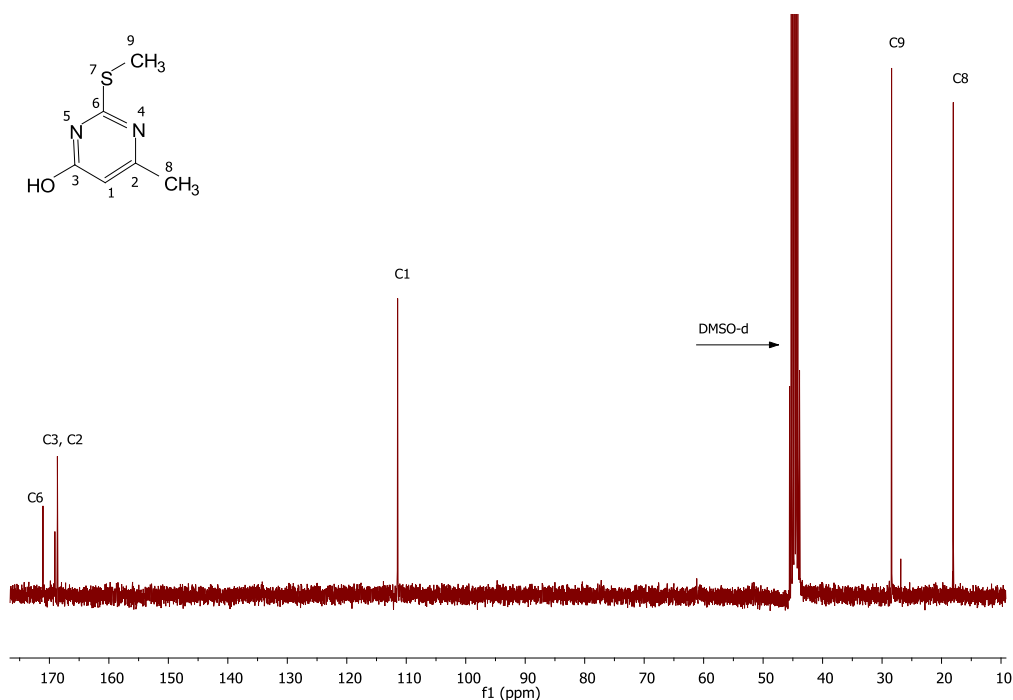


Figure 4.9 <sup>13</sup>C-NMR spectrum of 4-hydroxy-6-methyl-2-(methylthio)-pyrimidine and the assignment of the relevant peaks.

A peak is observed at 171 ppm, designated to the methine carbon (C6) in the aromatic ring adjacent to the sulphur and the two nitrogens. The electron withdrawing ability of the sulphur and nitrogens, the hybridization of the carbon and the anisotropy effect of the ring have an outcome of a more downfielded shift of the methine carbon (C6) compared to literature values.<sup>17</sup>

The other two methine carbons (C3, C2) in the aromatic ring that are adjacent to the nitrogens have almost the same chemical environment and are observed at 169 ppm and 168 ppm respectively. The methine carbon (C3) that has oxygen attached to it will be the one slightly more downfield from the other methine carbon (C2) due to oxygen being more electronegative than carbon (C9), deshielding the methine carbon (C3), and causing an increase in the chemical shift. The peak at 111 ppm is designated to the methylene carbon in the aromatic ring (C1). The methyl carbons (C8 and C9) are observed at 28.3 ppm and 18 ppm respectively. The methyl carbon (C9) adjacent the sulphur group is deshielded more due to the sulphur being more electronegative causing a higher chemical shift.<sup>17</sup>

### 4.5.3 Characterization of 4-chloro-6-methyl-2-(methylthio)-pyrimidine

#### 4.5.3.1 $^1\text{H-NMR}$

The  $^1\text{H-NMR}$  spectrum of 4-chloro-6-methyl-2-(methylthio)-pyrimidine and the assignments of the relevant peaks are shown in Figure 4.10

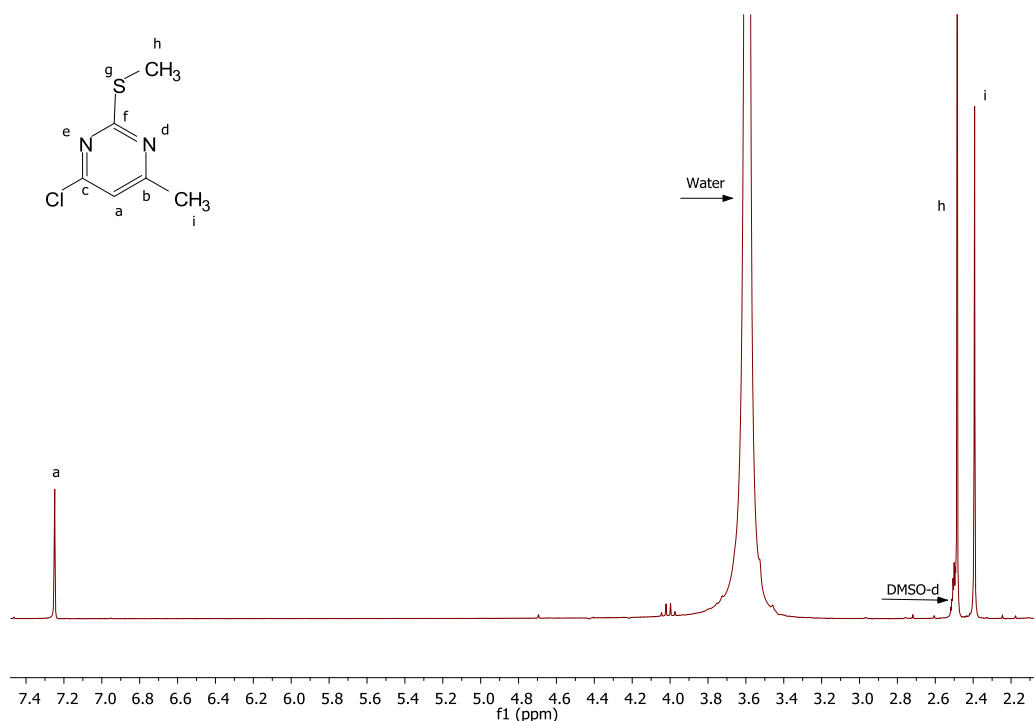


Figure 4.10  $^1\text{H-NMR}$  spectrum of 4-chloro-6-methyl-2-(methylthio)-pyrimidine and the assignment of the peaks.

A peak at 7.2 ppm is designated to the aromatic proton (a). A chemical shift is observed in the aromatic proton (a) compared to the 4-hydroxy-6-methyl-2-(methylthio)-pyrimidine aromatic protons (a) that is observed at 5.88 ppm (Refer to Figure 4.8). The upfield chemical shift of the OH aromatic protons can be explained by the lone pair interactions on the O atom. When lone electron pairs on the oxygen are *anti* to a C-H bond, the proton is shifted upfield.<sup>18</sup>

The methyl protons (h, i) integrate 3:3:1 relative to the aromatic proton in the aromatic ring (a). The peaks are observed at 2.48 ppm and 2.39 ppm respectively. The protons designated to (h) are more downfield compared to protons (i) due to the electronegativity of the sulphur atom causing deshielding of the methyl hydrogens (h).

4.5.3.2  $^{13}\text{C}$ -NMR

The results obtained from the  $^1\text{H}$ -NMR spectrum were confirmed by  $^{13}\text{C}$ -NMR spectroscopy. Figure 4.11 shows the  $^{13}\text{C}$ -NMR spectrum of 4-chloro-6-methyl-2-(methylthio)-pyrimidine and the assignment of the relevant peaks.

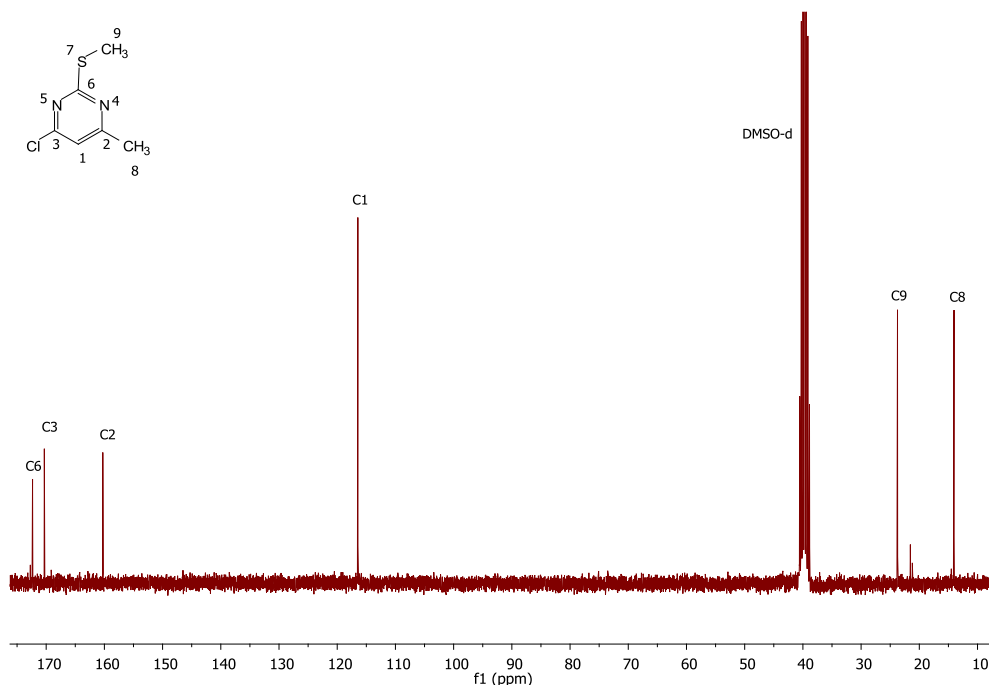


Figure 4.11  $^{13}\text{C}$ -NMR spectrum of 4-chloro-6-methyl-2-(methylthio)-pyrimidine and the assignment of the peaks.

A peak is observed at 172.4 ppm, designated to the methine carbon in the aromatic ring adjacent to the sulphur and the two nitrogens. The electron withdrawing ability of the sulphur and nitrogens, the hybridization of the carbon and the anisotropy effect of the ring have an influence of the position of the peak. These effects cause a more downfield shift of the methine carbon (C6). The other two methine carbons (C3, C2) in the aromatic ring that is adjacent to the nitrogens have almost the same chemical environment and are observed at 170.3 ppm and 160.2 ppm respectively. The methine carbon (C3) that has the chlorine atom attached to it will be the one slightly more downfield from the other methine carbon (C2) due to chlorine being more electronegative than the carbon (C9), deshielding the carbon, causing an increase in the chemical shift. The peak at 116.4 ppm is designated to the methylene carbon in the aromatic ring (C1). The methyl adjacent to the sulphur is designated to the peak observed at 23.7 ppm (C8). The methyl carbon (C9) adjacent the sulphur group is deshielded more from the sulphur

causing a higher chemical shift.<sup>17</sup> The methyl carbon on the aromatic ring is observed at 14 ppm (C9).<sup>17</sup>

#### 4.5.4 Characterization of 4-iodo-6-methyl-2-(methylthio)-pyrimidine

##### 4.5.4.1 <sup>1</sup>H-NMR

Figure 4.12 shows the <sup>1</sup>H-NMR spectrum of 4-iodo-6-methyl-2-(methylthio)-pyrimidine and the assignments of the relevant peaks.

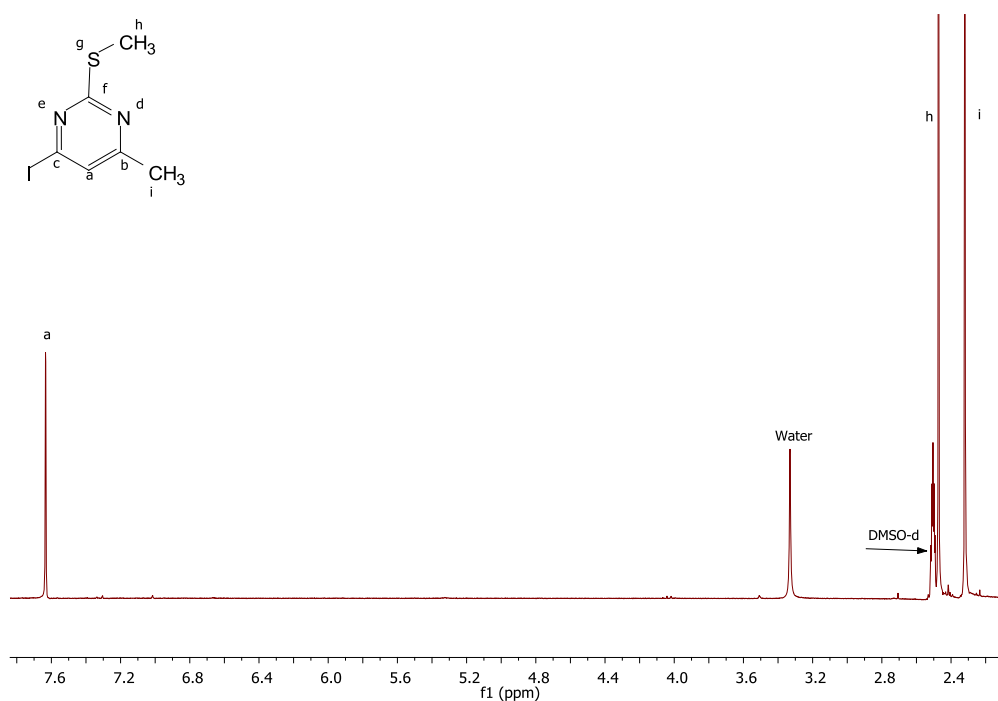


Figure 4.12 <sup>1</sup>H-NMR spectrum of 4-iodo-6-methyl-2-(methylthio)-pyrimidine and the assignment of the relative peaks.

A peak at 7.63 ppm is designated to the aromatic proton (a). A chemical shift is observed in proton (a) compared to the 4-Chloro-6-methyl-2-(methylthio)-pyrimidine proton (a) that is observed at 7.2 ppm (refer to Figure 4.10).<sup>17</sup> The methyl protons (h, i) integrate 3:3:1 relative to the aromatic proton in the aromatic ring (a). The peaks are observed at 2.46 ppm and 2.31 ppm respectively. The protons designated to (h) are more downfield compared to protons (i) due to the electronegativity of the sulphur atom causing deshielding of the methyl hydrogens (h).



4.5.4.2  $^{13}\text{C}$ -NMR

The results obtained from the  $^1\text{H}$ -NMR spectrum were confirmed by  $^{13}\text{C}$ -NMR spectroscopy. The  $^{13}\text{C}$ -NMR spectrum of 4-iodo-6-methyl-2-(methylthio)-pyrimidine and the assignment of the relevant peaks are shown in Figure 4.13.

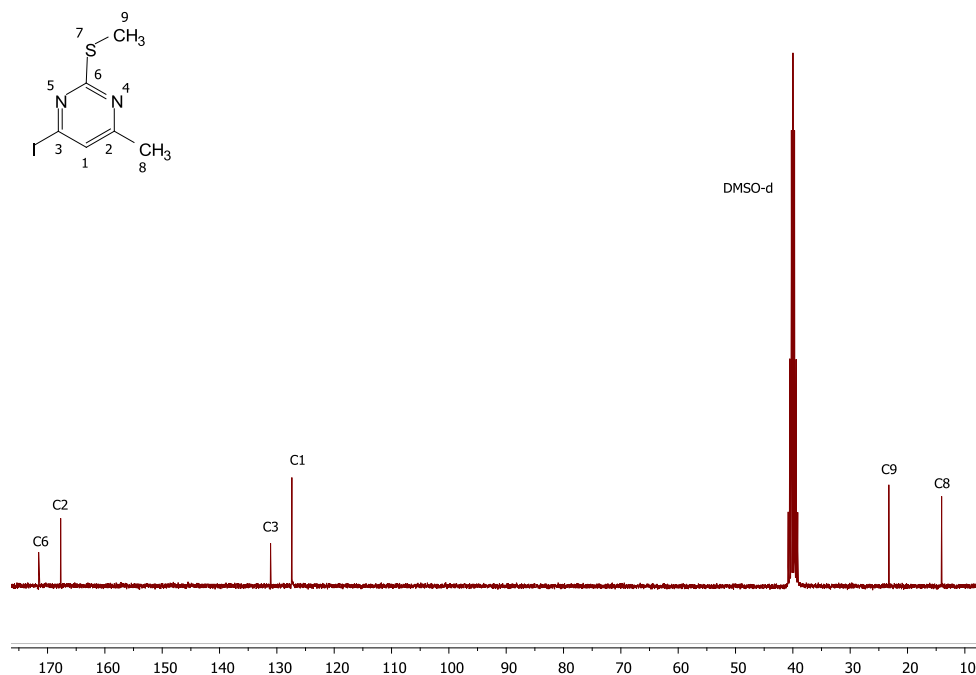


Figure 4.13  $^{13}\text{C}$ -NMR spectrum of 4-iodo-6-methyl-2-(methylthio)-pyrimidine and the assignment of the peaks.

The same assignments of peaks are observed as with 4-chloro-6-methyl-2-(methylthio)-pyrimidine (Refer to Figure 4.11), some of the peaks shifted, but a similar spectrum is observed. A peak is observed at 171.2 ppm, designated to the methine carbon in the aromatic ring adjacent to the sulphur and the two nitrogens (C6). The electron withdrawing ability of the sulphur and nitrogens, the hybridization of the carbon and the anisotropy effect of the ring have an influence of the position of the peak. These effects cause a more downfield shift of the methine carbon (C6). The other two methine carbons (C3, C2) in the aromatic ring that is adjacent to the nitrogens have almost the same chemical environment and are observed at 167.6 ppm and 130.8 ppm respectively. The methine carbon (C3) that has the iodine atom attached to it will be the one slightly more downfield from the other methine carbon (C2) due to iodo being more electronegative than the carbon (C9), deshielding the carbon, causing an increase in the chemical shift. The peak at 127.1 ppm is designated to the methylene carbon in

the aromatic ring (C1). The methyl (C9) adjacent to the sulphur is designated to the peak observed at 23.1 ppm. The methyl carbon (C9) is deshielded more due to the sulphur being electronegative, causing a higher chemical shift.<sup>17</sup> The methyl carbon on the aromatic ring is observed at 14 ppm (C8).<sup>17</sup>

#### 4.5.5 Characterization of 4-methyl-2-(methylthio)-6-((trimethylsilyl) ethynyl) pyrimidine

##### 4.5.5.1 <sup>1</sup>H-NMR

Figure 4.14 shows the <sup>1</sup>H-NMR spectrum of 4-methyl-2-(methylthio)-6-((trimethylsilyl) ethynyl) pyrimidine and the assignments of the relevant peaks.

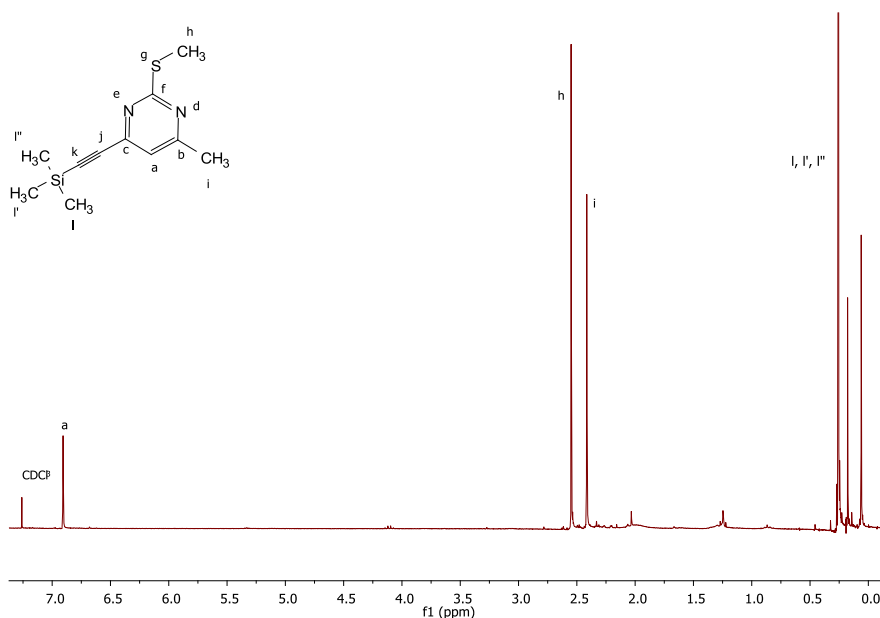


Figure 4.14 <sup>1</sup>H-NMR spectrum of 4-methyl-2-(methylthio)-6-((trimethylsilyl) ethynyl) pyrimidine and the assignment of the peaks.

The same peak absorptions are expected for 4-methyl-2-(methylthio)-6-((trimethylsilyl) ethynyl) pyrimidine than for 4-iodo-6-methyl-2-(methylthio)-pyrimidine (Refer to Figure 4.12), except the 4-methyl-2-(methylthio)-6-((trimethylsilyl) ethynyl) pyrimidine should show a peak in the range of 0.01 - 2.00 ppm indicative of the TMS protons (l, l', l'').

A peak at 6.9 ppm is designated to the aromatic proton (a). A chemical shift is observed in proton (a) compared to the 4-iodo-6-methyl-2-(methylthio)-pyrimidine proton (a) that is observed at 7.63 ppm (Refer to Figure 4.12). Due to no electronegative atom being present, that deshields the proton, the peak is observed at a upfield chemical shift compared to 4-iodo-6-methyl-2-(methylthio)-pyrimidine proton. The acetylenic moiety also shields the proton (a) due to anisotropic shielding by the adjacent  $\pi$  bonds. The methyl protons (h, i) integrate 3:3:1 relative to the aromatic proton in the aromatic ring (a). The peaks are observed at 2.54 ppm and 2.41 ppm respectively. The protons designated to (h) are more downfield compared to protons (i) due to the electronegativity of the sulphur atom causing deshielding of the methyl hydrogens (h). The TMS alkyne protecting group is observed at 0.24 ppm. The protons of this moiety are more shielded than most other known moieties. TMS protons appear at the end of the range (ppm).

#### 4.5.5.2 $^{13}\text{C}$ -NMR

The results obtained from the  $^1\text{H}$ -NMR spectrum were confirmed by  $^{13}\text{C}$ -NMR spectroscopy. Figure 4.15 shows the  $^{13}\text{C}$ -NMR spectrum of 4-methyl-2-(methylthio)-6-((trimethylsilyl) ethynyl) pyrimidine and the assignment of the relevant peaks.

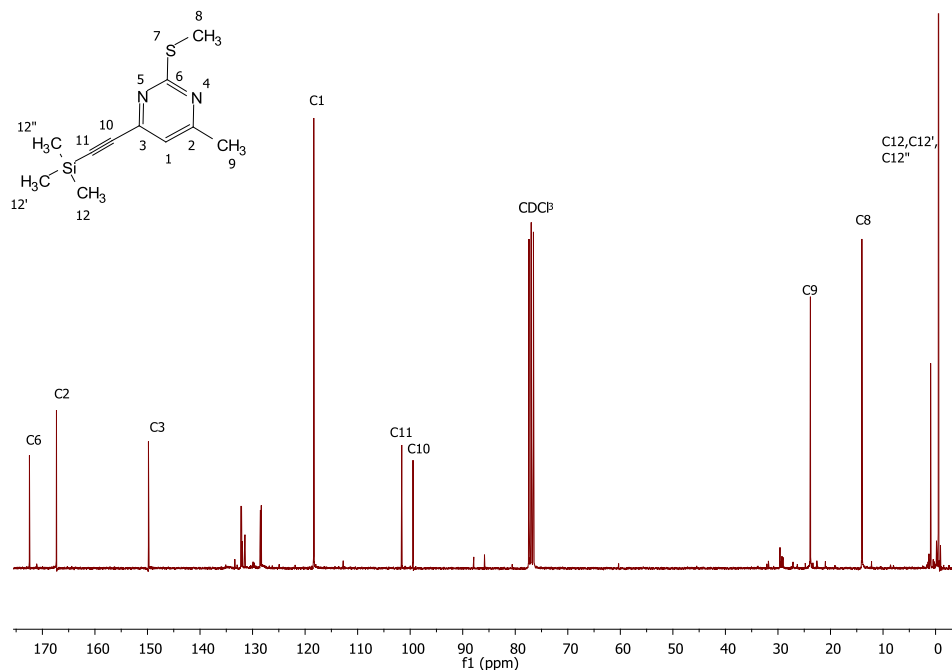


Figure 4.15  $^{13}\text{C}$ -NMR spectrum of 4-methyl-2-(methylthio)-6-((trimethylsilyl) ethynyl) pyrimidine and the assignment of the peaks.

A peak is observed at 172.5 ppm, designated to the methine carbon in the aromatic ring adjacent to the sulphur and the two nitrogens (C6). The electron withdrawing ability of the sulphur and nitrogens, the hybridization of the carbon and the anisotropy effect of the ring have an influence of the position of the peak. These effects cause a more downfield shift of the methine carbon (C6). The other two methine carbons (C3, C2) in the aromatic ring that is adjacent to the nitrogens have different chemical environments due to no halogen atom being present but an acetylenic alkyl chain instead. The methine carbon (C2) that has the methyl group attached to it is observed at 167.4 ppm. The methine carbon (C3) is observed at 149.9 ppm. The shift of these peaks from the 4-iodo-6-methyl-2-(methylthio)-pyrimidine spectra can be explained by the acetylenic alkyl chain present. The unsaturated carbon chain has a shielding effect on C3 due to shielding by the adjacent  $\pi$  bonds, causing the methine peak to be upfield from C2 carbon. The peak at 118.5 ppm is designated to the methylene carbon in the aromatic ring (C1). The methyl (C9) adjacent to the sulphur is designated to the peak observed at 23.8 ppm. The methyl carbon (C9) adjacent the sulphur group is deshielded more due to the sulphur being electronegative, causing a higher chemical shift.<sup>17</sup> The methyl carbon on the aromatic ring is observed at 14.1 ppm (C9).<sup>17</sup> Two peaks are observed at 101.7 ppm and 99.4 ppm designated to C10 and C11 respectively. The C10 carbon is more downfield due to a nitrogen atom present one carbon away and having an electronegative effect on the carbon. The deshielding effect in  $^{13}\text{C}$ -NMR is the same as in  $^1\text{H}$ -NMR. The shift is greater in  $^{13}\text{C}$ -NMR due to the electronegative atom is directly attached to the carbon (C-X) and not one bond away as with  $^1\text{H}$ -NMR where the electronegative atom is attached to the carbon and the proton is attached to the carbon as well (H-C-X). In  $^{13}\text{C}$ -NMR, an electronegative atom also causes a downfield shift in the  $\alpha$  and  $\beta$  carbons, but leads to a small upfield shift for the  $\gamma$  carbon. In this structure the  $\alpha$  carbons are C3 and C6. The  $\beta$  carbons are C1 and C10 and the  $\gamma$  carbons are C2, C9 and C11. C10 being the  $\beta$  carbon and C11 the  $\gamma$  carbon, C10 will be more downfield than C11. The TMS carbons also have a shielding effect on C11 causing a more upfield shift. The peak at  $\sim 0$  ppm correlates to the TMS carbons.

The presence of the acetylene carbons and the TMS carbons confirm the successful synthesis of 4-methyl-2-(methylethio)-6-((trimethylsilyl) ethynyl) pyrimidine via the Sonigashira coupling reaction.

## 4.5.6 Characterization of 4-methyl-2-(methylsulfonyl)-6-((trimethylsilyl) ethynyl) pyrimidine

### 4.5.6.1 $^1\text{H-NMR}$

Figure 4.16 shows the  $^1\text{H-NMR}$  spectrum of 4-methyl-2-(methylsulfonyl)-6-((trimethylsilyl) ethynyl) pyrimidine and the assignments of the relevant peaks.

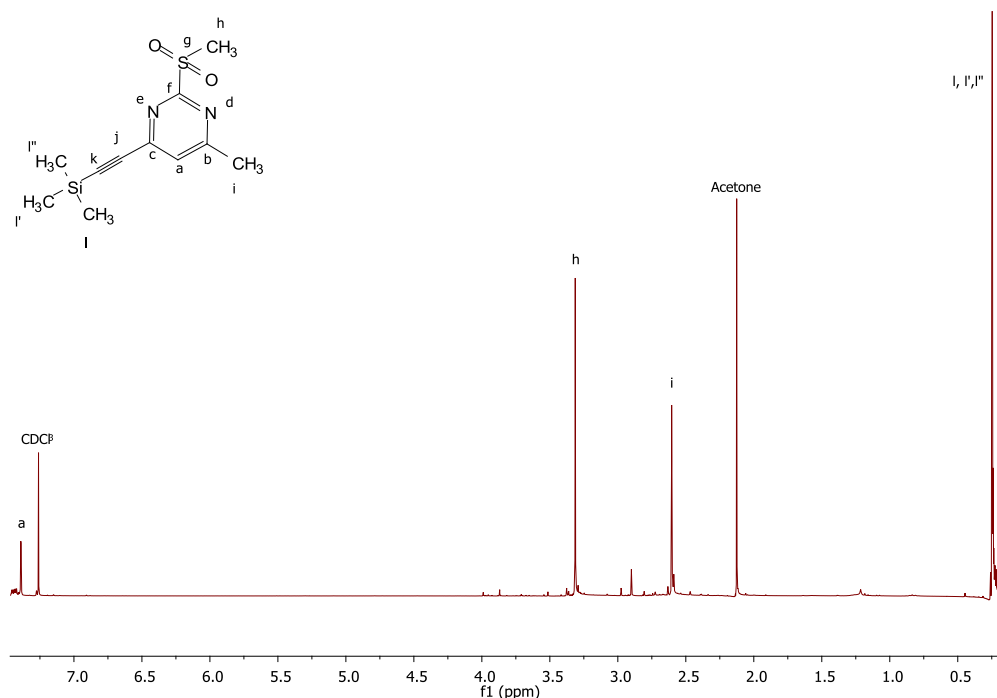


Figure 4.16  $^1\text{H-NMR}$  spectrum of 4-methyl-2-(methylsulfonyl)-6-((trimethylsilyl) ethynyl) pyrimidine and the assignment of the peaks.

The same peaks are observed as in the 4-methyl-2-(methylthio)-6-((trimethylsilyl) ethynyl) pyrimidine compound (Refer to Figure 4.14), some of the peaks shifted, but the same chemical shifts are observed.

A peak at 7.3 ppm is designated to the aromatic proton (a). The methyl protons (h, i) integrate 3:3:1 relative to the aromatic proton in the aromatic ring (a). The peaks are observed at 3.31 ppm and 2.6 ppm respectively. The protons designated to (h) are more downfield compared to protons (i) due to the electronegativity of the sulphur and oxygen atoms causing the methyl hydrogens to become deshielded (h). Comparing the  $^1\text{H-NMR}$  spectrum of 4-methyl-2-

(methylthio)-6-((trimethylsilyl) ethynyl) pyrimidine (Refer to Figure 4.14) and 4-methyl-2-(methylsulfonyl)-6-((trimethylsilyl) ethynyl) pyrimidine the methyl protons (h) is more downfield in the latter spectrum. This observation can possibly be explained due to the sulphur and two oxygens deshielding the methyl protons more than just the sulphur in 4-methyl-2-(methylthio)-6-((trimethylsilyl) ethynyl) pyrimidine, therefore the increase in the chemical shift from 2.54 ppm (Refer to Figure 4.14) to 3.31 ppm. The alkyne protecting group TMS is observed at 0.25 ppm. The protons of this moiety are more shielded than most other known moieties. TMS protons come out at the end of the range (ppm).

#### 4.5.6.2 $^{13}\text{C}$ -NMR

The results obtained from the  $^1\text{H}$ -NMR spectrum were confirmed by  $^{13}\text{C}$ -NMR spectroscopy. Figure 4.17 shows the  $^{13}\text{C}$ -NMR spectrum of 4-methyl-2-(methylsulfonyl)-6-((trimethylsilyl) ethynyl) pyrimidine and the assignment of the relevant peaks.

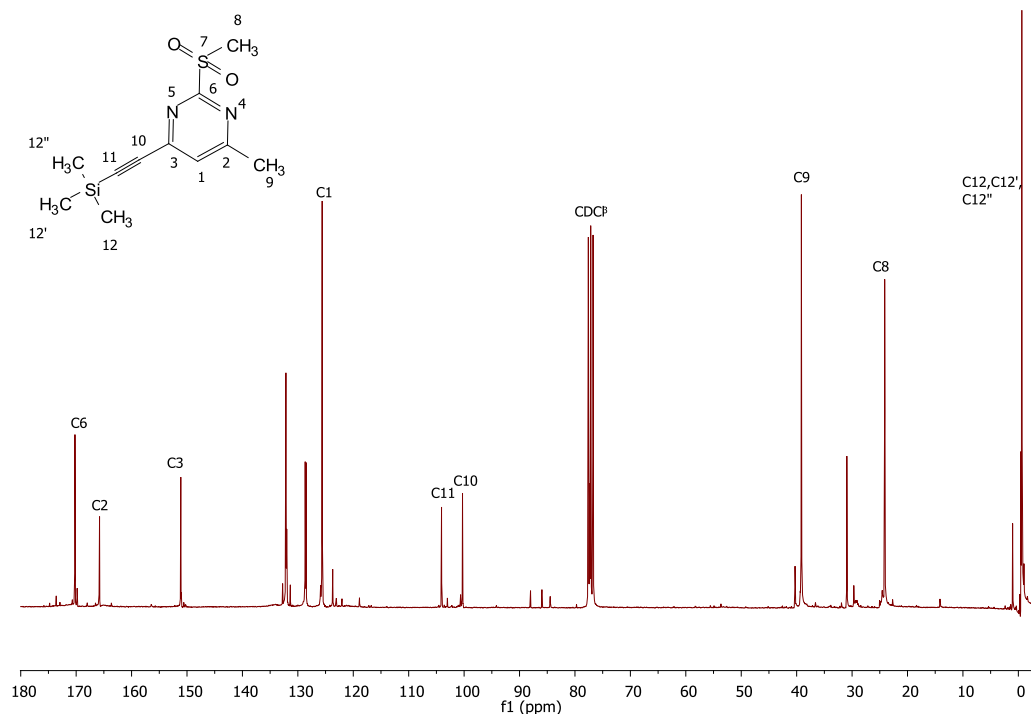


Figure 4.17  $^{13}\text{C}$ -NMR spectrum of 4-methyl-2-(methylsulfonyl)-6-((trimethylsilyl) ethynyl) pyrimidine and the assignment of the peaks.

The spectrum shows some smaller peak present. This is due to small amounts of starting material left in the crude product. The starting material was not necessary to remove, as it would

not influence the next reaction steps. A similar spectrum is observed for 4-methyl-2-(methylsulfonyl)-6-((trimethylsilyl) ethynyl) pyrimidine as for 4-methyl-2-(methylethio)-6-((trimethylsilyl) ethynyl) pyrimidine (Refer to Figure 4.15) A peak is observed at 170.2 ppm, designated to the methine carbon in the aromatic ring adjacent to the sulphur and the two nitrogens (C6). The electron withdrawing ability of the sulphur and nitrogens, the hybridization of the carbon and the anisotropy effect of the ring have an influence of the position of the peak. These effects cause a more downfield shift of the methine carbon (C6).

The methine carbon (C2) that has the methyl group attached to it is observed at 165.8 ppm. The methine carbon (C3) is observed at 151.1 ppm. The peak at 125.8 ppm is designated to the methylene carbon in the aromatic ring (C1).

The methyl (C9) adjacent to the sulphur is designated to the peak observed at 39.1 ppm. The C9 carbon adjacent to the sulphur and two oxygen atoms is deshielded more due to these atoms being highly electron-withdrawing, causing a higher chemical shift in comparison to 4-methyl-2-(methylethio)-6-((trimethylsilyl) ethynyl) pyrimidine  $^{13}\text{C}$ -NMR spectra (refer Figure 4.17).<sup>17</sup> The C8 carbon was observed at 23.8 ppm. The C9 carbon in this spectra have shifted to 39.1 ppm due to the extra two oxygens present deshielding the methyl carbon even more causing a higher chemical shift.

The methyl carbon on the aromatic ring is observed at 24.11 ppm (C9).<sup>17</sup> Two peaks are observed at 104 ppm and 100.2 ppm designated to C10 and C11 respectively. The same explanation as stated in Section 4.5.5.2 for the more downfield shift of the C10 carbon is applicable here. The peak at ~ 0 ppm correlates to the TMS carbons.

The shifts of the peaks stated above confirm the successful synthesis of 4-methyl-2-(methylsulfonyl)-6-((trimethylsilyl) ethynyl) pyrimidine via an oxidation reaction.

## 4.5.7 Characterization of *N*-(4-methyl-6-((trimethylsilyl) ethynyl) pyrimidin-2-yl)-*N*-phenylformamide

### 4.5.7.1 $^1\text{H-NMR}$

Figure 4.18 shows the  $^1\text{H-NMR}$  spectrum of *N*-(4-methyl-6-((trimethylsilyl) ethynyl) pyrimidin-2-yl)-*N*-phenylformamide and the assignments of the relevant peaks.

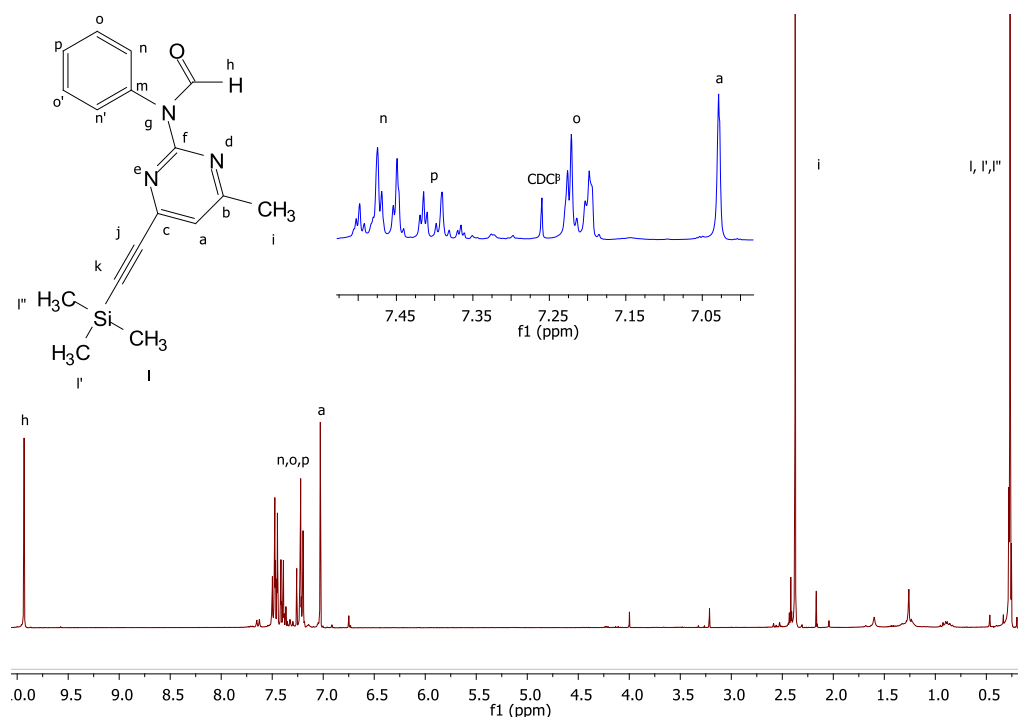


Figure 4.18  $^1\text{H-NMR}$  spectrum of *N*-(4-methyl-6-((trimethylsilyl) ethynyl) pyrimidin-2-yl)-*N*-phenylformamide and the assignment of the peaks.

The same peaks are observed as in the 4-methyl-2-(methylsulfonyl)-6-((trimethylsilyl) ethynyl) pyrimidine compound (Refer to Figure 4.16), except the disappearance of the methyl protons adjacent the sulphur atom, the appearance of new aromatic peaks and an aldehyde proton peak.

A peak downfield at 9.93 ppm is characteristic of aldehyde protons. Between 7.17 - 7.51 ppm the new aromatic protons are observed. The peaks between 7.44 - 7.51 ppm are designated to the aromatic protons (n, n'). Between 7.33 - 7.44 ppm the aromatic proton (p) is observed and between 7.17 - 7.25 ppm the peaks are designated to the aromatic protons (o, o'). These peaks



integrate 2:1:2, which correlate to the 5 new aromatic protons presence. The appearance of the aldehyde proton peak (h), aromatic proton peaks (n, o, p) and the disappearance of the methyl protons (h) at 3.31 ppm (Refer to Figure 4.16) preliminary confirms the synthesis of this compound.

A peak at 7.02 ppm is designated to the aromatic proton (a). The methyl protons (i) are observed at 2.37 ppm and integrate 3:1 relative to the aromatic proton in the pyrimidine ring (a) and 1:1 to the aldehyde proton (h). The alkyne protecting group TMS is observed at 0.26 ppm. The protons of this moiety are more shielded than most other known moieties. TMS protons come out at the end of the range (ppm).

#### 4.5.7.2 $^{13}\text{C}$ -NMR

The results obtained from the  $^1\text{H}$ -NMR spectrum were confirmed by  $^{13}\text{C}$ -NMR spectroscopy. The  $^{13}\text{C}$ -NMR spectrum of *N*-(4-methyl-6-((trimethylsilyl) ethynyl) pyrimidin-2-yl)-*N*-phenylformamide and the assignment of the relevant peaks are shown in Figure 4.19.

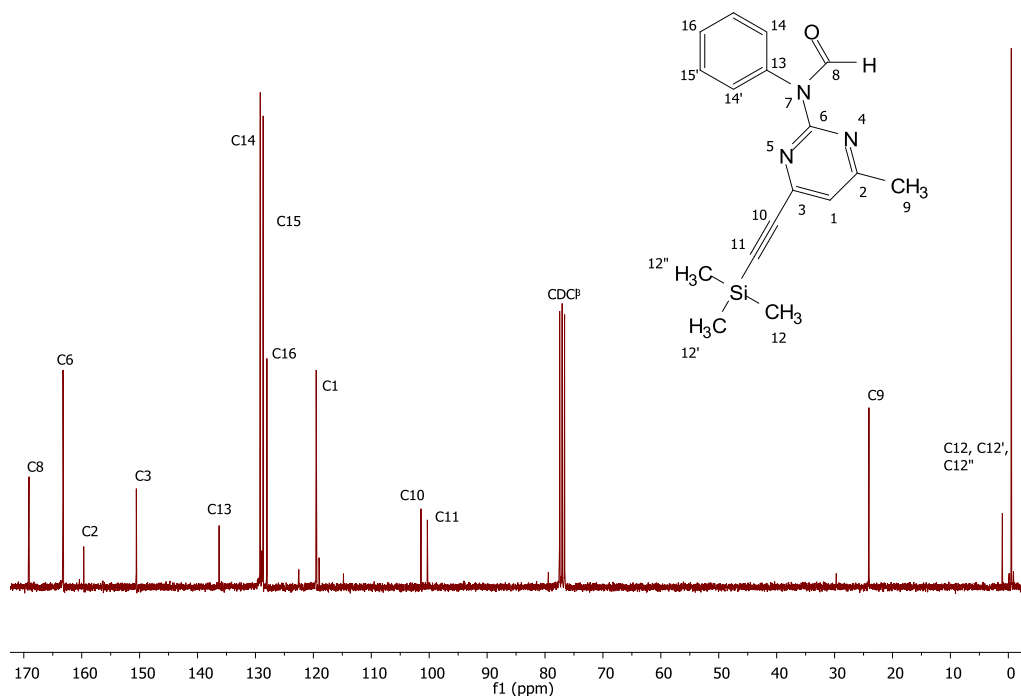


Figure 4.19  $^{13}\text{C}$ -NMR spectrum of *N*-(4-methyl-6-((trimethylsilyl) ethynyl) pyrimidin-2-yl)-*N*-phenylformamide and the assignment of the peaks.

The same peaks are observed as in the 4-methyl-2-(methylsulfonyl)-6-((trimethylsilyl) ethynyl) pyrimidine compound (Refer to Figure 4.17), except the disappearance of the methyl protons adjacent the sulphur atom, the appearance of new aromatic peaks and an aldehyde carbon peak appearing.

A peak is observed at 169.2 ppm, designated to the aldehyde carbon (C8). In literature the most profound range in which aldehydes absorb is 185 - 220 ppm, due to the shielding effect of two aromatic rings the peak is observed at a lower chemical shift.<sup>17</sup> A peak is observed at 163.4 ppm, designated to the methine carbon in the aromatic ring adjacent to the newly introduced nitrogen and the two nitrogens in the pyrimidine ring (C6). The electron withdrawing ability, the hybridization of the carbon and the anisotropy effect of the ring have an influence of the position of the peak.

The methine carbon (C2) that has the methyl group attached to it is observed at 159.58 ppm. The other methine carbon (C3) is observed at 150.5 ppm. The unsaturated carbon chain has a shielding effect on C3 due to the unsaturated carbon chain having a shielding effect on C3 due to shielding by the adjacent  $\pi$  bonds, causing the methine peak to be upfield from C2 carbon. The aromatic carbons (C13, C14, C15 and C16) are respectively observed at 136.3 ppm, 129.2 ppm, 128.7 ppm and 128.1 ppm. The peak at 119.5 ppm is designated to the methylene carbon in the pyrimidine ring (C1). The methyl carbon adjacent the sulphur atom has disappeared (Refer to Figure 4.17, C8). A peak at 23.9 ppm is observed that is characteristic of the methyl carbon on the pyrimidine ring (C9).

Two peaks observed at 101.4 ppm and 100.3 ppm are designated to C10 and C11 respectively. The same explanation as stated in Section 4.5.5.2 is applicable here for the more downfield shift of the C10 carbon. The peak at 1.05 ppm correlates to the TMS carbons (C12).

An aldehyde carbon (C8) and aromatic carbons (C13, C14, C15, C16) appearing and the disappearance of the methyl carbon stated above confirm the successful synthesis of *N*-(4-methyl-6-((trimethylsilyl) ethynyl) pyrimidin-2-yl)-*N*-phenylformamide

## 4.5.8 Characterization of *N*-(4-ethynyl-6-methylpyrimidin-2-yl)-*N*-phenylformamide

### 4.5.8.1 $^1\text{H-NMR}$

Figure 4.20 shows the  $^1\text{H-NMR}$  spectrum of *N*-(4-ethynyl-6-methylpyrimidin-2-yl)-*N*-phenylformamide and the assignments of the relevant peaks.

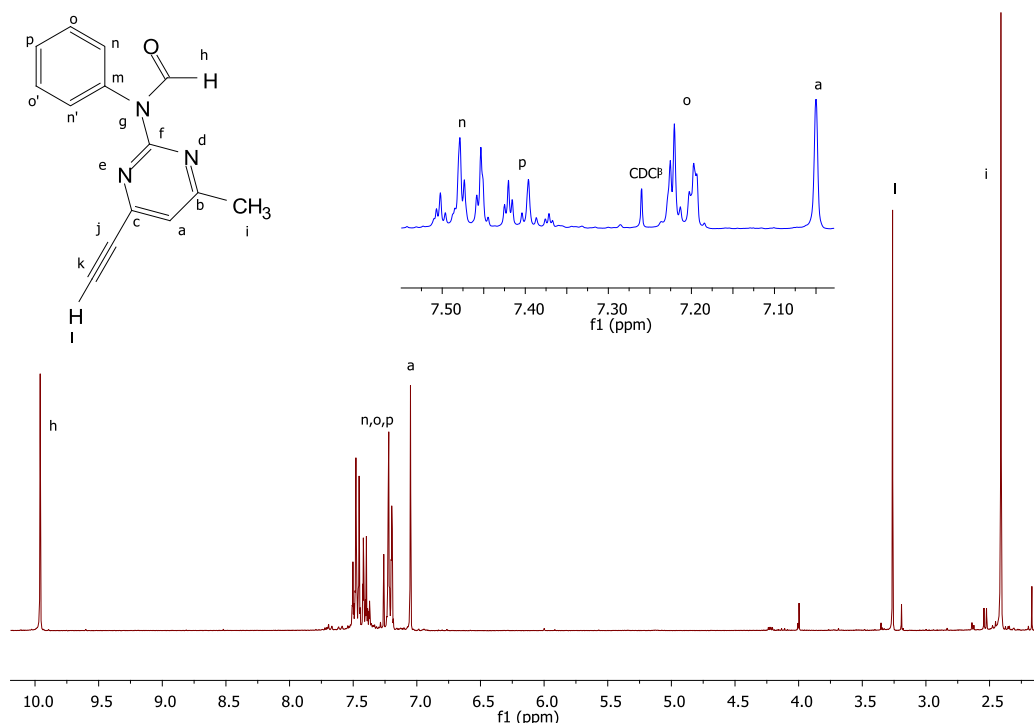


Figure 4.20  $^1\text{H-NMR}$  spectrum of *N*-(4-ethynyl-6-methylpyrimidin-2-yl)-*N*-phenylformamide and the assignment of the peaks.

Similar peaks are observed for *N*-(4-ethynyl-6-methylpyrimidin-2-yl)-*N*-phenylformamide as for *N*-(4-methyl-6-((trimethylsilyl) ethynyl) pyrimidin-2-yl)-*N*-phenylformamide (Refer to Figure 4.18). The difference is seen in the disappearance of the trimethylsilyl peak at 0.26 ppm and the appearance of the acetylic proton peak.

A peak downfield at 9.95 ppm is characteristic of aldehyde proton (h). Between 7.15 - 7.51 ppm the aromatic protons are observed (n, o, p). The peaks between 7.45 - 7.51 ppm are designated to the aromatic (n, n') protons. Between 7.35 - 7.45 ppm the aromatic proton (p) is observed and

between 7.17 - 7.23 ppm the peaks are designated to the aromatic (o, o') protons. These peaks integrate 2:1:2 which correlate to the 5 aromatic protons presence.

The appearance of the acetylic proton at 3.26 ppm (l) and the disappearance of the trimethylsilyl protons (Refer to Figure 4.18) at 0.26 ppm preliminary confirm the synthesis of this compound.

A peak at 7.05 ppm is designated to the aromatic proton (a). The methyl protons (i) are observed at 2.41 ppm and integrate 3:1 relative to the aromatic proton in the pyrimidine ring (a) and 1:1 to the aldehyde proton (h).

#### 4.5.8.2 $^{13}\text{C}$ -NMR

The results obtained from the  $^1\text{H}$ -NMR spectrum were confirmed by  $^{13}\text{C}$ -NMR spectroscopy. Figure 4.21 shows the  $^{13}\text{C}$ -NMR spectrum of *N*-(4-ethynyl-6-methylpyrimidin-2-yl)-*N*-phenylformamide and the assignment of the relevant peaks.

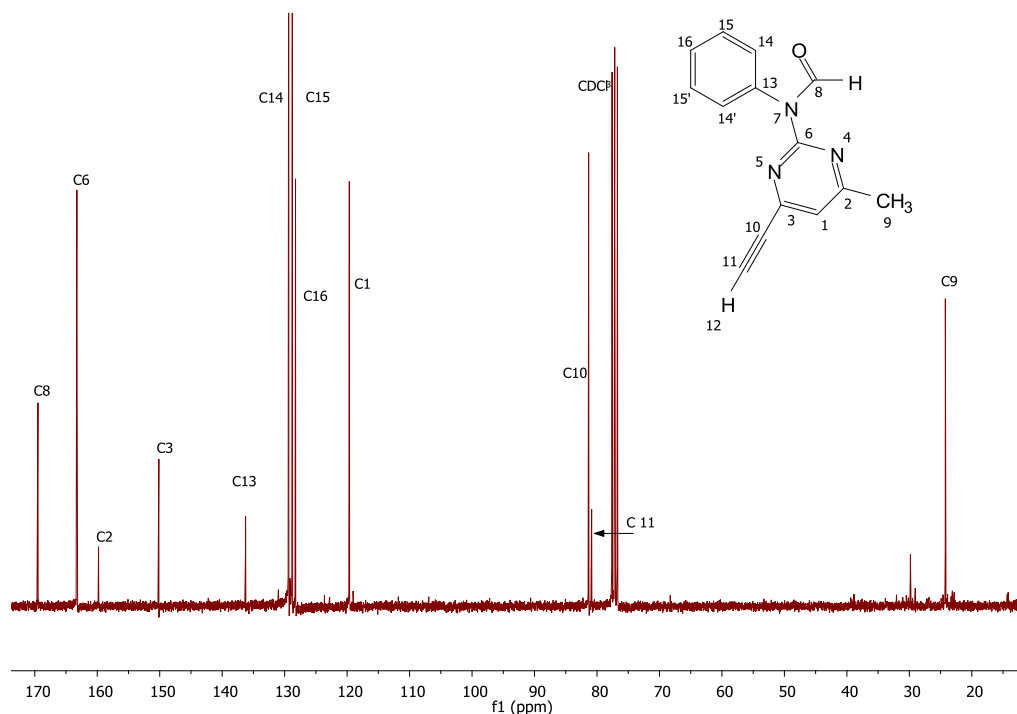


Figure 4.21  $^{13}\text{C}$ -NMR spectrum of *N*-(4-ethynyl-6-methylpyrimidin-2-yl)-*N*-phenylformamide and the assignment of the peaks.

Similar peaks are observed for *N*-(4-ethynyl-6-methylpyrimidin-2-yl)-*N*-phenylformamide as for *N*-(4-methyl-6-((trimethylsilyl) ethynyl) pyrimidin-2-yl)-*N*-phenylformamide (Refer to Figure 4.19). The difference is seen in the disappearance of the trimethylsilyl peak at 1.05 ppm and the results that have on the acetylic carbons in the carbon chain.

A peak is observed at 169.49 ppm, designated to the aldehyde carbon (C8). In literature, the most profound range in which aldehydes absorb is 185 - 220 ppm, due to the shielding effect of two aromatic rings the peak is observed at a lower chemical shift.<sup>17</sup> A peak is observed at 163.34 ppm, designated to the methine carbon in the aromatic ring adjacent to the three nitrogens (C6). The electron withdrawing ability, the hybridization of the carbon and the anisotropy effect of the ring have an influence of the position of the peak.

The methine carbon (C2) that has the methyl group attached to it is observed at 159.83 ppm. The other methine carbon (C3) is observed at 150.2 ppm. The unsaturated carbon chain has a shielding effect on C3 due to the unsaturated carbon chain having a shielding effect on C3 due to shielding by the adjacent  $\pi$  bonds, causing the methine peak to be upfield from C2 carbon. The aromatic carbons (C13, C14, C15 and C16) are respectively observed at 136.29 ppm, 129.39 ppm, 128.9 ppm and 128.25 ppm. The peak at 119.55 ppm is designated to the methylene carbon in the pyrimidine ring (C1).

C10 and C11 are observed at 81.3 ppm and 80.8 ppm, respectively. A shift is seen in these two peaks (Refer to Figure 4.19). This can be explained due to the deshielding TMS group not present, the peaks absorption is found to be more upfield.<sup>17</sup> A peak at 24 ppm is observed that is characteristic of the methyl carbon on the pyrimidine ring (C9).

The disappearance of the TMS carbons (C12) and the shift in the alkyl chain's carbons stated above confirm the successful synthesis of *N*-(4-ethynyl-6-methylpyrimidin-2-yl)-*N*-phenylformamide.

## 4.5.9 Characterization of 4-ethynyl-6-methyl-*N*-phenylpyrimidin-2-amine

### 4.5.9.1 $^1\text{H-NMR}$

The  $^1\text{H-NMR}$  spectrum of 4-ethynyl-6-methyl-*N*-phenylpyrimidin-2-amine and the assignments of the relevant peaks are shown in Figure 4.22.

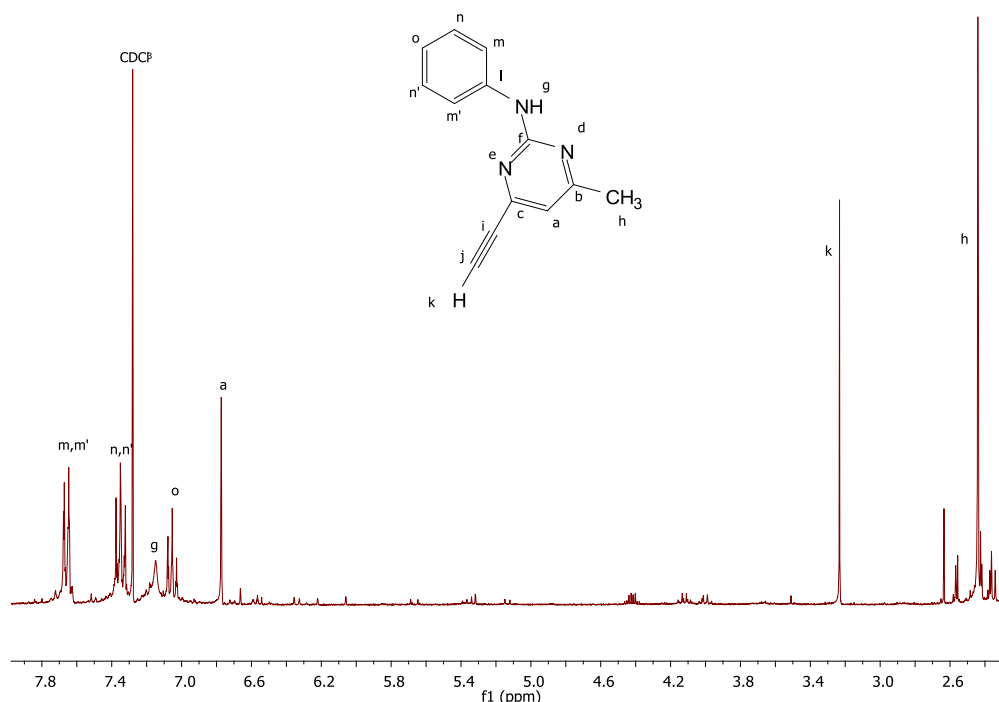


Figure 4.22  $^1\text{H-NMR}$  spectrum of 4-ethynyl-6-methyl-*N*-phenylpyrimidin-2-amine and the assignment of the peaks.

Similar peaks are observed for 4-ethynyl-6-methyl-*N*-phenylpyrimidin-2-amine than for *N*-(4-ethynyl-6-methylpyrimidin-2-yl)-*N*-phenylformamide. A difference is observed in the disappearance of the aldehyde peak at 9.95 ppm (Refer to Figure 4.22).

Between 6.99 - 7.67 ppm the aromatic protons are observed (n, o, p) and the amine proton (g). The peaks between 6.99- 7.05 ppm are designated to the aromatic (o) proton. Amine hydrogens exhibit hydrogen bonding that can have extremely variable absorption positions over a wide range. The position of the peak depends on the concentration, solvent, amount of hydrogen bonding and the temperature.<sup>17</sup> The more hydrogen bonding that occur, the more deshielded a proton become, appearing more downfield. A broad peak at 7.09 - 7.12 ppm correlates to the

amine hydrogen of the compound (g). Between 7.28 - 7.38 ppm the aromatic proton (n, n') is observed and between 7.59 - 7.70 ppm the peaks are designated to the aromatic (m, m') protons. These peaks integrate 2:2:1, which correlates to the 5 aromatic protons presence.

A peak at 6.75 ppm is designated to the aromatic proton (a). A peak at 3.21 ppm is designated to the acetylenic hydrogen (k). The methyl protons (h) are observed at 2.42 ppm and integrate 3:1 relative to the aromatic proton in the pyrimidine ring (a) and 3:5 to the aromatic protons (m, n, and o).

The disappearance of aldehyde proton (Refer to Figure 4.20) at 9.95 ppm preliminarily confirms the synthesis of this compound.

#### 4.5.9.2 $^{13}\text{C}$ -NMR

The results obtained from the  $^1\text{H}$ -NMR spectrum were confirmed by  $^{13}\text{C}$ -NMR spectroscopy. Figure 4.23 shows the  $^{13}\text{C}$ -NMR spectrum of 4-ethynyl-6-methyl-*N*-phenylpyrimidin-2-amine and the assignment of the relevant peaks.

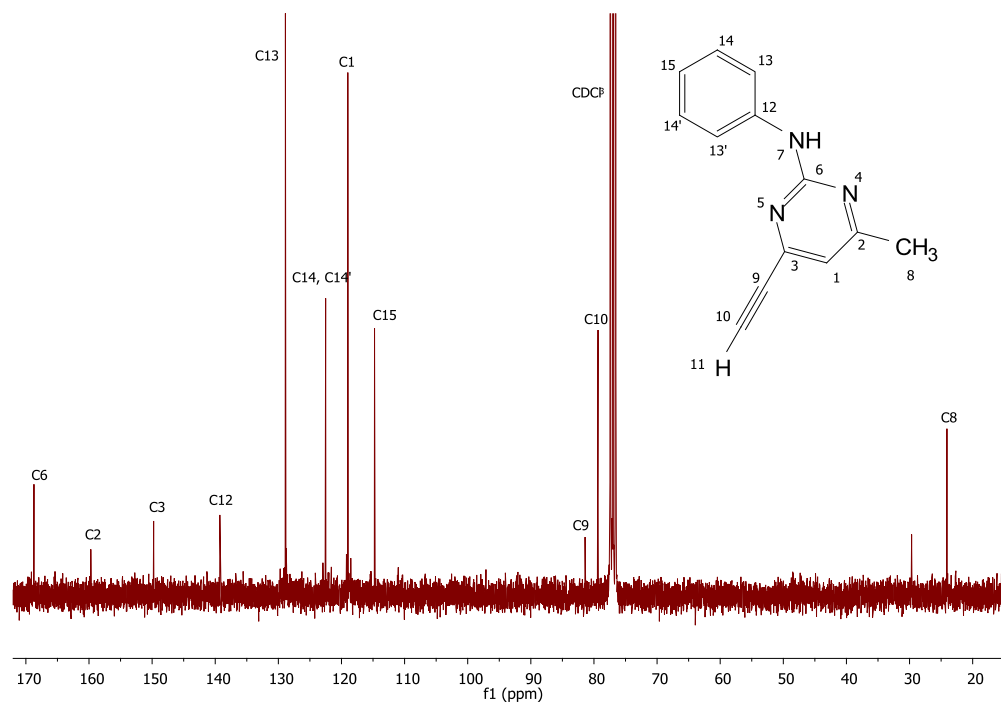


Figure 4.23  $^{13}\text{C}$ -NMR spectrum of 4-ethynyl-6-methyl-*N*-phenylpyrimidin-2-amine and the assignment of the peaks.

Similar peaks are observed for 4-ethynyl-6-methyl-*N*-phenylpyrimidin-2-amine than for *N*-(4-ethynyl-6-methylpyrimidin-2-yl)-*N*-phenylformamide. A difference is observed in the shift of the peaks and a disappearance of the aldehyde carbon (Refer to Figure 4.21).

A peak is observed at 168.78 ppm, designated to the methine carbon in the aromatic ring adjacent to the three nitrogens (C6). The electron withdrawing ability, the hybridization of the carbon and the anisotropy effect of the ring have an influence of the position of the peak.

The methine carbon (C2) that has the methyl group attached to it is observed at 159.97 ppm. The other methine carbon (C3) is observed at 150.07 ppm. The unsaturated carbon chain has a shielding effect on C3 due to anisotropy, causing the methine peak to be up field from C2 carbon. The aromatic carbons (C12, C13, C14, and C15) are respectively observed at 139.45 ppm, 128.9 ppm, 122.7 ppm and 114.94 ppm. The peak at 119.1 ppm is designated to the methylene carbon in the pyrimidine ring (C1). C9 and C10 are observed at 81.39 ppm and 79.53 ppm respectively. A peak at 24.25 ppm is observed that is characteristic of the methyl carbon on the pyrimidine ring (C9).

The disappearance of the TMS carbons (C12) and the disappearance of the aldehyde carbon confirm the successful synthesis of 4-ethynyl-6-methyl-*N*-phenylpyrimidin-2-amine.



#### 4.5.10 Characterization of poly(4-vinylbenzyl chloride-*alt*-maleic anhydride) copolymer (P(S<sub>Cl</sub>-*alt*-MANh))

##### 4.5.10.1 <sup>1</sup>H-NMR

Refer to Figure 4.24 for the <sup>1</sup>H-NMR spectrum of P(S<sub>Cl</sub>-*alt*-MANh) copolymer and the assignments of the relevant peaks.

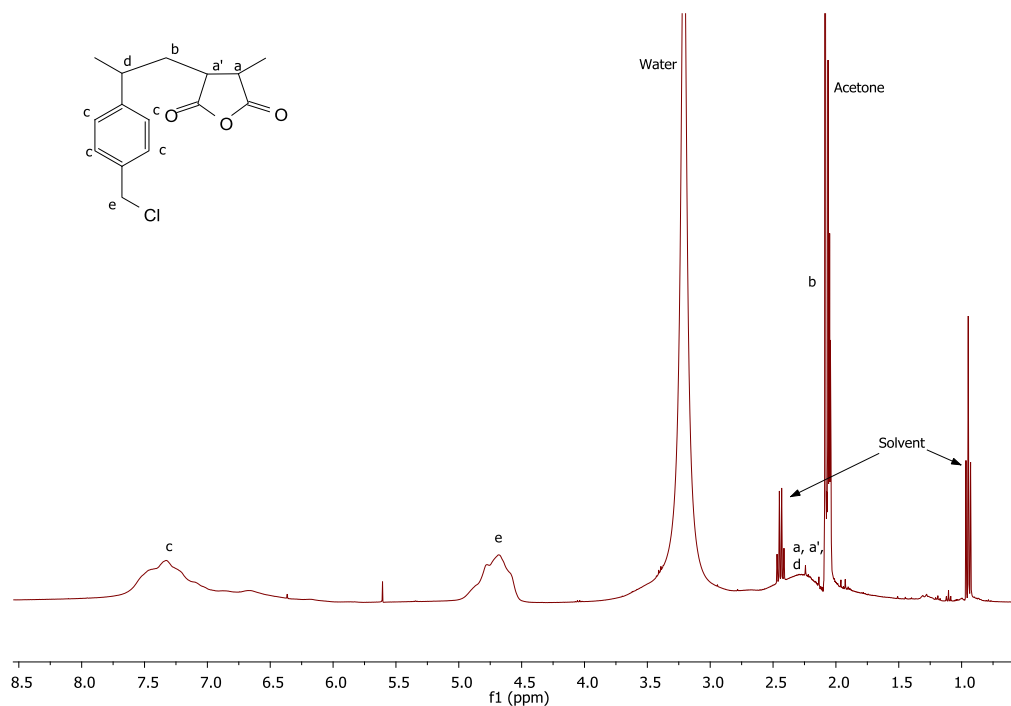


Figure 4.24 <sup>1</sup>H-NMR spectrum of poly(4-vinylbenzyl chloride-*alt*-maleic anhydride) copolymer and the assignment of the peaks.

P(S<sub>Cl</sub>-*alt*-MANh) is characterized by a poorly resolved resonance peak at 6.5 - 7.7 ppm that is ascribed to the four protons of the benzene ring unit (c). The methylene (b) and methine protons (a, a', d) originate from the maleic anhydride and 4-vinylbenzyl chloride monomers forming the backbone of the polymer respectively.<sup>11,19</sup> The backbone peaks are observed as a broad peak at 2.1 - 2.5 ppm (a, a', d) that are poorly resolved due to peak overlapping and 2.08 ppm (b).<sup>11,20</sup> The appearance of a broad peak at 4.5 - 4.9 ppm is indicative of the chloromethyl protons (e), providing evidence of the 4-vinylbenzyl chloride residue.<sup>11,12,21</sup> The peak integrates 2: 4 compared to the aromatic protons (c).<sup>11</sup>

It is difficult to calculate the respective maleic anhydride contents due to poor peak resolution. Although it is difficult to calculate the maleic anhydride contents in the polymer, the same trend as P(St-*alt*-MAh) copolymer (SMA) is expected (refer Section 3.2 in Chapter 3).

#### 4.5.10.2 $^{13}\text{C}$ -NMR

The results obtained from the  $^1\text{H}$ -NMR spectrum were confirmed by  $^{13}\text{C}$ -NMR spectroscopy. The  $^{13}\text{C}$ -NMR spectrum of P( $\text{S}_{\text{Cl}}$ -*alt*-MAh) and the assignment of the relevant peaks are shown in Figure 4.25.

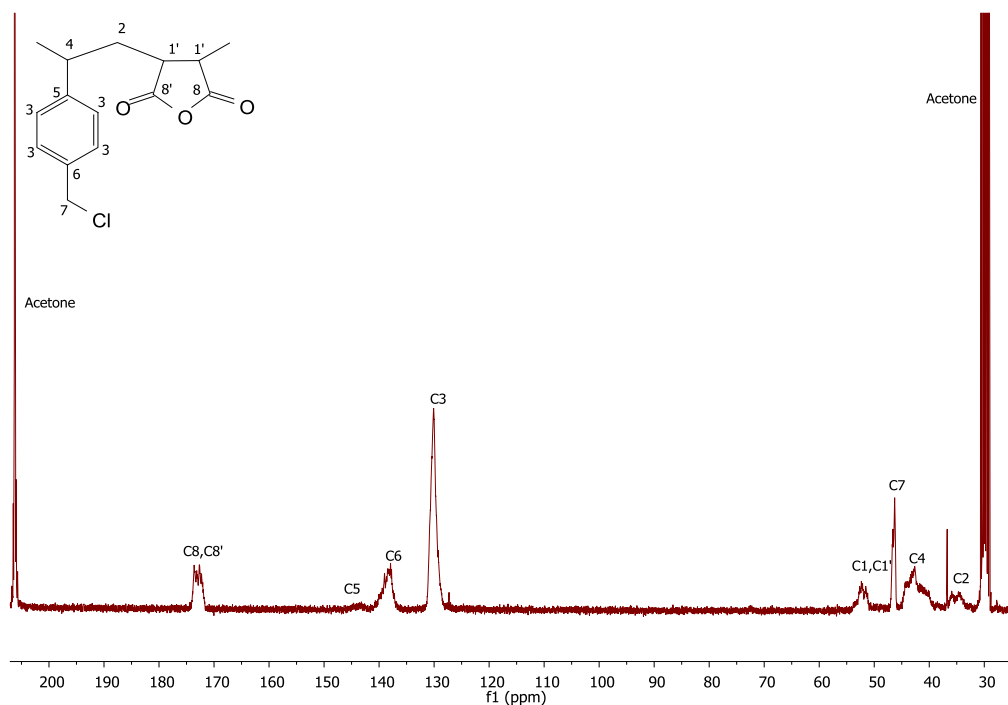


Figure 4.25  $^{13}\text{C}$ -NMR spectrum of poly(4-vinylbenzyl chloride-*alt*-maleic anhydride) copolymer and the assignment of the peaks.

A peak is observed at 172.9 ppm, designated to the carbonyl carbons of the maleic anhydride unit (C8, C8'). Peaks observed at 143 ppm, 138.6 ppm and 129.8 ppm corresponds to the aromatic carbons of the styrene unit (C5, C6, and C3). Peaks at 51.9 ppm 38.9 - 44.7 ppm and 35 ppm are poorly resolved and are designated to the methine carbons (C1 and C4) and methylene carbon (C2) of the polymer backbone. The peak at 46.4 ppm is indicative of a chloromethyl carbon (C7) which is in good agreement with literature.<sup>21</sup> C7 being more downfield than the methylene carbon C2 due to the more electron withdrawing chlorine moiety being

adjacent to the methylene carbon C7.<sup>21</sup> The chloromethyl carbon peak is also in good agreement with literature.<sup>21</sup>

#### 4.5.11 Characterization of poly(4-vinylbenzyl azide-*alt*-maleic anhydride) copolymer (P(S<sub>Cl</sub>-*alt*-MAnh))

##### 4.5.11.1 <sup>1</sup>H-NMR

Refer to Figure 4.26 for the <sup>1</sup>H-NMR spectrum of P(S<sub>N</sub>-*alt*-MAnh) and the assignments of the relevant peaks.

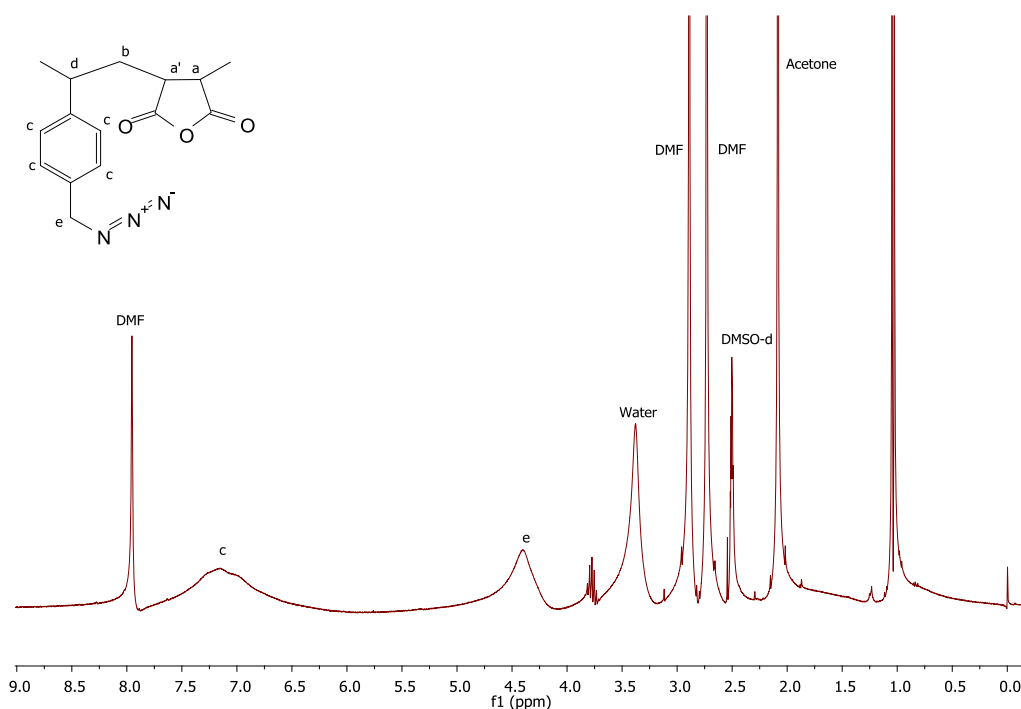


Figure 4.26 <sup>1</sup>H-NMR spectrum of poly(4-vinylbenzyl azide-*alt*-maleic anhydride) copolymer and the assignment of the peaks.

P(S<sub>N</sub>-*alt*-MAnh) is characterized by a poorly resolved resonance peak at 6.5 - 7.5 ppm that is ascribed to the four protons of the benzene ring moiety (c). The broad peak at 4.2 - 4.6 ppm is indicative of the benzylic methylene groups (e) adjacent the azide moiety. The resonance of the benzylic methylene groups shifted significantly upfield from 4.5 - 4.9 ppm (Refer to Figure 4.24, for P(S<sub>Cl</sub>-*alt*-MAnh)) to 4.2 - 4.6 ppm (for P(S<sub>N</sub>-*alt*-MAnh)).<sup>21</sup> The shift of the methylene protons

(e) is in good agreement with literature.<sup>12,21</sup> The shift of the peak is confirmation of the substitution reaction that took place and the absence of a resonance peak at 4.5 - 4.9 ppm suggests that the substitution reaction had occurred to completion. The peak integrates 2: 4 compared to the aromatic protons (c).<sup>11</sup>

#### 4.5.11.2 <sup>13</sup>C-NMR

The results obtained from the <sup>1</sup>H-NMR spectrum were confirmed by <sup>13</sup>C-NMR spectroscopy. The <sup>13</sup>C-NMR spectrum of P(S<sub>N</sub>-*alt*-MAH) and the assignment of the relevant peaks are shown in Figure 4.27.

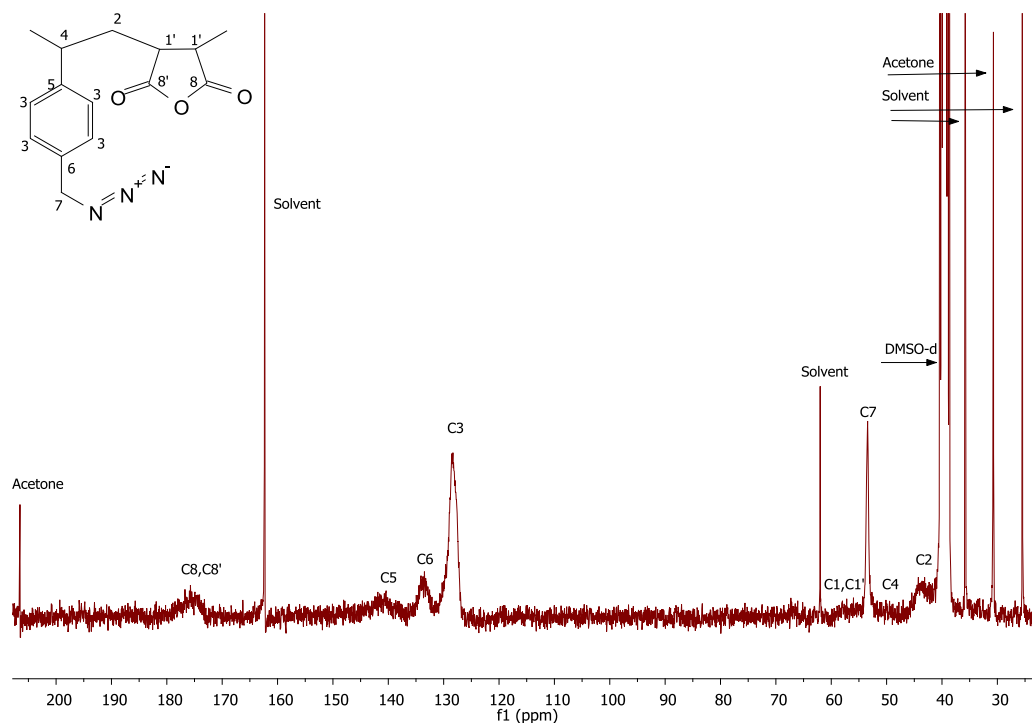


Figure 4.27 <sup>13</sup>C-NMR spectrum of poly(4-vinylbenzyl azide-*alt*-maleic anhydride) copolymer and the assignment of the peaks.

A peak is observed at 175 ppm, designated to the carbonyl carbons of the maleic anhydride unit (C8, C8'). Peaks observed at 138 - 144 ppm, 133 ppm and 128 ppm corresponds to the aromatic carbons of the styrene unit (C5, C6, and C3). Peaks at 55 - 60.1 ppm, 46.2 - 50.2 ppm and 42 ppm are poorly resolved and are designated to the methine carbons (C1 and C4) and methylene carbon (C2) of the polymer backbone, respectively. The peak at 53 ppm is indicative of the benzylic methylene carbon (C7) adjacent the azide moiety.<sup>21,22</sup> The C7 carbon being more

downfield in the P(S<sub>N</sub>-*alt*-MAh) polymer compared to the C7 carbon in P(S<sub>Cl</sub>-*alt*-MAh) (Refer to Figure 4.25) due to the more electron withdrawing azide moiety deshielding the carbon more. The higher chemical shift of the benzylic methylene carbon (53 ppm) compared to the chloromethyl carbon (Refer to Figure 4.25, 46.4 ppm) confirms the formation of an azide functionality and the substitution reaction being completed and successful.

## 4.5.12 Characterization of functionalized anilinyrimidine<sub>7</sub>-derivative copolymer (P(S<sub>AP7</sub>-alt-MAnh)).

### 4.5.12.1 <sup>1</sup>H-NMR

Refer to Figure 4.28 for the <sup>1</sup>H-NMR spectrum of the functionalized anilinyrimidine<sub>7</sub>-derivative copolymer (P(S<sub>AP7</sub>-alt-MAnh)) and the assignments of the relevant peaks.

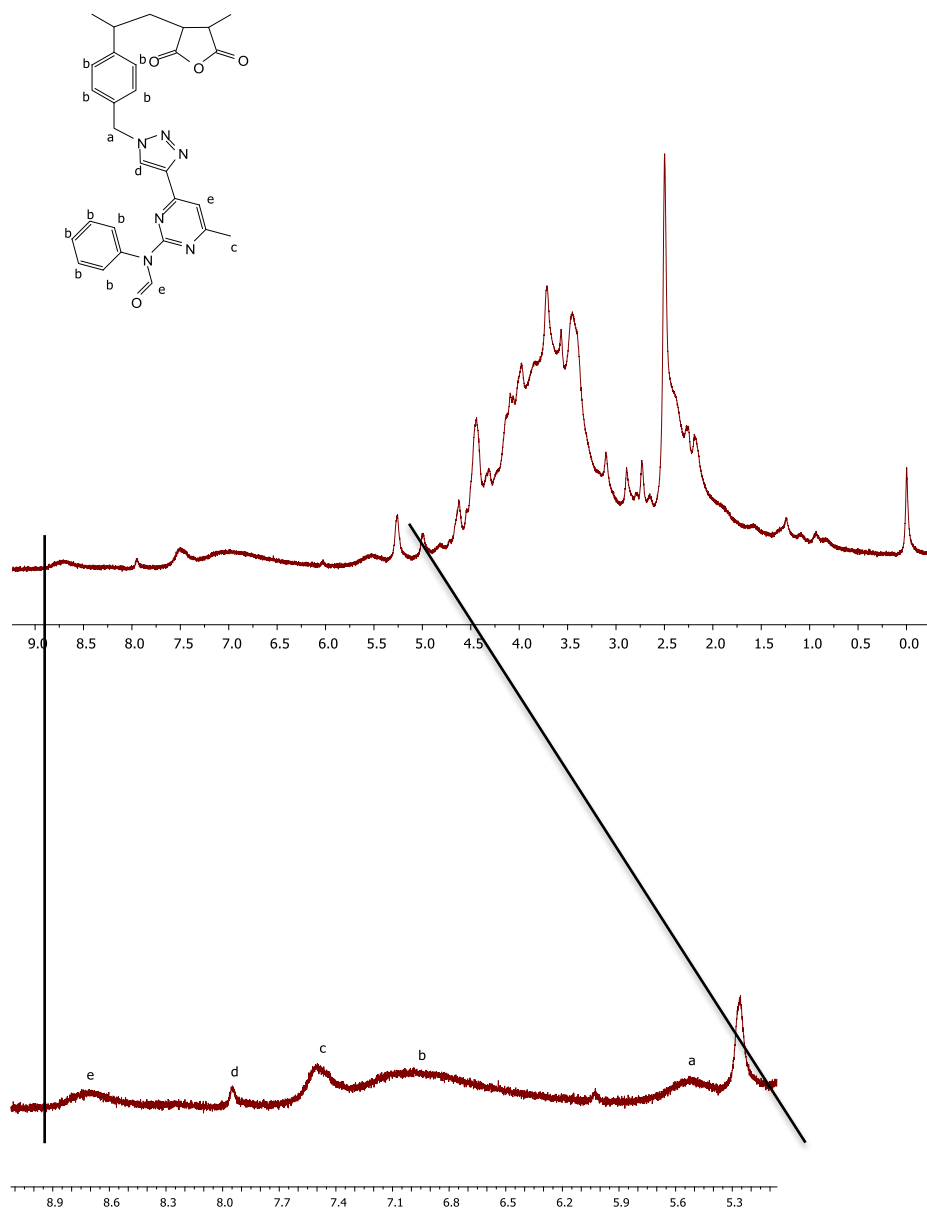


Figure 4.28 <sup>13</sup>C-NMR spectra of functionalized anilinyrimidine<sub>7</sub>-derivative copolymer (P(S<sub>AP7</sub>-alt-MAnh)) and the assignment of the peaks.

Although the  $^1\text{H-NMR}$  spectrum have overlapping peaks, the shift in the peak of the benzylic methylene adjacent to the azide moiety to the methylene proton adjacent to the newly introduced triazole ring, the newly introduced aromatic, aldehyde and methyl protons can be observed between 5.38 - 8.91 ppm.<sup>11,21,22</sup> After performing the copper (I)-catalyzed Azide-Alkyne Cyclo-addition (CuAAC), the signal of the benzylic methylene protons at 4.2 - 4.6 ppm (Refer to Figure 4.26) shifted downfield to 5.39 - 5.62 ppm with an integration of 2 protons (a) (for  $\text{P}(\text{S}_{\text{AP7-}alt\text{-MAh}})$ ).<sup>21</sup> The shift of the benzylic methylene protons adjacent to the newly introduced triazole moiety is in good agreement with literature.<sup>21</sup> The aromatic protons (b) appear at 6.63 - 7.31 ppm that integrates to 9 protons. During the click reaction, the acetylenic proton (l) at 3.26 ppm for *N*-(4-ethynyl-6-methylpyrimidin-2-yl)-*N*-phenylformamide (compound 7, Refer to Figure 4.20) become the C-H proton (d) on the triazole ring. This proton appears downfield at 7.95 pm for  $\text{P}(\text{S}_{\text{AP7-}alt\text{-MAh}})$  that integrates to 1 proton.<sup>21</sup> Both the aromatic proton at 7.05 ppm and the aldehyde proton for compound 7 shifted downfield to 8.57 - 8.84 ppm (e), the peak integrates to 2 protons.<sup>21</sup> The methyl protons (c) on the compound appear at 7.36 - 7.59 ppm, the shift is in good agreement with literature.<sup>21</sup> The shift of the benzylic methylene protons adjacent to the triazole moiety and the appearance of new aromatic, aldehyde and methyl protons confirm the successful synthesis of  $\text{P}(\text{S}_{\text{AP7-}alt\text{-MAh}})$  polymer.<sup>21</sup>

#### 4.5.13 Characterization of $\text{P}(\text{S}_{\text{Cl-}alt\text{-MAh}}$ ), $\text{P}(\text{S}_{\text{Cl-}alt\text{-MAh}}$ ) and $\text{P}(\text{S}_{\text{AP7-}alt\text{-MAh}}$ ) copolymers using ATR-FTIR spectroscopy

$\text{P}(\text{S}_{\text{Cl-}alt\text{-MAh}}$ ),  $\text{P}(\text{S}_{\text{N-}alt\text{-MAh}}$ ) and  $\text{P}(\text{S}_{\text{AP7-}alt\text{-MAh}}$ ) were dried at 60 °C under vacuum to remove any residual solvent and were characterized using ATR-FTIR. Refer to Figure 4.29 for the representative ATR-FTIR spectra of  $\text{P}(\text{S}_{\text{Cl-}alt\text{-MAh}}$ ) (top),  $\text{P}(\text{S}_{\text{N-}alt\text{-MAh}}$ ) (middle) and  $\text{P}(\text{S}_{\text{AP7-}alt\text{-MAh}}$ ) (bottom).

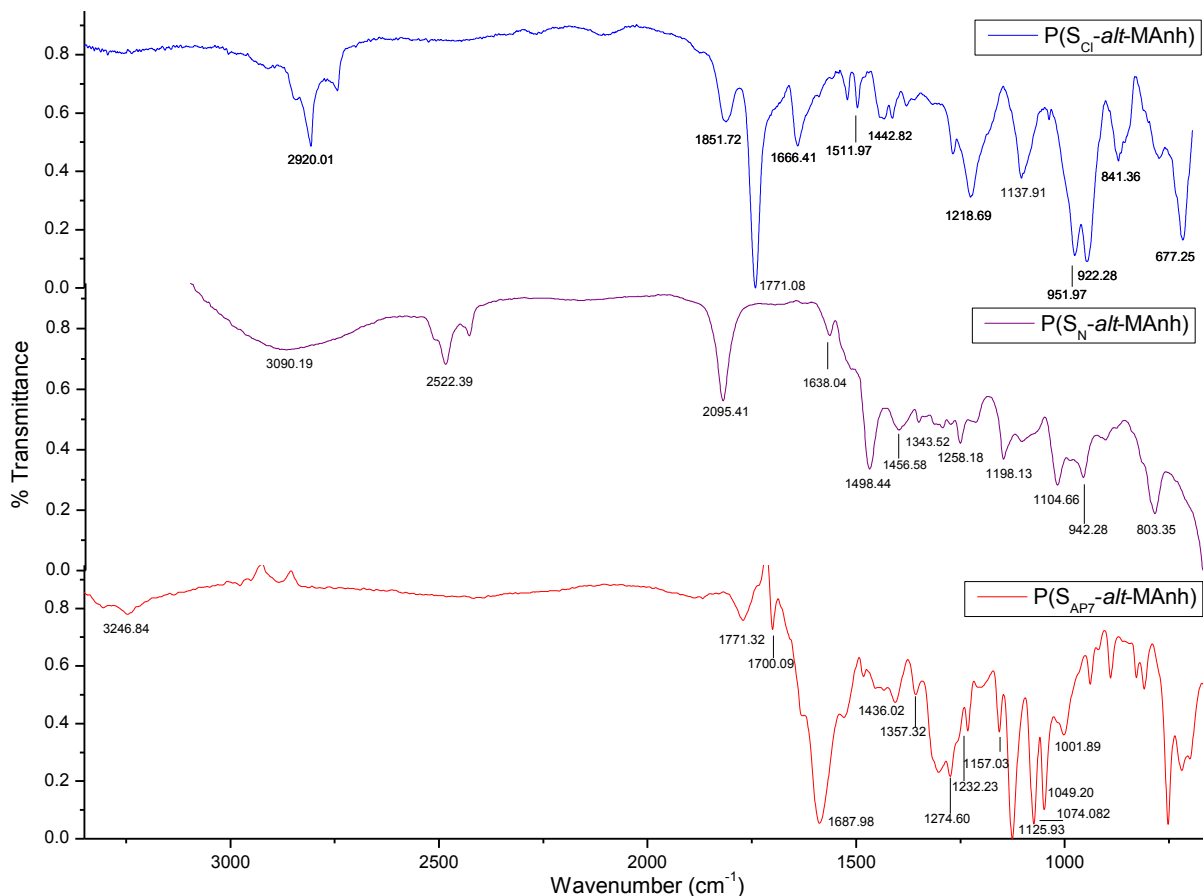


Figure 4.29 ATR-FTIR spectra of (a)  $P(S_{Cl}\text{-alt-MAh})$  (top), (b)  $P(S_{N}\text{-alt-MAh})$  (middle) and (c)  $P(S_{AP7}\text{-alt-MAh})$  (bottom).

$P(S_{Cl}\text{-alt-MAh})$  is characterized by a pair of bands of the carbonyls absorbing at  $1771.08\text{cm}^{-1}$  and  $1851.72\text{cm}^{-1}$  (Refer to Figure 4.29 (top)) due to the symmetrical and asymmetrical carbonyl stretch vibrations of the anhydride moiety. A characteristic band appears at  $1218.69\text{cm}^{-1}$  corresponding to the C-O stretch vibrations of the cyclic five-membered anhydride. The small band at  $3106.01\text{cm}^{-1}$  are due to  $\text{sp}^2$  aromatic C-H bending vibrations of the polymer chain and the bands at  $2920.01\text{cm}^{-1}$  are due to the  $\text{sp}^3$  aliphatic C-H stretch vibrations of the polymer chain and the methylene unit on the 4-vinylbenzyl residue. The bands at  $1442.82\text{cm}^{-1}$  and  $1511.97\text{cm}^{-1}$  corresponds to the C=C stretching vibrations of the aromatic ring and the C-H stretching vibrations of the polymer chain. These results are in good agreement with literature.<sup>19,20,23,24</sup>

The azide polymer ( $P(S_{N}\text{-alt-MAh})$ ) was confirmed by the characteristic appearance of a strong absorption band at  $2095.14\text{cm}^{-1}$  due to the presence of azido groups (Refer to Figure 4.29 (middle)).<sup>21,22</sup>



FTIR spectroscopy analysis of the anilinopyrimidine<sub>7</sub>-derivative copolymer (P(S<sub>AP7</sub>-*alt*-MANh)) (Refer to Figure 4.29 (bottom)) confirmed the complete disappearance of the characteristic signal of the azido group at 2095.14 cm<sup>-1</sup>. The band at 2095.14 cm<sup>-1</sup> is absent in the spectrum of P(S<sub>AP7</sub>-*alt*-MANh) (bottom) indicating that the azido functionality had participated in the click reaction.<sup>21</sup> The formation of a 1,2,3-triazole ring in the chain is further confirmed at ~ 3200 cm<sup>-1</sup> due to the C-H stretch vibration and the in-plane out-of-plane vibrations of the C-H group at 1074.08 cm<sup>-1</sup> and 1049.20 cm<sup>-1</sup> with the triazole ring-in-plane bending vibration band present at 1001 cm<sup>-1</sup>.<sup>22</sup>

The C-N stretch vibrations are difficult to assign due to mixing of bands are possible in the region.<sup>22,25</sup> The C=N stretch vibrations and the maleic anhydride's ring opening bands are overlapping at ~ 1687.98 cm<sup>-1</sup>.<sup>25</sup> Stretch vibration bands characteristic of N-C and C-N bonds are present at 1450.89 cm<sup>-1</sup> and 1436.02 cm<sup>-1</sup>. N-H in-plane and N-N bending vibrations are present at 1157.03 cm<sup>-1</sup> and 1274.60 cm<sup>-1</sup> respectively.<sup>25</sup>

Taken together, the NMR and FTIR spectra confirmed the successful synthesis of P(S<sub>Cl</sub>-*alt*-MANh), P(S<sub>N</sub>-*alt*-MANh) and P(S<sub>AP7</sub>-*alt*-MANh) copolymers.

#### 4.5.14 SEM analysis: Characterization of single needle- and single ball electrospun P(S<sub>Cl</sub>-*alt*-MANh) polymer nanofibers

The P(S<sub>Cl</sub>-*alt*-MANh) polymer was dissolved in a suitable 1:1 solvent system, DMF: THF, at a concentration for an acceptable number of polymer chain entanglement. The polymer solution was single needle and single ball electrospun. Single needle electrospinning was done at different condition varying in electric field strength and spinning distance. SEM images with regard to fiber diameter and fiber morphology indicated that the optimum polymer concentration was 25 wt. %. The conditions at which the single ball electrospinning process was conducted varied in electric field strength, spinning distance, humidity and rotating speed of the glass ball. SEM images (Refer to Figure 4.30) with regard to fiber diameter and fiber morphology indicated that the optimum polymer concentration was 25 wt. %.

Analysis of the SEM images indicated that the average fiber diameter for the single needle electrospun  $P(S_{Cr}\text{-}alt\text{-}MANh)$  polymer nanofibers was  $515 \pm 83$  nm and for the single ball electrospun  $P(S_{Cr}\text{-}alt\text{-}MANh)$  polymer nanofibers was  $585 \pm 113$  nm.

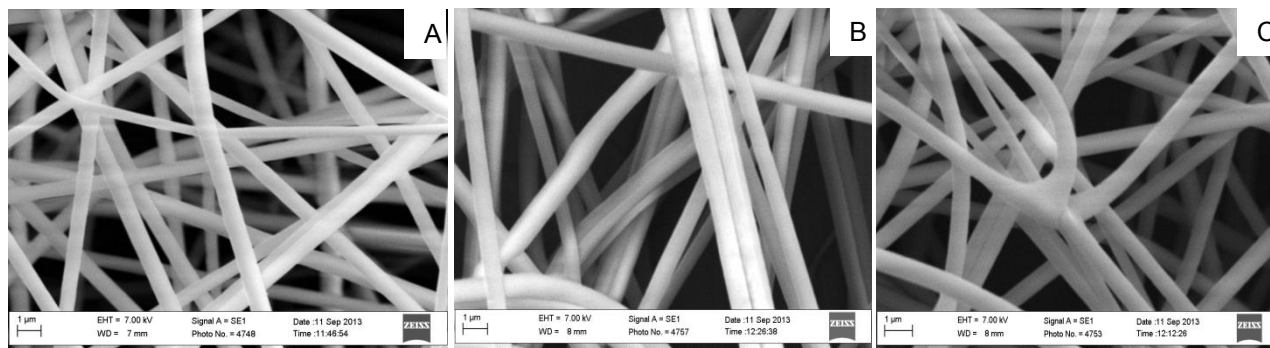


Figure 4.30 SEM images of  $P(S_{Cr}\text{-}alt\text{-}MANh)$  polymer nanofibers using single needle and single ball electrospinning. Image A was obtained using the single needle electrospinning process: Polymer concentration 25 wt. %; applied voltage 16 kV, ambient humidity <50%, temperature 20 °C, 15 cm spinning distance and a flow rate of  $0.2 \text{ mL}\cdot\text{min}^{-1}$ . Images B and C were obtained using the single ball electrospinning process: Polymer concentration 25 wt. %, applied voltage 55 kV, 10 cm spinning distance and an ambient humidity <50%.

#### 4.5.15 SEM analysis: Characterization of single needle- and single ball electrospun $P(S_N\text{-}alt\text{-}MANh)$ polymer nanofibers

The electrospinning process was unsuccessful, refer Section 4.4.2, no fibers were obtained to be able to characterize.

#### 4.5.16 SEM and ATR-FTIR analysis: Characterization of post-electrospinning modified $P(S_N\text{-}alt\text{-}MAh)$ polymer nanofibers

When  $P(S_{Cl}\text{-}alt\text{-}MAh)$  nanofibers were surface-functionalized, the fibers retained the nanofibrous structure and integrity. Refer to Figure 4.31 for the representative SEM images A and B of functionalized nanofibers without washing and images C and D that are functionalized nanofibers that were thoroughly washed. It is clear from the SEM images that the nanofibrous structure was preserved during functionalization. This is vital for the benefit of the high surface area to volume ration of the functionalized fibers.

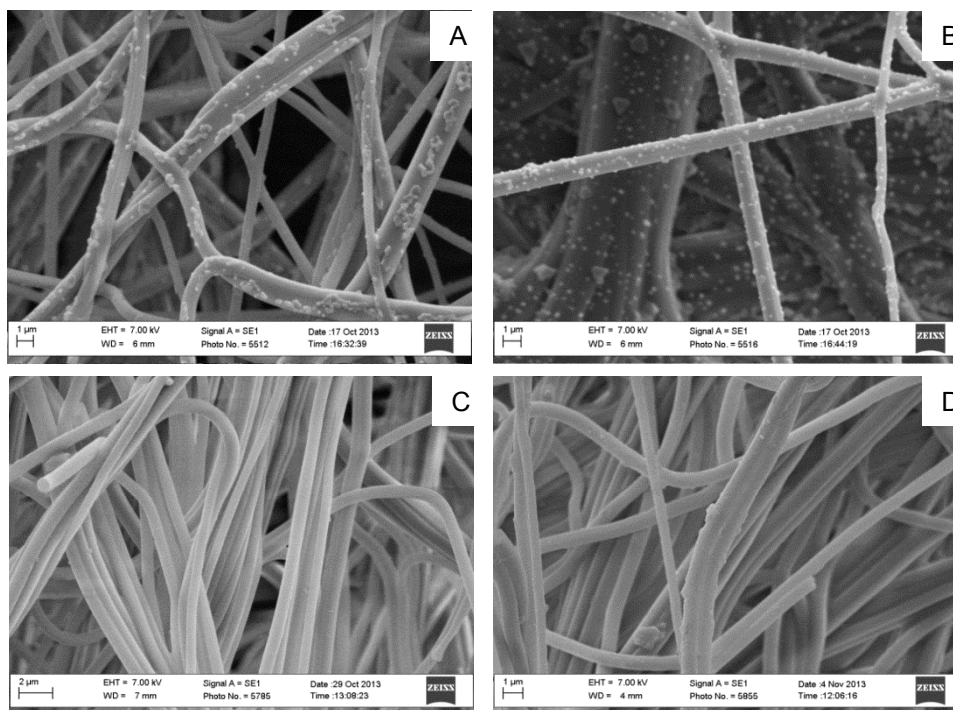


*Figure 4.31 SEM images of the post-electrospinning of  $P(S_{Cl}\text{-}alt\text{-}MAh)$  nanofibers to obtain azide functionalized  $P(S_N\text{-}alt\text{-}MAh)$  nanofibers. Images A and B are functionalized polymer nanofibers without washing (crystals present on surface of nanofibers). Images C and D are functionalized polymer nanofibers that were thoroughly washed.*

In the event of a successful post-electrospinning modification reaction, the azide moiety will substitute the chloride moiety on the polymer. From the ATR-FTIR spectra, the most important band is the formation of the strong characteristic absorption band at  $2095.14\text{ cm}^{-1}$  due to the presence of azido groups.<sup>21,22</sup>

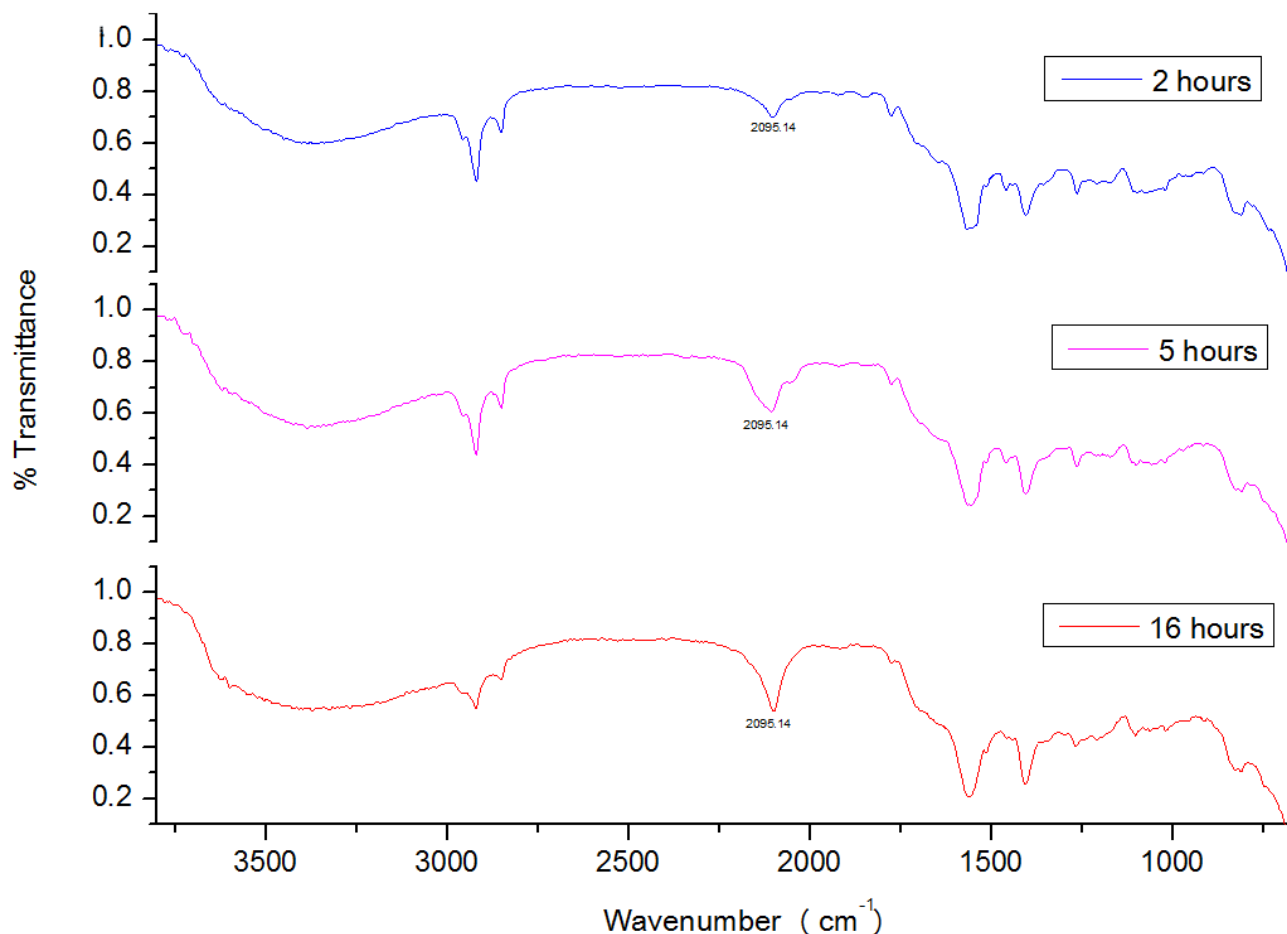


Figure 4.32 ATR-FTIR spectra of (a)  $P(S_{Cr}\text{-alt-}MANh)$  polymer nanofibers modified for 2 hours (top), (b)  $P(S_{Cr}\text{-alt-}MANh)$  polymer nanofibers modified for 5 hours (middle), (c)  $P(S_{Cr}\text{-alt-}MANh)$  polymer nanofibers modified for 16 hours (bottom).

The modification reaction was monitored after 2 hours, 5 hours and 16 hours to establish the reaction time needed for substantial substitution to occur. After 2 hours (Refer to Figure 4.32 (top)) a small bump could be seen at  $2095.14\text{ cm}^{-1}$ . After 16 hours (Refer to Figure 4.32 (bottom)) a sharper and more characteristic band appeared. The solvent system chosen caused ring-opening of the maleic anhydride residue to occur.<sup>26</sup> The solvent system had to be chosen to be able to preserve the nanofibrous structure during the substitution reaction. It was more

important to preserve the nanofibrous structure compared to the closed maleic anhydride unit. The ring opened maleic anhydride did not compete in the functionalization reaction that followed.

#### 4.5.17 SEM and ATR-FTIR analysis: Characterization of post-electrospinning functionalized anilinopyrimidine<sub>7</sub>-derivative polymer nanofibers (P(S<sub>AP7</sub>-*alt*-MANh))

P(S<sub>N</sub>-*alt*-MANh) nanofibers were surface-functionalized with *N*-(4-ethynyl-6-methylpyrimidin-2-yl)-*N*-phenylformamide (anilinopyrimidine<sub>7</sub>-derivative). During the functionalization the fibers retained their nanofibrous structure and integrity. Refer to Figure 4.33 for the representative SEM images A and B of functionalized nanofibers. It is clear from the SEM images that the nanofibrous structure was preserved during functionalization. This is vital for the benefit of the high surface area to volume ratio of the functionalized polymer nanofibers.

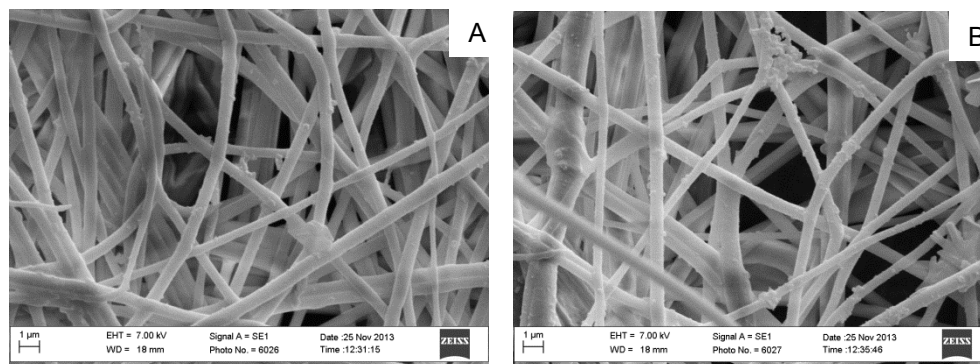


Figure 4.33 SEM images of functionalized anilinopyrimidine<sub>7</sub>-derivative polymer nanofibers (P(S<sub>AP7</sub>-*alt*-MANh)).

Comparing the ATR-FTIR spectrum of the post-electrospinning surface-functionalization reaction of the polymer nanofibers (Refer to Figure 4.34) to the anilinopyrimidine<sub>7</sub>-derivative polymer (P(S<sub>AP7</sub>-*alt*-MANh)) (refer Section 4.5.13, Figure 4.29) similar bands are observed with different intensities.

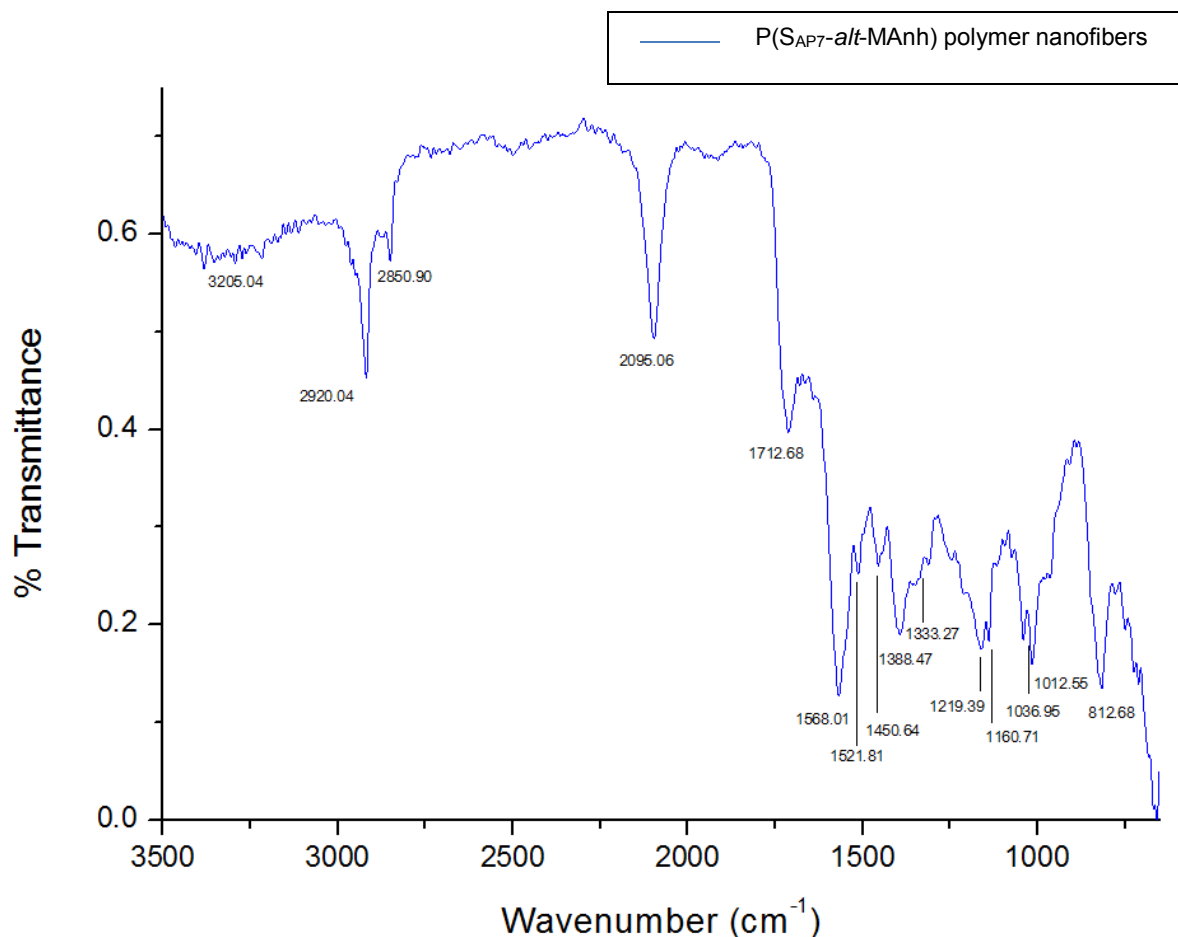


Figure 4.34 ATR-FTIR spectra of post-electrospinning modification to yield functionalization anilinopyrimidine- $\gamma$ -derivative polymer nanofibers ( $P(S_{AP7}\text{-alt-MAnh})$ ).

The formation of a 1,2,3-triazole ring in the chain is confirmed by a band appearing at  $\sim 3200\text{ cm}^{-1}$  due to the C-H stretch vibration and the in-plane out-of-plane vibrations of the C-H group at  $1073.15\text{ cm}^{-1}$  and  $1019.54\text{ cm}^{-1}$ .<sup>22</sup>

The C-N stretch vibrations are difficult to assign due to the possible overlap of bands in the region.<sup>22,25</sup> The C=N stretch vibrations and the maleic anhydride's ring opening bands are overlapping at  $\sim 1710.04\text{ cm}^{-1}$ .<sup>25</sup> Due to azide polymer nanofibers still present it is difficult to characterize the FTIR spectrum due to peak overlapping.

## 4.6 Conclusion

In the present chapter, the synthesis is described of a new polymer for anti-fungal use against *B. cinerea*. All fungicide-derivatives were successfully synthesized, including *N*-(4-ethynyl-6-methylpyrimidin-2-yl)-*N*-phenylformamide (anilinopyrimidine<sub>7</sub>-derivative) and 4-ethynyl-6-methyl-*N*-phenylpyrimidin-2-amine (anilinopyrimidine<sub>8</sub>-derivative). This method, involving the covalent attachment of specifically synthesized fungicide-derivatives to a material surface, has the possibility of being effective against *B. cinerea*.<sup>27</sup>

The functionalization reaction of the P(S<sub>N</sub>-*alt*-MANh) polymer with the anilinopyrimidine<sub>7</sub>-derivative was successful in yielding anilinopyrimidine<sub>7</sub>-derivative copolymer (P(S<sub>AP7</sub>-*alt*-MANh)). This reaction was successful, but electrospinning this polymer could not be done until now, due to time constraints and under the giving chemical conditions.

To obtain the functionalized polymer nanofibers the modification was done post-electrospinning. It is the first time every that P(S<sub>Cl</sub>-*alt*-MANh) polymer has been electrospun into polymer nanofibers. In literature it could not be found that this polymer has been electrospun before. P(S<sub>Cl</sub>-*alt*-MANh) polymer nanofibers were successfully modified to obtain P(S<sub>N</sub>-*alt*-MANh) nanofibers. The final anilinopyrimidine<sub>7</sub>-derivative polymer nanofibers (P(S<sub>AP7</sub>-*alt*-MANh)) was synthesized through further post-electrospinning modification reactions. The post-electrospinning functionalization reaction of P(S<sub>N</sub>-*alt*-MANh) nanofibers needs to be optimized. Different solvents compared to the polymer needs to be used as the nanofibrous structure need to be preserved. Under the giving chemical conditions the azido moiety did not disappear completely.

## 4.7 Experimental

### 4.7.1 Chemicals

Thiourea (Sigma Aldrich > 99%), methyl iodide (Sigma Aldrich > 99%), sodium carbonate (Merck chemicals), ethylacetoacetate (Riedel de Haen), acetic acid (Merck chemicals), phosphorous oxychloride (Merck chemicals, >99%), magnesium sulphite (Merck chemicals), hydroiodic acid (Analar chemicals), sodium thiosulphate (Merck chemicals), ammonium chloride (Merck

chemicals), Cu(I)I (Sigma Aldrich, >99%), Bis(triphenylphosphine)-palladium(II) dichloride (Sigma Aldrich >98%), oxone (Organic chemistry), iso-propylether (Sigma Aldrich 99+%), sodium hydride (Sigma Aldrich, 60% dispersed in mineral oil), formanilide (Sigma Aldrich, 99%), sodium azide (Riedel de Haen), sodium hydroxide pellets >85% (Merck Chemicals), Copper(I) bromide (Cu(I)Br) (Sigma Aldrich), copper sulphate penta hydride (Sigma Aldrich, >99%), ascorbic acid (Sigma Aldrich), L(+) ascorbic acid (Fluka, >99%), *N,N,N',N'',N'''*-pentamethyldiethylenetriamine (PMDETA) (Sigma Aldrich, 99%), 4-Vinylbenzyl chloride monomer 99.5% (Fluka chemika), maleic anhydride 99% (Sigma-Aldrich), formanilide (Aldrich, 99%), acetonitrile (Sigma)m methyl ethyl ketone  $\geq 99.7\%$  (Sigma-Aldrich), isopropanol (Kimix), and diethyl Ether (Kimix), ethyl acetate (Kimix), dichloromethane (Kimix), ethanol (Kimix), chloroform (Kimix), methanol (Kimix), hexane (Kimix), were used without purification. 2, 2' Azobis (isobutyronitrile) (AIBN) (Riedel de Haen) was recrystallized twice using methanol and dried under vacuum before use. Tetrahydrofuran (Kimix), *N,N*-dimethylformamide (Kimix), Triethylamine (Sigma Aldrich) and methanol (Kimix) were distilled and kept on 4 Å molecular sieves.

## 4.7.2 Characterization techniques

### 4.7.2.1 Nuclear magnetic resonance spectroscopy (NMR)

A Varian Inova 300 MHz and 400 MHz NMR spectrometer and Varian Inova 600 MHz NMR spectrometer were used for the NMR analysis. After the samples were run Mestrenova computer software was used to analyze the spectrums that were obtained. Characterization and integration was done on the program.

Deuterated dimethyl sulfoxide (Sigma-Aldrich®, 99.9 atom % DMSO- $d_6$ ), deuterated acetone (Sigma-Aldrich®, 99.9 atom % Acetone- $d_6$ ) and deuterated chloroform (Sigma-Aldrich®, 99.9 atom %  $CDCl_3$ ) was used to prepare NMR samples.

### 4.7.2.2 Attenuated total reflectance Fourier transform infrared (ATR-FTIR) spectroscopy

Infrared spectra were recorded using a Nicolet FTIR spectrometer (model Nexus) from Thermo-Fischer equipped with a Smart Golden Gate ATR accessory with a diamond/ZnSe internal



reflection crystal. The spectra were recorded from  $3250\text{ cm}^{-1}$  to  $905\text{ cm}^{-1}$  with a spectral resolution of  $8\text{ cm}^{-1}$  and the sum of 64 individual scans.

Samples were run in solid state and no sample preparation was necessary. Omnic software was used for data acquisition and processing of the data was done using Origin software.

#### 4.7.2.3 Scanning electron microscopy (SEM)

Images of SMA polymer, SMI polymer, SMI-qC<sub>12</sub> polymer and SMI-qC<sub>12</sub> polymer with sodium metabisulfite salt that was electrospun were obtained using a Leo® 1430VP Scanning Electron Microscope (SEM). For each fiber mat that was analysed, small squares, approximately 0.5 cm x 0.5 cm, were cut out and attached to a SEM stub using carbon double sided tape. The carbon tape is used to make sure good conductivity between the SEM stub and the sample is established. Prior to imaging the SEM stubs were sputter coated with gold under vacuum for 3 minutes. After imaging the images were analysed using an imaging analysis program, SEM Image Studio, to obtain data regarding fiber diameter. An average of 100 fiber diameters was measured per sample and the average fiber diameter and the standard deviation were calculated using Microsoft Excel 2010.

#### 4.7.2.4 Size exclusion chromatography (SEC)

Molar mass and dispersity ( $\mathcal{D}$ ) were obtained using size exclusion chromatography (SEC). SEC analysis was carried out on a DMAc solvent system. The SEC instrument consists of a Waters 1515 isocratic HPLC pump, a Waters 717 plus auto-sampler, Waters 600E system controller (run by Breeze Version 3.30 SPA) and a Waters in-line Degasser AF. A Waters 2414 differential refractometer was used at  $30\text{ }^{\circ}\text{C}$  in series with a Waters 2487 dual wavelength absorbance UV/Vis detector operating at variable wavelengths. DMAc was used as eluent at flow rates of  $1\text{ ml min}^{-1}$ . The column oven was kept at  $30\text{ }^{\circ}\text{C}$  and the injection volume was  $100\text{ }\mu\text{l}$ . Two PLgel (Polymer Laboratories)  $5\text{ }\mu\text{m}$  Mixed-C (300 x 7.5 mm) columns and a pre-column (PLgel  $5\text{ }\mu\text{m}$  Guard, 50 x 7.5 mm) were used. Calibration was done using narrow polystyrene standards ranging from 580 to  $2 \times 10^6\text{ g.mol}^{-1}$ . All molecular weights were reported as polystyrene equivalents. Data acquisition was done using Millennium software, version 4.

Samples were prepared dissolving samples in BHT stabilized THF (2mg/ml). Sample solutions were filtered via syringe through  $0.45\text{ }\mu\text{m}$  nylon filters before subjected to analysis.

#### 4.7.3 Synthesis of S-methylisothiourea using thiourea and methyl iodide

In a three-neck round bottom flask 5.211 g (68 mmol) thiourea was dissolved in 70 mL anhydrous methanol. After the thiourea was completely dissolved, 10.68 g (4.7 mL, 74.8 mmol) methyl iodide (MeI) was carefully added dropwise to the solution. The solution was stirred for 1.5 hours at room temperature, if heat is applied straight after the MeI will degrade. After stirring the reaction mixture the heat was gradually increased, the reaction was allowed to reflux for 30 min after which was left to cool to room temperature. Solvent was removed using reduced pressure. The crude product, dark red/orange crystals were recrystallized from acetonitrile to yield 13.3918 g S-methylisothiourea colourless needle-like crystals. Obtaining a 90.3% yield.

$^1\text{H-NMR}$  ( $\text{CDCl}_3$ ):  $\delta$  (ppm) = 8.7 - 9.05 (s, 3H N-H, N-H<sub>2</sub>), 3.56 (s, 3H, -CH<sub>3</sub>).

$^{13}\text{C-NMR}$  ( $\text{CDCl}_3$ ):  $\delta$  (ppm) = 171 (C), 13.9 (S-CH<sub>3</sub>).

#### 4.7.4 Synthesis of 4-hydroxy-6-methyl-2-(methylthio)-pyrimidine from S-methylisothiourea and ethyl acetoacetate

In a three-neck round bottom flask sodium bicarbonate (3.9199 g, 36.69 mmol) was dissolved in 11.5 mL deionised water. After the solution became clear, 8.001 g (36.69 mmol) S-methylisothiourea was added, after which the solution became white and very viscous. 13 mL water was added to dissolve the solids. 2.34 mL (18.344 mmol) ethyl acetoacetate was added at once and the reaction turned a light green/yellow colour. The reaction mixture was left to stir for 60 hours at room temperature. Overnight it turned a milky colour. The reaction mixture was neutralized with acetic acid, precipitating a white solid. The solids were collected and washed with water, dried under vacuum to yield 2.547 g 4-hydroxy-6-methyl-2-(methylthio)-pyrimidine, giving an 88.8% yield.

$^1\text{H-NMR}$  ( $\text{CDCl}_3$ ):  $\delta$  (ppm) = 5.88 (s, 1H, C-H), 3.65 - 4.5 (s broad, 1H, -C-OH), 2.4 (s, 3H, S-CH<sub>3</sub>), 2.1 (s, 3H, C-CH<sub>3</sub>).

$^{13}\text{C-NMR}$  ( $\text{CDCl}_3$ ):  $\delta$  (ppm) = 171 (S-C, aromatic), 169 (C-OH), 168 (C-CH<sub>3</sub>), 111 (C, aromatic), 28.3 (S-CH<sub>3</sub>-), 18 (C-CH<sub>3</sub>).

#### 4.7.5 Synthesis of 4-chloro-6-methyl-2-(methylthio)-pyrimidine from 4-hydroxy-6-methyl-2-(methylthio)-pyrimidine and phosphorous oxychloride

0.77 g (4.929 mmol) 4-Hydroxy-6-methyl-2-(methylthio)-pyrimidine was added to a three-neck round bottom flask. The starting material melts at room temperature. Phosphorous oxychloride is in a 10:1 excess, between 7.5-10 mL  $\text{POCl}_3$  was added dropwise very carefully. When  $\text{POCl}_3$  come in contact with the 4-hydroxy-6-methyl-2-(methylthio)-pyrimidine compound, boiling/bubbling is observed and heat is released. The solution changes colour from white to light yellow and forms small pieces of solid material. As refluxing occurs the solution turns first a bright orange and then a darker red and lastly back to original yellow colour. The reaction mixture was left at reflux temperature for 3 hours, cooled to room temperature and poured over crushed ice. This step was done with extreme caution as phosphorous oxychloride is highly dangerous and exothermic if in contact with water. The resultant aqueous mixture was extracted with ethyl acetate, the organic layer washed with saturated sodium bicarbonate, followed by a water wash. The resultant mixture was left to dry over magnesium sulphate and dried in vacuum to yield of 4-chloro-6-methyl-2-(methylthio)-pyrimidine in 88.4% yield.

$^1\text{H-NMR}$  ( $\text{CDCl}_3$ ):  $\delta$  (ppm) = 7.2 (s, 1H, C-H), 2.48 (s, 3H, S- $\text{CH}_3$ ), 2.39 (s, 3H, C- $\text{CH}_3$ ).

$^{13}\text{C-NMR}$  ( $\text{CDCl}_3$ ):  $\delta$  (ppm) = 172.4 (S-C, aromatic), 170.3 (C-Cl), 160.7 (C- $\text{CH}_3$ ), 116.4 (C, aromatic), 23.7 (S- $\text{CH}_3$ -), 14 (C- $\text{CH}_3$ ).

#### 4.7.6 Synthesis of 4-iodo-6-methyl-2-(methylthio)-pyrimidine from 4-chloro-6-methyl-2-(methylthio)-pyrimidine and hydroiodic acid

In a two-neck round bottom flask 4.926 g (28.6 mmol) of 4-Chloro-6-methyl-2-(methylthio)-pyrimidine was added and 8.7 mL (194.6 mmol) of HI acid was slowly added dropwise. The addition was done while in an ice bath to keep the reaction at low temperature as HI are highly exothermic. After the addition the reaction flask was added to a pre-heated oil bath at 50 °C. The reaction was left to react for 24 hours. The reaction mixture was allowed to cool down to room temperature after which the solid residue was filtered off, collected with water. The water mixture was neutralized till pH 8 with aqueous sodium bicarbonate and extracted with ethyl

acetate. The organic layer, a dark red layer, was washed with aqueous sodium thiosulphate and further washed with water, dried with magnesium sulphate and the solvent was removed under vacuum. The residual solids were rinsed with hexane to give 4.095 g of light brown 4-iodo-6-methyl-2-(methylthio)-pyrimidine solid obtaining a yield of 53%.

$^1\text{H-NMR}$  ( $\text{CDCl}_3$ ):  $\delta$  (ppm) = 7.63 (s, 1H, C-H), 2.46 (s, 3H, S- $\text{CH}_3$ ), 2.31 (s, 3H, C- $\text{CH}_3$ ).

$^{13}\text{C-NMR}$  ( $\text{CDCl}_3$ ):  $\delta$  (ppm) = 171.2 (S-C, aromatic), 167.6 (C-I), 130.8 (C- $\text{CH}_3$ ), 127.1 (C, aromatic), 23.1 (S- $\text{CH}_3$ -), 14 (C- $\text{CH}_3$ ).

#### 4.7.7 Palladium cross-coupling reaction yielding 4-methyl-2-(methylthio)-6-((trimethylsilyl) ethynyl) pyrimidine

The freeze-pump-thaw method was used in preparation of an air-free experiment. 20 ml freshly dried triethylamine (TEA) was used and the freeze-pump-thaw cycle was repeated four times and then degassed using Ar for 1 hour. Under argon flow 38.8 mg (0.21 mmol) copper (I) I and 105.68 mg (0.21 mmol) bis (triphenylphosphine) palladium (II) dichloride ( $\text{Pd}(\text{PPh}_3)_2\text{Cl}_2$ ) catalyst was added. The solution stayed yellow which is an indication of the catalyst's activity still present. If the solution turned a dark brown/black the catalyst came in contact with oxygen or water and lost its reactivity. 1.37 g (5.16 mmol) 4-iodo-6-methyl-2-(methylthio)-pyrimidine was added to the solution under argon flow after which 0.79 mL (7.75 mmol) trimethylsilylacetylene was added. The solution turned a light brown colour. The reaction mixture was placed in a preheated 60 °C oil bath for 36 hours. The colour after 12 hours in the oil bath became a dark brown. The reaction mixture was quenched with a saturated aqueous solution of ammonium chloride ( $\text{NH}_4\text{Cl}$ ) and extracted with ethyl acetate (EA). The organic layer was washed with water and dried over magnesium sulphate ( $\text{MgSO}_4$ ).

In this step the desired compound was obtained in fairly good yield but with contamination due to the formation of side products. Column chromatography was needed to purify the compound. Crude product was purified by column chromatography (95 pentane: 5 EA) to obtain 992 mg 4-methyl-2-(methylthio)-6-((trimethylsilyl) ethynyl) pyrimidine giving a yield of 81.2%.

Under experimental conditions, the desired product is obtained as the major compound, but considerable amounts of side products are formed when the reaction is performed at room

temperature. The best results are obtainable using TEA as base, Pd (PPh<sub>3</sub>)<sub>2</sub>Cl<sub>2</sub> as catalyst, elevated temperatures and a 1.5:1 alkyne/iodide ratio.

<sup>1</sup>H-NMR (CDCl<sub>3</sub>): δ (ppm) = 6.9 (s, 1H, C-H), 2.54 (s, 3H, S-CH<sub>3</sub>), 2.41 (s, 3H, C-CH<sub>3</sub>), 0.24 (s, 9H, Si-CH<sub>3</sub>).

<sup>13</sup>C-NMR (CDCl<sub>3</sub>): δ (ppm) = 172.5 (S-C, aromatic), 167.4 (C-CH<sub>3</sub>), 149.9 (C aromatic), 118.5 (C, aromatic), 101.7 (Si-C≡), 99.4 (≡C-), 23.8 (S-CH<sub>3</sub>-), 14.1 (C-CH<sub>3</sub>), 0 (Si-CH<sub>3</sub>).

#### 4.7.8 Synthesis of 4-methyl-2-(methylsulfonyl)-6-((trimethylsilyl) ethynyl) pyrimidine via an oxidation reaction of 4-methyl-2-(methylthio)-6-((trimethylsilyl) ethynyl) pyrimidine

To a solution of 381.2 mg (1.613 mmol) 4-methyl-2-(methylthio)-6-((trimethylsilyl) ethynyl) pyrimidine in 2 mL of a 8:1 methanol: water mixture was 1.533 mg (2.42 mmol) oxone added below 35 °C. 1.5 mL water was added and the reaction mixture was stirred at room temperature for 5 hours. The solution was extracted with chloroform, the organic layers combined and solvent was removed using reduced pressure. The remaining liquid was rinsed using isopropyl ether (IPE) to give 327.4 mg 4-methyl-2-(methylsulfonyl)-6-((trimethylsilyl) ethynyl) pyrimidine and a yield of 75.6%.

<sup>1</sup>H-NMR (CDCl<sub>3</sub>): δ (ppm) = 7.3 (s, 1H, C-H), 3.31 (s, 3H, S-CH<sub>3</sub>), 2.6 (s, 3H, C-CH<sub>3</sub>), 0.25 (s, 9H, Si-CH<sub>3</sub>).

<sup>13</sup>C-NMR (CDCl<sub>3</sub>): δ (ppm) = 170.2 (S-C, aromatic), 165.8 (C-CH<sub>3</sub>), 151.1 (C aromatic), 125.8 (C, aromatic), 104 (Si-C≡), 100.2 (≡C-), 39.1 (S-CH<sub>3</sub>-), 24.11 (C-CH<sub>3</sub>), 0 (Si-CH<sub>3</sub>).

#### 4.7.9 Synthesis of *N*-(4-methyl-6-((trimethylsilyl) ethynyl) pyrimidin-2-yl)-*N*-phenylformamide via the addition of formanilide to 4-methyl-2-(methylsulfonyl)-6-((trimethylsilyl) ethynyl) pyrimidine

Sodium hydride was washed hexane (3 times) followed by washing with toluene (3 times). 435.5 mg (3.57 mmol) Formanilide was added to a 76.1 mg (3.25 mmol) sodium hydride in 10 mL toluene solution. The addition of formanilide caused boiling and foaming to occur. The solution occurred as a white milky colour. The mixture was emerged in a preheated oil bath of 50 °C for 30 minutes after which it was added to 797.9 mg (2.97 mmol) of the methylsulfonylpyrimidine. The mixture was stirred at room temperature for 15 hours, poured onto ice water and extracted with ethyl acetate. The organic layer was dried using MgSO<sub>4</sub> and solvent was removed under reduced pressure. The crude liquid was washed with IPE to obtain 244.6 mg 4-methyl-2-(methylsulfonyl)-6-((trimethylsilyl) ethynyl) pyrimidine having a yield of 26.6%.

<sup>1</sup>H-NMR (CDCl<sub>3</sub>): δ (ppm) = 9.93 (1H, -CH=O), 7.17 - 7.51 (5H, aromatic), 7.02 (s, 1H, C-H), 2.37 (s, 3H, C-CH<sub>3</sub>), 0.26 (s, 9H, Si-CH<sub>3</sub>).

<sup>13</sup>C-NMR (CDCl<sub>3</sub>): δ (ppm) = 169.2 (-CH=O), 163.4 (C-N), 159.58 (C-CH<sub>3</sub>), 150.5 (C aromatic), 136.3, 129.2, 128.7, 128.1 (C, aromatic), 119.5 (C, aromatic), 101.4 (Si-C≡), 100.3 (≡C-), 23.9 (C-CH<sub>3</sub>), 1.05 (Si-CH<sub>3</sub>).

Mass spec (m/z): 310.

#### 4.7.10 TBAF-mediated desilylation of *N*-(4-methyl-6-((trimethylsilyl) ethynyl) pyrimidin-2-yl)-*N*-phenylformamide to yield *N*-(4-ethynyl-6-methylpyrimidin-2-yl)-*N*-phenylformamide

50 ml of THF was added to 320.8 mg (1.357 mmol) of *N*-(4-methyl-6-((trimethylsilyl) ethynyl) pyrimidin-2-yl)-*N*-phenylformamide. 709.6 mg (2.714 mmol) TBAF in water (75 wt. %) was added to 5 mL THF. Both the THF solutions were added together in one step. The reaction was monitored using thin layer chromatography (TLC) plates in a 1:1 solution of pentane: ethyl acetate. The reaction mixture was filtered over a silica plug to remove any excess TBAF in the reaction mixture. Solvent was removed using reduced pressure to obtain 190.26 mg *N*-(4-ethynyl-6-methylpyrimidin-2-yl)-*N*-phenylformamide having a reaction yield of 94%.

$^1\text{H-NMR}$  ( $\text{CDCl}_3$ ):  $\delta$  (ppm) = 9.95 (1H,  $-\text{CH}=\text{O}$ ), 7.35 - 7.45 (5H, aromatic), 7.05 (s, 1H, C-H), 3.26 (1H,  $\text{H-C}\equiv$ ), 2.41 (s, 3H, C- $\text{CH}_3$ ).

$^{13}\text{C-NMR}$  ( $\text{CDCl}_3$ ):  $\delta$  (ppm) = 169.49 ( $-\text{CH}=\text{O}$ ), 163.34 (C-N), 159.83 (C- $\text{CH}_3$ ), 150.2 (C aromatic), 136.29, 129.39, 128.9, 128.25 (C, aromatic), 119.55 (C, aromatic), 81.3 (Si-C $\equiv$ ), 80.8 ( $\equiv\text{C-}$ ), 24 (C- $\text{CH}_3$ ).

Mass spec (m/z): 268.

#### 4.7.10 Synthesis of 4-ethynyl-6-methyl-*N*-phenylpyrimidin-2-amine via an oxidation reaction of *N*-(4-methyl-6-((trimethylsilyl) ethynyl) pyrimidin-2-yl)-*N*-phenylformamide

1 mL of an ethanol/THF (2:1) solution was added to 83.7 mg (0.2704 mmol) *N*-(4-methyl-6-((trimethylsilyl) ethynyl) pyrimidin-2-yl)-*N*-phenylformamide. Aqueous sodium hydroxide (3 M, 0.25 ml) was added and the reaction was left to stir at room temperature overnight. The reaction mixture was poured over water and extracted with ethyl acetate. The organic layer was washed with a saturated sodium chloride solution and dried over  $\text{MgSO}_4$ . The solvent was removed using reduced pressure and the compound was purified using column chromatography (95 Dichloromethane (DCM): 5 Methanol (MeOH)) obtaining 38.1 mg *N*-(4-methyl-6-((trimethylsilyl) ethynyl) pyrimidin-2-yl)-*N*-phenylformamide having a yield of 48.1%.

$^1\text{H-NMR}$  ( $\text{CDCl}_3$ ):  $\delta$  (ppm) = 6.99 - 7.67 (5H, aromatic and N-H), 6.75 (s, 1H, C-H), 3.21 (1H,  $\text{H-C}\equiv$ ), 2.41 (s, 3H, C- $\text{CH}_3$ ).

$^{13}\text{C-NMR}$  ( $\text{CDCl}_3$ ):  $\delta$  (ppm) = 168.78 (C-N), 159.97 (C- $\text{CH}_3$ ), 150.7 (C aromatic), 139.45, 128.9, 122.7, 114.94 (C, aromatic), 119.1 (C, aromatic), 81.39 (Si-C $\equiv$ ), 79.53 ( $\equiv\text{C-}$ ), 24.25 (C- $\text{CH}_3$ ).

Mass spec (m/z): 240.

#### 4.7.11 Synthesis of poly(4-vinylbenzyl chloride-*alt*-maleic anhydride) copolymer (P(S<sub>Cl</sub>-*alt*-MAh))

Conventional radical copolymerization was used to synthesize an alternating copolymer of 4-vinylbenzyl chloride and maleic anhydride in a 1:1 molar ratio chloride: maleic anhydride.<sup>20</sup>

Maleic anhydride (MAh) (15.2 g, 153 mmol), 4-vinylbenzyl chloride monomer (23.3 g, 153 mmol) and 2, 2' azobis (isobutyronitrile) (AIBN, 50 mg, 2.14 mmol) were dissolved in 250 mL methyl ethyl ketone (MEK). The reaction mixture was purged with Argon (Ar) for 45 min at room temperature and emerged into a 60 °C preheated oil bath. The Ar needle was taken out of the solution, but kept in the round bottom flask for another 50 min. After 50 min the Ar needle was removed and temperature was increased to 80 °C. The reaction mixture was stirred overnight for 24 hours. The reaction mixture was allowed to cool to room temperature after which the polymer was precipitate in diethyl ether. The P(S<sub>Cl</sub>-*alt*-MAh) polymer was isolated and dried in vacuum at 40 °C overnight to remove any unreacted monomer and residual solvent.<sup>11</sup> Analyses were done using SEC.  $M_n = 101662\text{g/mol}$ ,  $\bar{D} = 1.90$ , MAh content: 45 - 50%)

Major IR absorptions: 3106.01, 2920.01, 1851.72, 1771.08, 1666.41, 1511.97, 1442.82, 1218.69, 1137.91, 951.97, 922.28, 841.36, 677.25  $\text{cm}^{-1}$ .

<sup>1</sup>H-NMR (CDCl<sub>3</sub>):  $\delta$  (ppm) = 6.5 - 7.7 (s broad, 4H aromatic), 4.5 - 4.9 (s broad 2H, -CH-CH<sub>2</sub>-Cl), 2.1 - 2.5 (s broad, 3H, -CH-), 2.08 (s, 2H, -CH<sub>2</sub>-).

<sup>13</sup>C-NMR (CDCl<sub>3</sub>):  $\delta$  (ppm) = 172.9 (-O-C=O), 143 (aromatic C), 138.6 (aromatic C), 129.8 (aromatic -C=), 51.9 (-CH-CH-), 46.4 (CH<sub>2</sub>-Cl), 44.7 - 38.9 (-CH-), 35 (-CH<sub>2</sub>).



#### 4.7.12 Synthesis of functionalized poly(4-vinylbenzyl azide-*alt*-maleic anhydride) (P(S<sub>N</sub>-*alt*-MAh)) copolymer

The terminal nitrogen of the sodium azide is mildly nucleophilic. The chloride on the polymer can be substituted via a nucleophilic substitution reaction. P(S<sub>Cl</sub>-*alt*-MAh) copolymer (2.01 g, 7.86 mmol Chloride (Cl) functionality) was dissolved in 30 mL DMF. 1.53 g of sodium azide was placed in a 250 mL three neck round bottom. 8 mL DMF was placed in the round bottom to suspend the sodium azide and the polymer solution was slowly dripped into the round bottom over 60 min. The reaction mixture was left to stir for 24 hours at room temperature. After the reaction time the polymer was precipitated in diethyl ether and dried under vacuum at 40 °C for 4 hours to remove any residual solvent.

Major IR absorptions: 3090.19, 2522.39, 2095.41, 1638.04, 1498.44, 1456.58, 1258.18, 1198.13, 1104.66, 942.28, 803.35 cm<sup>-1</sup>.

<sup>1</sup>H-NMR (CDCl<sub>3</sub>): δ (ppm) = 6.5 - 7.5 (s broad, 4H aromatic), 4.2 - 4.6 (2H, -CH<sub>2</sub>-N<sub>3</sub>), 2.08 (s, 2H, -CH-CH<sub>2</sub>-CH-), 2.4 (s broad, 3H, -CH-).

<sup>13</sup>C-NMR (CDCl<sub>3</sub>): δ (ppm) = 175 (-O-C=O), 138 - 144 (aromatic C), 133 (aromatic C), 128 (aromatic -C=) 55 - 60.1 (CH<sub>2</sub>-CH-CH-), 46.2 - 50.2 (CH<sub>2</sub>-CH-CH-), 42 (-CH<sub>2</sub>).

#### 4.7.13 Synthesis of functionalized polymer by immobilizing *N*-(4-ethynyl-6-methylpyrimidin-2-yl)-*N*-phenylformamide on to P(S<sub>N</sub>-*alt*-MAh)) copolymer yielding anilinopyrimidine<sub>7</sub>-derivative copolymer (P(S<sub>AP7</sub>-*alt*-MAh))

160 mg (0.608 mmol) P(S<sub>N</sub>-*alt*-MAh) copolymer was dissolved in 5 mL of DMF and placed in a 50 mL Schlenk tube. 360 mg (1.216 mmol) Anilinopyrimidine<sub>7</sub>-derivative was added to the polymer solution. PMDETA ligand (15.5 mg, 0.0912 mmol) was added to the mixture of P(S<sub>N</sub>-*alt*-MAh) polymer and compound. The mixture was degassed using Ar for 20 minutes. After degassing the reaction mixture 26.16 mg (0.1824 mmol) Cu(I)Br and 144.54 mg (0.7296 mmol) sodium ascorbic acid were added as quick as possible. The reaction

mixture was degassed for a further 5 minutes and left under Ar to stir for 16 hours. After the reaction time the polymer solution was precipitated in diethyl ether to remove any unreacted compound and residual solvent.

Major IR absorptions:  $\sim 3200$ , 2095.14,  $\sim 1687.98$ , 1450.89, 1436.02, 1274.60, 1157.03, 1074.08, 1049.20, 1001  $\text{cm}^{-1}$ .

$^1\text{H-NMR}$  ( $\text{CDCl}_3$ ):  $\delta$  (ppm) = 8.7 (2H, aromatic H on compound and  $-\text{CH}=\text{O}$ ), 7.95 (1H, C-H triazole), 7.5 (3H, C- $\text{CH}_3$ ), 6.78 - 7.41 (s broad, 9H aromatic), 5.31 - 5.75 (2H,  $-\text{CH}_2-\text{N}_3$ ).

#### 4.7.14 Single needle electrospinning of poly(4-vinylbenzyl chloride-*alt*-maleic anhydride) copolymer ( $\text{P}(\text{S}_{\text{Cl-}}\text{-}i\text{alt}\text{-MANh})$ )

$\text{P}(\text{S}_{\text{Cl-}}\text{-}i\text{alt}\text{-MANh})$  copolymer was dissolved in a 1:1 THF/DMF solution to a concentration of 25 wt. %. Electrospinning took place in a top to bottom direction. The prepared solution was placed in a single needle electrospinning setup prepared beforehand, refer Section 3.4.1 in Chapter 3. The setup involved a 1 mL plastic syringe with a 21 Gauge blunted needle. The syringe is placed upside and connected to a syringe pump (Harvard, Model 33 Twin Syringe Pump). The high power voltage supply is capable of generating positive DC voltages from 0 to 25 kV, the opposite electrodes of the high voltage supply was connected to the blunt needle and the a aluminum covered collector. The positive charge was set at 8 kV and the negative at -8 kV. The flow rate of the solution was set at 0.18 mL/min and the optimum spinning distance was found to be 15 cm. Environmental conditions while electrospinning were ambient humidity <50% and temperature 20 °C. The collected electrospun nanofibers were placed under vacuum at 40 °C to remove any residual solvent that might be present.

#### 4.7.15 Single ball electrospinning of poly(4-vinyl benzyl chloride-*alt*-maleic anhydride) copolymer ( $\text{P}(\text{S}_{\text{Cl-}}\text{-}i\text{alt}\text{-MANh})$ )

$\text{P}(\text{S}_{\text{Cl-}}\text{-}i\text{alt}\text{-MANh})$  copolymer was dissolved in a 1:1 DMF/THF mixture. The concentration of the polymer in the solvent was 25 wt. %. The prepared solution was placed in the solution holder.

Refer to Figure 3.5 (in Section 3.4.2, Chapter 3) for the schematic illustration of the basic ball electrospinning setup. The rotating drum collector was placed various spinning distances but an optimum spinning distance was 10 cm. The positive electrode of a Matsusada high voltage power supply was attached to the cup holder and the negative electrode of another high voltage supply was attached to the rotating drum collector. The positive high voltage supply is capable of generating positive DC voltages from 0 to 160 kV and was set at 35 kV. The high voltage power supply of the negative electrode is capable of generating -25 kV and was set to maximum. The rotating ball was attached to an electrical device set at 7.5 kV and the drum collector at -12 kV. The nanofibers that collected were placed under vacuum at 40 °C to remove any residual solvent that might be present.

#### 4.7.16 Single needle- and single ball electrospinning of poly(4-vinyl benzyl azide-*alt*-maleic anhydride) copolymer (P(S<sub>N</sub>-*alt*-MAh))

Refer section 4.4.2 for details regarding the dissolution of the polymer. No fibers were obtained from single needle or single ball electrospinning the polymer solution.

#### 4.7.17 Post-electrospinning modification of P(S<sub>Cl</sub>-*alt*-MAh) polymer nanofibers to yield P(S<sub>N</sub>-*alt*-MAh) polymer nanofibers

P(S<sub>Cl</sub>-*alt*-MAh) polymer nanofibers are placed in a non-solvent for the fibers itself but the same solvent dissolves the inorganic NaN<sub>3</sub> salt. An isopropanol/water solution mixture (90: 10) was chosen as the solvent. Fibers could stay in the solvent for longer than 48 hours and no degradation of polymer nanofibrous structure is observed. 143.4 mg (2.204 mmol) sodium azide is added to 15 ml isopropanol/water solvent. It is made sure that all inorganic salt is dissolved before 186.86 mg (0.735 mmol Cl functionality) of P(S<sub>Cl</sub>-*alt*-MAh) nanofibers are placed within solution. A magnetic stir bar is added and round bottom is placed in a 70 °C pre-heated oil bath. The reaction mixture was left to react for 24 hours. The fibers were taken out of solution and washed in clean isopropanol/water three times to make sure any residual sodium azide and newly formed sodium chloride is removed from the surface of nanofibers. Fibers are dried under vacuum at 40 °C for 4 hours to remove any residual solvent.

For the azide substitution reaction to occur a suitable solvent had to be chosen to dissolve the  $\text{NaN}_3$  but preserve the nanofibrous structure of the polymer nanofibers. The optimum solvent was found to be a 90:10 mixture of isopropanol/water. The only disadvantage of using water is the hydrolysis of the maleic anhydride moiety, although ring opening of the maleic anhydride unit occurred, a maleic acid did not influence the attachment of the anilinopyrimidine<sub>7</sub>-derivative.

#### 4.7.18 Post-electrospinning functionalization of $\text{P}(\text{S}_{\text{N}}\text{-}i\text{alt}\text{-MAh})$ polymer nanofibers by immobilizing $N$ -(4-ethynyl-6-methylpyrimidin-2-yl)- $N$ -phenylformamide onto polymer nanofibers yielding anilinopyrimidine<sub>7</sub>-derivative polymer nanofibers ( $\text{P}(\text{S}_{\text{AP7}}\text{-}i\text{alt}\text{-MAh})$ )

5 mg (0.019 mmol  $\text{N}_3$  functionality)  $\text{P}(\text{S}_{\text{N}}\text{-}i\text{alt}\text{-MAh})$  polymer nanofibers is added to 5 mL acetonitrile in a 50 mL round bottom. 4.53 mg (0.0209 mmol) Anilinopyrimidine<sub>7</sub>-derivative and 1.92 mg (0.019 mmol) triethylamine (TEA) is added and the reaction and the reaction mixture is degassed using Ar. After 20 min 0.72 mg (0.0038 mmol)  $\text{Cu}(\text{I})\text{I}$  is added quickly. The reaction mixture was left under Ar for another 20 min. The reaction was left overnight for 24 hours. After 24 hours the fibers are removed from the reaction flask and washed three times with clean acetonitrile. The functionalized polymer nanofibers are dried under vacuum at 40 °C for 4 hours to remove any residual solvent.

Although the attachment of the anilinopyrimidine<sub>7</sub>-derivative ( $N$ -(4-ethynyl-6-methylpyrimidin-2-yl)- $N$ -phenylformamide) onto the polymer nanofibers seems like a straight forward reaction, it was difficult to find an appropriate solvent for the reaction.

Some of the reaction steps were challenging by having numerous side reactions occurring under the detailed reaction conditions. Reactions were optimized as far as possible but due to unexplained reactions occurring very low yields were obtained in the last steps. The obtained quantity of mepanipyrim derivatives was sufficient for both analysis and anti-fungal studies.

## 4.8 References

1. Serey, R. A.; Torres, R.; Latorre, B. A. *Ciencia e investigación agraria*. **2007**, 3, 215-224.
2. de Kock, P.J de; Holtz, G. S. *Arf. J. Enol. Vitic.* **1994**, 23, 33-40.
3. Myresiotis, C.K.; Karaoglanidis, G.S.; Tzavella-Klonari, K. *Plant Dis.* **2007**, 91, 407-413.
4. Couderchet, M. *Vitis*. **2003**, 4, 165-171.
5. Nagata, T.; Masuda, K.; Maeno, S.; Miura, I. *Pest Manag. Sci.* **2004**, 4, 399-407.
6. Bshena, O. E. S. *Synthesis of Permanent Non-Leaching Antimicrobial Polymer Nanofibers*, PhD thesis, University of Stellenbosch, Stellenbosch. **2012**.
7. Rowley, G. L.; Greenleaf, A. L.; Kenyon, G. L. *J. Am. Chem. Soc.* **1971**, 21, 5542-5551.
8. Aly, A. A.; Nour-El-Din, A. M. *Arkivoc.* **2008**, 153-194.
9. Omar, N. M. A. *Studies on nitrogen heterocyclic systems*, PhD thesis, Zagazig University, Egypt. **2003**.
10. Wang, H.; Wen, K.; Wang, L.; Xiang, Y.; Xu, X.; Shen, Y.; Sun, Z. *Molecules*. **2012**, 4, 4533-4544.
11. Fleet, R.; Van Den Dungen, Eric TA; Klumperman, B. S. *Afr. J. Sci.* **2011**, 3-4, 01-11.
12. Yin, J.; Ge, Z.; Liu, H.; Liu, S. *J. Polym. Sci. A: Polym Chem.* **2009**, 10, 2608-2619.
13. Mansfeld, U.; Pietsch, C.; Hoogenboom, R.; Becer, C. R.; Ulrich, S. *J. Polym. Chem.* **2010**, 1, 1560-1598.

14. Lia, N.; Binder, W.H. *J. Mater. Chem.* **2011**, 27, 16717–16734.
15. Lammens, M.; Skey, J.; Wallyn, S.; O'Reilly, R.; Du Prez, F. *Chem. Commun.* **2010**, 46, 8719–8721.
16. Shenoy, S. L.; Bates, W. D.; Frisch, H. L.; Wnek, G. E. *Polymer.* **2005**, 10, 3372-3384.
17. Pavia, D. L. *Introduction to spectroscopy*; CengageBrain. com: **2009** .
18. Reich, H. J. Chem 605 - Structure Determination Using Spectroscopic Methods.  
<http://www.chem.wisc.edu/areas/reich/chem605/index.htm>.
19. Tang, C.; Ye, S.; Liu, H. *Polymer.* **2007**, 15, 4482-4491.
20. Jeong, J.; Byoun, Y.; Ko, S.; Lee, Y. *J. Ind. Eng. Chem .* **2001**, 5, 310-315.
21. Wu, Y.; Kuo, S. J. *Polym. Chem.* **2012**, 11, 3100-3111.
22. Srividhya, D.; Manjunathan, S.; Nithyanandan, S.; Balamurugan, S.; Senthil, S. *Chin. J. Polym. Sci.* **2009**, 6, 761-770.
23. Stoilova, O.; Ignatova, M.; Manolova, N.; Godjevargova, T.; Mita, D.; Rashkov, I. *Eur. Polym. J.* **2010**, 10, 1966-1974.
24. Chen, G.; Zhang, Y.; Zhou, X.; Xu, J. J. *Appl. Surf. Sci.* **2006**, 3, 1107-1110.
25. Komaraiah, A.; Ramakrishna, K.; Sailu, B.; Reddy, P. *Arkivoc.* **2007**, 14, 110-116.
26. Mishra, G.; McArthur, S. L. *Langmuir.* **2010**, 12, 9645-9658.
27. Lin, J.; Qiu, S.; Lewis, K.; Klibanov, A. M. *Biotechnol. Bioeng.* **2003**, 2, 168-172.

## CHAPTER V: ANTI-FUNGAL STUDIES BETWEEN FUNCTIONALIZED POLYMERS AND *Botrytis cinerea*

### 5.1 Introduction

*Botrytis cinerea* Pers.: Fr., the causal agent of grey mould, causes annual table grape spoilage during storage, and is therefore a high risk of loss to farmers and consumers.<sup>1,2</sup> Fruit can be infected in the field or during storage by inoculum present in the environment. *Botrytis cinerea* is mainly controlled in the field by means of chemical fungicides and in storage using sulphur dioxide (SO<sub>2</sub>) generating sheets or weekly fumigations thereof.<sup>3-5</sup>

As discussed in previous chapters the current methods of control *B. cinerea* have drawbacks and have led to the invention of possible new *B. cinerea* control methods for the use in storage rooms.<sup>6,7</sup>

The two different functionalized polymers were evaluated in this chapter as anti-fungal platforms against *B. cinerea*. The first polymer, poly(styrene-*alt*-maleic anhydride) (SMA), was functionalized to yield poly(Styrene-*alt*-[(N-dodecyl)-N, N-dimethyl]-3-propyl maleimide) copolymer (SMI-qC<sub>12</sub>) and electrospun to produce functionalized polymer nanofibers. The nanofibers were further surface-functionalized via an ionic transfer exchange to incorporate sodium metabisulfite within the polymer nanofibers after electrospinning (as described in Chapter 3). Nanofibers with an average fiber diameter in the range of ~ 410 - 465 nm were produced. The second polymer, poly(4-vinylbenzyl chloride-*alt*-maleic anhydride) (VBC), was functionalized before and after the electrospinning process. The polymer was functionalized with fungicide-derivatives (as described in Chapter 4). Nanofibers with an average fiber diameter in the range of ~ 515 - 585 nm were produced.

In both procedures the chosen functionalization-agents (sodium metabisulfite and fungicide-derivatives) in this study were based on previous research (as described in Chapter 2).

These functionalized polymers were developed as potential *B. cinerea* control platforms during the storage of grapes. An anti-fungal pilot study was carried out using the different functionalized polymers and fungicide-sensitive *B. cinerea* isolates to evaluate whether *B. cinerea* can be inhibited. In this chapter we report the anti-fungal study between the functionalized polymers and *B. cinerea*.

## 5.2 Materials and methods

### 5.2.1 *B. cinerea* isolates and preparation

Two *B. cinerea* isolates were provided by Dr. C. Lennox, Department Plant Pathology, University of Stellenbosch. Isolates were collected during 2010 from an experimental plot in a commercial orchard from a farm in the Ceres region of the Western Cape. These isolates are considered to be natural, having no exposure to botryticides for a period of five years before sampling. Isolates were cultured onto 9-mm potato dextrose agar (PDA) (Biolab, Merck, Modderfontein, South Africa) plates and incubated at 23 °C in the dark. Spore suspensions were prepared from 14 day old cultures with a final concentration of  $1 \times 10^3$  spores. $\mu\text{L}^{-1}$ .

### 5.2.2 Functionalized polymer preparation

#### 5.2.2.1 Functionalized SMI-qC<sub>12</sub> nanofibrous mats with incorporated sodium metabisulfite salt

The SMI-qC<sub>12</sub> polymer was synthesized (Chapter 3, section 3.3.4). Shortly, the polymer and sodium metabisulfite salt was simultaneously dissolved in a solvent and electrospun into polymer nanofibrous mats. After crosslinking, the nanofibers became insoluble and were emerged in a saturated sodium metabisulfite solution to increase the amount of salt incorporate within the polymer nanofibers. The salt was incorporated within the polymer system via ionic transfer exchange. Using the single ball electrospinning-setup nanofibrous mats were obtained. A polymer concentration of 25 wt. % was found to be sufficient for acceptable number of polymer chain entanglements and the salt concentration in the solution was 0.6 wt. %.

#### 5.2.2.2 Fungicide-derivatives

The fungicide-derivatives, *N*-(4-ethynyl-6-methylpyrimidin-2-yl)-*N*-phenylformamide (anilinopyrimidine<sub>7</sub>-derivative) and 4-ethynyl-6-methyl-*N*-phenylpyrimidin-2-amine



(anilinopyrimidine<sub>8</sub>-derivative) were synthesized (as described in Chapter 4, sections 4.2.8 and 4.2.10). The fungicide-derivatives were stored in the dark at 4 °C under argon atmosphere to maintain and preserve possible fungicide activity.

### 5.2.3 Media preparation

For the sensitivity assay using sodium metabisulfite, PDA amended with streptomycin sulfate, was prepared in 9-mm Petri-dishes.

For the sensitivity assay using the synthesized organic compound, minimal medium modified from the Difco Czapek-Cok (CDA) recipe was used.<sup>8</sup> Due to the close chemical relationship of the compound to mepanipyrim, the CDA medium was used to avoid possible interactions of the compound with complex components of an undefined medium, such as PDA, that were observed in previous studies conducted.<sup>8,9</sup> One liter of medium contained: 10g glucose, 3 g NaNO<sub>3</sub>, 1 g KH<sub>2</sub>PO<sub>4</sub>, 1 g K<sub>2</sub>HPO<sub>4</sub> 0.5 g MgSO<sub>4</sub>·7H<sub>2</sub>O, 0.5 g KCl and 0.01 g FeSO<sub>4</sub>·7H<sub>2</sub>O.

### 5.2.4 Conidial and mycelium sensitivity assay

#### 5.2.4.1 Conidial germination sensitivity using SMI-qC<sub>12</sub> nanofibrous mats with incorporated sodium metabisulfite salt

The amended fibrous mats were irradiated with UV-light and attached to the inner lid of the Petri dish using irradiated double-sided tape. Fibrous mats with sodium metabisulfate and neat fibres were used. Control plates did not have fibrous mats attached to the inner lid. Aliquots of 300 µL from the respective spore suspension were spread on the medium surface.<sup>10</sup> Plates were incubated for 24 hours at 24 °C in the dark. Three replications were done for each isolate.

The effect of sodium metabisulfite upon conidial germination was evaluated looking at the germ tube elongation and morphologies.<sup>11,12</sup> Germ tubes at least 1.5 times that of the spore length and unbranched were considered germinated and counted.<sup>11,12</sup> Using a stereomicroscope, thirty spores were counted per replicate and the percentage inhibition of germination calculated. Germ-tubes are normally straight and without any branching. If the spore would be inhibited it is

clearly identifiable as abnormalities in the base morphology of the germ-tube either being tightly coiled or highly branched. Inhibition is therefore seen as a disruption of the micro tubular component of the germ-tube either being highly branched or tightly coiled.<sup>10</sup>

#### 5.2.4.2 Mycelium sensitivity assay to fungicide-derivatives

Mycelium growth of the two isolates was tested on CDA medium amended with the fungicide-derivatives (synthesized in Section 4.2 in Chapter 4). The fungicide-derivatives were dissolved with acetone for final concentrations of 0.01, 0.05 and 0.1 mg/L in one liter of medium. The final acetone concentration per liter of medium was 0.01%. Control plates were also done in triplicate for each isolate and only contained acetone. Inoculated plates were incubated in the dark at 24 °C for 3 - 4 days.

Colony diameters were measured at two right angles using a digital calliper.<sup>8,13,14</sup> The mean radial growth of the colonies at the different concentrations was expressed as the percentage mean radial growth on unamended CDA subtracted from 100 to give the percentage inhibition.<sup>15</sup>

## 5.3 Results

### 5.3.1 Conidial sensitivity assay regarding functionalized SMI-qC<sub>12</sub> polymer nanofibers

The presence of sodium metabisulfite inhibits spore germination by more than 60% (refer Table 5.1). Germination of conidia was evaluated, where the germ tube was shorter than 1.5 the size of the spore head.<sup>16</sup> The control plates had 3.33% inhibition (96.7% germinated). Plates containing only neat fibers had 10% inhibition and the plates with sodium metabisulfite fibers a showed inhibition of 60%.

*Table 5.1 The percentage of conidial inhibition of two different isolates of B. cinerea using sodium metabisulfite. In each experiment 30 spores were evaluated for germination*

Pathogen/ Isolate	Experiment	Inhibition of spore germination				% Inhibition	
		1	2	3	avg		
<i>Botrytis cinerea</i>	Control	1 (29)	2 (28)	1 (29)	1 (29)	3.33	
	Isolate	Neat fibers	5 (25)	2 (28)	3 (27)	3 (27)	10
	1	Fibers and active salt	21 (9)	19 (11)	14 (16)	18 (12)	60
	Control	3 (27)	2 (28)	1 (29)	2 (28)	6.67	
	Isolate	Neat fibers	2 (29)	4 (26)	5 (25)	4 (26)	13.33
	2	Fibers and active salt	18 (12)	14 (16)	16 (14)	16 (14)	53.33

<sup>a</sup> The value in brackets is the number of conidium that germinated. The value outside of the brackets is the number of spores that did not germinate.

### 5.3.2 Mycelium sensitivity assay regarding the synthesized fungicide-derivatives

The assay was done to determine the inhibition of mycelium growth using synthesized fungicide-derivatives. Both anilinopyrimidine<sub>7</sub>-derivative and anilinopyrimidine<sub>8</sub>-derivative demonstrated antifungal activity against the two isolates (refer Table 5.2).

Table 5.2 The Percentage inhibition of mycelium growth is expressed as a function of concentration against the two *B. cinerea* isolates.

Fungicide-derivatives	Concentration mg/L	% Inhibition	
		Isolate 1	Isolate 2
Fungicide <sub>7</sub> -derivative	0.00	0	0
	0.01	-	-
	0.05	98.42	100
	0.1	100	100
	0.00	0	0
Fungicide <sub>8</sub> -derivative	0.01	96.93	77.31
	0.05	97.25	100
	0.1	97.55	100

<sup>a</sup> Although in both experiments the concentration of anilinopyrimidine<sub>7</sub>-derivative at 0.01 mg.L<sup>-1</sup> did not set and growth could not be established, a clear inhibition of mycelium growth is observed at the next two concentrations.

### 5.3.3 Inhibition assay of mycelium growth using functionalized anilinopyrimidine<sub>7</sub>-derivative copolymer (P(S<sub>AP7</sub>-*alt*-MA<sub>nh</sub>)) against *B. cinerea*

Due to time constrains the last step of the study could not be performed. In future work, it would be recommended to do assays regarding the final product. This would require the compound to be covalently attached to the polymer, where the advantage would be that no leaching out of fungicide.

## 5.4 Discussion and conclusion

### 5.4.1 Discussion on conidial sensitivity assay regarding functionalized SMI-qC<sub>12</sub> polymer nanofibers

From Table 5.1 the inhibition of conidial germination in the presence of sodium metabisulfite is presented and an increase in the percentage inhibition of conidial germination between the control plates and the salt containing fibers are indicated. Conidial germination of *B. cinerea* in general medium (PDA) was inhibited by 60% using sodium metabisulfite incorporated SMI-qC<sub>12</sub> nanofibers. A difference was also observed in germ-tube morphologies in the different experiments being the control, neat fibers and functionalized fibers. In the presence of sodium metabisulfite, the germ-tubes were highly branched and/or tightly coiled, indicating an inhibition effect.

### 5.4.2 Discussion on mycelium sensitivity assay regarding the synthesized fungicide-derivatives

The results, although this was only a pilot study, indicated that both fungicide-derivatives have strong fungicidal activity.<sup>17</sup> At the lowest concentration of 0.01 mg/L anilinopyrimidine<sub>7</sub>-derivative showed full inhibition of mycelium growth. At highest concentration (0.1 mg/L) full inhibition is observed for both compounds (refer Table 5.2).<sup>17</sup>

Against both isolates (isolate 1 and isolate 2) it was observed that anilinopyrimidine<sub>7</sub>-derivative showed full inhibition, except for concentration 0.05 mg.L<sup>-1</sup> against isolate 1.

Anilinopyrimidine<sub>8</sub>-derivative showed good anti-fungal properties against the isolates. Full inhibition of mycelium growth was observed for concentrations 0.05 and 0.1 mg.L<sup>-1</sup> against isolate 2. Against isolate 1 more than 96.5% inhibition is observed for all concentrations. Anti-fungal results show promising results for both anilinopyrimidine-derivatives.

Comparing anilinopyrimidine<sub>7</sub>-derivative to anilinopyrimidine<sub>8</sub>-derivative it is suggested that anilinopyrimidine<sub>7</sub>-derivative is slightly more active against both isolates although both compounds showed excellent anti-fungal activity.

### 5.4.3 Conclusion

The study focused on the spoilage of grapes during post-harvest storage periods. The use of fungicides in the field are effective, but cannot be used during storage due to residue levels on the surface of the berries. Accumulating residue levels are restricted due to toxicity towards humans.<sup>18</sup> During postharvest storage, grey mould is prevented with SO<sub>2</sub> gas by initially fumigating the fruit, followed by weekly fumigations. During transport fumigations are not possible and are done by means of SO<sub>2</sub> generating sheets present in the packaging.<sup>18,19</sup>

The first limitation of SO<sub>2</sub> gas as fumigation agent is that it exhibits anti-fungal activity against *B. cinerea*, but does not kill dormant infections present within the berry tissue during storage. This leads to subsequent development of grey mould at a later stage when favourable conditions arise.<sup>19</sup> A high SO<sub>2</sub> concentration is therefore needed to control inoculum present on the berry surface, but if it is too high damage can occur. Secondly, SO<sub>2</sub> generating sheets are only placed on top of the box. When SO<sub>2</sub> is released, the gas is only from one side of the packaging system. The berries close to the generating sheet therefore experience higher SO<sub>2</sub> concentrations than the fruit at the bottom of the packaging. For this reason, a control method is needed that can effectively control *B. cinerea* during storage but does not involve accumulating residues on the berry surface.

The two afore mentioned control methods of controlling *B. cinerea* includes SO<sub>2</sub> fumigation using SO<sub>2</sub> generating sheets during storage and fungicide application in the field but have limited success. To date no literature have showed the successful inhibition of *B. cinerea* during storage.<sup>1</sup> It is thus of importance to establish effective treatments or control methods with low toxic risk and resistance development of the pathogen.<sup>7</sup>

Polymer nanofibers were synthesized that entailed sodium metabisulfite to be incorporated with the nanofibrous structure. Instead of having a SO<sub>2</sub> generating sheet on the top of the box these nanofibrous mats can be wrapped around the fruit. With only one generating sheet on top of the fruit box, more sodium metabisulfite is needed to release SO<sub>2</sub> gas within the whole box of fruit. Through having a material wrapped around the fruit, less sodium metabisulfite is needed. Fungicide-derivatives were synthesized and attached to a polymer system. This allows no residues to be present on the fruit surface, with anti-fungal activity staying intact and no leaching out of the active ingredient is possible.

The sensitivity assays was done as a pilot study, future research will be needed to conclude this work fully, with this working providing a sufficient platform as a proof of concept.

## 5.5 References

1. Barth, M.; Hankinson, T.R.; Zhuang, H.; Breidt, F. *Food Microbiol.* **2009**, 27, 135.
2. Forster, B.; Staub, T. *Crop prot.* **1996**, 6, 529-537.
3. Mustonen, H.M. *Aust. J. Exp. Agr.* **1992**, 32, 389-393.
4. Zutahy, Y.; Lichter, A.; Kaplunov, T.; Lurie, S. *Postharvest Biol. Technol.* **2008**, 50, 12-17.
5. Nelson, K. E.; Gentry, J. P. *Am. J. Enol. Vitic.* **1966**, 4, 290-301.
6. Nagata, T.; Masuda, K.; Maeno, S.; Miura, I. *Pest. Manag. Sci.* **2004**, 4, 399-407.
7. Serey, R. A.; Torres, R.; Latorre, B. A. *Ciencia e investigación agraria.* **2007**, 3, 215-224.
8. Yourman, L.; Jeffers, S. *Plant Dis.* **1999**, 6, 569-575.
9. Vaughan, S. J.; Steel, C. C.; Ash, G. J. *Australas. Plant Pathol.* **2001**, 4, 367-368.
10. Weber, R.; Hahn, M. J. *Plant Dis. Protect.* **2011**, 118, 17-25.
11. Chapeland, F.; Fritz, R.; Lanen, C.; Gredt, M.; Leroux, P. *Pestic. Biochem. Physiol.* **1999**, 2, 85-100.
12. Lin, J.; Qiu, S.; Lewis, K.; Klibanov, A. M. *Biotechnol. Bioeng.* **2003**, 2, 168-172.
13. Begum, F.; Mahal, F. a. A., Shahidul J. *Life Earth Sci.* **2010**, 5, 23-27.
14. Northover, J.; Matteoni, J. *Plant Dis.* **1986**, 5, 398-402.

15. Lennox, C. L.; Spotts, R. A. *Plant Dis.* **2003**, 6, 645-649.
16. Lin, J.; Qiu, S.; Lewis, K.; Klibanov, A. M. *Biotechnol. Bioeng.* **2003**, 2, 168-172.
17. de Kock, P.J; Holtz, G. S. *Arf. J. Enol. Vitic.* **1994**, 23, 33-40.
18. Palou, L.; Crisosto, C. H.; Garner, D.; Basinal, L. M.; Smilanick, J. L.; Zoffoli, J. P. *Am. J. Enol. Vitic.* **2002**, 2, 110-115.
19. Cantín, C. M.; Palou, L.; Bremer, V.; Michailides, T. J.; Crisosto, C. H. *Postharvest Biol. Technol.* **2011**, 2, 150-158.



## CHAPTER VI: CONCLUSIONS AND RECOMMENDATIONS FOR FUTURE RESEARCH

### 6.1 Conclusions

The synthesis and characterization of two functionalized polymer nanofibrous systems (mats) were presented in this thesis. The nanofibrous mats were utilized as platforms for the inhibition of *B. cinerea* growth that can potentially be used for packaging of table grapes. This chapter discusses the main findings and recommendations for this study.

#### 6.1.1 Functionalization of polymers

##### 6.1.1.1 Functionalization of SMI-qC<sub>12</sub> polymer nanofibers with incorporated sodium metabisulfite

An alternating poly(styrene-*alt*-maleic anhydride) (SMA) copolymer was successfully synthesized using conventional radical polymerization. SMA with a 50% maleic anhydride content was synthesized with a dispersity of 4.09 and a weight average molecular weight ( $M_w$ ) of 198 000 g/mol. SMA was modified through a nucleophilic reaction with 3-(*N,N*-dimethylamino)-1-propylamine (DMAPA) to yield poly(styrene-*alt*-[*N*-3-(*N,N*'-dimethylamino) propyl maleimide]) copolymer (SMI) which was further quaternized with bromododecane (Br-C<sub>12</sub>) to yield the relevant quaternized poly(styrene-*alt*-[(*N*-dodecyl)-*N,N*-dimethyl]-3-propyl maleimide]) copolymer (SMI-qC<sub>12</sub>). The obtained polymers were fully characterized using <sup>1</sup>H-NMR, <sup>13</sup>C-NMR and ATR-FTIR spectroscopy.

The obtained polymers were successfully electrospun into polymer nanofibrous mats using single needle and single ball electrospinning techniques. SEM analysis of the obtained polymer mats showed that the average fiber diameter ranged between 410 and 465 nm.

The deposition of sodium metabisulfite salt with highest possible concentration (215 mg sodium metabisulfite salt per 445 mg polymer mat) was successfully achieved through a multi-step process. Initially, the SMI-qC<sub>12</sub> nanofibers were crosslinked via heat treatment in order to preserve the nanofibrous structure upon contact with solvents. By submerging the obtained crosslinked nanofibers into a sodium metabisulfite saturated solution in DMF/THF, the deposition of sodium metabisulfite was achieved through an ion exchange reaction between the bromide anion and the anionic sodium metabisulfite salt.

#### 6.1.1.2 Synthesis of functionalized polymer through immobilization of anilinopyrimidine-derivatives onto poly(4-vinylbenzyl azide-*alt*-maleic anhydride) copolymer yielding anilinopyrimidine-derivative polymers

Anilinopyrimidine-derivatives with suitable functional groups were successfully synthesized as confirmed by <sup>1</sup>H-NMR, <sup>13</sup>C-NMR. Although the fungicide mepanipyrim is commercially available, its use in this study was limited as it does not have the necessary functional groups needed for the polymer modification. The synthesis of the desired anilinopyrimidine-derivatives was achieved in a multi-step synthetic route. Although the last steps of the process only gave low yields, the obtained anilinopyrimidine-derivatives amount was sufficient for both analysis and anti-fungal studies.

Alternating poly(4-vinylbenzyl chloride-*alt*-maleic anhydride) copolymer (P(S<sub>Cl</sub>-*alt*-MAh)) was successfully synthesized via radical copolymerization of 4-vinylbenzyl chloride (S<sub>Cl</sub>) with maleic anhydride (MAh) followed by pre- and post-electrospinning modification with sodium azide to yield poly(4-vinylbenzyl azide-*alt*-maleic anhydride) copolymer (P(S<sub>N</sub>-*alt*-MAh)). The azide moieties were then used in a click reaction with anilinopyrimidine<sub>7</sub>-derivative that resulted in polymer chains with covalently bonded anti-fungi moieties (anilinopyrimidine<sub>7</sub>-derivative polymer) (P(S<sub>AP7</sub>-*alt*-MAh)). The modification of the polymer and the polymer nanofibers were confirmed with <sup>1</sup>H-NMR, <sup>13</sup>C-NMR, and ATR-FTIR.

## 6.1.2 Anti-fungal studies

Anti-fungal properties of the prepared, sodium metabisulfite imbedded polymer nanofibers and Anilinopyrimidine-derivative polymer against *Botrytis cinerea* were studied.

The successful inhibition of *B. cinerea* using the salt incorporated nanofibers was confirmed by evaluation of the conidial sensitivity assay. The sodium metabisulfite imbedded nanofibers showed anti-fungi activity with up to 60% inhibition of conidial germination.

The anti-fungal activity of free anilinopyrimidine-derivatives against *B. cinerea* was carried out at different anilinopyrimidine-derivative concentrations. The results indicated that even at very low concentrations (0.01 mg/L) of anilinopyrimidine-derivatives, an almost full inhibition of *B. cinerea* mycelium growth was observed.

Overall, this study showed that the use of nanofibers imbedded with sodium metabisulfite or anilinopyrimidine-derivatives as anti-fungal methods is both effective as a sufficient approach that can potentially revolutionize the grape-packaging industry.

## 6.2 Recommendations for future research

This study opened a new promising avenue to the grape-packaging industry, however a few further investigation that can potentially improve the anti-fungi activity. Among these needed studies are:

- (1) Optimizing the maximum quantity of salt that can be imbedded within the polymer nanofibers which will give the best anti-fungi activity.
- (2) To investigate other polymers of different nature that may have anti-fungal properties as pristine polymer and additionally reducing the final cost.
- (3) Investigating the anti-fungal activities of the anilinopyrimidine<sub>7</sub>-derivative polymer as well as investigating other alternative synthetic methods for anilinopyrimidine-derivatives that may increase the yield.

- (4) To investigate the anti-fungal activities of these methods against other postharvest pathogens.
- (5) To investigate a wider spectrum of fungicides that have shown anti-fungal activity, modifying the fungicides to yield fungicides with suitable functional groups to be attached to a polymer system and testing them against *Botrytis cinerea* and other plant pathogens.

## ACKNOWLEDGMENTS

I would like to thank my supervisors Prof B Klumperman, Dr L Cronje and an extended thanks to Prof van Otterlo who have been determined to guide and teach me throughout my study.

I would also like to thank the Department of Postharvest Technology and especially Prof L Opara, for welcoming me and giving me the opportunity to study further through supporting me financially.

I would like to thank the Institute of Polymer Science at the University of Stellenbosch who welcomed me and provided me with the opportunity to do my further studies here.

I would like to thank the research group of Prof Klumperman, every person in the lab who spent hours in the lab with me, made me smile and contributed to my study. A big thanks to Waled who took me in in the beginning and showed me around, helped me find my feet, all the discussions we had and especially your willingness to share your knowledge.

I would like to thank the Department of Plant Pathology, in specific Dr C Lennox and Jessica Rochefort who has gone out of their way to make my anti-fungal testing possible and helping me with the plant pathology chapter.

Ek wil ongelooflik baie dankie sê aan die volgende drie mense wat my bygestaan het met die skryf: Leone, Jessica en Lizl. Baie dankie vir die ure wat julle ingesit het. 'n Dankie is nie genoeg nie!

Ek wil in besonder dankie sê aan my ouers, Pieter en Elize Harmzen, vir julle onbaatsigtelike liefde en ondersteuning. Dankie vir al julle moontlike leiding en die liefde waarmee julle my groot gemaak het en my gedra het. Dankie vir die ondersteuning en die hulp om my studies klaar te maak, spesifiek my meesters graad. Ek wil ook 'n spesiale dankie sê vir die mense naaste aan my wat al soos familie: Retha en Corne, julle het my gedra, in baie maniere ondersteun, selfs die dae as ek nie meer geweet het watter kant toe nie, dae as ek gewonder het of die tesis gaan klaar kom of dae as reaksies maande gevat het om te werk. Dankie vir al julle ondersteuning en liefde.

## **Erika Harmzen**